Membrane-model systems to study EGFR-ARNO interaction

Dissertation

zur

Erlangung des Doktorgrades (Dr. rer. nat.)

der

Mathematisch-Naturwissenschaftlichen Fakultät

der

Rheinischen Friedrich-Wilhelms-Universität Bonn

vorgelegt von

Martina Bettio

aus Treviso

Bonn 2016

Angefertigt mit Genehmigung der Mathematisch-Naturwissenschaftlichen
Fakultät der Rheinischen Friedrich-Wilhelms-Universität Bonn

1. Gutachter: Professor Dr. Michael Famulok

2. Gutachter: Professor Dr. Thorsten Lang

Tag der Promotion: 25.11.2016

Erscheinungsjahr: 2017

Part of this thesis is published in:

Hussein, M.; **Bettio, M.**; Schmitz, A.; Hannam, J. S.; Theus, J.; Mayer, G.; Dosa, S.; Gütschow, M.; Famulok, M. (2013): Cyplecksins are covalent inhibitors of the pleckstrin homology domain of cytohesin. In *Angew. Chem. Int. Ed.*, Vol. 52 (36): pp. 9529-9533. DOI: 10.1002/anie.201302207

Table of Contents

Table of Contents

List of Figures

List of Figures

List of Figures

List of Tables

List of Abbreviations

°C	degree Celsius
Δ	delta
A280	absorption coefficient at 280 nm
ADP	adenosine-diphosphate
AFM	atomic force microscopy
Amp	ampicillin
Apo A-1	Apolipoprotein A-1
APS	ammonium persulfate
Arf	ADP ribosylation factors
ARNO	ARF nucleotide binding site opener
ATP	adenosine-5´-triphosphate
BSA	bovine serum albumin
CHAPSO	3-[(3-cholamidopropyl)dimethylammonio]-1-propanesulfonate
c_L	total lipid concentration
CMC	critical micelle concentration
Da	Dalton
DAGK	diacylglycerol kinase
DHPC	1,2-dihexanoyl-sn-glycero-3-phosphocholine
DMPC	1,2-dimyristoyl-sn-glycero-3-phosphocholine
DMSO	dimethyl sulfoxide
ε280	extinction coefficient at 280 nm
ECD	extracellular binding domain
E. coli	*Escherichia coli*
EDTA	ethylenediaminetetraacetic acid
EGF	epidermal growth factor
EGFR	epidermal growth factor receptor
EM	electron microscopy
ErbB	v-erb-a erythroblastic leukemia viral oncogene homolog
ERK	extracellular regulated kinase
FCS	fetal calf serum
FPLC	fast protein liquid chromatography
GAP	GTPase-activating protein
GDP	guanosine-diphosphate
GEF	guanine-nucleotide exchange factor
GEP	guanine exchange protein
GPCR	G protein-coupled receptor
Grb2	growth factor receptor-bound protein 2
GTP	guanosine-5´-triphosphate
h	hour

HB-EGF	heparin-binding EGF-like growth factor
HDL	high density lipoprotein
HER	human epidermal growth factor receptor
His-tag	polyhistidine-tag
HPLC	high pressure liquid chromatography
ICAM-1	intercellular adhesion molecule 1
i.e.	*id est*
IEX	ion exchange chromatography
IGF1	insulin-like growth factor 1
IFI	inducible feedback inhibitor
IP3	inositol-1,4,5-triphosphate
IPTG	isopropyl β-D-1-thiogalactopyranoside
IR	insulin receptor
IUPAC	international union of pure and applied chemistry
JM	juxtamembrane
Kd	dissociation constant
L	liter
Lac	lac operon
LB	Luria Bertani
LUT	look up table
Lz	leucine zipper
M	molar
min	minute
MAP	mitogen activated protein
MAPK	mitogen activated protein kinase
MEK	mitogen activated protein kinase kinase
MSP1	membrane scaffold protein 1
MSP1D1	membrane scaffold protein 1 deleted 1
MST	microscale thermophoresis
mTOR	mammalian target of rapamycin
MuSK	muscle-specific kinase
MW	molecular weight
Ni-NTA	nickel-nitrilotriacetic acid
NMR	nuclear magnetic resonance
NRG	neuregulin
OD_{600}	optical density at 600 nm
o/n	overnight
PAGE	polyacrylamide gel electrophoresis
PBR	polybasic region
PC	phosphatidylcholine
PCC	Pearson correlation coefficient
PDGF	platelet-derived growth factor

PDGFR	platelet-derived growth factor receptor
PE	phosphatidylethanolamine
PFA	paraformaldehyde
PH	pleckstrin homology
pI	isoelectric point
PI	phosphatidylinositol
PI3-K	phosphoinositide 3-kinase
PIP_2	phosphatidylinositol-4,5-bisphosphate
PIP_3	phosphatidylinositol-3,4,5-triphosphate
PKC	protein kinase C
PLCγ	phospholipase C γ
PS	phosphatidylserine
PSI	pound-force per square inch
PTB	phosphotyrosine-binding
Raf	rapidly accelerated fibrosarcoma
Ras	rat sarcoma GTPase
Rho	ras like GTPase
RNA	ribonucleic acid
ROI	region of interest
RSD	relative standard deviation
RTK	receptor tyrosine kinase
SDS	sodiumdodecylesulfate
sec	seconds
Secin	Sec7 inhibitor
SH2	src homology 2
SH3	src homology 3
SNARE	soluble N-ethylmaleimide-sensitive-factor attachment receptor
SOCS	suppressor of cytokine signaling
SOS	son of sevenless
STAT	signal transducer and activation of transcription
Strep	steptavidin
TEMED	N,N,N´,N´-Tetramethylethylendiamid
TEV	tobacco etch virus
TGF-α	trasforming growth factor α
TKD	tyrosine kinase domain
TM	transmembrane
tRNA	transfer RNA
UV	ultraviolet
v/v	volume per volume
w/v	weight per weight
w/w	weight per weight

Zusammenfassung

Transmembranproteine machen 25% des Proteoms aus und sind verantwortlich für wichtige biologische Funktionen wie dem Transport von Molekülen, der Signaltransduktion und der Katalyse. Aufgrund dessen sind Transmembranproteine häufige pharmakologische Ziele und das Verständnis ihrer Aktivierungsmechanismen und Interaktionspartner ist eine der wichtigsten Aufgaben der pharmazeutischen und biochemischen Forschung. Als Forschungsobjekte stellen Transmembranproteine eine besondere Herausforderung dar, da sie in wässriger Lösung instabil sind und zur Aggregation neigen, sobald sie von der Plasmamembran getrennt werden.

Artifizielle membranähnliche Systeme erlauben es, die Strukturen der unterschiedlichen Membranproteine und deren Interaktionen mit der Membran oder mit anderen Proteinen zu analysieren. In dieser Doktorarbeit wurden mehrere Membranmodelle verwendet, um die Aktivierung und Regulierung des EGFR (engl: *Epidermal Growth Factor Receptor*) durch intrazellulare Faktoren, insbesondere Cytohesin-2 (auch: ARNO, engl.: *Arf nucleotide binding site opener*), zu erforschen. Der EGFR kontrolliert unterschiedliche Zellfunktionen und verstärkte Aktivität kann zur Entwicklung von Krebs führen. ARNO ist ein Guaninnukleotid-Austauschfaktor für Arf (ADP-Ribosylierungsfaktor) GTPasen. ARNO besitzt, neben der katalytisch aktiven Sec7-Domäne, ein PH-Modul (Pleckstrin Homologie), welches mit anionische Lipiden auf der Plasmamembran interagieren kann. Durch die Benutzung von einem artifiziellen Membransystem, hier Nanodiscs, wurden die Bedingungen für die Interaktion zwischen ARNO und der Plasmamembran nachgestellt. Darüber hinaus wurden Nanodiscs als Plattform für die Untersuchung von niedermolekularen Inhibitoren der PH-Domäne, nämlich Cyplecksine (Cytohesin Pleckstrin Homologie Inhibitoren) verwendet. Es lässt sich schließen, dass Nanodiscs nicht nur geeignete Systeme sind, um Protein-Membran-Interaktionen zu untersuchen, sondern auch genutzt werden können, um niedermolekulare Inhibitoren zu testen.

Des Weiteren wurden EGFR-Interaktionen und die ARNO-abhängige EGFR-Aktivierung, die sich in einer Autophosphorylierung des Rezeptors widerspiegelt, zunächst in Mizellen und anschließend in komplexeren artifiziellen Systemen wie Bizellen, Nanodiscs und *Plasma Membrane Sheets* untersucht. Aus der Literatur ist bereits bekannt, dass ARNO die Phosphorylierung von EGFR in Zellsystemen und bei löslichen interzellularen Domänen des EGFR in membranfreien Experimenten verstärkt.

Zusammenfassung

Abhängig von dem Membransystem wurde eine schwache Interaktion zwischen der Sec7-Domäne von ARNO und dem JM (Juxtamembran) Segment des EGFR beobachtet. ARNO-abhängige EGFR-Stimulation wurde jedoch im Membransystem nicht festgestellt. Eine mögliche Erklärung hierfür ist, dass mehrere Kofaktoren für die Phosphorylierung und Aktivierung des EGFR notwendig sein können, die in vereinfachten Membransystemen nicht anwesend sind.

Dennoch wurde mit Hilfe von *Membrane Sheets* eine Kolokalisierung von ARNO und EGFR auf der Plasmamembran beobachtet, die einer Interaktion zwischen den beiden Proteinen entsprechen kann. Außerdem wurden auch Effekte von ARNO auf die EGFR-Cluster beobachtet. Durch die Verringerung des Ausmaßes der Cluster-Bildung könnte der intrazellulare Teil des Rezeptors für cytosolische Faktoren zugängig werden. Diese Erkenntnisse können den Weg für ein tieferes Verständnis von EGFR-Aktivierungsmechanismen durch ARNO bereiten.

I. Abstract

Transmembrane proteins are involved in important biological functions, such as in transport of molecules, and in signal transduction. They represent almost 25 % of the proteome and constitute important drug targets. The study of transmembrane proteins has been a major challenge for biochemical research over the past decades. Transmembrane proteins are unstable and prone to aggregation when examined apart from the plasma membrane. Artificial, yet native-like membrane systems have allowed for the identification of the structure and function of several transmembrane proteins. In this thesis, the analysis of different membrane-model systems to study a particular transmembrane protein, namely EGFR (epidermal growth factor receptor) is reported. Moreover, the interactions of EGFR with a cytosolic factor, i.e. ARNO (Arf nucleotide binding site opener), is analyzed. EGFR is involved in many cellular functions and alteration of its activity often leads to cancer development. ARNO acts as a GEF (guanine nucleotide exchange factor) for Arf (ADP ribosylation factor), due to its Sec7 domain. Furthermore, ARNO contains a PH (pleckstrin homology) domain, important for interactions with anionic lipids at the plasma membrane. By using nanodiscs, the conditions for the interaction between ARNO and anionic lipids in a membrane-like system were recreated. In addition, nanodiscs were used as a system to study a recently developed small-molecule inhibitor for the PH domain. Summarizing, nanodiscs were identified to be not only a suitable system to study protein-membrane interactions, but to be a viable *in vitro* system to study small-molecule compounds. Moreover, starting with receptor-micelles and proceeding to more complex artificial systems, such as bicelles, nanodiscs, and membrane sheets, ARNO-dependent EGFR phosphorylation and the interaction between the two proteins were evaluated. It has been previously reported that ARNO enhances EGFR phosphorylation in living cells, as well as the phosphorylation of the soluble intracellular domain of EGFR in membrane-free experiments. Depending on the membrane system, weak interactions between the Sec7 domain of ARNO and the JM (juxtamembrane) region of EGFR were observed. Nevertheless, ARNO-dependent EGFR activation was not observed in membrane-like systems. By using membrane sheets, the co-localization between ARNO and EGFR at the plasma membrane was detected. Furthermore, ARNO may have an effect on EGFR by decreasing receptor clustering and making EGFR more accessible for intracellular co-factors. These findings can open the way for a deeper understanding of the activation mechanisms of EGFR via ARNO.

II. Introduction

II.1 The plasma membrane - an overview

The plasma membrane is a biological barrier that controls which substances can enter cells. The major constituent of the eukaryotic plasma membrane are phospholipids. The other components are sphingolipids and cholesterol (Simons, Sampaio 2011). Phospholipids are composed of two hydrophobic fatty acid chains and one polar head group (O'Connor, Adams 2010). The fatty acids can have different lengths, normally ranging between 14 to 24 carbon atoms. The fatty acid chains are arranged in a back-to-back bilayer, minimizing their contact with the aqueous environment. Meanwhile, the hydrophilic head group faces towards the external part and the cytoplasmic side of the cell (Alberts et al. 2002). The phospholipid bilayer is largely stabilized by the cholesterol, which makes up ~30 % of the membrane.

The first model of the plasma membrane proposed by Singer and Nicolson in 1972 described the phospholipid bilayer as a fluid mosaic in which proteins are randomly distributed into the membrane (Singer, Nicolson 1972). In their fluid mosaic model, Singer and Nicolson distinguished between two different types of membrane proteins: peripheral membrane proteins and integral membrane proteins (or transmembrane proteins). Peripheral proteins are only weakly associated with the membrane, and their interaction can be modulated by changing the pH or ionic strength. On the other hand, transmembrane proteins span through the phospholipid bilayer, meaning they can be removed using strong conditions, such as detergents.

The model proposed by Singer and Nicolson in 1972 has been refined during the years (Goñi 2014). Recent biochemical and biophysical research has focused on the role of protein-lipid and protein-protein interaction at the cell membrane (Krause, Regen 2014).

Negatively charged phospholipids, like PS (phosphatidylserine) and PI (phosphatidylinositol), are present in the inner leaflet of the plasma membrane. Between 20-25 % of all negatively charged lipids are PS, making them the most abundant negatively charged lipids at the plasma membrane (Leventis, Grinstein 2010). In contrast, PIs are relatively rare and can be phosphorylated at the positions of 3, 4 and/or 5, forming PIP_ns (phosphatidylinositol polyphosphates) (Lemmon 2008). The amount of PIP_2

(phosphatidylinositol-4,5-bisphosphate) at the plasma membrane is estimated to be between 0.5-1 % of all negatively charged lipids (Li et al. 2014).

While PIP_2 has many different functions, it can be broken into two main roles: it regulates the organization of transmembrane proteins, such as EGFR (epidermal growth factor receptor), and the recruitment of membrane proteins to the plasma membrane. As recently published by Wang et al. (2014), EGFR is organized in cluster at the plasma membrane, due to the ionic interaction between PIP_2 and a particular domain of the receptor. The formation of EGFR clusters is implicated in the receptor activation and signaling. Furthermore, peripheral proteins can be recruited at the plasma membrane due to lipid-protein interactions. Specific protein domains are responsible for the binding to the plasma membrane, or with particular phospholipid groups in the membrane (Lemmon 2008). One such example is the PH (pleckstrin homology) domain. The PH domain, as described in Section II.4.1.1, was first identified as a ~100 amino acids sequence presents twice in pleckstrin, the major substrate of PKC (protein kinase C) in platelets (Imaoka, Lynham, Haslam 1983). The PH domain is responsible for the interaction with anionic lipids, such as PIP_2 and PIP_3 (phosphatidylinositol-3,4,5-triphosphate) at the plasma membrane. In the past years, the classes of proteins containing a PH domain has been extremely enlarged (Lemmon, Ferguson 2000).

As previously mentioned, the plasma membrane is also an important site of protein-protein interaction. One example is provided by the Ras (rat sarcoma) superfamily of small GTPases, which is composed of several subfamily like Ras family, the Rho (Ras homolog gene) family and the Arf (ADP Ribosylation Factor) family (Wennerberg et al. 2005). The activity of the Ras superfamily is regulated via GEFs (guanine nucleotide exchange factors) and GAPs (GTPase-activating proteins). GEFs and GAPs allow GTP loading and hydrolysis, respectively (Di Paolo, De Camilli 2006). The Ras superfamily switches between a GDP-inactive to a GTP-active conformation. In turn, this process is made possible by the recruitment of GEFs and GAPs to the plasma membrane by the interaction with PIP_ns. One example of a class of GEFs is cytohesins. Cytohesins interact with PIP_2 or PIP_3 at the plasma membrane (Kolanus 2007). A detailed description of cytohesins can be found below in Section II.4.1.

Transmembrane proteins are also key components of the plasma membrane. They regulate the traffic of substances from the extracellular to the intracellular space, are important for the activation of signaling cascades, and for the cellular homeostasis (Rigaud 2002). The three major classes of transmembrane proteins that are found at the

plasma membrane are: ion channels, G protein-coupled receptors (GPCRs) and receptor tyrosine kinases (RTKs). For the purpose of this thesis, only RTKs will be treated in Section II.3.1.

Following the model proposed by Singer and Nicolson, transmembrane proteins are considered to be "swimming" in a lipid sea and are not concentrated on particular spots on the membrane. This model was adapted across the years, to come to a more complete representation of the plasma membrane depicted by Engelman (2005). Engelman affirmed that "membranes are more like a mosaic then a fluid" due to the presence of organized transmembrane protein patches. Furthermore, there is additional evidence that lipids at the plasma membrane are organized into microdomains, termed lipid rafts (Simons, Vaz 2004). Lipid rafts consist of sphingolipids and cholesterol groups that can be used as a platform for membrane proteins clustering. In the model of Simons and Vaz (2004), the sphingolipids associate laterally and any void spaces remaining are filled by cholesterol that functions as a spacer. Sphingolipid–cholesterol rafts are insoluble in the detergent Triton X-100 and they partition into a low density layer during gradient centrifugation (Simons, Ikonen 1997). Moreover, lipid rafts can recruit specific proteins: for example, it is reported that SNAREs (soluble N-ethylmaleimide-sensitive-factor attachment receptor) are not homogeneously distributed on the plasma membrane, but they are concentrated in ~100 nm cholesterol-dependent microdomains. The depletion of cholesterol causes the destruction of SNAREs clusters (Lang 2003). The formation of protein clusters can therefore be induced by lipid-lipid interactions, and lipid-protein interaction and second messengers, such as calcium (Zilly et al. 2011).

II.2 Membrane-model systems

The extreme complexity of the plasma membrane leads to the necessity of developing of membrane-model systems. Membrane surrogates provide a useful tool for studying lipid-protein and protein-interaction in a native-like environment. To overcome the complexity of biological membranes, different membrane-model systems have been developed. Several parameters have to been taken into consideration to select an accurate artificial system. For example, the architecture of the membrane system and the lipid composition depend on the type of protein or on the biological question that are analyzed. Furthermore, there are several obstacles during the purification of transmembrane proteins, e.g. solubility, precipitation and inactivity once proteins are extracted from the

membrane. Membrane-model system can be used to stabilize transmembrane proteins, once they are extracted from the natural environment, and to study their structure and function. In the following sub-sections, several membrane-model systems are described, highlighting their advantages and disadvantages, and pointing out some of their possible applications.

II.2.1 Micelles

Detergents are the most commonly used agents to solubilize membrane proteins. Detergents form micelles in aqueous solutions. Figure 1 illustrates the micelle structure. Micelles are defined according to the IUPAC (international union of pure and applied chemistry) terminology (Nic et al. 2009) as a "particle of colloidal dimensions that exists in equilibrium with the molecules or ions in solution from which it is formed". During the formation of micelles in aqueous solution, the hydrophobic tails of the detergent tend to orient themselves away from the water, forming the core of the micelle. This re-orientation also has the effect of pointing the hydrophilic heads of the detergent towards the water solvent. There are several parameters that influence the formation of micelles, such as pH, temperature, and ionic strength (Tanford 1974). The CMC (critical micelle concentration) is the concentration of detergent above which micelles are formed. Above the CMC, micelles and monodispersed molecules co-exist in a dynamic equilibrium (Domingues et al. 1997). The hydrophobic core of the micelles interacts with the hydrophobic region of the protein and forms a soluble detergent-protein complex (Garavito, Ferguson-Miller 2001).

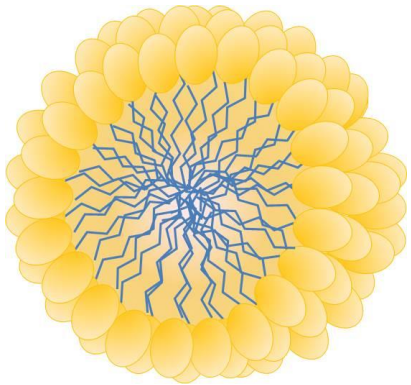

Figure 1: Micelle structure

The hydrophobic tails (blue) form the core of micelle, while the hydrophilic head groups (yellow) are in contact with the surrounding solvent.

Detergents are often the first choice solution to extract proteins from the lipid environment for further biophysical and biological studies (Arnold, Linke 2008).

Since micelles are an extremely simple membrane system, they also have limitations. First, micelles are not bilayers as opposed to the plasma membrane, and second, certain detergents used for the formation of micelles can disrupt lipid-lipid or protein-lipid interactions, which are important to conserve the structure of proteins. The choice of the detergent to stabilize the membrane protein must be determined empirically on a case-by-case basis, and thus can be a time-consuming process. For these reasons, other membrane-like systems were considered.

II.2.2 Bicelles

Bicelles are a phospholipid bilayer formed from short- and long-chain phospholipids, typically 1,2-dihexanoyl-sn-glycero-3-phosphocholine (DHPC) and 1,2-dimyristoyl-sn-glycero-3-phosphocholine (DMPC), respectively. The structure of bicelles is depicted in Figure 2. The ground work for the study of bicelles was established by Sanders and Prestegard (1990) when they investigated the formation of phospholipid bilayer formed by DMPC and detergent, typically CHAPSO. The first investigation on the structure of bicelles was performed by Sanders, Landis (1995). The central part of the bicelle is formed by long-chain phospholipids, while the edges of the rim of the bicelle are protected by short-chain phospholipids.

Several parameters affect the structure and formation of bicelles. One such parameter is the ratio between the long- and short-chain phospholipids, typically denoted by the parameter "q". Another common parameter is the total lipid concentration (c_L). For q ratios roughly >3, bicelles are big aggregates that can be oriented by a magnetic field. For this reason, they are often used for solid-state NMR (nuclear magnetic resonance) to study the structure of phospholipid bilayers and membrane proteins (Prosser et al. 2006). In contrast, when the q ratio is small (q<1), the bicelles are small and cannot be aligned with the magnetic field. In this situation, they are termed isotropic bicelles and they were often used for high-resolution NMR (Whiles et al. 2002). Furthermore, Glover et al. (2001) showed that bicelles at low q ratio are stable in a wide range of temperatures. However, they also showed that if $c_L \leq 1$ % w/w, the short-chain lipids dissociate from the bicelles (Glover et al. 2001).

Bicelles are used to study proteins interacting with the membrane or for the reconstitution of transmembrane proteins. Several proteins were successfully studied and reconstituted in bicelles, such as Arf1 (Liu et al. 2010) and GPCR (Serebryany et al. 2012).

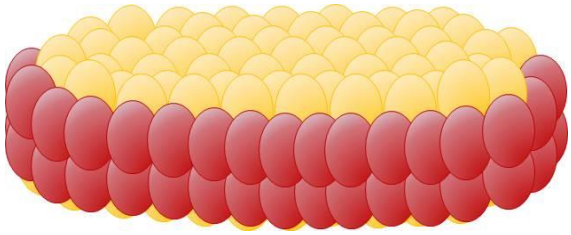

Figure 2: Bicelle structure

The long chain phospholipids (yellow) form the lipid bilayer, while the short chain lipids (red) surround the central part, protecting the hydrophobic chains from the surrounding solvent. The hydrophobic tails all point towards the inside of the bicelles.

Different protocols are available for the reconstitution of transmembrane proteins (Avanti Polar Lipids Website a). One such example, transmembrane proteins can be lyophilized and mixed with a phospholipid powder. Upon rehydration, bicelles containing the transmembrane protein are spontaneously formed. However, this procedure only works if the proteins are highly resistant and highly stable. Moreover, if proteins are soluble without detergents, they can be simply added to pre-formed bicelles for the reconstitution into the bilayer. Other approaches require the presence of pre-formed lipid vesicles. Upon the addition of protein and a detergent, the vesicles are disrupted and the bicelles containing the desired proteins are formed. Nevertheless, this requires a careful detergent titration and furthermore, the determination of the q ratio can be challenging, since some phospholipids can be difficult to solubilize.

Bicelles present two major advantages compared to micelles: 1) bicelles resemble the structure of biological membranes, since they present a bilayer structure; 2) The presence of lipids and not only detergent creates a more native-like environment for the reconstitution of transmembrane proteins (Lu et al. 2012). Furthermore, recent studies showed that the composition of the bicelles can be modified with negatively charged phospholipids, allowing for the study of important protein-membrane interactions (Struppe et al. 2000).

Other studies have shown that the structure of proteins inserted into micelles is significantly different than the structure of proteins inserted into bicelles. For example, Sanders and Landis (1995) showed that the enzyme DAGK (diacylglycerol kinase) is

active only in bicelles, while no activity was detected in micelles. Dürr et al. (2012) reported a list of proteins that conserved their activity and/or structure in bicelles, but where important protein features were lost in micelles. The same properties were recently collected by Mineev et al. (2015) for the transmembrane region and juxtamembrane region of EGFR.

All these facts show that bicelles present a good membrane model system for the reconstitution of transmembrane proteins. Nevertheless, bicelles require careful titration, and the insertion of the proteins can be challenging and time-consuming.

II.2.3 Nanodiscs

Nanodiscs are another membrane model system suitable for the study of membrane proteins and their interactions with the phospholipid bilayer. Bayburt and Sligar (2003) were the first to identify the self-assembly properties of lipid mixtures into a disc-shaped bilayer when incubated with a modified form of the human Apo A-1 (Apolipoprotein A-1). Apo A-1 is composed of 243 amino acid residues, and contains an N-terminal domain of 44 amino acid residues, as well as a C-terminal lipid binding domain formed mainly of by α-helices.

Apo A-1 is the major component of the HDL (high density lipoprotein) and it constitutes almost 70 % of HDL total mass (Brouillette et al. 2001). Apo A-1 is involved in the reverse transport of the cholesterol from peripheral tissue to the liver. Apo A-1 has been studied for its ability to bind free lipids in the serum and to form nascent discoidal HDL (Nath et al. 2007). Bayburt and Sligar (2003) have produced a mutated form of the Apo A-1, without its N-terminal globular domain, not required for lipid binding. This mutated form of Apo A-1 is named MSP1 (membrane scaffold protein 1). Two membrane scaffold proteins surround the edges of the disc bilayer in a head-to-tail conformation. Figure 3 shows the structures of nanodisc.

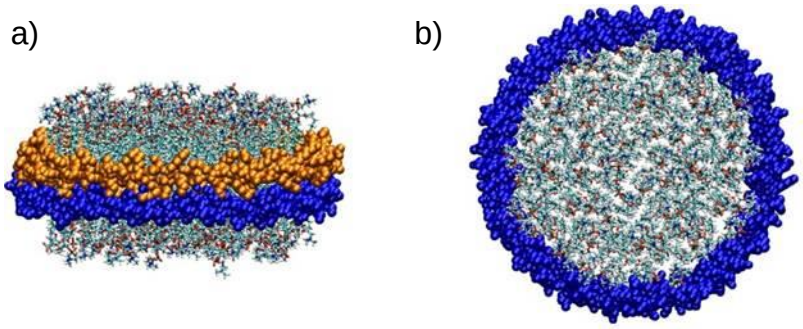

Figure 3: Nanodisc structure

a) Side view of nanodiscs formed by two membrane scaffold proteins (in orange and in blue). **b)** Top view of nanodiscs. Figure taken from Bayburt, Sligar (2010).

The diameter of nanodiscs is regulated by the length of the scaffold protein. Different membrane scaffold proteins are available to generate nanodiscs of variable sizes. Typically nanodiscs contain around 150 phospholipid molecules and have a diameter between 10 and 16 nm, depending on the type of MSP used. For example, the MSP1D1 (membrane scaffold protein 1 deleted 1) contains an N-terminal deletion of 11 amino acid residues and it is used to produce nanodiscs with a diameter of 10 nm. Furthermore, the thickness of the nanodiscs ranges between 4.5 and 5.5 nm, depending on the length of the fatty acid chain of the phospholipids used (Denisov et al. 2004).

Nanodiscs can self-assemble starting from a detergent, phospholipids and scaffold protein mixture. Once the detergent is removed with hydrophobic beads or by dialysis, the nanodiscs are formed. The ratio between MSP and phospholipids is critical for proper nanodiscs formation: an excess of phospholipids causes the formation of aggregates. If on the other hand, the amount of lipids is too low, MSP can form unstable lipid-poor structures (Bayburt, Sligar 2010).

Nanodiscs were used to reconstitute a lot of different transmembrane proteins, such as bacteriorhodopsin, cytochrome P450 and some GPCRs. For the insertion of transmembrane proteins into nanodiscs an important parameter is the ratio between the concentration of scaffold protein and the transmembrane proteins. Once the ratio is established, depending on the type of detergent used for the solubilization of the transmembrane protein, the amount of the hydrophobic beads should also be titrated.

Since nanodiscs are suitable for the reconstitution of transmembrane proteins, they are commonly used for NMR study to determine protein structures (Glück et al. 2009). Another of the advantages of using nanodiscs is that their lipid composition can be

variated. One such example, the insertion of anionic lipids into nanodiscs is useful to study the membrane recruitment of proteins containing PH modules.

Nanodiscs are stable for weeks, and became recently commercially available, avoiding the tedious protein purification procedures. Nanodiscs are commonly used for NMR (Hagn et al. 2013), cryo EM (electron microscopy) (Pandit et al. 2011) and SPR (surface plasmon resonance) (Glück et al. 2011). For the preparation of nanodiscs, it is crucial to carefully establish the correct proportions of the membrane scaffold protein and phospholipids. Furthermore, also the insertion of the transmembrane protein into the disc bilayer required well defined settings. For example, if an excess of the transmembrane protein is added to the MSP-phospholipids solution, the protein can precipitate and forms aggregates. On the other hand, if a low protein amount is added, only a small part of the formed nanodiscs could contain the transmembrane protein.

II.2.4 Membrane sheets

The membrane models described above are completely artificial systems, in which the structure of the plasma membrane is rudimental maintained, but the composition and heterogeneity of the plasma membrane cannot be reached. Membrane sheets provide the right system to conserve not only the architecture of the membrane, but also its composition.

The preparation of membrane sheets begins by leaving the cells to adhere overnight onto a glass support coated with poly-lysine. Subsequently, adherent cells are immersed in an appropriate buffer and a single ultrasound pulse is used to “unroof” the cells. Through this pulse, only the basal membrane, attached secretory vesicles and some intracellular proteins interacting with the membrane remain attached to the cover slip (Lang 2003). The preparation of membrane sheets is described in Figure 4. Afterwards, the sheets are fixed with PFA (paraformaldehyde).

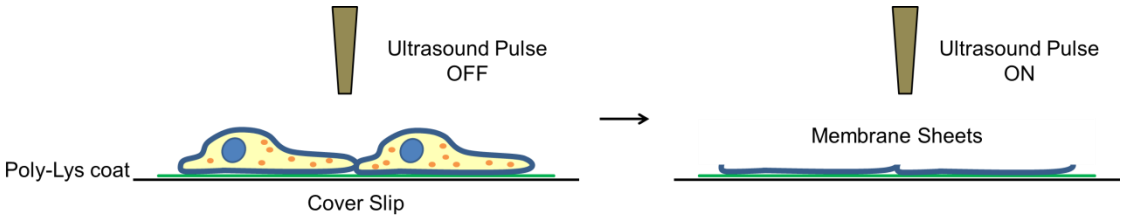

Figure 4: Schematic preparation of membrane sheets

Cells are adherent onto poly-lysine coated cover slips. An ultrasound pulse causes the cells to be "unroofed", leaving behind only the basal membrane, which remains attached to the glass support.

Membrane sheets can be used for direct membrane imaging usually with fluorescence or light microscopy, or further incubated with immunofluorescent antibodies. Membrane sheets are used in several applications and, in contrast to whole cell assay, allow exposing the intracellular membrane leaflet directly to reagents. They are often used for atomic force microscopy (AFM) and electron microscopy (EM), since a high protein density at the plasma membrane is necessary for these methods (Perez et al. 2006). Furthermore, plasma membrane sheets were recently used to monitor endocytosis (Wu et al. 2010) and in modulation studies of ion channels (Tsuboi et al. 2004). Yet another particularly interesting application of membrane sheets is their use in protein clustering (Lang 2001).

Since membrane sheets are tightly attached to the cover slip via their basal membrane, the use of antibodies against the extracellular part of membrane proteins can be difficult. Membrane sheets must be used directly after preparation. The plasma membrane sheets conserve their structure for only ~1 hour after preparation, otherwise degradation processes are initiated.

II.3 The epidermal growth factor receptor (EGFR)

II.3.1 Receptor Tyrosine Kinases (RTKs)

As mentioned above, RTKs are one of the major classes of transmembrane proteins present at the plasma membrane. RTKs are a crucial regulator of different cellular functions, such as cellular growth, differentiation and survival. Transmembrane receptors receive extracellular stimuli and transmit these signals to different intracellular pathways. The function of RTKs is to transfer a γ-phosphate of the adenosine-5´-triphosphate (ATP) to hydroxyl groups of tyrosine residues on target proteins (Hunter 1998). RTKs are normally present as monomer on the cell surface in the inactive state. The IR (insulin receptor) and IGF1 (insulin-like growth factor 1) receptor are exceptions because they exist as a disulfide linked dimer at the cell surface. IR is a member of the RTKs family involved in the regulation of glucose homeostasis (Taniguchi et al. 2006). It is present as $\alpha_2\beta_2$ heterotetramer at the cell membrane (Hubbard 2013).

EGFR also represents a peculiar case: recent studies showed that the receptor can be present as inactive dimer at the cell surface (Clayton 2005; Whitson et al. 2004).

Humans have 58 known RTKs, which can be further grouped into 20 subfamilies, based on their primary structure (Figure 5). RTKs are composed of an extracellular domain (ECD), which is important for the ligand binding, a single α-helix transmembrane (TM) domain and an intracellular component. The intracellular section can be further divided into a kinase core, a C-terminal tail containing phosphorylatable tyrosine residues, and a regulatory juxtamembrane (JM) region (Lemmon, Schlessinger 2010).

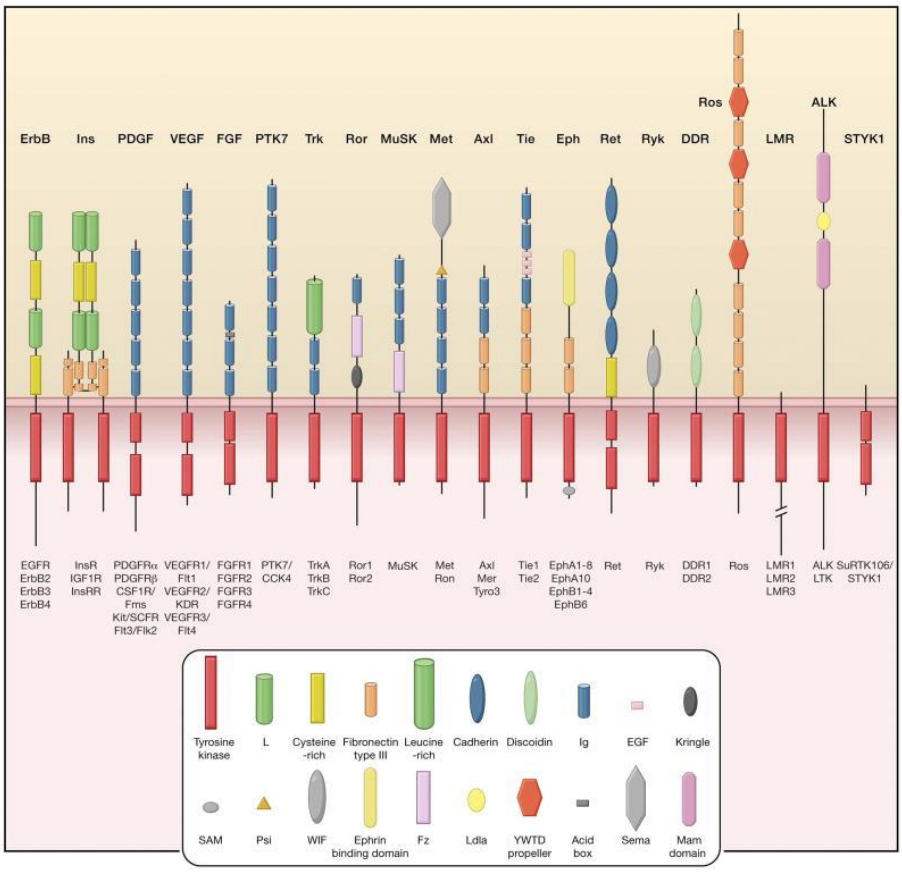

Figure 5: The 20 members of the human RTKs families

Humans known RTKs are divided into 20 families. The different domains are listed in the legend. The family names are indicated with bold letters. ErbB: Named from the viral oncogene v-erb-B, an avian erythroblastosis virus. Ins: Insulin receptor family. PDGF: Platelet-derived growth factor receptor family. VEGF: Vascular endothelial growth factor receptor family. FGF: Fibroblast growth factor receptor family. PTK: Protein tyrosine kinase receptor family. Trk: Tropomyosin receptor kinase family. Ror: Receptor orphan family. MuSK: Muscle-specific kinase family. Met: Hepatocyte growth factor receptor family. Axl: A Tyro3 protein tyrosine kinase receptor family. Tie: Tyrosine kinase receptor family in endothelial cells. Eph: Ephrin receptor family. Ret: Rearranged during transfection receptor. Ryk: Receptor related to tyrosine kinases. DDR: Discoidal domain receptor family. Ros: Proto-oncogene tyrosine-protein kinase family. LMR: Lemur receptor family. ALK: Anaplastic lymphoma kinase receptor family. STYK1: Serine/threonine/tyrosine kinase 1 family. This figure is taken from Lemmon and Schlessinger (2010); The figure caption is adapted from Blume-Jensen and Hunter (2001).

For the activation of RTKs, an extracellular ligand binds to the extracellular part of the receptor. Upon the ligand binding, the oligomerization and conformational rearrangements of the extracellular domain take place. Subsequently, the intracellular domains dimerize. In this way, the receptor can phosphorylate several tyrosine residues that act as docking sites for intracellular proteins.

II.3.2 The EGFR and the ErbB family

The EGFR/ErbB1 receptor is a 170 kDa transmembrane protein belonging to the ErbB family of RTKs. The ErbB family is comprised of three other members, namely Her2/ErbB2, Her3/ErbB3, and Her4/ErbB4 receptors (Olayioye 2000). The EGFR and the ErbB family present a homology in the domains division comparable to the other RTKs.

In particular EGFR has a glycosylated ECD of 620 amino acid residues, a TM region with a single α-helix, a JM domain, a large tyrosine kinase domain (TKD) followed by a C-terminal tail containing 5 phosphorylation sites (Lemmon et al. 2014). The ECD can be further divided into 4 subdomains (I, II, III and IV). Details are provided in Section II.3.3.

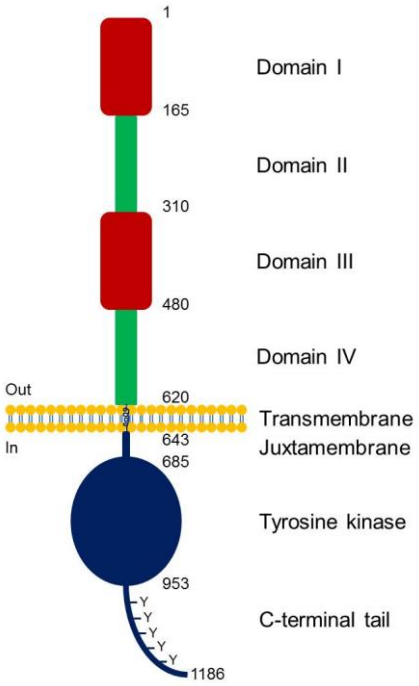

Figure 6: Domains organization of EGFR

The extracellular region (1-620) contains four domains: domain I (1-165), domain II (165-310), domain III (310-480) and domain IV (480-620). The transmembrane region is connecting the extracellular domain with the intracellular part. The juxtamembrane region (643-685) separates the tyrosine kinase domain from the membrane. The C-terminal tail contains five phosphorylation sites. This figure is adapted from Lemmon et al. (2014).

The ErbB family regulates important cellular functions, such as cell growth, proliferation, survival, and differentiation. Aberrant function of EGFR is a hallmark of different human cancers, such as breast cancer, non-small cell lung cancer and colorectal cancer (Johnston et al. 2006).

ErbB receptor family has different ligands that can interact with the ECD and can activate different intracellular pathways. An exception is Her2, since no specific ligand has yet been identified and it forms heterodimers with other members of the ErbB family (Yarden 2001). Several ligands are known for ErbB family members. For example, epidermal growth factor (EGF), transforming growth factor α (TGF-α), and amphiregulin bind exclusively to EGFR, while the heparin-binding EGF-like growth factor (HB-EGF), epiregulin and betacellulin can bind also to Her4. Neuregulins are produced from four different genes and can bind to Her3 as well as Her4 (Fuller et al. 2008). Upon ligand binding, the dimerization of the receptor monomer on the plasma membrane takes place. EGFR can dimerize with another EGFR monomer, forming a homodimer, or it can dimerize with other members of the ErbB family, forming heterodimers (Figure 7). Her3 has impaired kinase activity, and it can only form heterodimers to be activated (Berger et al. 2004).

The phosphorylated tyrosine residues on the C-terminal tail, serve as binding sites for intracellular proteins containing Src homology 2 (SH2) domain and phosphotyrosine-binding (PTB) domain (Schlessinger, Lemmon 2003). The two major downstream signaling pathways activated by ErbB receptors are MAPK (mitogen-activated protein kinase) and PKB (protein kinase B), also known as Akt, pathways (Mendelsohn, Baselga 2000). MAP kinase signaling starts upon that Grb2 (growth factor receptor-bound protein 2) binds to the phosphorylated receptor via its SH2 domain. Subsequently, the protein SOS (son of sevenless), a guanine nucleotide exchange factor, docks to Grb2 via a SH3 domain. Active SOS catalyzes the GDP-GTP exchange on Ras (rat sarcoma) protein. Ras can bind to Raf (rapidly accelerated fibrosarcoma), a serine-threonine protein kinase, then Raf can phosphorylate and activate MEK (mitogen-activated protein kinase kinase). MEK can then activate the MAP kinase downstream signaling. MAPK cascade is an important regulator of gene transcription and cell proliferation (Haley, Gullick 2009).

The second classical pathway activated by ErbB receptors is PI3K (phosphatidylinositol-4,5-bisphosphate 3-kinase)/Akt signaling. PI3K, once activated, starts to catalyze the conversion of PIP_2 to PIP_3. The second messenger PIP_3 can interact with the PH domain of Akt at the plasma membrane. The protein Akt can then indirectly phosphorylate the protein mTOR (mammalian target of rapamycin), which is important for the activation of survival stimuli (Cantley 2002; Haley, Gullick 2009).

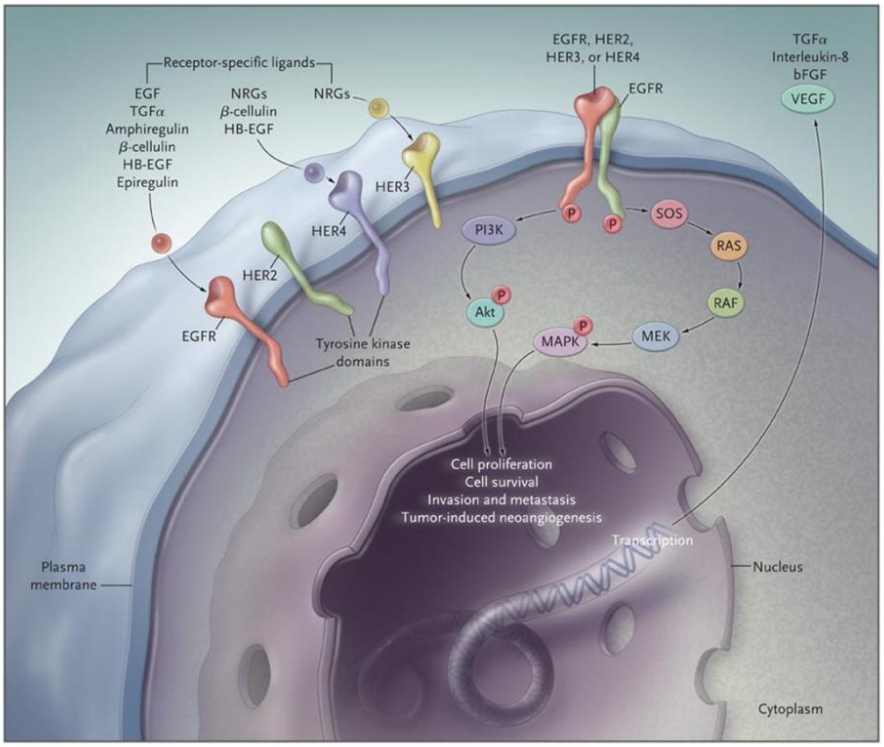

Figure 7: ErbB homo- or hetero-dimerization at the plasma membrane and activation of different intracellular cascades

Upon ligand binding, receptors of the ErbB family dimerize, forming homodimers (for example EGFR-EGFR) or heterodimers (EGFR-Her2/ EGFR-Her3/ EGFR-Her4). The dimerize receptors are then phosphorylated and can activate different signal cascades. The major signal pathways activated are the RAS–RAF–MEK–MAPK pathway, which controls gene transcription, cell-cycle progression and the PI3K-Akt cascade that regulates the production of anti-apoptotic and pro-survival signals. Reproduced with permission from Ciardiello and Tortora (2008), Copyright Massachusetts Medical Society.

II.3.3 The EGFR activation mechanism

II.3.3.1 The ligand binding induces a conformational rearrangement of the extracellular domain

The extracellular domain of the EGFR is responsible for ligand binding. Two ligand molecules bind to two different receptor monomers leading to receptor dimerization. Crystallographic structures have clarify the structure of the EGFR extracellular domain upon ligand binding (Garrett et al. 2002; Ogiso et al. 2002). EGFR extracellular domain can be divided in four subdomains: I, II, III and IV. The domains I and III contain leucine rich regions, while domains II and IV contain disulfide-bound modules (Burgess et al. 2003). One ligand molecule simultaneously contacts domain I and III. The activation is driven by a "dimerization arm" that is protruding from domain II

and induces a dramatic conformational change that leads to the dimer formation. In the absence of the ligand, the dimerization arm is hidden, contacting domain IV in an auto-inhibited or tethered conformation (Figure 8a). Ligand binding disrupts the auto-inhibited structure and exposes the dimerization arm resulting in the extended conformation (Figure 8b) (Ferguson et al. 2003; Ferguson 2008). Domain IV plays a minor role in the stabilization of the ligand binding (Dawson et al. 2005). The dimerization interface between two receptor monomers presents a back-to-back conformation, due to the extended contact of domains II (Figure 8c).

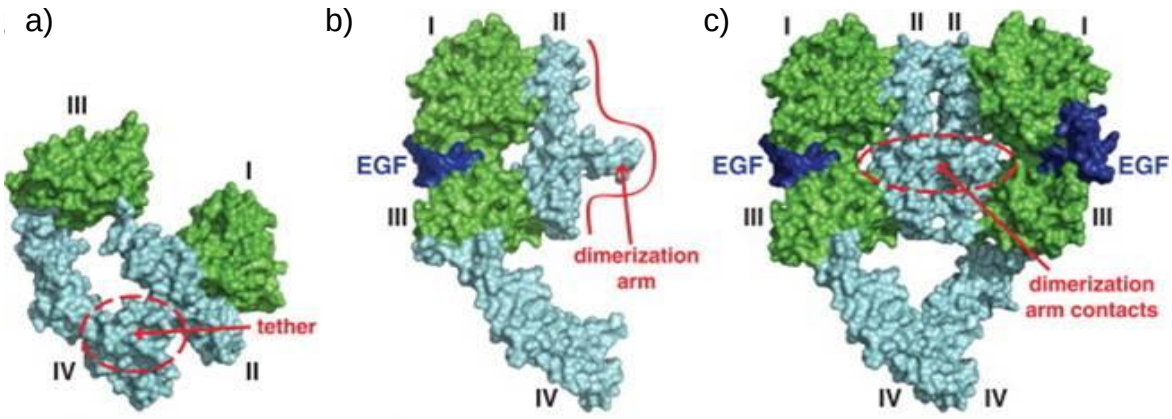

Figure 8: Structure of the human EGFR extracellular domain before and after ligand binding

a) Tether conformation upon EGF binding (PDB 1NQL). Domains I and III are green, while domains II and IV are blue. **b)** Model for the monomeric extended conformation upon EGF binding (PDB 3NJP). The ligand contacts domains I and III. The dimerization arm is now exposed. **c)** The structure for the 2:2 (EGF:EGFR) back-to-back dimer (PDB 3NJP). The dimerization arm contact is circled in red. This figure is taken from Bessman et al. (2014).

II.3.3.2 The activation of the kinase domain requires the formation of the asymmetric dimer

The ligand binding and dimerization of the extracellular domain also lead to the dimerization of the kinase domain. The kinase domain is composed of a small N-lobe and a larger C-lobe. Between the N- and C-lobe there is an important regulatory element, namely the activation-loop. The phosphorylation of one or several tyrosine residues in the activation loop is critical for the activation of several RTKs, such as IR (insulin receptor) (Bose, Zhang 2009). EGFR represents a peculiar case, because the phosphorylation of the activation-loop is not necessary for the activation of the kinase domain (Gotoh et al. 1992). Zhang et al. (2006) were the first to understand that for complete activation, the

formation of an asymmetric dimer is necessary. In the asymmetric dimer, the C-lobe of one kinase domain (activator) contacts the N-lobe of the other kinase domain (receiver) (Figure 9). The formation of the asymmetric dimer for EGFR is similar to that of a cyclin bound to a cyclin-dependent protein kinase (Jura et al. 2009a; Zhang et al 2006). The N-lobe contains five β-strands and one αC-helix that is important for the receptor regulation, while the C-lobe is mostly formed by α-helices (Roskoski 2014; Stamos et al. 2002). ATP binds between the β1- and β2 strands of the N-lobe to a conserved GxGxxG (G: glycine; x: variable amino acid residues) ATP-phosphate binding loop, which is referred to as a P-loop. The P-loop is important in positioning the β- and γ-phosphate of ATP for catalysis (Roskoski 2014).

A conserved glutamate residue in the αC is fundamental for the formation of a salt bridge with a lysine residue in the β3-strand, as well as for the formation of the active conformation (Roskoski 2014). Furthermore, a conserved DFG (D: aspartic acid; F: phenylalanine; G: glycine) motif is present at the N-terminal part of the activation loop. An aspartic acid residue coordinates one magnesium ion, which is important for ATP binding (Jura et al. 2011). The JM region located subsequently to the TM domain helps to keep the kinase domains in the asymmetric conformation (Jura et al. 2009a). The detailed role of the JM domain is discussed in Section II.3.3.3. A general activation mechanism is described in Figure 10.

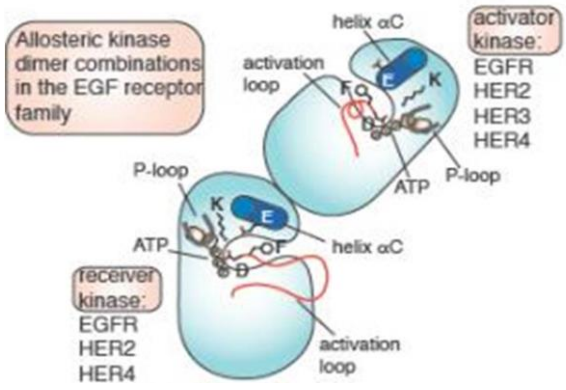

Figure 9: Asymmetric dimer formation

The kinase domain of the ErbB family forms an asymmetric dimer in the active state. The monomer, which is called the activator, contacts the N-lobe of the second monomer (i.e. the labelled receiver) with its C-lobe. Her3 presents only low kinase activity and for this reason its kinase domain cannot function as receiver (Jura et al. 2009b). The αC-helix, activation loop and ATP binding pocket are represented schematically. This figure is taken from Jura et al. (2011).

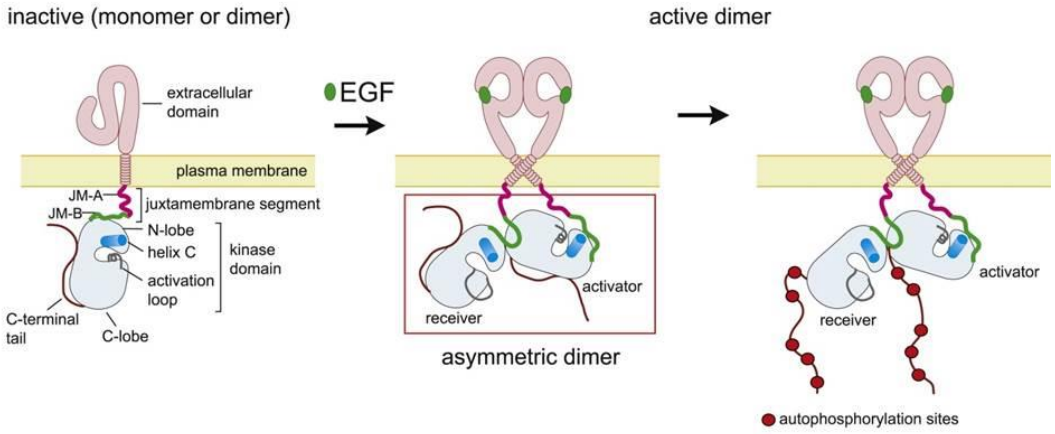

Figure 10: Schematic activation model for EGFR

In the left panel, the receptor is present at the membrane as a monomer or an inactive dimer (middle panel). EGF binding leads to receptor dimerization and formation of the asymmetric dimer (right panel). As a result, the phosphorylation of the tyrosine residues takes place. This figure is taken from Jura et al. (2009a).

II.3.3.3 The role of the transmembrane and juxtamembrane regions in EGFR activation

The conformational change on the extracellular side of the receptor has to be transmitted to the intracellular side for the complete receptor activation. The exact mechanisms by which the signals are transduced from the ECD (extracellular domain) remain largely unknown. The transmembrane (TM) region is a hydrophobic segment made up of 23 amino acids that spans from residues 621 to 644 of the EGFR sequence, which connects the extra- and intracellular domains. Studies from Mendrola et al. (2002) have led to reconsideration of the role of the TM domain in the receptor dimerization. Mendrola et al. (2002) reported that the TM domain of the ErbB family can self-associate in the membrane due to GxxxG (G: glycine; x: not specific amino acid residue) dimerization-specific modules. The EGFR TM region contains two GxxxG motifs, one at the N-terminal and one at the C-terminal. These motifs are commonly used in transmembrane α-helices as dimerization surfaces (Russ, Engelman 2000). Furthermore, a mutation from valine to glutamic acid in position 645 of the TM region of the related ErbB2 receptor is sufficient to drive oncogenic transformation. This is probably due to a significant orientation change in the α-helix of the TM motif that enhances the activation of the receptor (Sharpe et al. 2000). It was also shown that the ECD and TM region of EGFR can dimerize with a 10^5-fold higher affinity than the single ECD in solution (Tanner, Kyte 1999). Arkhipov et al. (2013) and the related study of Endres et al. (2013)

published a NMR-model in which the N-terminal GxxxG motifs on the TM regions interact to help the dimer formation.

In addition, the JM region plays a key role for the regulation of EGFR. The JM domain spans residues 645-682 and it can be further divided in two parts: JM-A (645-663) and JM-B (664-682) (Jura et al. 2009a).

Normally, the JM of the other members of the RTK family has an auto-inhibitory function. For example, the JM of IR contains ~35 amino acids and three tyrosine (Tyr) residues (965, 972 and 984). Tyr965 is important for endocytosis, while the Tyr972 is a docking site for IRS (insulin receptor substrate) proteins. Mutations on these two tyrosine residues, however, do not affect receptor kinase activity. Tyr984 is not a phosphorylation site, but mutating it drastically increases the catalytically activity of the receptor. In the unphosphorylated state, the JM masks a part of the kinase domain which is important for ATP coordination (Hubbard 2004). Other auto-inhibitory mechanisms are described for Ephrin receptors, MuSK (Muscle-specific kinase) receptor and PDGF (Platelet-derived growth factor) receptor (Hubbard 2004).

For EGFR, the JM plays a crucial role for the activation. Thiel and Carpenter (2007) showed that the deletion of the JM domain causes the loss of phosphorylation on the intracellular domain. In particular, the JM-B segment forms a structure referred to as the "juxtamembrane latch". The juxtamembrane latch starts from the N-lobe of the receiver and has the effect of stabilizing the C-lobe of the activator in the asymmetric conformation.

The JM-A segment contains several basic amino acid residues. Jura et al. (2009a) showed that the JM-A segments on both kinase domains are necessary to form antiparallel α-helices, helping the dimerization and stabilization of the asymmetric dimer. Endres et al. (2013) and the related paper of Arkhipov et al. (2013) both propose that the TM and JM domains are also presented in an auto-inhibited conformation. As mentioned above, the TM region presents two GxxxG dimerization motifs, one at the N-terminal and one at the C-terminus. According to this model, based on NMR data, the TM domain dimerizes at the C-termini in the inhibitory state. The basic JM regions are sequestered at the membrane. In particular the "LRRLL" (L: leucine; R: arginine) motif on the JM-A can interact with anionic lipids at the plasma membrane. The TM domain forms a dimer at the N-terminal GxxxG module and the JM domains are pulled out from the membrane to stabilize the asymmetric dimer only upon ligand binding and a rearrangement of the extracellular module (Lemmon et al. 2014). This possible activation mechanism is

reported in Figure 11. Further investigation on the role of the TM and JM regions is necessary to understand the complete activation mechanism of EGFR.

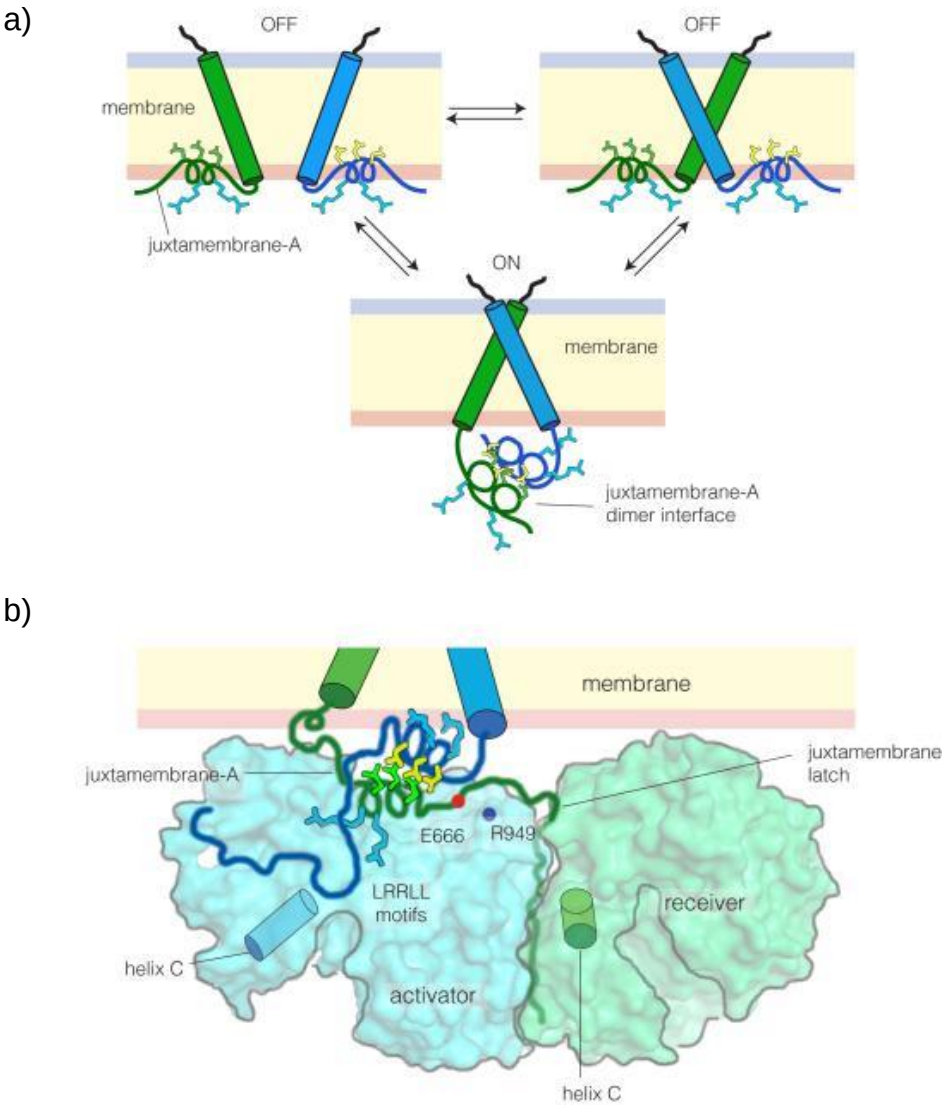

Figure 11: Model for the structural rearrangement of the TM, JM and kinase domains

a) The model shows the TM and JM-A domains as monomers in the inactive state or as an inactive dimer. Upon activation, the rearrangement of the TM domain displaces the JM region from the membrane to form the antiparallel α-helices. The LRRLL motif on the JM-A is highlighted: the leucine side chains are in yellow and green, while the arginine side chains are in blue. **b)** The model shows the asymmetric dimer formation at the plasma membrane. The juxtamembrane latch helps to position a glutamate residue (E666) of the receiver close to an arginine residue (R949) of the activator to anchor the JM-A segment. This Figure is taken from Endres et al. (2013).

II.4 Cytoplasmic regulators of EGFR activity

The activity of EGFR is regulated by several negative feedback signals. Inhibitory mechanisms are initiated directly after EGFR activation. The receptor activity is modulated via endocytosis and dephosphorylation. Other mechanism involves *de novo* protein synthesis. For human EGFR, four different inducible feedback inhibitors (IFIs) are known: leucine-rich and immunoglobulin-like domains protein 1 (LRIG1), suppressor of cytokine signaling 4 and 5 (SOCS4 and SOCS5) and mitogen-induced gene 6 (MIG6) (Segatto et al. 2011). The MIG6 protein is a well-known IFI that stabilizes the catalytic domain in the inactive conformation, probably preventing the formation of the juxtamembrane latch (Jura et al. 2009a; Zhang et al. 2007).

Positive cytosolic regulatory elements for RTKs are extremely rare. Until now only two are known: Dok-7 (docking protein 7) for MuSK (muscle-specific receptor tyrosine kinase) (Inoue et al. 2009) and cytohesins for EGF-receptor (Bill 2011). Cytohesins were identified by Bill (2011) as positive regulatory elements for the EGFR. They were postulated to enhance the formation of the asymmetric dimer. Cytohesins are described in Section II.4.1.

II.4.1 The Cytohesins and Arfs protein

The cytohesins are a group of proteins acting as guanine nucleotide exchange factors (GEFs) for Arfs (ADP rybosilation factors) (Kolanus 2007). Arf proteins are member of the small-guanine nucleotide-binding proteins of the Ras superfamily. Arfs regulate several biological processes such as vesicular trafficking and organelle structures. Arf proteins switch between a GTP-bound active state and a GDP-bound inactive state (Donaldson, Jackson 2011). The hydrolysis of the GDP is operated by GAPs, while the exchange to GTP is operated by GEFs. Arf proteins can be divided into three classes based on the amino acid sequence. Specifically, class I, which is composed of Arf1, Arf2 and Arf3, regulates vesicles formation and budding; class II comprises Arf4 and Arf5 and they play a role in Golgi transport; finally, Arf6, the only member of class III, regulates the structural organization of the cell membrane and the transport from endosomes to the membrane (D'Souza-Schorey, Chavrier 2006).

Cytohesins promote the GDP-GTP exchange on Arf1 and Arf6. The cytohesin family includes four members: cytohesin-1, cytohesin-2 (ARNO), cytohesin-3 (Grp-1) and cytohesin-4. Cytohesin-4 is only present in the immune cells (Kolanus 2007).
The cytohesins are small proteins of around 47 kDa. All cytohesins share homology in the domain division: an N-terminal coiled-coil region, a central Sec7 domain, and a C-terminal PH domain, which is flanked by a short polybasic region (PBR). The coiled-coil region is important for protein-protein interactions and dimerization of cytohesins. The Sec7 domain is responsible for GEF activity. The PH domain is necessary for membrane interactions, and the polybasic region is important for the interaction with PS on the cell plasma membrane (Figure 12).

Figure 12: Schematic of domain division of cytohesins

Starting from the N-terminal (N-term) part, cytohesins contain a coiled-coil (CC) domain (blue), a central Sec7 domain (green), and a C-terminal (C-term) pleckstrin homology (PH) domain (purple), flanked by a short polybasic region (PBR) (grey). This Figure is adapted from Kolanus (2007)

Kolanus et al. (1996) identified cytohesin-1 as an interacting partner for integrin-β in immune cells. The overexpression of cytohesin-1 or its Sec7 domain induces the binding of integrin-β to ICAM-1 (intercellular adhesion molecule 1). Hafner et al. (2006) showed that the inhibition of the Sec7 domain via SecinH3 leads to insulin resistance in human hepatic cells, probably hindering the binding of IRS1 to insulin receptor. ARNO was recently identified as a cytoplasmic enhancer for EGFR (Bill 2011). The Sec7 domain of ARNO was sufficient to enhance the phosphorylation of the receptor independently from its GEF activity. This led to the conclusion that ARNO acts as an allosteric enhancer for EGFR, probably contributing to the formation of the asymmetric dimer.

II.4.1.1 The PH domains of cytohesins and their inhibitor

The PH domain is an approximately 100 amino acid domain present at the C-terminal part of the cytohesin sequence. The PH domain was first discovered in pleckstrin, the substrate of PKC (protein kinase C) in platelets (Imaoka, Lynham, Haslam 1983). PH domains are presents in a variety of proteins and it is estimated that around 252 human proteins possess a PH domain. However, only 10 % of the identified PH domains

can specifically interact with the cell membrane, while the function for most of them still remains unknown (Lemmon et al. 2002). The structure of the PH domain comprises a seven-stranded β-sandwich with a C-terminal α-helix (Lemmon, Ferguson 2000). The surface of the PH domain is extremely polarized, presenting a negative and a positive charge on the two opposite sides. Of the 10 % of PH domains responsible for the interaction with the plasma membrane, the positive surface interacts with phosphoinositides on the cell surface in a concentration-dependent manner (Lemmon et al. 2002). In particular, the PH domain of the cytohesins can interact with PIP_3 or PIP_2 depending on the splicing variants present at the β1/β2 loop. The two glycine variant binds PIP_3 with high affinity, while the three glycine variant can bind to PIP_2 and PIP_3 with micromolar affinities (Kolanus 2007).

To further elucidate the function of cytohesins, a new PH-inhibitor was recently identified via an aptamer displacement assay in Famulok's group (Hussein et al. 2013). Cyplecksins (cytohesin pleckstrin homology domain inhibitors) belong to the family of the bromo-barbituric acids and they contain one substituent in position 1 and two in position 5. The mechanism involves a covalent attachment of cyplecksins to the PH domain. These small molecule compounds inhibit the PH domain-dependent recruitment of cytohesins to the plasma membrane.

III. Aim of the Project

The study of membrane proteins in a native-like environment is an interesting perspective and one of the major challenges in pharmaceutical and biochemical research. The understanding of the activation mechanism of membrane proteins, e.g. receptor tyrosine kinases, in a native-like environment can lead to the development of new pharmacological strategies to counteract their uncontrolled activation in pathological conditions. However, transmembrane proteins are often hard to study due to purification, aggregation and instability problems (Bayburt, Sligar 2003). The activation mechanism of the receptor tyrosine kinase EGFR is only partially understood. Recently, ARNO was identified as an interaction partner for EGFR (Bill 2011). It was suggested that ARNO has a direct influence on EGFR phosphorylation in cellular systems. The effect of ARNO on EGFR phosphorylation was also observed in membrane-free experiments using the soluble intracellular part of the receptor.

Thus, the aim of this research project was to test different native-like membrane systems for their suitability to analyze EGFR-ARNO interactions and EGFR activation. In particular, micelles, bicelles, nanodiscs and membrane sheets were used for this purpose.

At first, nanodiscs were used as a platform to observe the recruitment of ARNO to membranes. The phospholipid composition of the nanodiscs was optimized by adding anionic lipids for the binding of the ARNO PH domain to the nanodiscs. In order to test this model system, small-molecules targeting the PH domain of cytohesins, called cyplecksins, were investigated for their ability to inhibit membrane recruitment of ARNO.

In a second step, the insertion of purified EGFR or particular subdomains of the receptor into micelles, bicelles and nanodiscs was optimized. Biochemical and biophysical assays were performed to answer the questions: Is it possible to reproduce the effect of ARNO on EGFR phosphorylation in artificial membrane systems? And: Are simplified membrane-model systems a suitable model to study ARNO-EGFR interactions?

As none of the reconstituted membrane systems were determined to be completely suitable for these purposes, a more complex, native-like membrane system, i.e. membrane sheets, were used. Membrane sheets were used to understand whether ARNO directly interacts with EGFR and, if so, which domains are necessary for the interaction.

IV. Results

IV.1 Nanodiscs as a model system to study membrane-ARNO interactions

In order to understand protein functions in a native-like environment and their interactions with the surrounding lipids, artificial membrane system are required. Sligar and co-workers first described and produced nanodiscs for the insertion and study of transmembrane proteins (Sligar's Laboratory Website). Nanodiscs are a phospholipid bilayer, surrounded by two amphipathic helical molecules, termed membrane scaffold proteins (MSPs) (Bayburt et al. 2002).

The production of nanodiscs using natural phospholipids and the interaction with the pleckstrin homology (PH) domain of the cytohesin-2 (also termed ARNO) are described in this Section. The PH domain of ARNO binds to PIP_2 or PIP_3 on the inner leaflet of the plasma membrane (Kolanus 2007). Nanodiscs were used as a platform to observe the PIP_2-dependent membrane recruitment of ARNO PH domain. Recently, small-molecules targeting the PH domain of cytohesins, namely cyplecksins (cytohesin pleckstrin homology domain inhibitors) were identified in the Famulok's laboratory (Hussein et al. 2013). Cyplecksins bind the PH domain covalently and compete for the binding of soluble PIP-derivatives. Nanodiscs were used to test whether cyplecksins are able to inhibit the membrane recruitment of the PH domain of ARNO in a native-like environment.

IV.1.1 Proteins Expression and Purification

IV.1.1.1 Cytohesin-2 (ARNO) PH domain

The PH domain interacts with PIP_ns present on the plasma membrane. This construct contains a SBP-tag (streptavidin-binding peptide, S) at the N-terminus followed by a TEV (tobacco etch virus, T) cleavage site. ST-ARNO-PH construct used is the three glycine variant and it binds PIP_2 and PIP_3 with similar affinity. ST-ARNO-PH was expressed and purified as reported in Paragraph VII.2.1 and it has a molecular weight of 19 kDa. Fractions from expression and purification were analyzed by SDS-PAGE (Figure

13). All the original gels can be found in the Appendix. The streptavidin-binding peptide tag on the protein was used for following pull-down experiments.

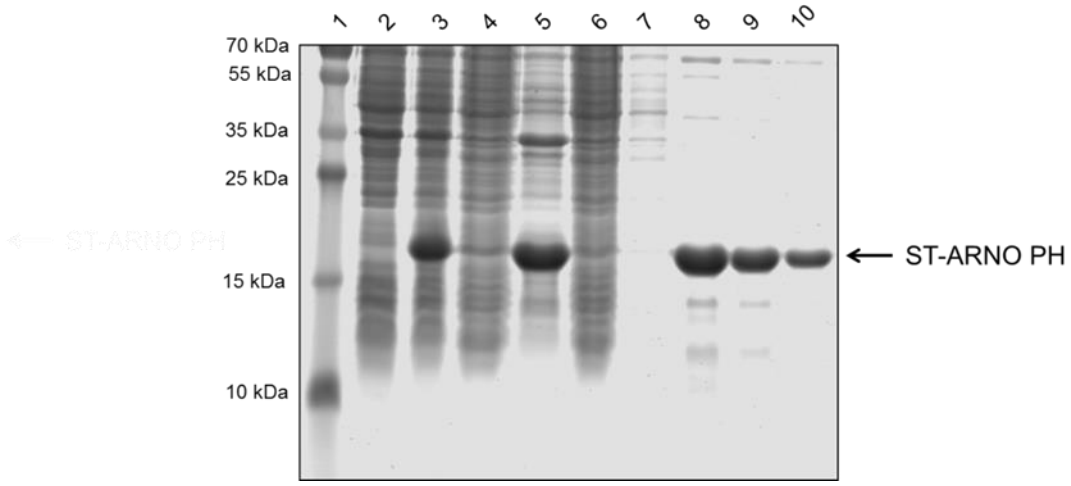

Figure 13: ST-ARNO PH expression and purification

15 % SDS-PAGE stained with Coomassie Brilliant Blue. Prestained molecular weight marker is loaded on lane 1. The induction of protein expression is observed comparing the total cell sample before (lane 2) and after induction (lane 3). ST-ARNO PH is visible at approximately 20 kDa. Lane 4 shows the cellular debris after centrifugation, lane 5 shows the cell lysate. Lane 6 shows the lysate after incubation with Strep-tactin beads. Lane 7 shows the wash step. From lane 8 to lane 10 the elution fractions are visible. Contaminants traces are visible at around 13 kDa and 11 kDa. Eluted fractions are pooled together and a buffer exchange step against ARNO storage buffer was performed. The sample after buffer exchange is not shown on the gel.

IV.1.1.2 Membrane scaffold protein 1 deleted 1 (MSP1D1)

MSP1 (membrane scaffold protein 1) is a truncated version of the human Apolipoprotein A-1, termed Apo A-1, in which the first 43 N-terminal amino acid residues are removed (Shih et al. 2007). MSP1 was modified as a further N-terminal deleted mutant, i.e. MSP1D1 (membrane scaffold protein 1 deleted 1), first expressed and purified by Denisov et al. (2004). MSP1D1 has a molecular weight of 24 kDa.

MSP1D1 was expressed as reported in Paragraph VII.2.1. MSP1D1 contains a Histidine-tag at the N-terminus followed by a spacer sequence and a TEV protease site. Fractions from expression and purification were analyzed by SDS-PAGE (Figure 14).

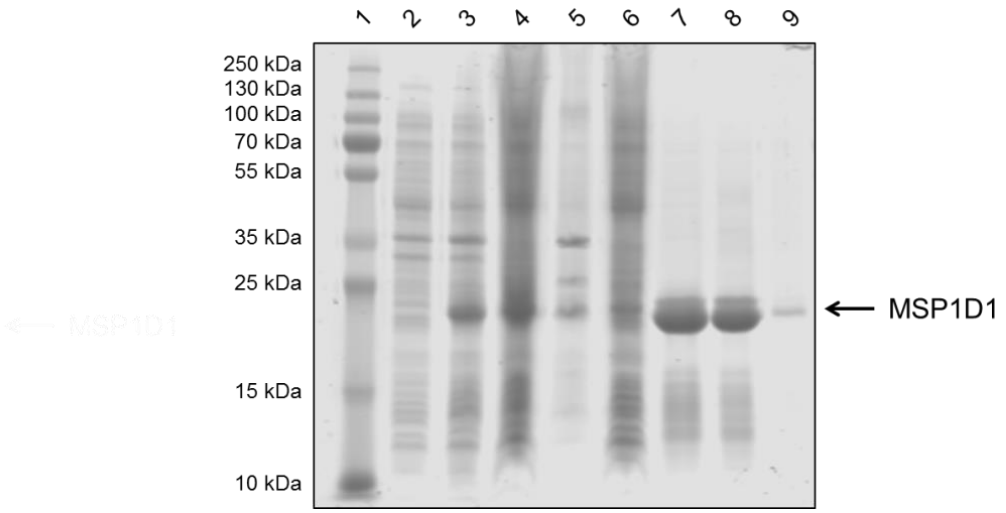

Figure 14: MSP1D1 expression and purification

12.5 % SDS-PAGE stained with Coomassie Brilliant Blue. Prestained molecular weight marker was loaded on lane 1. The induction of protein expression was observed comparing the total cell sample before (lane 2) and after induction (lane 3). MSP1D1 is visible at approximately 24 kDa. Lane 4 shows the cell lysate and lane 5 the cellular debris after centrifugation. Lane 6 shows the lysate after incubation with Ni-NTA beads. Lane 7 shows the eluted fraction. Contaminant traces are visible at around 13 kDa. Lane 8 shows the final protein product in dialysis buffer. Lane 9 shows the precipitate after overnight dialysis.

IV.1.2 The production of nanodiscs with natural phospholipids

Nanodiscs were used as a membrane model system to observe the recruitment of ARNO PH domain to the plasma membrane. The PH domain of cytohesins, depending on the splicing variants, contains two or three glycine residues that bind phosphoinositides with different affinities (Cronin et al. 2004; Klarlund et al. 2000). Two glycine residue splicing variants bind to PIP_3, while the three glycine residue splicing variants bind to PIP_2 and PIP_3 (Kolanus 2007).

Two different nanodisc types were produced. Nanodiscs containing only 80 mol % PC (phosphatidylcholine, egg, chicken) and 20 mol % PE (phosphatidylethanolamine, liver, bovine) were used as control. Nanodiscs containing 75 mol % PC, 20 mol % PE and 5 mol % PIP_2 (brain, porcine) were used to study the binding between ARNO PH domain and the membrane.

IV.1.2.1 Biophysical assays to confirm nanodiscs assembly with natural phospholipids

IV.1.2.1.1 Analytical gel filtration

Nanodiscs were prepared as reported in Section VII.2.5.1.1. High pressure liquid chromatography (HPLC)-analytical gel filtration on Superdex 200 10/300 column (packed by Volkmar Fieberg) with a 0.2 ml/min flow in MSP standard buffer was performed. Sligar and co-workers have shown that the protein catalase has the same retention time as nanodiscs (Figure 15) (Sligar's Laboratory Website). The absorption at 280 nm was used for the detection of proteins. Catalase was used as a reference for nanodisc assembly. Catalase has a molecular weight of 250 kDa and the elution time was 13.297 min.

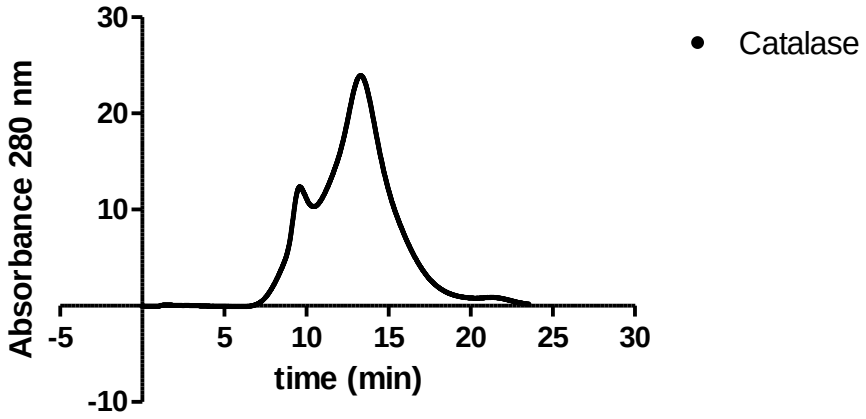

Figure 15: HPLC-analytical gel filtration of catalase

Gel filtration was performed on Superdex 200 10/300 GL column in MSP standard buffer with a 0.2 ml/min flow. Catalase eluted at 13.297 minutes. An aggregate peak at 9.577 minutes was eluted at the column void-volume.

In Figure 16 and 17 are reported the chromatograms of PCPE-nanodiscs and PIP_2-nanodiscs, respectively, with three different ratios of MSP1D1 to lipid: 1:20, 1:40 and 1:60.

For PCPE-nanodiscs, at the 1:60 ratio, a large aggregate peak was visible from the chromatogram and the nanodiscs peak was not eluted at the same retention time of the reference protein. At the 1:40 ratio, the elution time was comparable to the elution time of catalase, but still an aggregate peak was visible at around 10 minutes. At the 1:20 ratio, traces of free MSP1D1 were visible at around 16 min. To avoid aggregate formation and the presence of free MSP1D1 in solution, a 1:30 molecular ratio of MSP1D1:lipid was used.

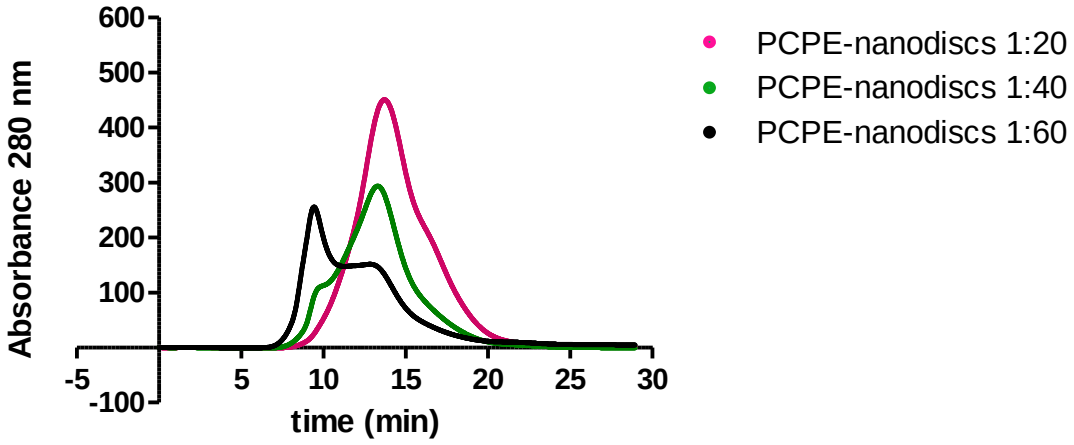

Figure 16: HPLC-analytical gel filtration of PCPE-nanodiscs

Gel filtration was performed on Superdex 200 10/300 GL column in MSP standard buffer with a 0.2 ml/min flow. Three different MSP to phospholipids molar ratio were tested: 1:60 in black, 1:40 in green and 1:20 in pink. In the 1:60 chromatogram, one aggregate peak was visible at 9.421 min, while the nanodiscs peak eluted at 12.834 min. In the 1:40 chromatogram, the nanodiscs peak was eluted at 13.289 min, while an aggregate peak was still visible at around 10 min. In the 1:20 chromatogram, nanodiscs eluted at 13.704 min, while the MSP1D1 shoulder was lightly visible at around 16 min. This indicated the presence of free MSP in the mixture. To avoid aggregate formations and the presence of free MSP1D, an intermediate ratio of 1:30 was chosen.

For PIP_2-nanodiscs, the 1:60 ratio showed a small aggregate peak eluting at the column void-volume. The main peak was not eluted at the same time as catalase. At the 1:40 ratio, the elution time was comparable to the elution time of catalase, but traces of aggregates were present at 9.8 minutes. At the 1:20 ratio, traces of free MSP1D1 were visible. For the PIP_2-nanodiscs a MSP:lipid ratio of 1:30 was also used.

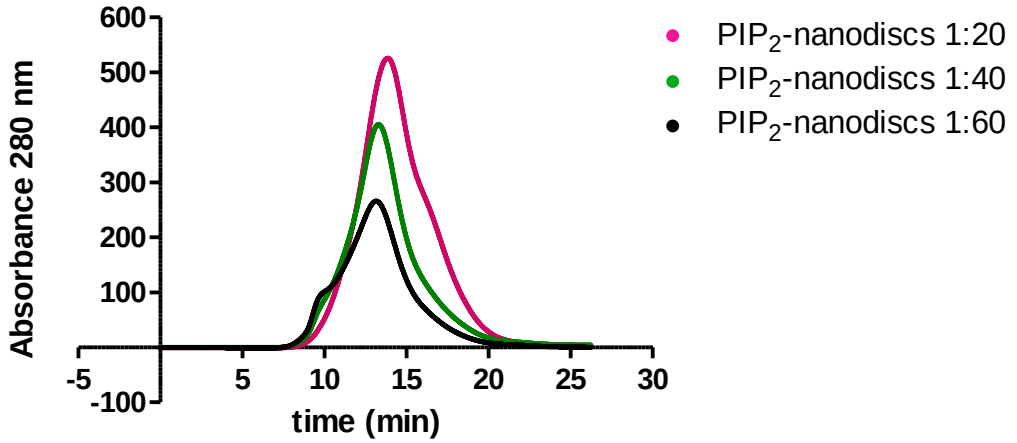

Figure 17: HPLC-analytical gel filtration of PIP_2-nanodiscs

Gel filtration was performed on Superdex 200 10/300 GL column in MSP standard buffer with a 0.2 ml/min flow. Three different MSP to lipids molar ratio were tested: 1:60 in black, 1:40 in green and 1:20 in pink. In the 1:60 chromatogram, the nanodiscs peak eluted at 13.150 min, before the catalase reference at 13.297 min and an aggregates peak was visible at around 10 min. In the 1:40 chromatogram, the nanodiscs peak was eluted at 13.291 min, as was the catalase reference but a small aggregates peak was visible at 9.8 min. In the 1:20 chromatogram, nanodiscs eluted at 13.855 min, after the catalase reference. Free traces of MSP were indicated by the shoulder at around 16 min visible in the chromatogram. Also for PIP_2-nanodiscs, to avoid aggregate formations and the presence of free MSP1D, an intermediate ratio of 1:30 was chosen.

IV.1.2.1.2 Dynamic light scattering (DLS)

The 1:30 MSP to phospholipid ratio for the nanodiscs assembly was confirmed with DLS (dynamic light scattering). DLS allows to measure of the volume of particles in solution according to their Brownian motions. PCPE-nanodiscs had a diameter of 16.18 nm and PIP_2-nanodiscs of 15.34 nm (Figure 18a and 18b, respectively). The nanodisc dimensions measured with DLS are around 5 nm bigger than the nanodisc dimensions reported in the literature, probably due to the presence of natural phospholipids that can alter the nanodisc dimensions (Bayburt et al. 2002).

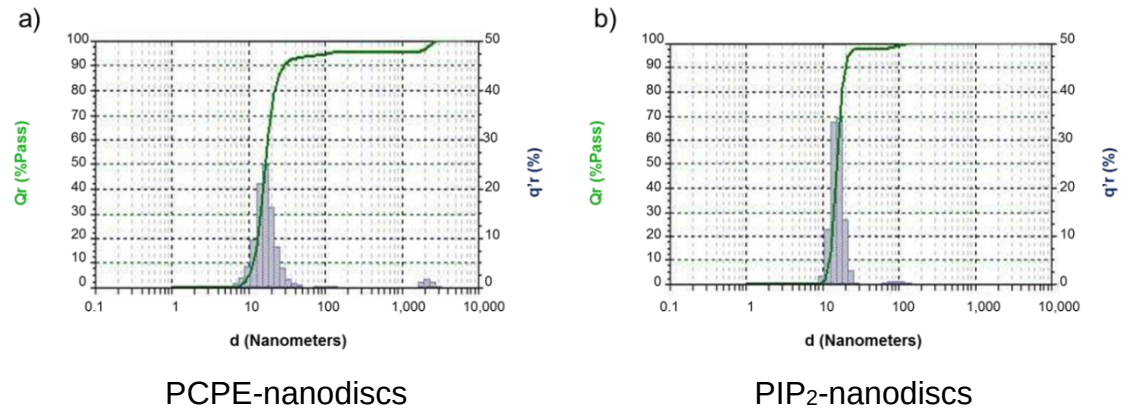

Figure 18: DLS analysis of nanodiscs with natural phospholipids

DLS was performed in the laboratory of Professor Gerd Bendas (University of Bonn). The x-axis indicates the hydrodynamic diameter (d) of the particles in nanometers. Qr indicates the distribution function of the particle size in percentage. $q^{l}r$ indicates the frequency distribution of the particle size in percentage. **a)** The measured diameter for PCPE-nanodiscs was 16.18 nm with a 94 % volume distribution. **b)** The measured diameter for PIP_2-nanodiscs was 15.34 nm with a 98 % volume distribution.

IV.1.2.2 ARNO PH domain interacts with PIP_2-nanodiscs

To validate the nanodiscs as a native-like membrane system to detect the PIP_2-dependent membrane recruitment of ARNO, a pull-down assay was performed. Nanodiscs with or without PIP_2 were incubated with ST-ARNO-PH. A general experiment schema is reported in Figure 19.

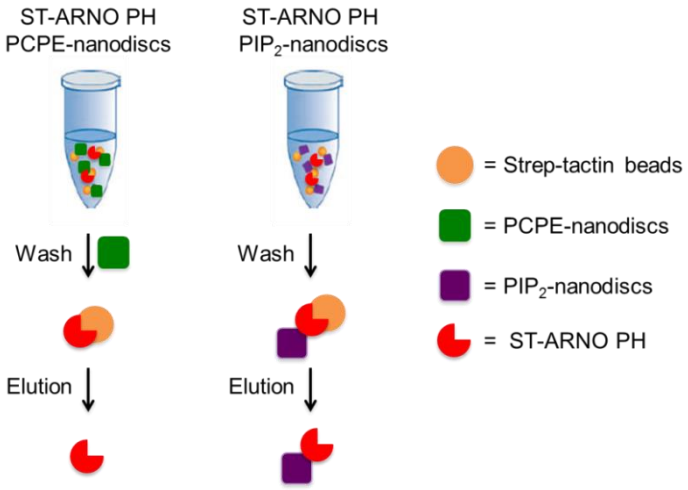

Figure 19: Pull-down assay with Strep-tactin magnetic beads

Strep-tactin magnetic beads were incubated with ST-ARNO PH and PIP_2-nanodiscs or PCPE-nanodiscs. A wash step was performed to remove unspecific interactions. Elutions were analyzed by SDS-PAGE. Eppendorf picture modified from Recenttec Website.

The pull-down assay was performed as reported in Section VII.2.9.1. In the Coomassie stained gels, only the protein fraction of the nanodiscs, i.e. MSP1D1, is visible.

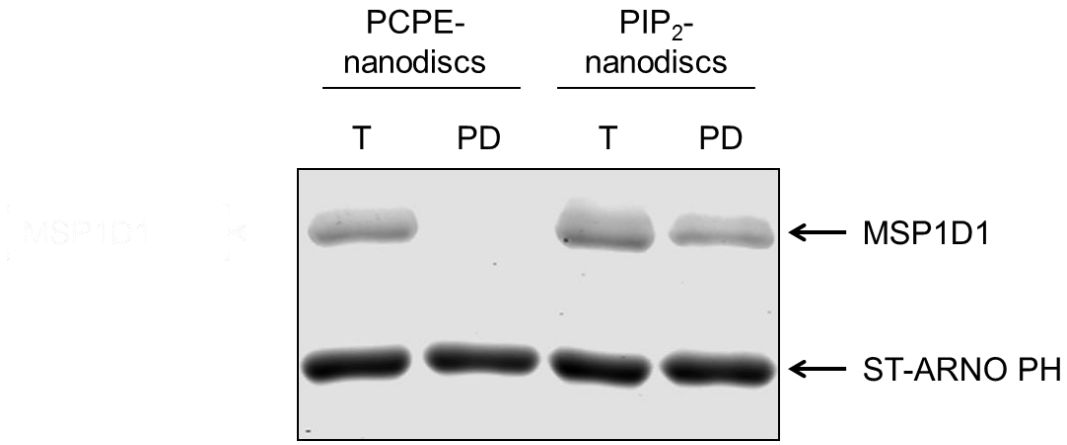

Figure 20: ARNO PH interacts with PIP_2-nanodiscs

The figure shows the pull-down assay performed with ST-ARNO PH and nanodiscs. ST-ARNO PH was immobilized on strep-tactin beads with PCPE-nanodiscs or PIP_2-nanodiscs in presence of 2 % DMSO. After incubation on ice, the bound proteins were eluted. The input or total (T) fractions and the pull-down (PD) fractions were analyzed by SDS-PAGE and visualized by Coomassie staining.

In the pull-down fraction PCPE-nanodiscs were not visible. ARNO PH binds only to PIP_2-containg nanodiscs (Figure 20), indicating that nanodiscs are a suitable model to reliably detect the PIP_2-dependent membrane recruitment of cytohesins.

IV.1.2.3 Cyplecksins inhibit the membrane recruitment of ARNO PH domain

ARNO PH binds to PIP_2-nanodiscs, as reported in Figure 20, while no interaction was detected with PCPE-nanodiscs. To analyze if cyplecksins (cytohesin pleckstrin homology domain inhibitors) inhibit membrane targeting of ARNO PH, PIP_2-nanodiscs were used. Cyplecksins were synthetized and tested by Dr. Mohammed Hussein from Famulok's group. In Figure 21 the structures of cyplecksins 1-3 and the inactive analogues MH 40 A and MH 40 B are reported.

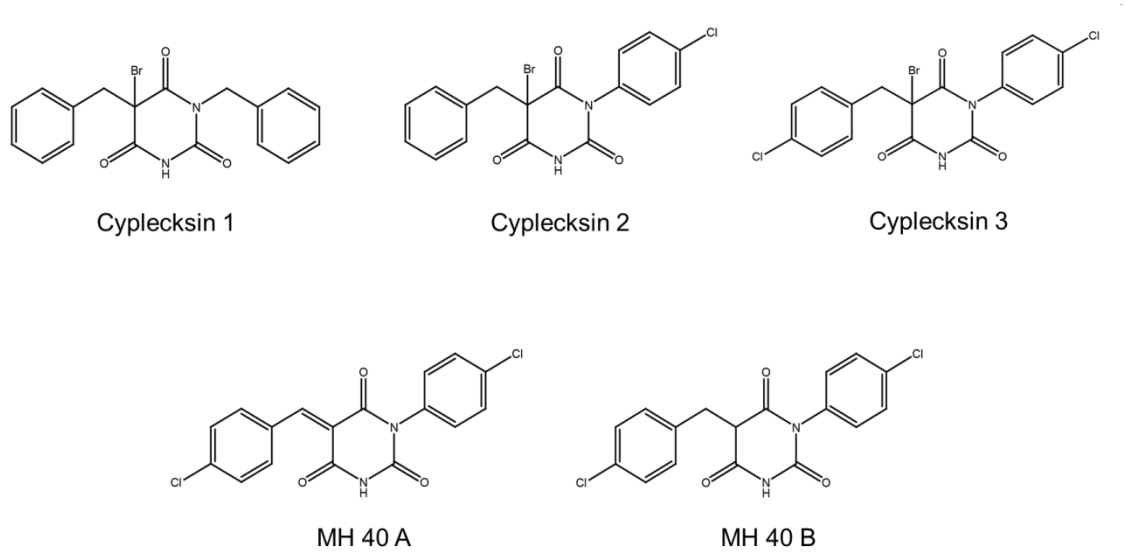

Figure 21: Structure of cyplecksins 1-3 and the inactive analogues MH 40 A and MH 40 B

A pull-down assay was performed as reported in Section VII.2.9.2. Cyplecksins or the inactive analogues MH 40 A and B were used at the concentration of 100 µM. The compounds were pre-incubated with bead-coupled ARNO PH and subsequently PIP_2-nanodiscs were added. Figure 22 shows the results of the pull-down assay.

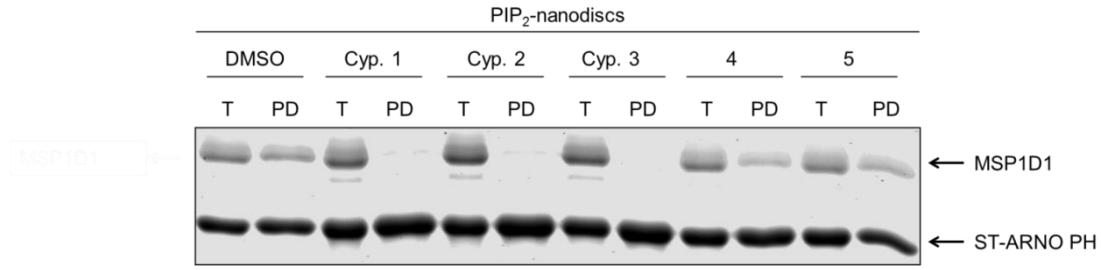

Figure 22: Cyplecksins inhibit ARNO PH interaction with PIP_2-nanodiscs

The pull-down assay was performed in presence of 2 % DMSO, 100 µM cyplecksins 1-3 (Cyp. 1, Cyp. 2 and Cyp. 3), MH 40 A (4) or MH 40 B (5). ARNO PH was pre-incubated with DMSO, cyplecksins or the inactive analogues. Subsequently PIP_2-nanodiscs were added. The mixtures were incubated with strep-tactin beads. The input or total (T) fractions and the pull-down (PD) fractions were analyzed by SDS-PAGE and visualized by Coomassie staining. Cyplecksins inhibit PIP_2-dependent membrane binding, while the interaction was still present when the inactive analogues MH 40 A and MH 40 B were used.

Cyplecksins 1-3 inhibit the binding between ARNO PH and PIP_2-nanodiscs. The co-elution between ARNO PH and PIP_2-nanodiscs was not affected by the inactive analogue MH 40 A and MH 40 B. Therefore, nanodiscs are a reliable system to test small-molecule inhibitors for protein-membrane interactions.

IV.2 Different membrane-like environments to study protein-protein interaction and activation

Cytohesins were identified as enhancer for the activation of the EGFR in living cells and for the intracellular domain of the receptor in solution by Bill (2011). Previous data from the Famulok's laboratory (personal communication from Anton Schmitz and Michael Famulok) suggested a direct interaction between the Sec7 domain of ARNO and the JM (juxtamembrane) region of EGFR. Starting from this point, the idea was to investigate the activation of EGFR via Sec7 using the phosphorylation level as a readout in evaluating different membrane surrogates. Furthermore, this PhD work intended to observe the interaction between ARNO and EGFR, starting from simplified system such as micelles, and ending with the more complex system, like membrane-sheets. Membrane surrogates provide a native-like environment to study protein activation and interaction.

IV.2.1 Micelles

Detergents are a tool to solubilize membrane proteins and they form micelles in an aqueous environment. The head group of the detergent is hydrophilic and it is in contact with the water, while the lipophilic tails form the core of the micelle. The formation of micelles occurs when the detergent concentration is above a threshold level, or CMC (critical micelle concentration) (Versace, Lazaridis 2015).

In the following chapters, the reconstitution of EGFR activity in micelles and the interaction studies with ARNO are presented.

IV.2.1.1 EGFR activity in micelles

To test the activity of EGFR reconstituted in a membrane-like environment, a phosphorylation assay was used. For this purpose, an already dimerized form of the receptor (lz-EGFR-TS) was expressed and purified from Sf9 (*Spodoptera frugiperda*) cells, as reported in Paragraph VII.2.1.9. The EGFR contains three major (Tyr 1068, 1148, and 1173) and two minor phosphorylation sites (Tyr 992 and 1086) located on the C-terminal tail (Bishayee et al. 1999; Downward et al. 1984). Phosphorylated tyrosine residues are used as docking sites for intracellular factors containing SH2 domain or PTB

domains, responsible for the activation of different signal cascades (Yarden, Sliwkowski 2001).

IV.2.1.1.1 Expression and Purification of lz-EGFR-TS

The lz-EGFR-TS contains an N-terminal leucine zipper (lz) dimerization motif replacing the extracellular domains. The construct has a Flag-tag at the N-terminal part and a C-terminal TEV (T) cleavage site followed by a SBP-tag (streptavidin binding peptide, S). A schematic representation of the construct is depicted in Figure 23.

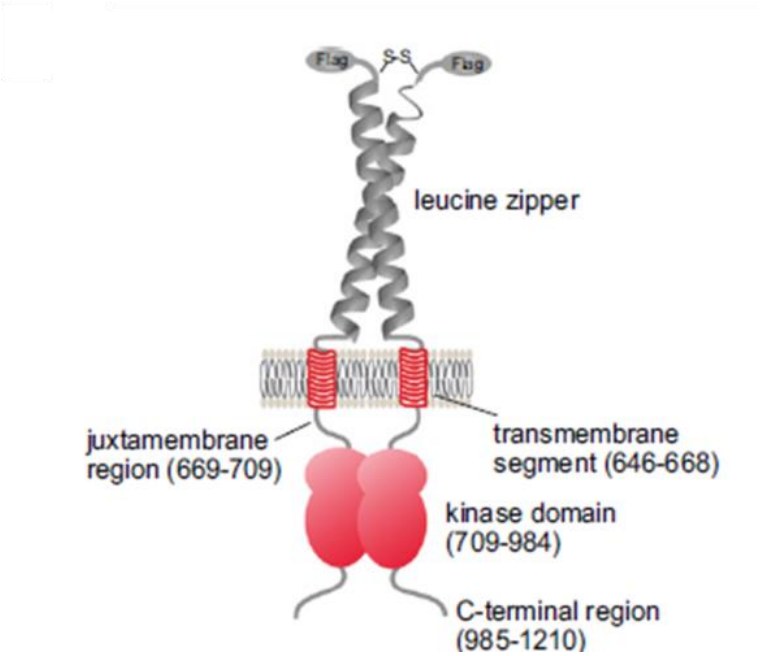

Figure 23: Schematic representation of the lz-EGFR-TS construct

Lz-EGFR-TS has an N-terminal Flag-tag and a C-terminal SBP-tag. The extracellular domain is replaced by a leucine zipper dimerization module. The Figure is taken from Bill (2011).

The constructs has a molecular weight of 76.6 kDa and was purified using the SBP-tag at the C-terminus. Purification conditions are reported in Section VII.2.1.9. In Figure 24 the SDS-PAGE and Coomassie staining of the purification is shown.

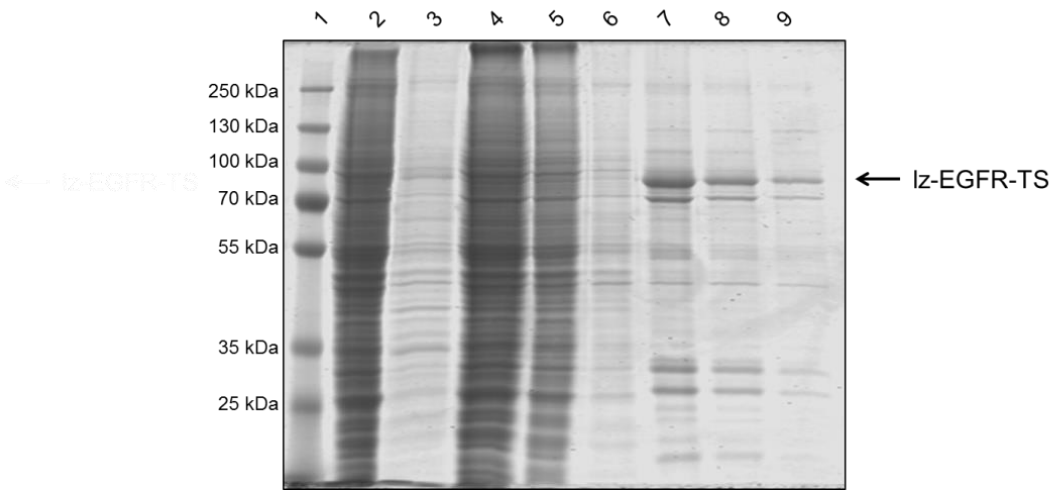

Figure 24: Purification of lz-EGFR-TS from Sf9 cells

10 % SDS-PAGE stained with Coomassie Brilliant Blue. Prestained molecular weight marker was loaded on lane 1. The cell lysate after infection is visible in lane 2. Lane 3 shows cellular debris and lane 4 presents the supernatant after beads incubation. Lanes 5 and 6 show the washing steps. From lane 7 to lane 9 the elution fractions 1, 2 and 3 are visible. Lz-EGFR-TS eluted at molecular weight of 77 kDa, as a double band. Due to high detergent concentrations used to solubilize the protein in the elution buffer, no further purification via gel filtration was performed. Contaminant traces are visible at between 55 kDa and 20 kDa.

Lz-EGFR-TS eluted as a double band at around 77 kDa. The upper band corresponded to the desired and expected protein, while some degradation products were visible at a lower molecular weight. To confirm that the eluted band at 77 kDa corresponded to lz-EGFR-TS, two different Western Blots using a streptavidin-conjugated dye and an anti-Flag antibody were performed (data not shown). The receptor was solubilized in 0.1 % Triton X-100.

IV.2.1.1.2 Phosphorylation Assay in micelles

To test if lz-EGFR-TS was active after purification in micelles, EGFR phosphorylation was used as readout. For a detailed protocol see Section VII.2.7.1. Lz-EGFR-TS after purification already had a measurable basal phosphorylation level. For this reason, the protein YopH, a tyrosine-protein phosphatase from *Yersinia pseudotuberculosis* at the concentration of 200 nM was used to dephosphorylate EGFR before the phosphorylation assay. The receptor at the concentration of 100 nM, solubilized in 0.1 % Triton X-100 micelles, was incubated with 1 mM ATP for 10 seconds or 20 seconds. The reaction was stopped by the addition of 20 mM EDTA, to chelate the magnesium present in the buffer and block ATP activity. Samples before and after ATP addition were taken and analyzed by SDS-PAGE and Western Blot (Figure 25) using an anti-pTyr antibody.

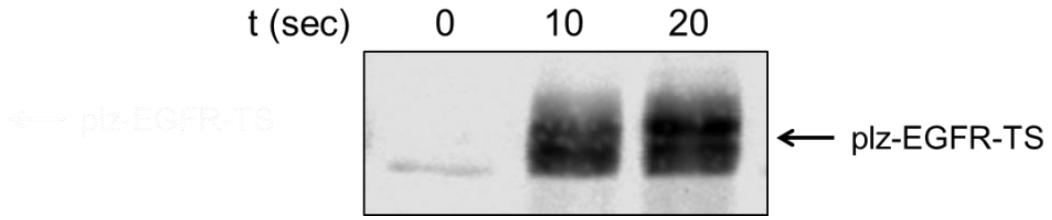

Figure 25: lz-EGFR-TS phosphorylation in micelles

Western Blot analysis is performed with anti-pTyr antibody. At time 0 seconds the receptor before ATP addition is visible. The receptor phosphorylation level measured within 10 seconds, and 20 seconds increased after ATP addition. Phosphorylation leads to the appearance of a double band.

Lz-EGFR-TS conserved its kinase activity upon purification. In Triton X-100 micelles, the receptor reached a high phosphorylation level within 20 seconds, similar to results reported in literature (Kholodenko et al. 1999; Wu et al. 2006). Micelles provide a membrane-like environment in which receptor activity can be studied.

IV.2.1.1.3 Influence of ARNO on EGFR phosphorylation in micelles

Bill (2011) reported that ARNO has a direct influence on EGFR activation in living cells and on EGFR soluble intracellular fraction in membrane-free assays. Furthermore, it was affirmed that the Sec7 domain is sufficient to enhance EGFR phosphorylation (Bill 2011). The Sec7 domain is known to be responsible for GEF function of the cytohesins (Cherfils et al. 1998). Starting from this background, to analyze EGFR phosphorylation in membrane-like systems, micelles containing lz-EGFR-TS were incubated with ARNO Sec7 (kindly provided by Yin Dongsheng from Famulok's group) or GST (glutathione S-transferase). GST protein was used as a negative control, to verify that only ARNO influences the EGFR phosphorylation level. The phosphorylation level was measured with a specific anti-pTyr antibody. Figure 26 shows the Western Blot with anti-pTyr antibody of micelles containing lz-EGFR-TS in presence of ARNO Sec7 or GST protein.

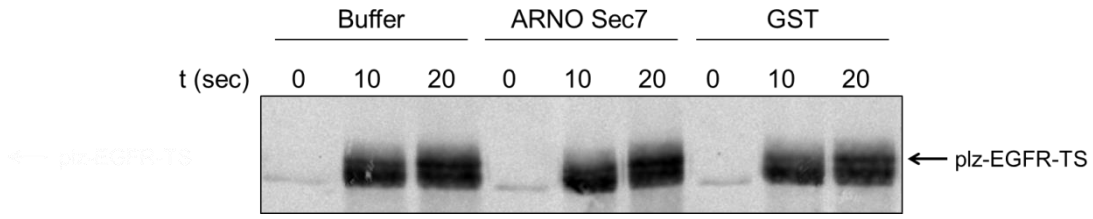

Figure 26: Influence of ARNO Sec7 on lz-EGFR-TS phosphorylation in micelles

Western Blot analysis is performed with anti-pTyr antibody. 0 second was evaluated to visualize the receptor prior to ATP addition. The receptor embedded in micelles was incubated with 1 mM ATP in buffer, 600 nM ARNO Sec7, or 600 nM GST, for 10 and 20 seconds, respectively. GST protein was used as negative control and it had no effect on EGFR stimulation. No enhancement of the phosphorylation level of the receptor was observed in presence of ARNO Sec7.

The reaction was started by adding ATP at the concentration of 1 mM, and samples were taken after 10 seconds and 20 seconds. BSA (bovine serum albumin) was added to the reaction to avoid unspecific interactions. No influence of ARNO on lz-EGFR-TS phosphorylation in micelles was observed. The same phosphorylation intensity was visible in presence or absence of ARNO and with the negative control.

IV.2.1.2 EGFR-ARNO interaction in micelles

As ARNO Sec7 did not enhance the phosphorylation of EGFR in micelles, other characterization of the physical interactions between ARNO and EGFR were evaluated. For this purpose, only the TM (transmembrane) and the JM (juxtamembrane) segments of the receptor were used. EGFR-TMJM is composed of amino acid residues 618 to 682 of EGFR (Red Brewer et al. 2009). The TM region contains a single α-helix spanning through the membrane. The JM domain helps to maintain the kinase domain in the active conformation, forming a structure termed "juxtamembrane latch" (Jura et al. 2009a).

Previous data collected by Famulok's group (personal communication from Benjamin Weiche, Anton Schmitz and Michael Famulok) suggested that the JM domain is the interaction site for ARNO Sec7 domain. Taking that into account, micelles containing a truncated EGFR construct were evaluated for ARNO Sec7 domain interaction by pull-down assay and crosslinking.

IV.2.1.2.1 Pull-down assay in micelles

IV.2.1.2.1.1 Expression and purification of HST-EGFR-TMJM

HST-EGFR-TMJM contains TM region and JM domain of EGFR fused to a His-tag (H) and a SBP-tag (S) at the N-terminus followed by a TEV (T) cleavage site. The construct was expressed and purified in *E. coli* in a pET28 expression system as reported in Section VII.2.1.8.1. A schematic representation of the protein structure is reported in Figure 27.

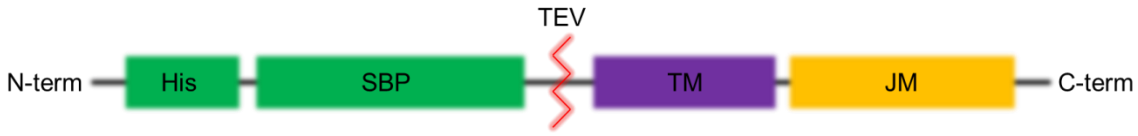

Figure 27: Schematic representation of HST-EGFR-TMJM construct

HST-EGFR-TMJM contains a His-tag and a SBP-tag (both in green) at the N-terminus. The TEV cleavage site is indicated by the red line. The TM domain (purple) is followed by the JM segment (yellow).

EGFR-TMJM could not be expressed as a soluble protein in bacteria, probably due to the presence of the hydrophobic TM segment that leads to the accumulation of the construct in inclusion bodies (Palmer, Wingfield 2012). Protein expression was induced by the addition of IPTG (isopropyl β-D-1-thiogalactopyranoside) in the culture medium, as visible in Figure 28. To extract the protein from the inclusion bodies, high concentrations of denaturing agents were required (Palmer, Wingfield 2012). Urea at a concentration of 8 M was used for this purpose. Cell extracts were then used for affinity chromatography with Ni-NTA beads allowing for interactions with the His-tag. HST-EGFR-TMJM after purification still contained visible traces of contaminants. The construct has a molecular weight of ~15 kDa. Due to the presence of high detergent concentrations, no further gel filtration step to purify the protein was possible. EGFR-TMJM micelles were formed with 0.2 % of sodium cholate.

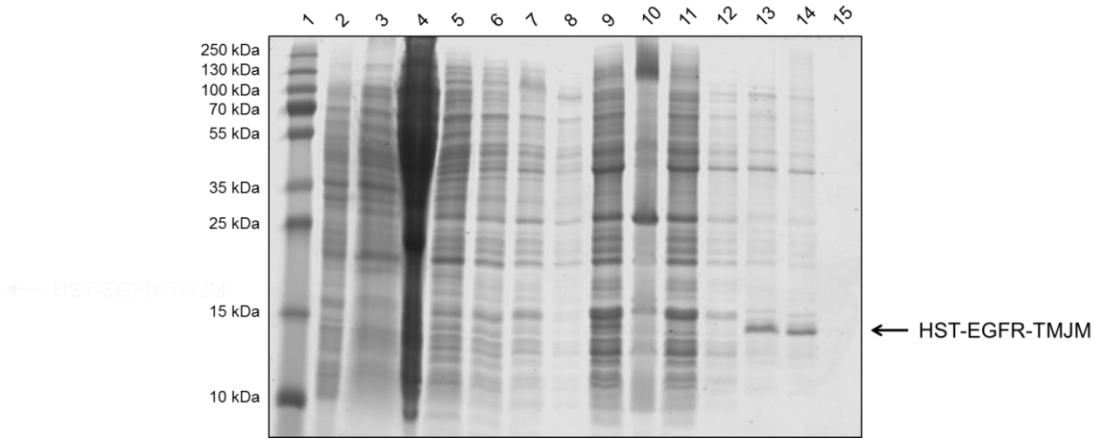

Figure 28: HST-EGFR-TMJM expression and purification from inclusion bodies

15 % SDS-PAGE stained with Coomassie Brilliant Blue. Prestained molecular weight marker was loaded on lane 1. In lane 2 is the total cell before induction, while in lane 3 after induction. HST-EGFR-TMJM is visible at ~15 kDa, but the expression was weak, and no induction band was visible. Lane 4 shows the cell lysate. From lane 5 to 8 the washing steps are visible. Lane 9 shows the cellular extract after incubation with 8 M urea. Lane 10 shows the cellular debris after centrifugation. Lane 11 shows the supernatant after incubation with Ni-NTA beads. Lane 12 illustrates another wash step before elution, visible in lane 13. Contaminant traces are visible at around 100 kDa, 50 kDa and 25 kDa. In lane 14 the supernatant after overnight dialysis in MSP standard buffer with 0.2 % sodium cholate is visible. In lane 15 no precipitate after dialysis is visible.

IV.2.1.2.1.2 Expression and purification of GST-ARNO Sec7

ARNO Sec7 was expressed as an N-terminal GST-fused construct. For the purification protocol see Paragraph VII.2.1. Samples, before and after protein induction, were collected and analyzed by SDS-PAGE (Figure 29). After protein induction, a band at 48 kDa became visible. This corresponds to the molecular weight of GST-ARNO Sec7. Glutathione beads, which bind the GST-tag on the protein complex, were used for the purification.

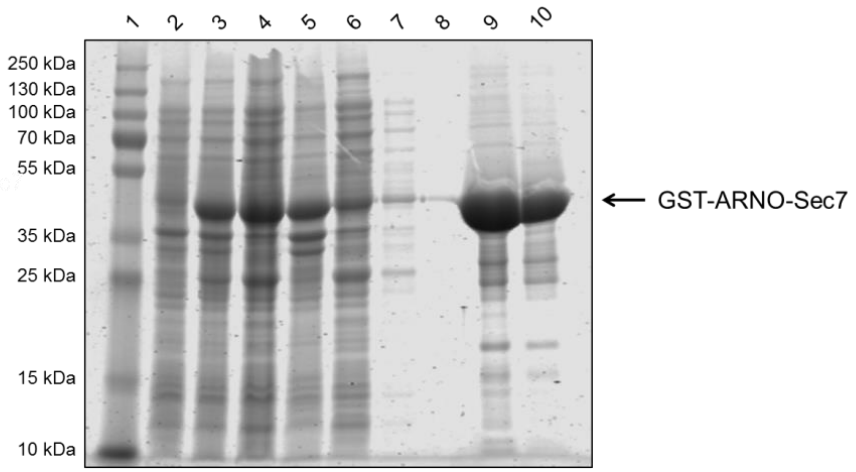

Figure 29: GST-ARNO Sec7 expression and purification

12.5 % SDS-PAGE stained with Coomassie Brilliant Blue. Prestained molecular weight marker was loaded on lane 1. The induction of protein expression was observed comparing the total cell before (lane 2) and after induction (lane 3). GST-ARNO Sec7 is visible at 48 kDa. Lane 4 shows the cell lysate, lane 5 cellular debris after centrifugation. Lane 6 shows the lysate after incubation with glutathione beads. Lanes 7 and 8 show the washing step. Lane 9 shows the eluted GST-ARNO Sec7 protein in high amount. In lane 10 the final protein product is visible. Contaminant traces are visible at around 25 kDa and 15 kDa.

To verify the functionality of GST-ARNO Sec7, its catalytic activity was then evaluated with a fluorescent-based guanine nucleotide exchange assay. For the protocol see Paragraph VII.2.8. Figure 30 shows the GDP-GTP exchange on a mutant Arf1 catalyzed by GST-ARNO Sec7. The deletion mutant Arf1 (NΔ17Arf1) is lacking the first N-terminal 17 amino acids, corresponding to its myristoylation site. The construct lost dependence on phospholipids for GTP binding (Kahn et al. 1992) and is therefore functional even in the absence of membranes. GST-ARNO Sec7 was active at nanomolar concentration, as shown in Figure 30.

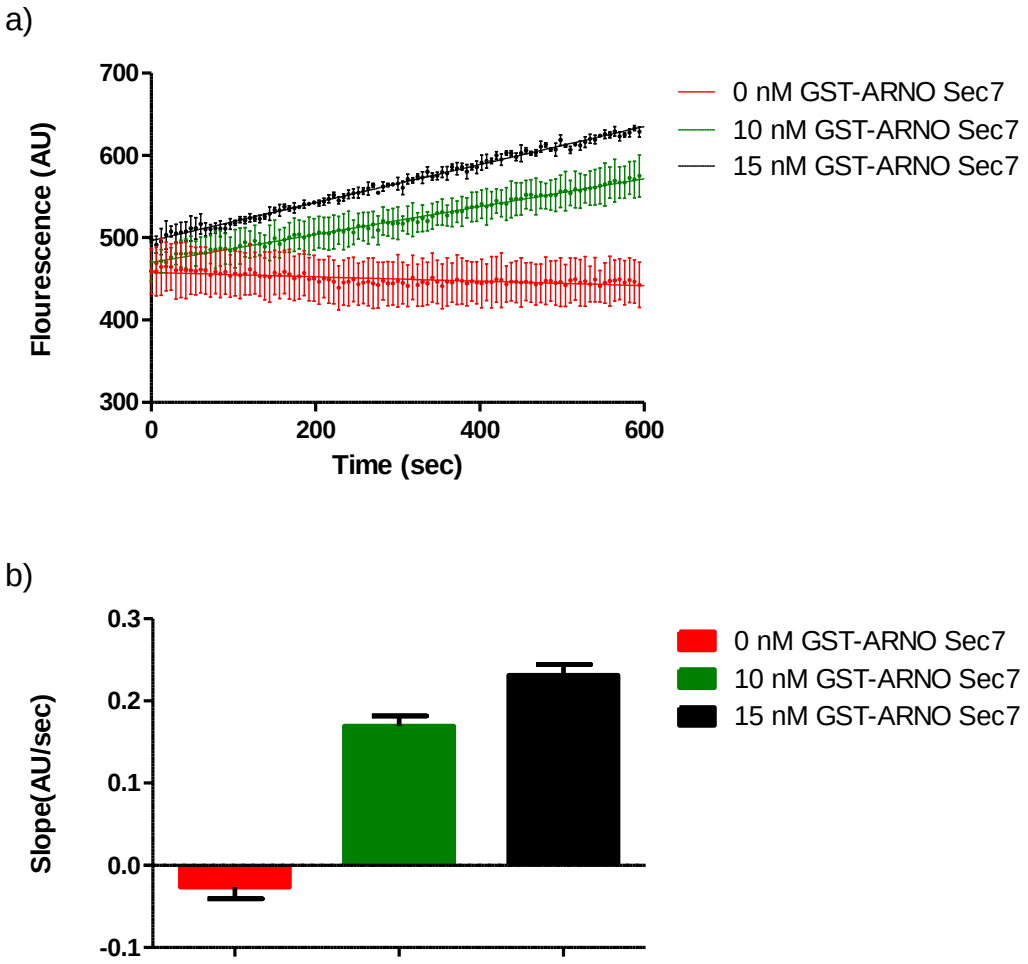

Figure 30: GST-ARNO Sec7 fluorescence-based GDP-GTP exchange assay on NΔ17Arf1

GST-ARNO Sec7 (0 nM, 10 nM or 15 nM) was incubated with GDP preloaded Arf1. The reaction was started upon addition of GTP. The GDP-GTP exchange was monitored via the tryptophan fluorescence (excitation 280 nm; emission 340 nm). **a)** Measure of tryptophan fluorescence upon GTP addition. **b)** The curves were fitted with the linear regression model and the slope were reported as bar chart, N=3.

IV.2.1.2.1.3 GST-pull-down assay

After confirming functionality of purified GST-ARNO Sec7, and the purification of EGFR, the interaction between the JM segment of EGFR and GST-ARNO Sec7 was evaluating using a GST-pull-down assay. For a detailed protocol see Section VII.2.9.3.

Micelles containing the TM domain and JM region of EGFR were pre-incubated with GST-ARNO Sec7 and subsequently with glutathione beads. Upon interaction, co-elution between ARNO and TMJM-micelles was expected. Samples of the loaded fraction, supernatant after bead incubation, eluate, and the beads were analyzed by SDS-PAGE (Figure 31).

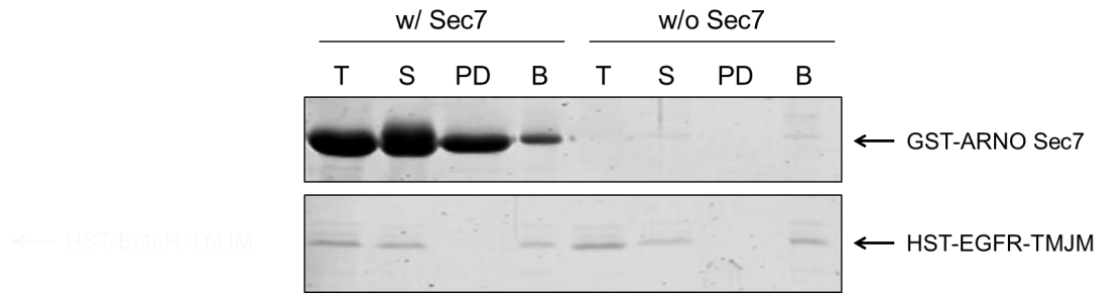

Figure 31: GST-pull-down of HST-EGFR-TMJM in micelles in presence of GST-ARNO Sec7

15 % SDS-PAGE stained with Coomassie Brilliant Blue. The protein pull-down was performed with glutathione beads in the presence (with: w/) or absence (without: w/o) of 30 µM GST-ARNO Sec7. HST-EGFR-TMJM embedded in sodium cholate micelles was used at the concentration of 10 µM. The beads were incubated with GST-ARNO Sec7 and EGFR-TMJM, or only with EGFR-TMJM as control. The total protein (**T**), supernatant after bead incubation (**S**), pull-down (**PD**) and bead (**B**) fractions were collected. Only GST-ARNO Sec7 is visible in the pulled down fraction, no EGFR-TMJM is co-eluted. The TMJM peptide may interact unspecific with the GST-beads, since it is present in the bead fraction of the reactions with or without Sec7.

From the pull-down assay no interaction between ARNO and EGFR-TMJM was detected. In the bead fraction, HST-EGFR-TMSM was visible indicating an unspecific interaction with the glutathione beads.

To avoid this problem, a reverse pull-down was performed, using strep-tactin beads instead of glutathione beads. Strep-tatctin beads bind to the SBP-tag at the N-terminus of HST-EGFR-TS construct. Also in this case, the elution of EGFR construct was not possible, as the protein remains attached to the beads (data not shown). Since it was not possible to observe EGFR-TMJM construct in the eluted fraction of both pull-down assays, other approaches were used to assay ARNO-EGFR interaction.

IV.2.1.2.2 Crosslinking assay in micelles

IV.2.1.2.2.1 Expression and purification of His-EGFR-TMJM-SBP

Due to the difficulties in obtaining the desired purity of the HST-EGFR-TMJM construct, another TMJM construct was expressed and purified for the following experiments. The new construct contained the SBP-tag at the C-terminal part instead of at the N-terminus which bears a 6xHis-tag (Figure 32). The SBP-tag contains 38 amino acid residues and its presence close to the His-tag in the previously used HST-EGFR-TMJM construct, could interfere with the proper binding of the His-tag to the Ni-NTA beads for the purification. The construct was expressed in *E. coli* in a pET28 expression system as reported in Section VII.2.1.8.1.

Figure 32: Schematic representation of His-EGFR-TMJM-SBP construct

The construct contains a 6xHis-tag (green) at the N-terminal part, followed by the TM (purple) and JM (yellow) regions. The SBP-tag (green) is present at the C-terminal part.

The construct has a molecular weight of ~14 kDa. The final His-EGFR-TMJM-SBP had a greater purity and yield than HST-EGFR-TMJM; nevertheless contaminant traces were still visible. Purification steps of His-EGFR-TMJM-SBP are illustrated in Figure 33.

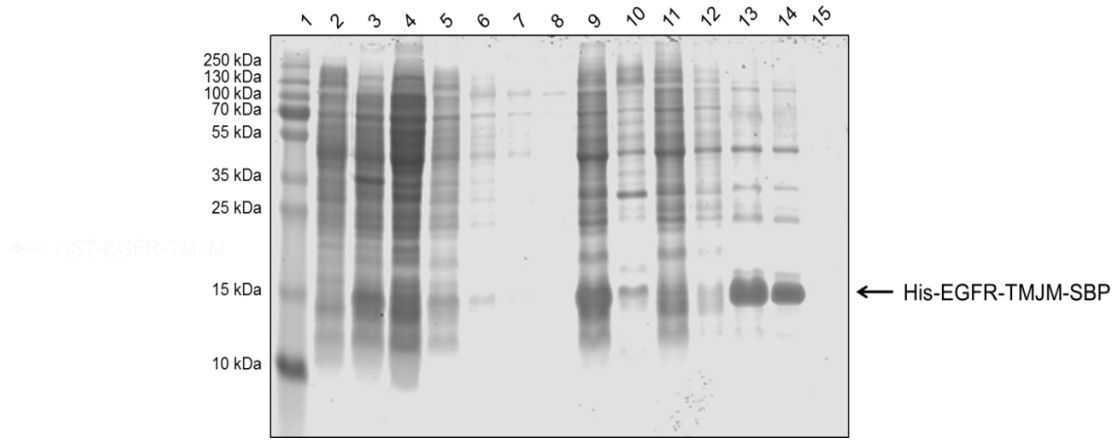

Figure 33: His-EGFR-TMJM-SBP expression and purification from inclusion bodies

15 % SDS-PAGE stained with Coomassie Brilliant Blue. Prestained molecular weight marker was loaded on lane 1. The induction of protein expression is observed comparing the cell lysate before (lane 2) and after induction (lane 3). His-EGFR-TMJM-SBP is visible at ~14 kDa. Lane 4 shows the cell lysate. Lane 5, 6, 7 and 8 shows the wash steps 1 to 4 respectively. Lane 9 shows the cellular extract after incubation with 8 M urea. Lane 10 shows cellular debris after centrifugation Lane 11 shows the supernatant after incubation with Ni-NTA (nickel-nitrilotriacetic acid) beads. Lane 12 illustrates the wash step 5. In lane 13 the eluted protein is visible. Contaminant traces are visible at ~55 kDa, 35 kDa, and 25 kDa. In lane 14 the supernatant after overnight dialysis in MSP standard buffer with 0.2 % sodium cholate is visible. In lane 15 no precipitate after dialysis is visible.

IV.2.1.2.2.2 Expression and purification of HT-ARNOΔPBR

ARNOΔPBR is an almost full-length ARNO construct, lacking the C-terminal polybasic region (PBR). The protein was expressed in *E. coli* as an N-terminal Histidine (H) fused construct in a pIBA101 vector, followed by a TEV (T) cleavage site. For the purification protocol see Paragraph VII.2.1. Samples, before and after protein induction, were collected and analyzed by SDS-PAGE (Figure 34). HT-ARNOΔPBR has a molecular weight of 47 kDa. The construct was expressed a basal level upon induction. Ni-NTA agarose beads were used for the purification. A high proportion of protein

remained insoluble, and was found in the precipitated fraction. Three separate elution steps were performed. The elution fractions were pooled together and a further gel filtration step was used to remove impurities (data not shown).

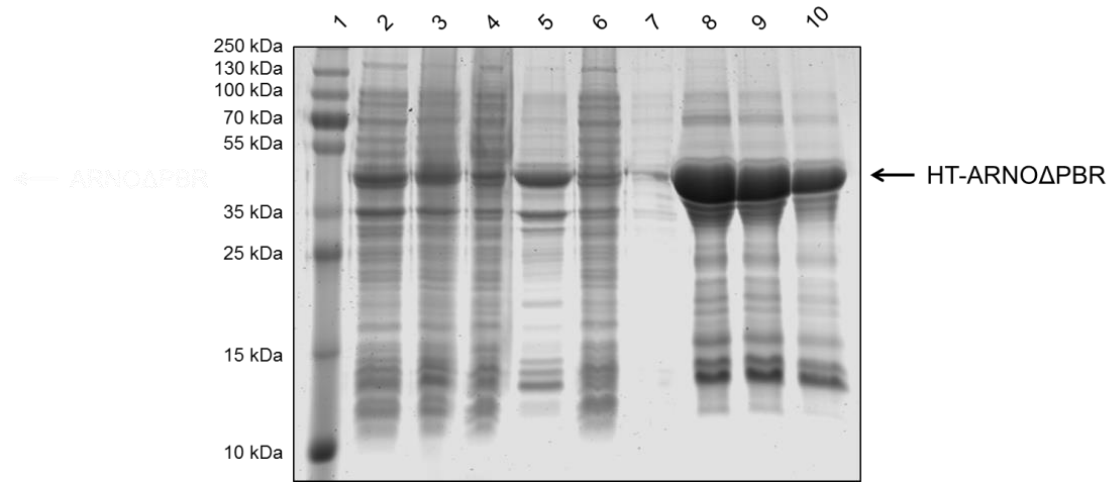

Figure 34: HT-ARNOΔPBR expression and purification

12.5 % SDS-PAGE stained with Coomassie Brilliant Blue. Prestained molecular weight marker was loaded on lane 1. HT-ARNOΔPBR has a molecular weight of 47 kDa. Before IPTG induction in lane 2, a basal expression level of the protein is visible. Upon IPTG addition, protein expression becomes stronger (lane 3). The total cell lysate is visible in lane 4. Cellular debris containing unfolded protein is visible in lane 5. The total cell lysate after bead incubation (lane 6) still shows protein traces. HT-ARNOΔPBR was washed (lane 7) one time before elution. Three different elutions were performed (from lane 8 to 10). The final protein product was gel filtrated to remove contaminants (not shown on the gel).

IV.2.1.2.2.3 Crosslinking

Crosslinking is a technique to stabilize molecular interactions. Protein-protein binding can be transient and difficult to detect. “Freezing" the moment of the interaction with a chemical crosslinker can allow the detection of weak and transient interactions (Thermo Scientific Pierce 2010). Crosslinking reagents are bi-functional compounds and covalently bind particular groups on the molecules (Peters, Richards 1977). The crosslinking reaction forms monomer, dimer, trimer, tetramer or high molecular weight complexes. The crosslinker concentration, the concentration of the interacting partners, and the reaction time should be carefully evaluated to avoid the formation of high molecular aggregates that cannot be analyzed by SDS-PAGE. Crosslinking between the same protein and unspecific crosslinking can also occur.

To analyze the interaction of ARNO with the His-EGFR-TMJM-SPB construct in sodium cholate micelles, the crosslinker bis(sulfosuccinimidyl)suberate (BS3,

ThermoFisher Scientific) was used. BS3 is a water-soluble crosslinker, with a spacer arm of 11.4 Å. BS3 reacts with primary amines at pH 7-9 (Thermo Scientific Pierce 2010).

Previous experiment in Famulok's group (personal communication from Benjamin Weiche, Anton Schmitz and Michael Famulok) provides support to the theory that the JM-A segment is responsible for binding to ARNO Sec7. As a proof of principle, only the JM peptide (kindly provided by Doctor Benjamin Weiche) was crosslinked with HT-ARNOΔPBR. For a detailed protocol see Section VII.2.10.1. Two different concentrations of crosslinker were initially used: 1.5 mM and 0.5 mM. The JM peptide has a molecular weight of 11 kDa, while HT-ARNOΔPBR has a molecular weight of 47 kDa. The crosslinked band between one ARNO monomer and one JM monomer was expected at ~55 kDa. Samples, before and after crosslinking, were collected and analyzed by SDS-PAGE (Figure 35).

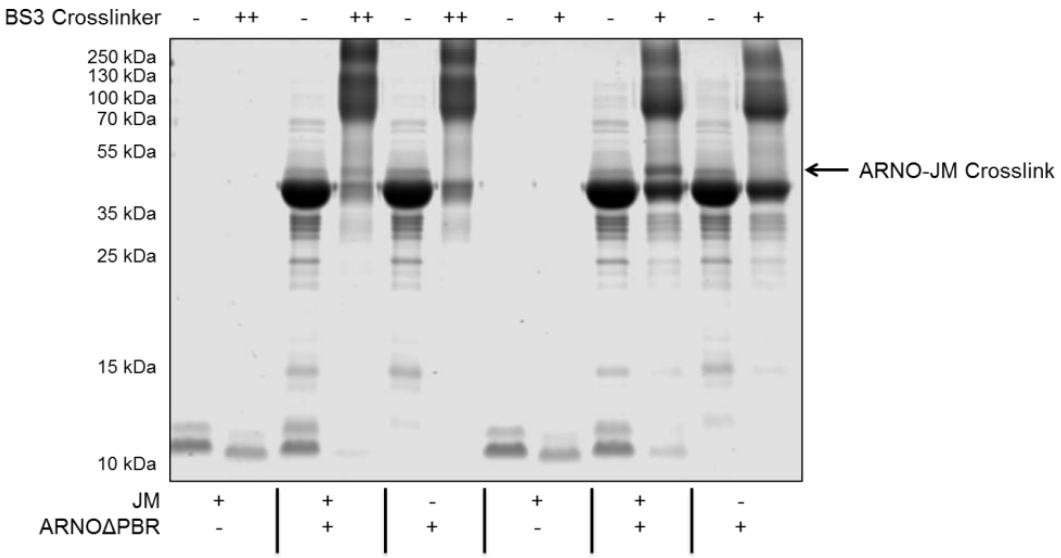

Figure 35: Crosslinking between ARNOΔPBR and JM peptide with different BS3 concentrations

15 % SDS-PAGE stained with Coomassie Brilliant Blue. The BS3 was used at two different concentrations: 1.5 mM (++) and 0.5 mM (+). HT-ARNOΔPBR concentration was 30 µM, while the JM peptide concentration was 10 µM. An additional band at ~55 kDa appears upon BS3 incubation only when ARNO and JM are present together. The ARNO-JM crosslinked complex was visibly stronger at the lower BS3 concentration. The crosslinked band size corresponds to a 1:1 interaction between the two proteins. ARNOΔPBR formed dimers at ~90 kDa and higher molecular aggregates. JM crosslinking was not visible. It is possible that the peptide formed larger aggregates that were not able to enter the gel matrix at the given percentage.

For the JM peptide no crosslinked band was visible in the gel, but the band intensity became weaker upon crosslinker addition. One possible explanation is that JM forms high molecular weight aggregates upon crosslinking. The aggregates were not able

to enter this percentage of gel during the run. ARNOΔPBR crosslinks formed dimers at ~90 kDa, and higher molecular weight complexes were also visible. JM crosslinks with ARNOΔPBR, and formed a 1:1 complex at ~55 kDa. This band interestingly showed a stronger intensity with lower BS3 concentration, while it became weaker when the concentration of the crosslinker was increased.

The same experiment was repeated with His-EGFR-TMJM-SBP construct embedded in sodium cholate micelles. The TM region and the JM domain of the insulin receptor (IR) in micelles were used as negative control. Hafner et al. (2006) reported that cytohesins play a role in the downstream signaling of IR, and no direct interaction between IR-JM and cytohesin seems to be necessary for this effect. The IR-TMJM construct provides a feasible negative control for interactions for evaluating the specific versus non-specific interactions between JM and ARNO.

The BS3 crosslinker was again used at the concentrations of 1.5 mM (Figure 36a) and 0.5 mM (Figure 36b). No crosslinking was visible between EGFR-TMJM and ARNO. Also EGFR-TMJM:EGFR-TMJM complexes, upon BS3 addition, were not visible. The band intensity of the EGFR-TMJM after crosslinking became weaker. Probably higher molecular weight structures were not able to enter the gel matrix. For the IR-TMJM construct, high molecular weight aggregates were present.

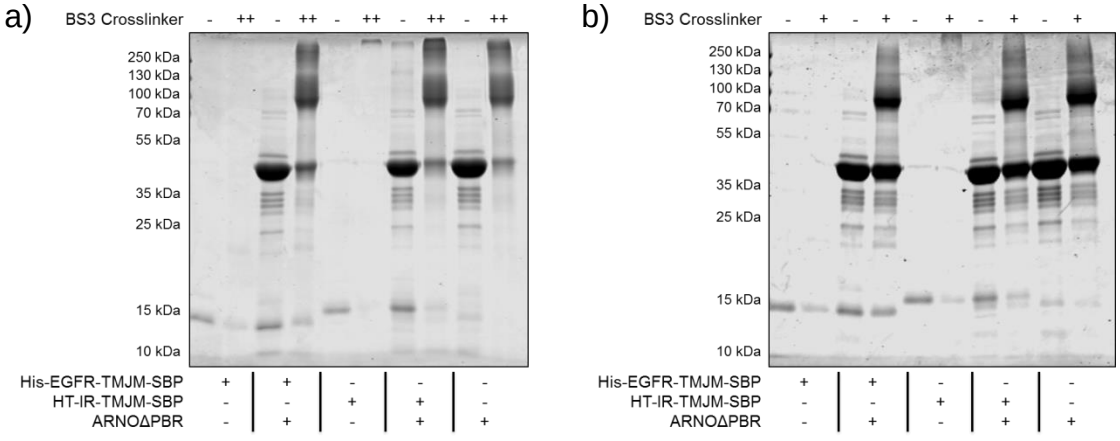

Figure 36 : Crosslinking between ARNOΔPBR and TMJM constructs in micelles

12.5 % SDS-PAGE stained with Coomassie Brilliant Blue. The BS3 was used at two different concentrations: **a)** 1.5 mM (++) and **b)** 0.5 mM (+). ARNOΔPBR concentration was 30 µM, while for the TMJM constructs was 10 µM. His-EGFR-TMJM-SBP did not crosslink with ARNO in micelles. Also for the EGFR-TMJM construct, upon BS3 addition, no crosslinking band was visible. For the IR-TMJM construct a high molecular weight aggregate was visible upon BS3 addition and, as expected, no crosslinked band with ARNOΔPBR.

From these results, micelles are not a suitable model for studying ARNO-EGFR interaction. It is probable that high concentrations of detergent that are necessary to keep the transmembrane protein in a soluble state represent an obstacle for the interaction itself. For this reason, other membrane systems were tested.

IV.2.2 Bicelles

Bicelles are often used as a membrane model system for the study of membrane proteins. Bicelles are discoidal phospholipids aggregates formed by long chain phospholipids, usually DMPC (1,2-dimyristoyl-sn-glycero-3-phosphocholine) or DPPC (1,2-dipalmitoyl-sn-glycero-3-phosphocholine), and short-chain lipid, such as DHPC (1,2-dihexanoyl-sn-glycero-3-phosphocholine) or detergent (CHAPSO) (Dürr et al. 2012; Glover et al. 2001). Previous studies used bicelles for solid-state NMR and have suggested that the bicelle formation is temperature, lipid concentration (c_L) and long-chain:short-chain lipid ratio (q) dependent. The central structure of bicelles is formed by the long chain phospholipids and their fatty acid chains, which are protected from contact with the water by a ring of short-chain lipid or detergent molecules (Ram, Prestegard 1988; Whiles et al. 2002)

Transmembrane proteins can be reconstituted into bicelles upon lyophilization. Bicelles were used as a membrane-like system to test the interaction between ARNO Sec7 and EGFR-TMJM. No phosphorylation studies were possible using the bicelles, due to the inability of recovering the kinase activity of EGFR after lyophilization (Rey L., May J. C. 2010).

IV.2.2.1 Bicelles assembly

DMPC/DHPC bicelles with q=0.25 and c_L=46 mM were prepared. For a detailed protocol see Section VII.2.4.1. The protocol was modified from Avanti Polar Lipid (Avanti Polar Lipids Website a). DMPC and DHPC were provided as a powder, and were solubilized in buffer. Subsequently heating and cooling down steps were performed until a homogenous solution was formed.

IV.2.2.1.1 Dynamic Light Scattering (DLS) of bicelles

Bicelles assembly was assayed with DLS (Figure 37) and the measured diameter was around 6 nm, comparable with the data reported in literature (Glover et al. 2001).

Results

Dilutions of bicelles were only possible if the DHPC concentration was kept at 10 mM to ensure bicelle integrity.

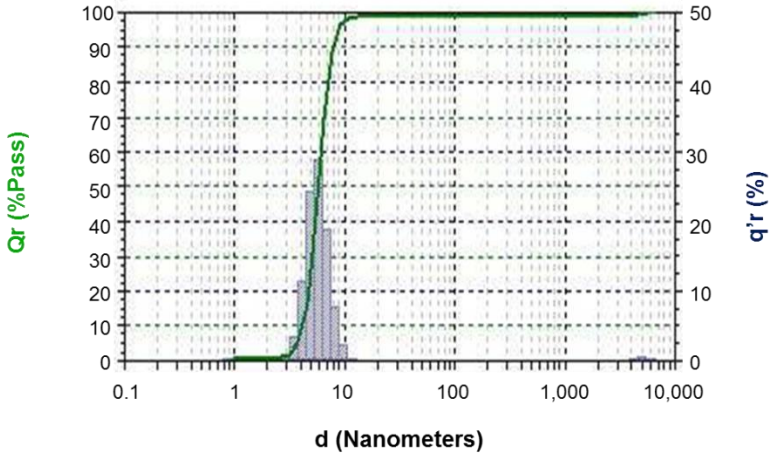

Figure 37: DLS to control the formation of bicelles

DLS was performed in the laboratory of Professor Gerd Bendas (University of Bonn). The x-axis indicates the hydrodynamic diameter (d) of the particles in nanometers. Qr indicates the distribution function of the particle size in percentage. $q^{I}r$ indicates the frequency distribution of the particle size in percentage. The measured diameter for DMPC/DHPC bicelles was 5.65 nm with a 99 % volume distribution.

Lyophilized His-EGFR-TMJM-SBP protein was reconstituted at the concentration of 300 µM in a solution of previously formed bicelles. The size of bicelles containing the transmembrane protein was analyzed with DLS (Figure 38). No change in the diameter of bicelles upon the reconstitution of the transmembrane protein was observed.

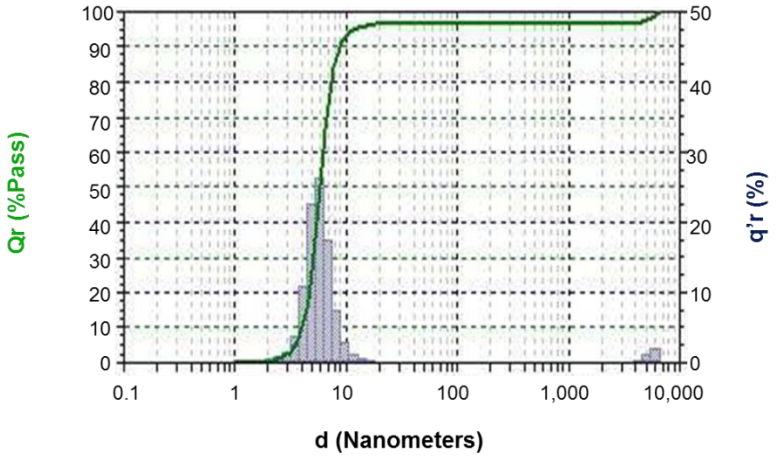

Figure 38: DLS of bicelles containing His-EGFR-TMJM-SBP

DLS was performed in the laboratory of Professor Gerd Bendas (University of Bonn). The x-axis indicates the hydrodynamic diameter (d) of the particles in nanometers. Qr indicates the distribution function of the particle size in percentage. $q^{I}r$ indicates the frequency distribution of the particle size in percentage. The measured diameter for DMPC/DHPC bicelles containing His-EGFR-TMJM-SBP was 5.66 nm with a 96.9 % volume distribution

To test if the peptide was embedded into the bicelles, fractions were taken during the assembly with lyophilized EGFR-TMJM and analyzed by centrifugation. As a control, EGFR-TMJM peptide was dissolved in buffer only and samples of supernatant and precipitate were analyzed by SDS-PAGE (Figure 39).

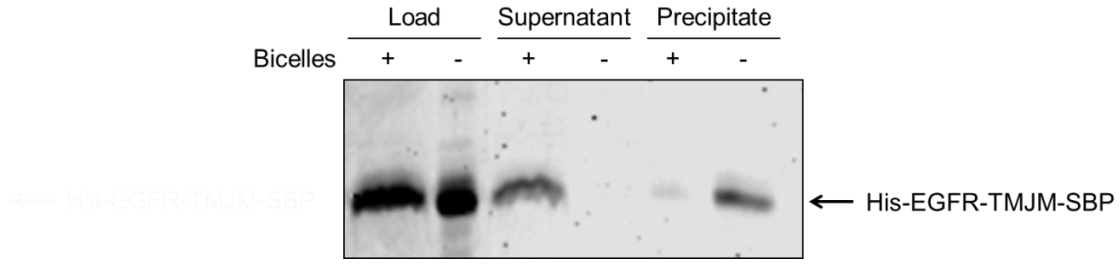

Figure 39: Control of His-EGFR-TMJM-SBP assembly into bicelles

15 % SDS-PAGE stained with Coomassie Brilliant Blue. Lyophilized His-EGFR-TMJM-SBP peptide at the concentration of 300 µM was mixed with 46 mM DMPC/DHPC bicelles or solubilized in 10 mM Phosphate Buffer pH 7.2. Fractions of both mixtures were taken as loading controls. Cycles of cooling and heating were performed and the final products were centrifuged. Samples of the supernatant and precipitate were collected and analyzed. No EGFR-TMJM band was visible in the supernatant where no bicelles were present, while the EGFR-TMJM band was visible in the supernatant of the bicelles sample. The precipitate fraction of the bicelle sample showed a lower amount of EGFR-TMJM peptide than the buffer fraction.

The same concentration of EGFR-TMJM was used for both mixtures. The peptide remains in solution only when bicelles are present; no traces of peptide in the buffer supernatant are visible. Precipitate is visible for both mixtures, but in lower amounts in the bicelle fraction.

IV.2.2.2 EGFR-ARNO interaction in bicelles

IV.2.2.2.1 Crosslinking in bicelles

Bicelles containing the TMJM region of EGFR were crosslinked with ARNOΔPBR (for a detailed protocol see Section VII.2.10.2). In Figure 40 the crosslinking experiment between the two proteins using BS3 as a crosslinker is evaluated. The SBP-tag of the EGFR-TMJM peptide was detected with a streptavidin-conjugated dye Western Blot, while ARNO was detected using an anti-ARNO antibody. The TMJM has a molecular weight of ~14 kDa, while HT-ARNOΔPBR is approximately 47 kDa. The same crosslinking band at ~60 kDa was detected using both antibodies, but the intensity was very weak. Dimeric EGFR-TMJM was visible from the streptavidin Western Blot also before BS3 addition (confirmed with Mass Analysis, data not shown) at ~25 kDa. In the anti-ARNO Western Blot a large quantity of unspecific bands were

visible, this complicated the identification of the crosslinking between the two proteins. Nevertheless, the crosslinked band size indicated in Figure 40 corresponds to a 1:1 interaction of ARNO with EGFR TMJM.

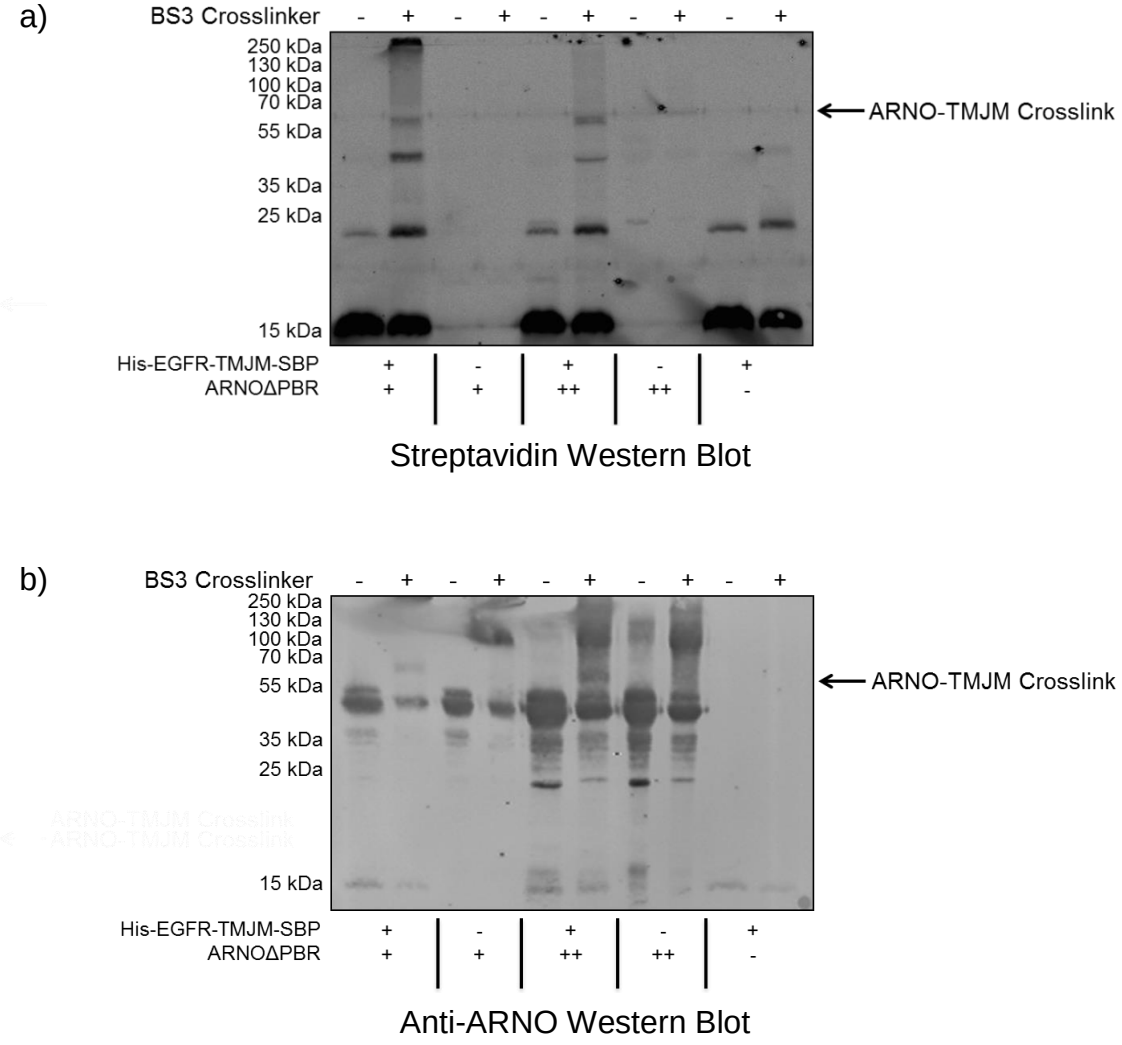

Figure 40: Crosslinking between ARNOΔPBR and EGFR-TMJM embedded into bicelles

BS3 crosslinking agent was incubated with two different HT-ARNOΔPBR concentrations, 10 µM (+) and 50 µM (++) respectively, and bicelles containing His-EGFR-TMJM-SBP. Analysis was performed by SDS-PAGE and **a)** Streptavidin Western Blot detecting the SBP-labeled EGFR-TMJM or **b)** anti-ARNO Western Blot. An additional band appeared upon BS3 incubation, only where ARNO and EGFR-TMJM were present together at ~60 kDa. The same band was detected in the streptavidin and anti-ARNO Western Blot. The crosslinked band indicates the interaction of one ARNO monomer with one EGFR-TMJM monomer.

To understand if ARNO Sec7 domain was responsible for the interaction with the JM domain, BS3 crosslinking was repeated with this construct. The Sec7 domain did not have an additional tag, and for this reason only a streptavidin Western Blot was performed. ARNO Sec7 has a molecular weight of 22 kDa, while EGFR-TMJM has a

molecular weight of 14 kDa. The expected crosslinking between one monomer of TMJM and Sec7 is ~35 kDa.

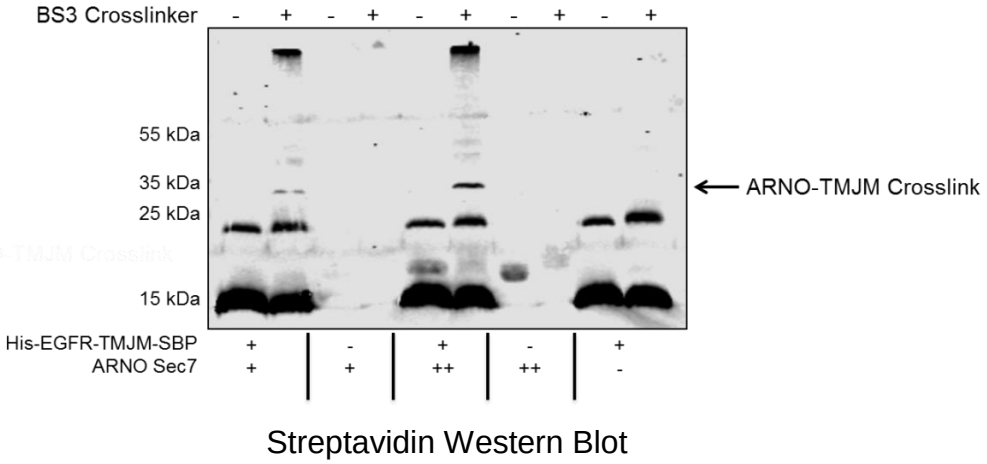

Figure 41: Crosslinking between ARNO Sec7 and EGFR-TMJM embedded into bicelles

BS3 was incubated with two different ARNO Sec7 concentrations, 10 µM (+) and 50 µM (++) respectively, and bicelles containing HT-EGFR-TMJM-SBP. Analysis was performed with SDS-PAGE and streptavidin Western Blot detecting the SBP-tagged EGFR-TMJM. An additional band appeared at 35 kDa upon BS3 incubation only where ARNO and EGFR-TMJM were present together. The crosslinking band indicates the interaction of one ARNO monomer with one EGFR-TMJM monomer.

The crosslinking between ARNO Sec7 and EGFR-TMJM is indicated in Figure 41 at around 35 kDa. The crosslinked band intensity increased with increasing ARNO concentration. The visible band size corresponds to a 1:1 complex between ARNO Sec7 and EGFR-TMJM. High molecular weight aggregates were also visible upon BS3 addition, but only in the presence of both proteins. The Sec7 domain appears to be sufficient for the interaction with the JM region.

To test whether the interaction between ARNO and JM is specific, two scrambled versions of the EGFR JM domains were produced. The JM domain can be further divided into two sub-regions: JM-A (residues 645-663) and JM-B (residues 664-682) (Jura et al. 2009a). The JM-A region is rich in arginine residues, and is necessary for the dimerization and stabilization of the asymmetric dimer. The JM-B segment is referred to as "juxtamembrane latch" and it wraps around the kinase domain to stabilize it (Jura et al. 2009a; Red Brewer et al. 2009).

NMR studies (not published yet) performed in collaboration with Dr. Manuel Etzkorn, from the University of Düsseldorf, provide additional support to the interaction between ARNO Sec7 and EGFR-JM. The JM-A is important for dimerization, by forming a coiled-coil structure. According to the program for the prediction of coiled-coil regions in proteins (COILs), in the JM-A scrambled version 1 (sc1), the coiled-coil motif is

partially conserved, while in the JM-A scrambled version 2 (sc2) there is no tendency to form the coiled-coil structure. In Table 1, the sequence of the JM wild-type and the two scrambled versions are reported.

Table 1: Sequences of JM domain wild-type and scrambled versions (sc) 1 and 2

	JM-A (residues 645-663)	JM-B (residues 664-682)
JM wild-type	RRRHIVRKRTLRRLLQERE	LVEPLTPSGEAPNQALLRI
JM sc1	PRQTEINRVLEITRRRLEL	LKLVASPALERQGRRPHRL
JM sc2	RELKHIQVRLRTERQLEPL	EIRAVNRSRLTPRLAGLPR

To reduce unspecific interactions during crosslinking, 10 µM BSA was added to the reaction. In Figure 42 it is possible to observe the streptavidin Western Blot crosslinking using BS3 of EGFR-TMJM wild type and the two scrambled versions, named scrambled version 1 (sc1) and scrambled version 2 (sc2), respectively. From the Western Blot, it was possible to identify the crosslinked band between ARNO Sec7 and wild-type EGFR-TMJM at ~35 kDa. However a weak interaction for EGFR-TMJM sc1 was observed and no crosslinking was visible for the EGFR-TMJM sc2.

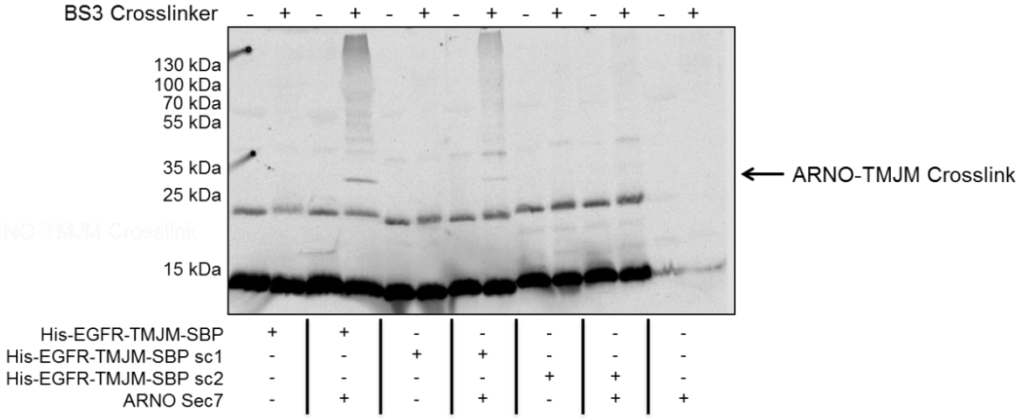

Figure 42: Crosslinking between ARNO Sec7 and EGFR-TMJM wild-type, sc1 and sc2 embedded into bicelles

Crosslinking agent BS3 was incubated with 10 µM ARNO Sec7 and bicelles containing His-EGFR-TMJM-SBP wild-type, scrambled version 1 (sc1), or 2 (sc2). The TMJM domain concentrations contained within the bicelles was 5 µM. Analysis was performed by SDS-PAGE and streptavidin Western Blot, detecting the SBP-labeled EGFR-TMJMs. A weak band at ~35 kDa was observed between the wild-type TMJM appeared upon incubation with BS3. Almost no interaction was detected upon incubation of the TMJM sc1 with the Sec7 domain, while no crosslinking was visible for TMJM sc2.

The interaction between ARNO Sec7 and the wild-type JM domain was once again visualized by the crosslinked band size at ~35 kDa, nevertheless the band intensity

was weak and hard to detect. Only a weaker crosslinked band size between Sec7 and TMJM sc1 was detected. In the TMJM sc1, the coiled-coil motif on the JM-A is partially conserved and probably for this reason, it was possible to observe a weak crosslinked band with ARNO Sec7. No crosslinking was detected with TMJM sc-2, in which both JM-A and JM-B segments were completely modified.

Multiple crosslinking conditions were tested to try to increase the efficiency of the reaction, but were without success. Mineev et al. (2015) recently observed the structure of the JM-A segment in DMPC/DHPC bicelles. Mineev et al. (2015) showed with NMR studies that the JM-A region in bicelles shows an unstructured random-coil conformation that forms a transient helix. These data are in agreement with the work by Endres et al. (2013). The JM in bicelles is solvent exposed and can interact with protein in solution. The unstructured JM domain could be more flexible and this could explain the weak nature of the interaction detected.

Furthermore, to support the theory that Sec7 is sufficient for the interaction, the PH domain of ARNO was used as negative control (Figure 43). The PH domain of ARNO contained a Flag-tag at the N-terminal part in order to perform a Flag Western Blot. The crosslinking was performed as before.

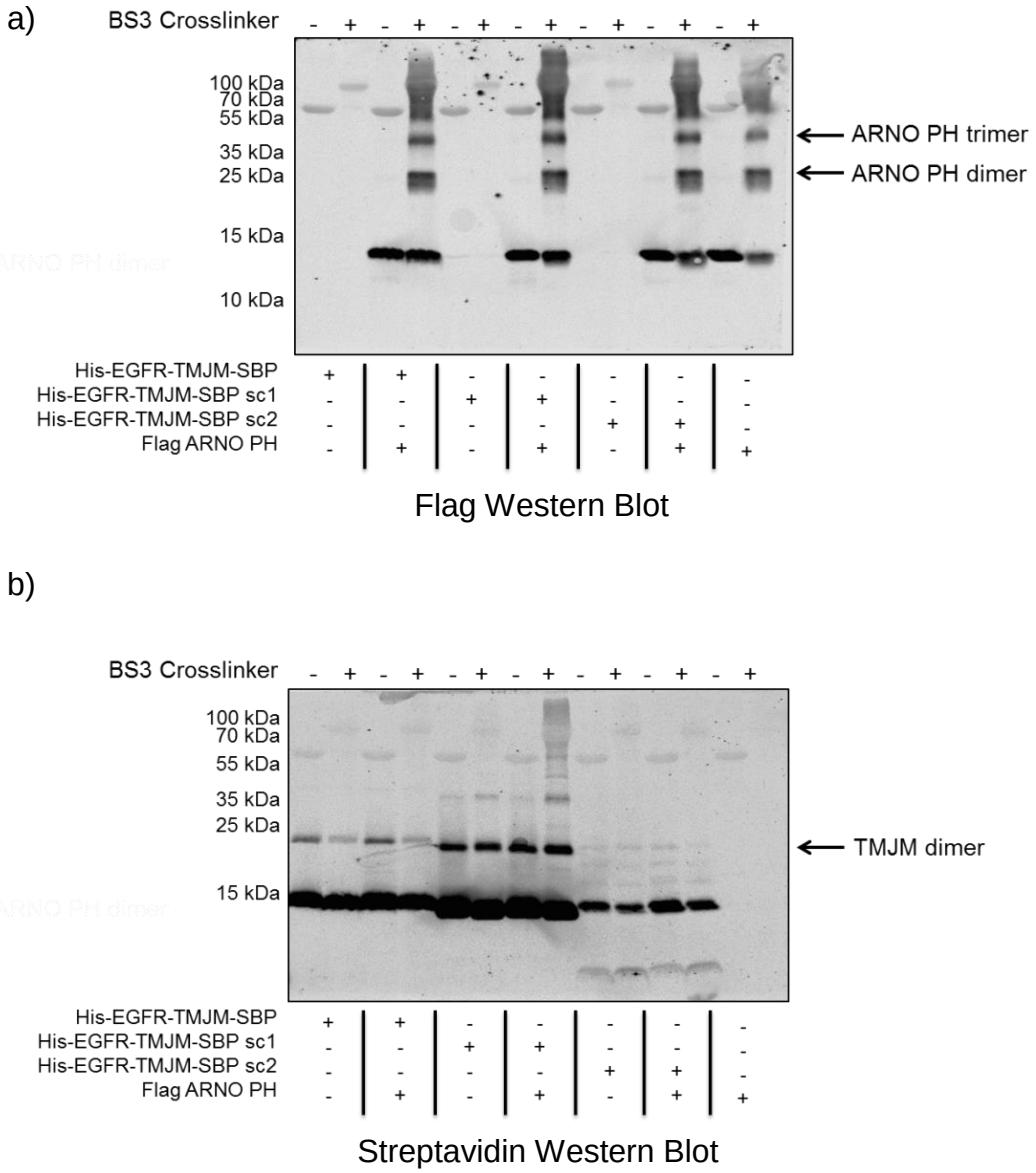

Figure 43: Crosslinking between ARNO PH and EGFR-TMJM wild-type, sc1 and sc2 embedded into bicelles

BS3 was incubated with 10 µM Flag ARNO PH and bicelles containing His-EGFR-TMJM-SBP wild-type and scrambled version 1 (sc1) and 2 (sc2). The TMJM domains contained within bicelles had a concentration of 5 µM. Analysis was performed by SDS-PAGE and **a)** anti-Flag Western Blot detecting the N-terminal part of ARNO PH domain and **b)** streptavidin Western Blot detecting the SBP-labeled EGFR-TMJMs. In figure **a)** no crosslinking between TMJM domains and ARNO PH is visible. Only monomeric, dimeric, and trimeric structures of ARNO PH were visible. In figure **b)** different TMJM concentrations were loaded on to the gel. For this reason, different intensities of TMJM dimers were visible from the Western Blot. Nevertheless, no interaction of ARNO PH with TMJM domains was detected.

ARNO PH as described before is necessary for the membrane recruitment and interaction with PIP_ns. The PH domain of ARNO does not seem to be directly involved in the interaction with the JM domain of the EGFR.

IV.2.3 Nanodiscs

IV.2.3.1 Nanodiscs production with synthetic phospholipids

To increase nanodiscs stability and avoid rapid degradation of phospholipids due to oxidation processes, synthetic phospholipids were used, such as DMPC (1,2-dimyristoyl-*sn*-glycero-3-phosphocholine) or DPPC (1,2-dipalmitoyl-*sn*-glycero-3-phosphocholine). DMPC has a 14:0 fatty chain, while DPPC has a 16:0 fatty chain. Nanodiscs assembly was performed as reported in Section VII.2.5.1.2. Since new phospholipids were used, a further lipid to MSP1D1 titration was necessary. The final MSP:lipid molar ratio used is 1:60 for DMPC and 1:70 for DPPC. Controls for nanodiscs assembly were performed.

IV.2.3.1.1 Analytical gel filtration to verify nanodiscs formation with synthetic phospholipids

FPLC (fast protein liquid chromatography) gel filtration was performed on a Superdex 200 10/300 GL (GE Healtcare) column in MSP standard buffer with a flow rate of 0.4 ml/min. Column calibration was performed using a gel filtration standard from Bio-rad. Catalase, used as control for nanodiscs assembly from Sligar and co-workers (Sligar's Laboratory Website), and γ-globulin present almost the same Stokes diameter, at 10.4 nm and 10.2 nm respectively (Le Maire et al. 2008).

Table 2: Gel filtration protein standards

Protein Standard	Stokes Diameter (nm)	Elution volume (mL)
Thyroglobulin (bovine)	17	8.76
γ-globulin (bovine)	10.2	12.24
Ovalbumin (chicken)	5.6	15.05
Myoglobin (horse)	3.8	17.42

DMPC- and DPPC-nanodisc chromatograms are visible in Figure 44 and 45, respectively.

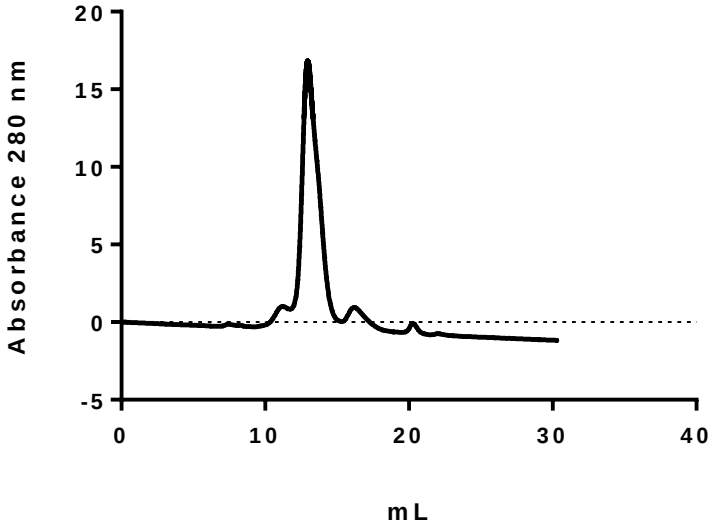

Figure 44: FPLC analytical gel filtration of DMPC-nanodiscs

Gel filtration was performed on Superdex 200 10/300 GL column in MSP standard buffer with a 0.4 ml/min flow rate. The aggregate peak elutes at 11.19 ml. Nanodiscs elute as mainly product at 12.96 ml.

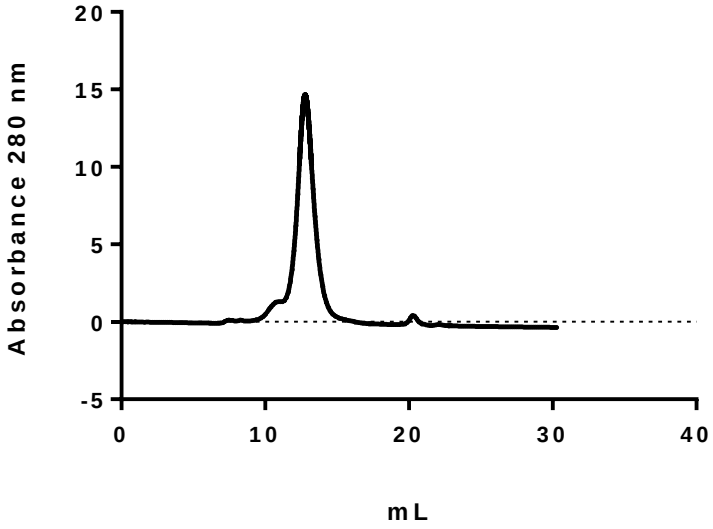

Figure 45: FPLC analytical gel filtration of DPPC-nanodiscs

Gel filtration was performed on Superdex 200 10/300 GL column in MSP standard buffer with a 0.4 ml/min flow rate. The aggregate peak elutes at 11.93 ml. Nanodiscs elute as mainly product at 12.78 ml.

DMPC- and DPPC-nanodiscs presented almost the same elution volume as γ-globulin, with a Stokes diameter of circa 10 nm, as reported in literature (Bayburt, Sligar 2010). A small aggregate peak was eluted at around 12 ml.

IV.2.3.1.2 Dynamic light scattering (DLS) to verify nanodiscs assembly with synthetic phospholipids

Nanodisc assembly was also confirmed via DLS, as reported in Section VII.2.5.3.1 DLS was performed in the group of Professor Gerd Bendas. The measured diameter for DMPC-nanodiscs was 9.87 nm, while DPPC of 11.07 nm. Synthetic nanodiscs show comparable dimensions to the one reported in literature (Bayburt et al. 2002).

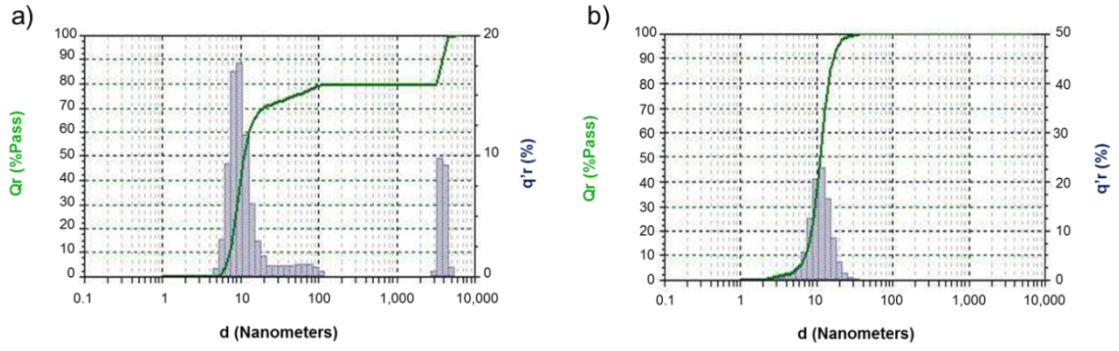

Figure 46: DLS analysis of nanodiscs with synthetic phospholipids

DLS is performed in the laboratory of Professor Gerd Bendas (University of Bonn). The x axis indicates the hydrodynamic diameters of the particles in nanometers. Qr indicates the particle size distribution function in percentage. $q^{l}r$ indicates the frequency distribution of particle size in percentage. **a)** The measured diameter for DMPC-nanodiscs was 9.87 nm with a 79.7 % volume distribution. Aggregate traces were detected at higher molecular range (3.880 µm). **b)** The measured diameter for DPPC-nanodiscs was 11.07 nm with a 100 % volume distribution.

IV.2.3.1.3 Negative Staining Electron Microscopy to verify nanodiscs assembly with synthetic phospholipids

Negative staining electron microscopy was performed in collaboration with Dr. Elmar Behrmann (Center of advanced European studies and research, Bonn) as a further control to confirm the correct nanodisc assembly and to control nanodisc dimensions (Figure 47). For the sample preparation see Section VII.2.5.3.4. Highly diluted nanodisc samples after gel filtration were analyzed in a low salt buffer. The diameter of single nanodisc particles were measured and resulted to be around 10 nm. Nanodiscs of bigger dimensions were measured around 18 nm, probably due to degradative processes occurring during sample preparation. Stacking effects and formation of long nanodisc chains were also observed. This phenomenon was probably caused by the air dryer effect during the sample preparation.

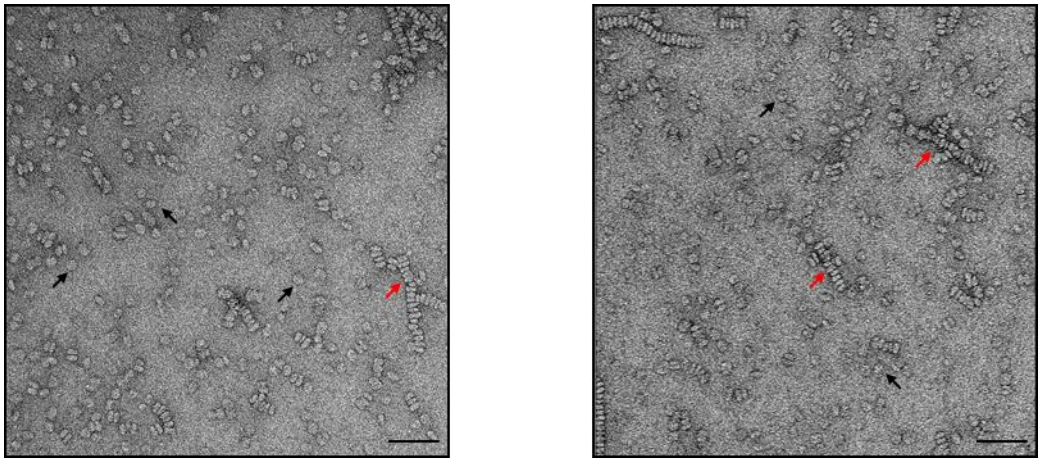

Figure 47: Negative Staining electron microscopy of nanodiscs

Nanodisc assembly was analyzed with negative staining electron microscopy. After gel filtration the samples were stained with uranylformate in low salt buffer. Scale bars indicate 70 nm. Single nanodiscs are indicated with black arrows, while nanodisc chains are indicated with red arrows.

IV.2.3.2 EGFR activity in nanodiscs

IV.2.3.2.1 Insertion of lz-EGFR-TS into nanodiscs

For the preparation of nanodiscs containing lz-EGFR-TS, the protocol reported in Section VII.2.5.2.1 was used. The receptor concentration 1 µM was used for the assembly. To confirm the assembly of the protein within the nanodiscs, an indirect control experiment was performed. Phospholipids and MSP protein with or without lz-EGFR-TS, and the receptor alone were incubated with Amberlite beads. Amberlite beads are used commonly during the nanodiscs formation to remove detergents. Lz-EGFR-TS precipitates if no detergent of lipid environment are present. Nanodiscs, nanodiscs containing lz-EGFR-TS, and lz-EGFR-TS alone were analyzed before and after Amberlite bead incubation and then centrifuged and run on a SDS-PAGE gel (Figure 48).

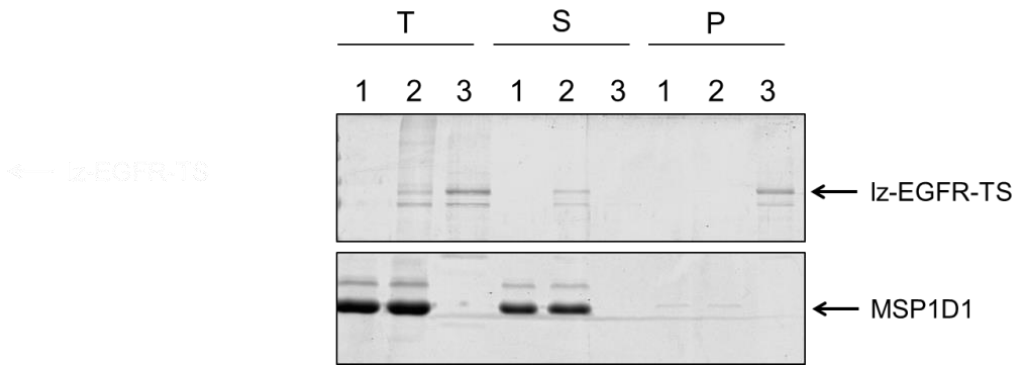

Figure 48: Control of lz-EGFR-TS assembly into nanodiscs

12.5 % SDS-PAGE stained with Coomassie Brilliant Blue. Empty nanodiscs (1), nanodiscs containing lz-EGFR-TS (2) or lz-EGFR-TS alone (3) were incubated overnight with Amberlite beads. Samples of the total mixtures (**T**) before incubation were taken. After overnight incubation, beads were removed and samples of the supernatant (**S**) and precipitates (**P**) were collected. The lz-EGFR-TS remains in solution only when nanodiscs are formed. The protein alone cannot stay in solution without detergent and it is visible in the precipitated fraction.

The lz-EGFR-TS was visible in the precipitated fraction, when no lipids were present. Transmembrane proteins, due to the presence of the hydrophobic domain, cannot stay in solution without detergent or lipids.

Nanodiscs provide a membrane-like environment, allowing the receptor to remain soluble even if the detergent is removed.

Analytical gel filtration was also performed to check the formation of the nanodiscs with lz-EGFR. Samples after gel filtration were collected and analyzed by SDS-PAGE and Coomassie Staining. Due to the high dilution of the samples during the assay and the already low concentration of the receptor used, no protein was detected on the gel (data not shown).

IV.2.3.2.2 Phosphorylation assay in nanodiscs

To test whether nanodiscs were a suitable model for the *in vitro* reconstitution of EGFR, the catalytic activity of lz-EGFR-TS was assayed with a phosphorylation assay. For a detailed protocol see Section VII.2.7.2. The reaction was started by the addition of 1 mM ATP and the activation was measured for 1 min, 3 min, 5 min and 10 min. The reaction was stopped by the addition of 6x SDS-PAGE Sample Buffer. Samples before and after ATP addition were collected and analyzed by SDS-PAGE and Western Blot using an anti-EGFR antibody and an anti-pTyr (phosphor-Tyrosine) antibody (Figure 49). In the pTyr Western Blot, upon ATP addition, it is possible to see a double band, due to the phosphorylation of the receptor.

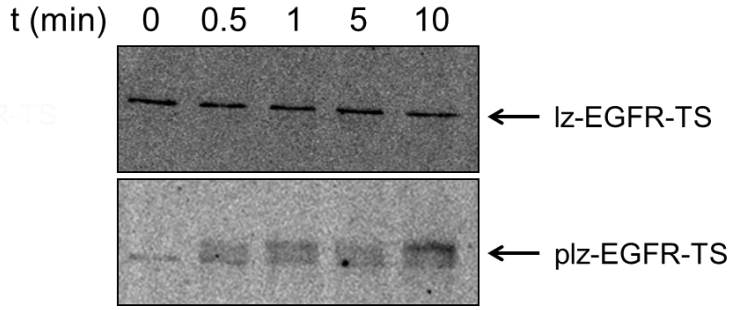

Figure 49: Phosphorylation of lz-EGFR-TS into nanodiscs

Western Blot analysis with anti-EGFR sc03 antibody (upper panel) and pTyr antibody (lower panel). At time 0, the receptor is visible before stimulation. The receptor phosphorylation level increases upon ATP addition after 30 seconds, 1 minute, 5 minutes and 10 minutes of stimulation. The total amount of receptor seemed to decrease upon ATP addition, but the anti-EGFR sc03 antibody binding is inhibited by phosphorylation.

Lz-EGFR-TS after purification exhibited a basal phosphorylation level. For this reason, receptor was dephosphorylated with YopH for further experiments. The kinetics of phosphorylation in nanodiscs seemed to be very slow and weak, compared to the one in micelles.

IV.2.3.2.3 Influence of ARNO on EGFR Phosphorylation in nanodiscs

The ARNO Sec7 influence on EGFR phosphorylation level into nanodiscs was assayed. Bill (2011) reported that ARNO Sec7 enhances lz-EGFR phosphorylation in living cells. To test whether this result is obtained also in nanodiscs, Lz-EGFR-TS was incubated with ARNO Sec7, or Flag-tagged ARNO Sec7, or Flag-tagged ARNO PH as negative control, in presence of 1 mM ATP for 1 minute or 3 minutes (Figure 50).

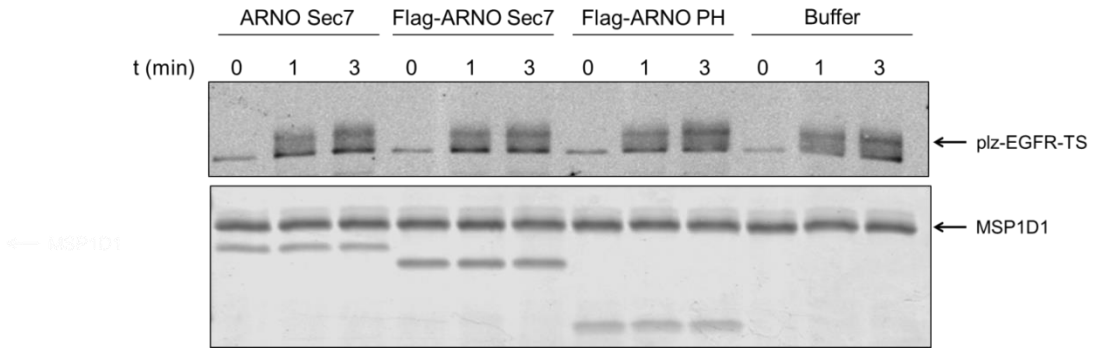

Figure 50: Phosphorylation of lz-EGFR-TS in nanodiscs in presence of ARNO Sec7, or Flag-ARNO Sec7, or Flag-ARNO PH

Western Blot with anti-pTyr antibody (upper panel) and 12.5 % SDS-PAGE stained with Coomassie Brilliant Blue (lower panel). Nanodiscs containing lz-EGFR-TS were incubated with 600 µM ARNO Sec7 (no tag), or 600 µM Flag-ARNO Sec7, or 600 µM Flag-ARNO PH or Buffer in presence of 200 nM YopH. Samples before stimulation (time 0) were taken. The stimulation starts upon 1 mM ATP addition and samples after 1 minute and 3 minutes were taken. No increase of the phosphorylation level in the presence of ARNO Sec7 or Flag-ARNO Sec7 was observed. Proteins are visible from the Coomassie staining. The presence of nanodiscs is indicated by the staining of the membrane scaffold protein.

Samples before and after ATP addition were collected and analyzed with anti-pTyr antibody. Protein presence is indicated with Coomassie staining. Two different Sec7 constructs were used, to exclude any tag influence on the experiment. As expected, ARNO PH has no effect on EGFR phosphorylation. However, an increase of EGFR phosphorylation was not observed after Sec7 addition too.

IV.2.3.3 EGFR-ARNO interaction in nanodiscs

To study if nanodiscs are a suitable model to study protein-protein interactions, the TM domain and the JM segment of the EGFR were embedded into the disc bilayer. The idea was to investigate the interaction between ARNO Sec7 and the JM domain, to elucidate the activation mechanism of EGFR.

IV.2.3.3.1 Insertion of EGFR-TMJM into nanodiscs

For the preparation of nanodiscs containing the transmembrane region of EGFR and the JM domain, a MSP:TMJM molar ratio of 3:1 was used. Nanodiscs containing the peptide were assembled as reported Section VII.2.5.2.2. Due to the small size of the His-EGFR-TMJM-SBP peptide inserted into nanodiscs, no shift in gel filtration chromatogram and no change in the DLS diameter of nanodiscs were observed.

Results

To confirm the correct nanodiscs-peptide assembly, an indirect control experiment was established. The EGFR-TMJM peptide was mixed only with the phospholipids, but no membrane scaffold protein was added to the mixtures. The same steps for nanodisc assembly were performed. After overnight incubation, Amberlite beads were removed and the mixtures were centrifuged for some minutes. Precipitate and supernatant were used for SDS-PAGE (Figure 51a) and streptavidin Western Blot (Figure 51b), recognizing the SBP-tag at the C-terminal part of the EGFR-TMJM construct.

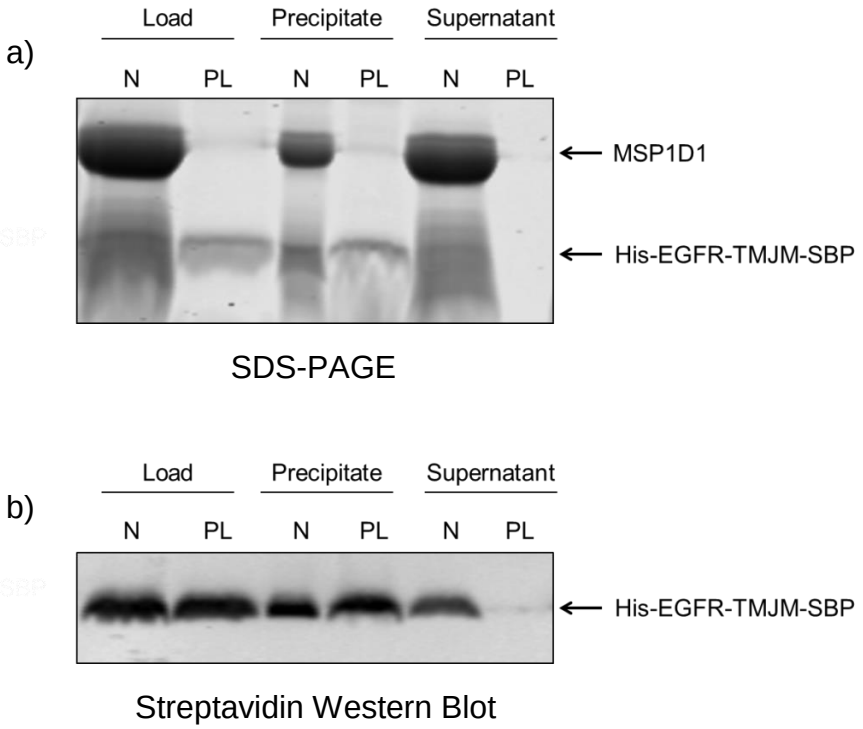

Figure 51: Control of EGFR-TMJM assembly into nanodiscs

A phospholipids-MSP1D1 mixture or phospholipids only were mixed with His-EGFR-TMJM-SBP. DMPC phospholipids were used. Fractions of both mixtures were taken as a loading control. The nanodiscs-TMJM mixture and phospholipids-TMJM mixture were incubated with Amberlite beads overnight. Fractions of the precipitate after centrifugation and of the supernatant were collected. **N**: Nanodiscs; **PL**: Phospholipids. **a)** 15 % SDS-PAGE stained with Coomassie Brilliant Blue. Smearing effects were due to phospholipids. The presence of the nanodiscs is highlighted by the membrane scaffold protein. No EGFR-TMJM band was visible in the supernatant of the lipid fraction. The EGFR-TMJM was not clearly visible in the supernatant of the nanodiscs sample. **b)** Western Blot performed using streptavidin-800 conjugated dye, recognizing the SBP-tag at the C-terminus of the TMJM peptide. The EGFR-TMJM was present only in the supernatant of the formed nanodiscs. Precipitation of the peptide was visible for nanodiscs and phospholipids fractions. No TMJM peptide was visible in the supernatant of the lipid mixture.

TMJM peptide was added in larger amount to be sure that the majority of nanodiscs contained the protein. Precipitation phenomena were visible for both mixtures.

The TMJM peptide stayed in solution only when nanodiscs were properly formed, while no peptide was visible in the Western Blot of the lipid-protein mixture.

IV.2.3.3.2 Pull-down assay to analyze the interaction of ARNO Sec7 with the JM domain of EGFR

IV.2.3.3.2.1 GST pull-down with nanodiscs

DMPC-nanodiscs containing the TM domain and JM region of EGFR were pre-incubated with GST-ARNO Sec7 and subsequently with glutathione beads. A sample of the loaded fraction, supernatant, eluate, and the beads were analyzed by SDS-PAGE and Western-Blot. To increase the binding capacity between nanodiscs containing TMJM and ARNO Sec7, a pull-down assay at 25 °C was performed (Figure 52). The protocol is reported in Section VII.2.9.4.

Lipid motility is increased at temperatures closer to the transition temperature. The transition temperature is defined as the temperature at which the lipids change physical state, from a structured gel phase to a fluid crystalline phase (Avanti Polar Lipids Website b). Close to the transition temperature, the membrane fluidity increases and therefore the interaction between membrane proteins and cytosolic proteins can be influenced (Simons, Vaz 2004). For DMPC, the transition temperature is 24 °C, for this reason the experiment was performed at room temperature.

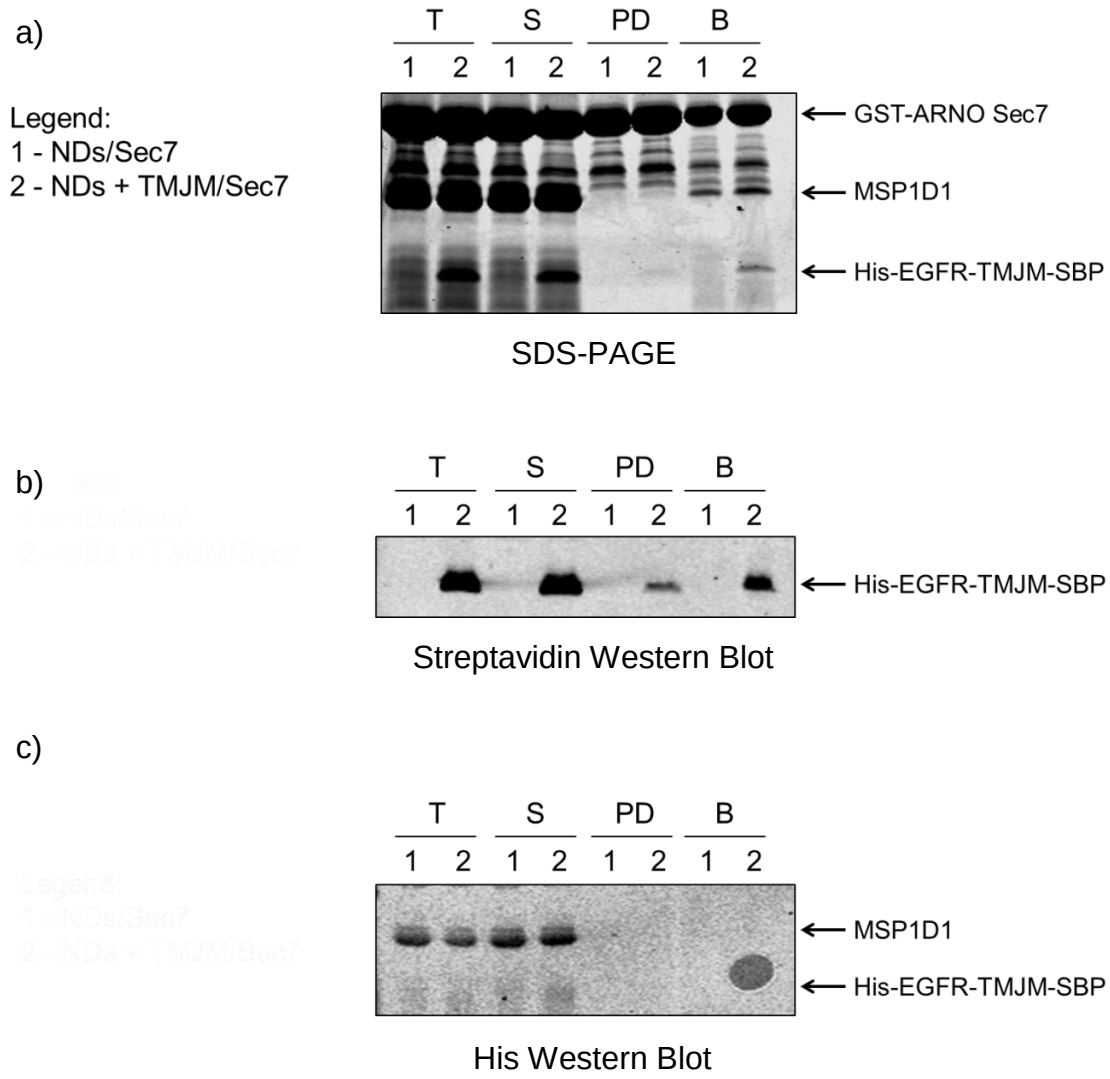

Figure 52: GST pull-down at 25 °C with DMPC-nanodiscs to analyze TMJM-Sec7 interaction

The pull down assay was performed with catalytically active GST-ARNO Sec7 and His-EGFR-TMJM-SBP containing nanodiscs (NDs+TMJM). Empty nanodiscs (NDs) were used as a control. Glutathione beads were incubated with nanodiscs with (+) or without (-) the TMJM domain and GST-ARNO Sec7 at 25 °C for 1 hour. The total protein (**T**), supernatant after beads incubation (**S**), pull-down (**PD**) and beads (**B**) fractions were collected and analyzed. **a)** 15 % SDS-PAGE stained with Coomassie Brilliant Blue. GST-ARNO Sec7, the scaffold protein of nanodiscs and the TMJM domain were visible. **b)** Western Blot performed with streptavidin-800 conjugated dye, recognizing the SBP-tag at the C-terminus of TMJM peptide. The TMJM domain was visible in the pull-down fraction. **c)** Western Blot performed with anti-His antibody detecting the N-terminal part of MSP1D1 protein and the N-terminal part of His-EGFR-TMJM-SBP construct. MSP1D1 was detected only in the total fraction and supernatant.

From the Coomassie staining (Figure 52a), GST beads showed low binding capacity, because almost the same band intensity was visible before and after beads incubation. In the pull-down fraction, a very weak band was visible for the TMJM

domain. No MSP1D1 band was visible in neither the pull-down fraction and in the bead fractions.

In the streptavidin Western Blot (Figure 52b) the TMJM co-eluted with Sec7. Unspecific binding of the EGFR-TMJM was visible in the bead fraction.

Also a Western Blot analysis using an anti-His antibody recognizing the N-terminal part of the membrane scaffold protein and the N-terminal part of the EGFR-TMJM was performed (Figure 52c). MSP1D1 was present only in the total fraction and in the supernatant. EGFR-TMJM was not detected, due to the low antibody sensitivity.

Furthermore, no MSP1D1 was detected in the pull-down and beads fraction in neither the SDS-PAGE and in the anti-His Western Blot. However, the TMJM was visible in the pull-down fraction of the streptavidin Western Blot, suggesting that the TMJM domain could be pulled out from the nanodiscs during the binding. The interaction might be sufficient to pull out the peptide form the lipid bilayer.

To understand if this problem could be due to the fact that DMPC-bilayer was not thick enough to allow the proper insertion of TMJM, DPPC-nanodiscs were used. DPPC, as previously mentioned, has a longer fatty acid chain of 16:0, compared to the 14:0 chain of DMPC. DPPC-nanodiscs with or without EGFR-TMJM, were incubated with GST-ARNO Sec7 or GST protein as a negative control at 37 °C (Figure 53). This temperature was chosen for two reasons: first, the lipid motility at this temperature is comparable to the physiologic one; second, DPPC has a transition temperature of 41 °C and the membrane fluidity should be high enough to allow a better interaction, but since it is not above the transition temperature, the peptide removal from the bilayer via Sec7 is avoided.

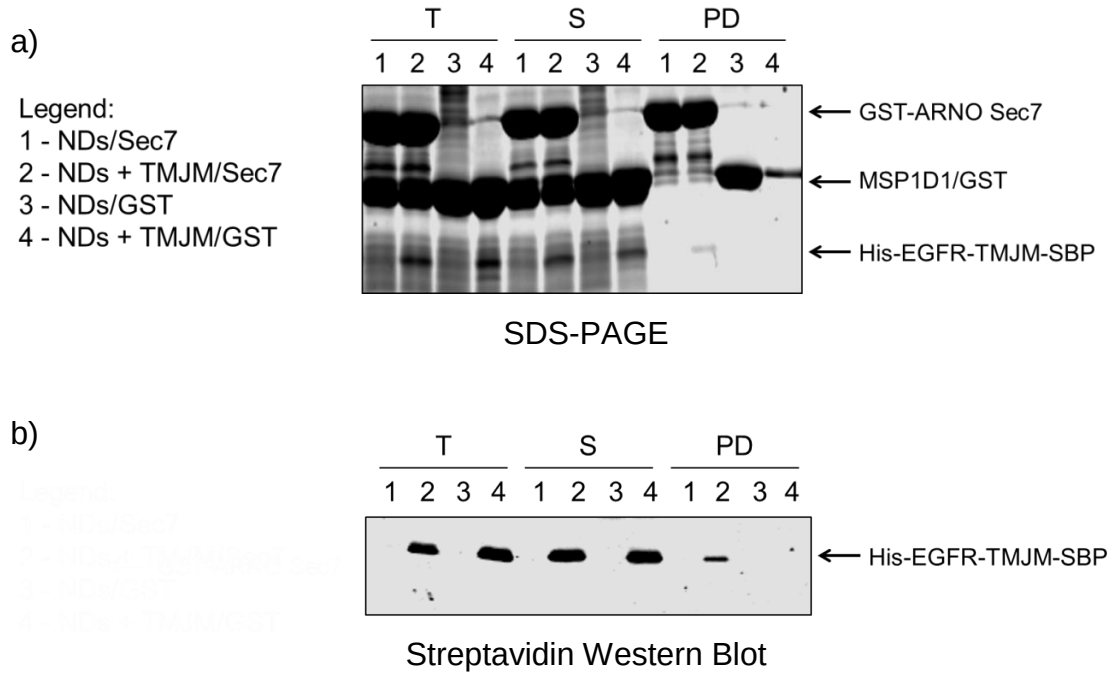

Figure 53: GST pull-down at 37 °C with DPPC-nanodiscs to analyze TMJM-Sec7 interaction

Glutathione beads were incubated with nanodiscs with (NDs+TMJM) or without (NDs) the TMJM domain and GST-ARNO Sec7 or GST protein as negative control at 37 °C for 1 hour. The total protein (**T**), supernatant after bead incubation (**S**) and pull-down (**PD**) fractions were collected and analyzed. **a)** 15 % SDS-PAGE stained with Coomassie Brilliant Blue. Four different proteins are visible in the total protein fractions: GST-ARNO Sec7, GST protein and nanodiscs scaffold protein, running at the same molecular weight, and EGFR-TMJM-SBP protein. In the pull-down fraction, TMJM peptide was visible only where DPPC-nanodiscs were incubated with ARNO-Sec7. The last lane, in which GST and nanodiscs with TMJM were loaded, was broken and part of the fraction was lost. **b)** Streptavidin Western Blot was performed with streptavidin-800 conjugated dye, recognizing the SBP-tag at the C-terminus of TMJM peptide. TMJM domain was visible in the pull-down fraction only in presence of ARNO Sec7. No unspecific binding between GST and TMJM was detected.

With DPPC-nanodiscs at 37 °C, the interaction between ARNO Sec7 and TMJM was weak but specific. No interaction of TMJM with GST protein was detected.

Comparing the pull-down assays performed at 25 °C and 37 °C, the co-elution between ARNO Sec7 and TMJM was higher at 37 °C with DPPC-nanodiscs. Since the membrane scaffold protein is an N-terminal truncated form of the human Apolipoprotein A-1 (Apo A-1), to verify the presence of MSP1D1 in the pull down fraction, a Western Blot using anti-Apo A-1 antibody was performed (data not shown). The antibody showed high unspecific binding and it was not possible to confirm the presence of the scaffold protein in the pulled down fractions. Since no other antibody was commercially available for MSP1D1 and the anti-His antibody previously used was unspecific, the detection of the protein in the pulled down fraction was not possible.

IV.2.3.3.2.2 Ni-NTA pull-down with nanodiscs

In order to test if the weak interaction shown in the GST-pull down was due to the low elution capacity, other beads for the pull-down were tested. Furthermore, to avoid the possibility that the TMJM was pulled out of the nanodiscs during the interaction with ARNO Sec7, the His-tag at the N-terminal part of the His-EGFR-TMJM-SBP was anchored to the Ni-NTA agarose beads for the pull-down. The His-tag of MSP1D1 was previously removed by TEV cleavage. A detailed protocol is reported in Section VII.2.9.5. DPPC-nanodiscs with or without the TMJM peptide were pre-incubated at 37 °C with the beads. After the pre-incubation, GST-ARNO Sec7 was added. In Figure 54, the SDS-PAGE and the GST Western Blot of the fractions are shown.

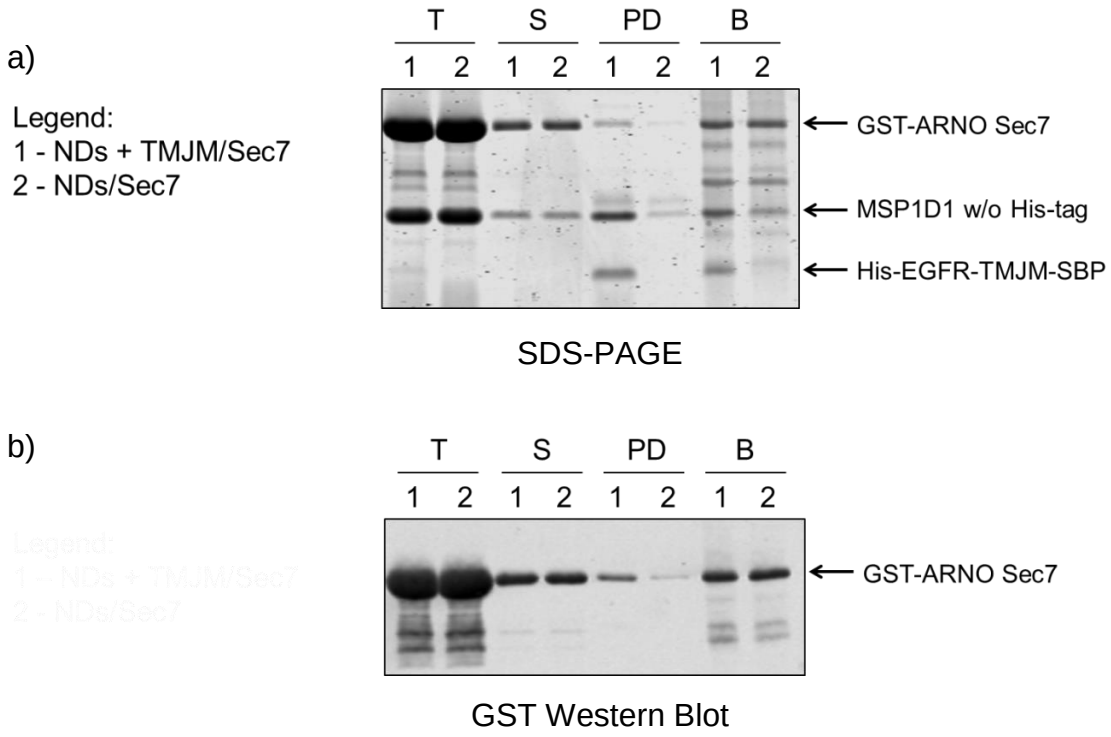

Figure 54: Ni-NTA Agarose beads pull-down at 37 °C to analyze TMJM-Sec7 interaction

The pull down assay was performed with catalytically active GST-ARNO Sec7 and His-EGFR-TMJM-SBP containing nanodiscs (NDs+TMJM). Empty nanodiscs (NDs) were used as control. MSP1D1 had no His-tag (w/o His-tag). This experiment was performed by the student Kevin Baβler, under my direct supervision. Ni-NTA Agarose beads were incubated with nanodiscs with or without the TMJM domain and GST-ARNO Sec7 at 37 °C for 1 hour. The total protein (**T**), supernatant after beads incubation (**S**), the pull-down (**PD**) and bead (**B**) fractions were collected and analyzed. **a)** 15 % SDS-PAGE stained with Coomassie Brilliant Blue. Three different proteins are visible in the total protein fractions: GST-ARNO Sec7, the nanodiscs scaffold protein, and His-EGFR-TMJM-SBP protein. ARNO Sec7 co-eluted only where TMJM was present. **b)** A Western Blot using an anti-GST antibody was performed. A higher GST-ARNO Sec7 amount was eluting in presence of the TMJM domain.

Results

GST-ARNO Sec7 eluted in higher amounts in presence of the EGFR-TMJM domain. Unspecific interactions of ARNO Sec7 with the nanodiscs or the Ni-NTA beads were visible in the pulled down fraction. From the Coomassie staining, it was visible that MSP1D1 was co-eluting with TMJM, indicating that the peptide was not removed from the bilayer upon interaction.

The same experiment was repeated at 25 °C, but no specific co-elution between ARNO and EGFR was detectable (data not shown). These findings support the idea that the temperature has a high contribution on the interaction and membrane fluidity. These preliminary results support the theory that the JM region interacts specifically but in a weaker and transient way with ARNO Sec7.

Due to challenges in increasing the pull-down efficiency and in reproducing the experiment using other types of Ni-NTA beads, other approaches were used to verify the interaction between ARNO Sec7 and the JM domain of EGFR.

IV.2.3.3.3 Crosslinking to analyze the interaction of ARNO Sec7 with the JM domain of EGFR

Nanodiscs containing the TMJM region of the EGFR were crosslinked with ARNOΔPBR (for a detailed protocol see Section VII.2.10.3). BS3 was used at the concentration of 0.5 mM for 5 minutes to crosslink ARNOΔPBR and EGFR-TMJM embedded into nanodiscs (Figure 55).

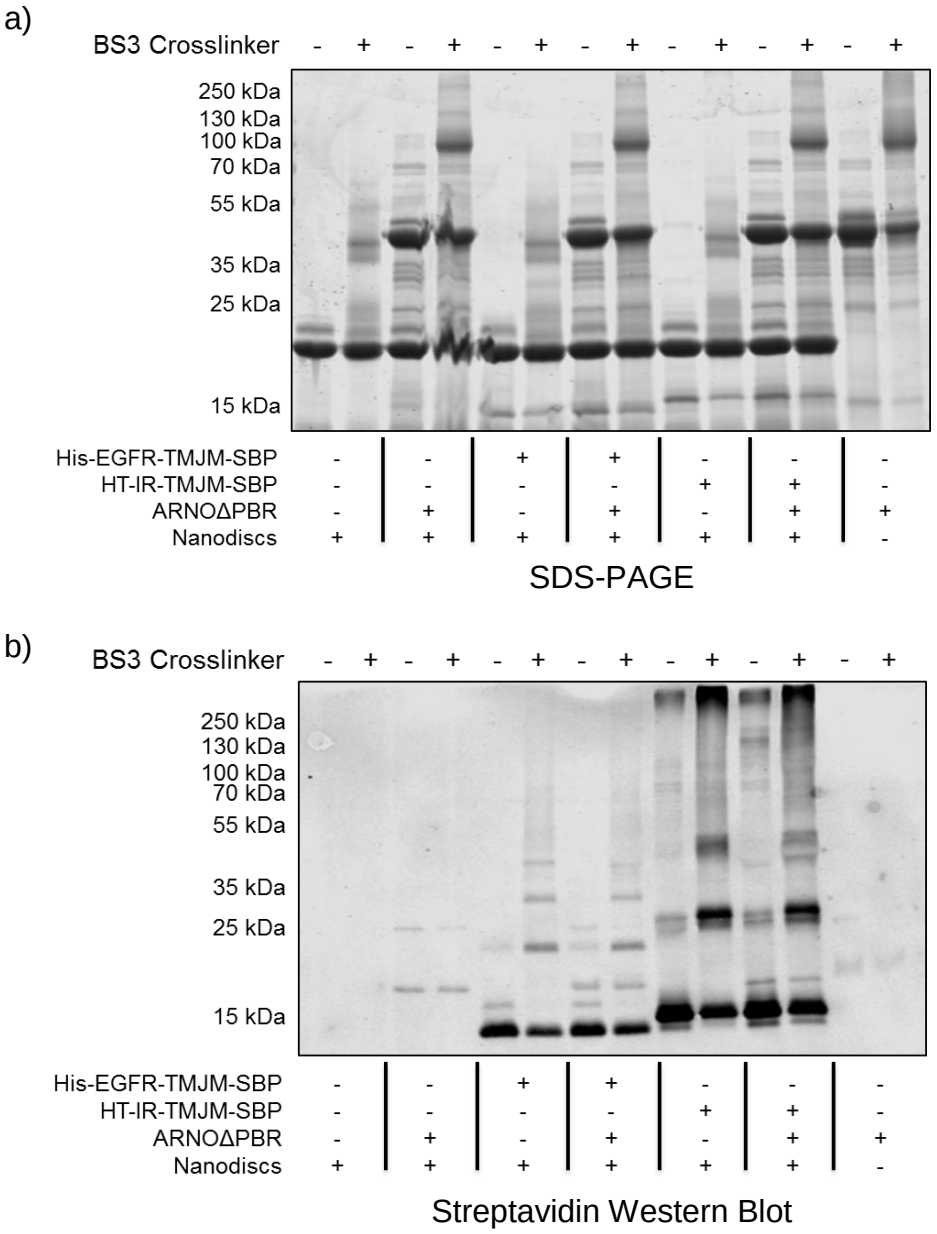

Figure 55: BS3 crosslinking with nanodiscs containing EGFR-TMJM and ARNOΔPBR

BS3 crosslinker at the concentration of 0.5 mM was incubated with 30 µM ARNOΔPBR and 20 µM nanodiscs containing His-EGFR-TMJM-SBP or HT-IR-TMJM-SBP (negative control). Samples before and after addition of the crosslinker were collected and analyzed by **a)** 15 % SDS-PAGE stained with Coomassie Brilliant Blue and **b)** Western blot using a streptavidin-800 conjugated dye. No crosslinking between ARNO and EGFR-TMJM was visible using BS3 crosslinker.

After BS3 addition, the gel analysis was complicated by the presence of a variety of different crosslinked bands. Nanodiscs containing HT-IR-TMJM-SBP were used as a negative control. The EGFR-TMJM was visible at 14 kDa. Before crosslinker addition, EGFR-TMJM as a dimer was present at around 25 kDa. A similar behavior was already seen for TMJM-micelles. MSP1D1 of nanodiscs has a molecular weight of 24 kDa. Upon BS3 addition, the crosslinking band of MSP1D1 was visible around 45 kDa.

ARNOΔPBR crosslinked at ~100 kDa. For a 1:1 complex between ARNO and EGFR-TMJM, it was expected a crosslinked band around 60 kDa, as already seen in bicelles (see Section IV.2.2.2.1), but no interaction was visible. HT-IR-TMJM-SBP had a similar molecular weight of EGFR-TMJM, and also for this peptide, there was already a dimerized construct at ~25 kDa. High molecular aggregates were also visible on the upper part of the gel. As expected, no crosslinking was observed between HT-IR-TMJM-SBP and ARNOΔPBR.

In order to understand if the difficulty in observing the interaction in nanodiscs with BS3 crosslinker was due to the fact that the JM region was inserted too deeply inside the phospholipid bilayer, a membrane permeable crosslinker was used. DSS (dissucimidyl suberate) is the membrane permeable analogue of BS3. DSS at a concentration of 0.5 mM was incubated for 5 minutes in the presence of 30 μM ARNOΔPBR and nanodiscs containing His-EGFR-TMJM-SBP or HT-IR-TMJM-SBP as a negative control.

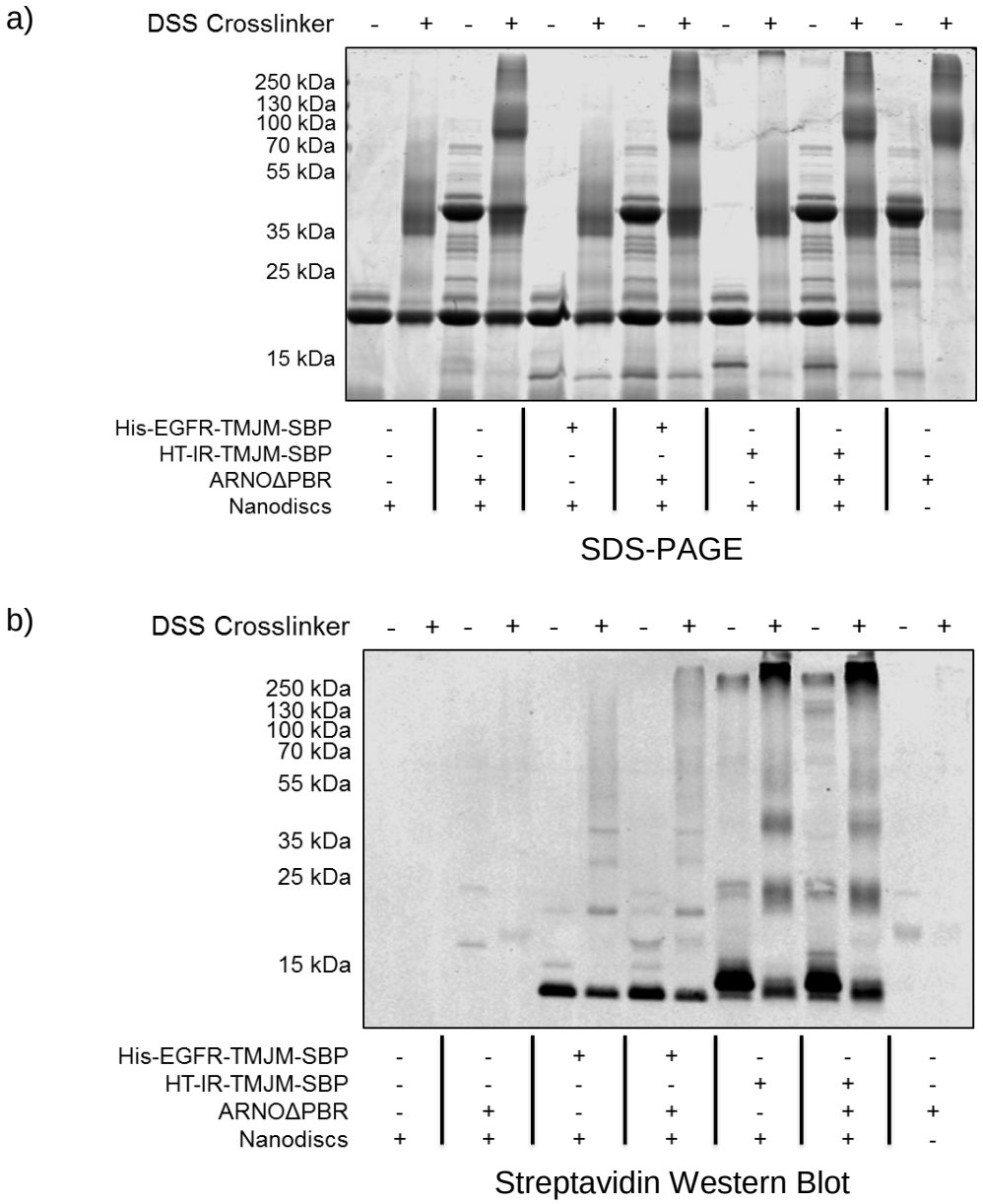

Figure 56: DSS crosslinking of nanodiscs containing EGFR-TMJM and ARNOΔPBR

DSS crosslinker at the concentration of 0.5 mM was incubated with 30 µM ARNOΔPBR and 20 µM nanodiscs containing His-EGFR-TMJM-SBP or HT-IR-TMJM-SBP (negative control). Samples before and after addition of the crosslinker were collected and analyzed with **a)** 15 % SDS-PAGE stained with Coomassie Brilliant Blue and **b)** Western blot using a Streptavidin-800 conjugated dye. No crosslinking between ARNO and EGFR-TMJM was visible using a membrane permeable crosslinker.

As previously reported, the expected crosslinked band for a 1:1 complex should be visible at around 60 kDa. Also using a membrane permeable crosslinker, no interaction between EGFR-TMJM and ARNO was visible. The same crosslinking behavior of BS3 was observed as well for the non-water soluble analogue DSS. The crosslinking in nanodiscs is not a suitable method to analyze ARNO-EGFR interactions.

IV.2.3.3.4 Microscale Thermophoresis (MST) to analyze the interaction of ARNO Sec7 with the JM domain of EGFR

Another technique, microscale thermophoresis (MST), was used to verify the interaction between ARNO Sec7 and the JM domain of the EGFR into nanodiscs.

MST measures the motion of molecules in solution when a temperature gradient is generated. Different parameters are important to determine thermophoretic movement: hydration shells, charge, and size of the molecules (Duhr, Braun 2006). Molecules to be detected have to be labeled with florescent dyes. The intrinsic tryptophan fluorescence can also be used. The interaction between one or more molecules affect the thermophoretic movements and a change in the fluorescence intensity can be detected (Jerabek-Willemsen et al. 2011). MST has the advantage that a small amount of protein and low concentrations of the interacting partners are required.

To perform MST, the MSP1D1 of nanodiscs was expressed and purified as a C-terminal fusion construct with the monomeric enhanced green fluorescence protein (MSP1D1-mEGFP). A further gel filtration step on a Superdex 200 10/300 GL column was necessary to remove the aggregates formed during nanodisc production. To estimate the labeled moiety, a dilution series of nanodiscs after gel filtration was analyzed with MST. The eluted nanodiscs were diluted 20 times in buffer and directly used to perform MST experiments. DPPC-nanodiscs containing the TMJM domain of EGFR or empty discs used as a negative control were incubated with different ARNO Sec7 concentrations from 50 µM to 1.5 nM. Three different MST powers (20 %, 40 % and 60 %) with a 20 % LED (Light Emitting Diode) power were used. In Figure 57 the typical thermophoresis (with temperature jump) results are reported. Exactly the same thermophoresis behavior was observed for the empty nanodiscs and for the nanodiscs containing the TMJM domain. No specific interaction between Sec7 and JM was detected. The same thermophoresis behavior is probably due to unspecific binding. To reduce the unspecific interaction, the measurement was repeated in presence of 1.5 mg/mL BSA, but no variation in the curves was visible (data not shown).

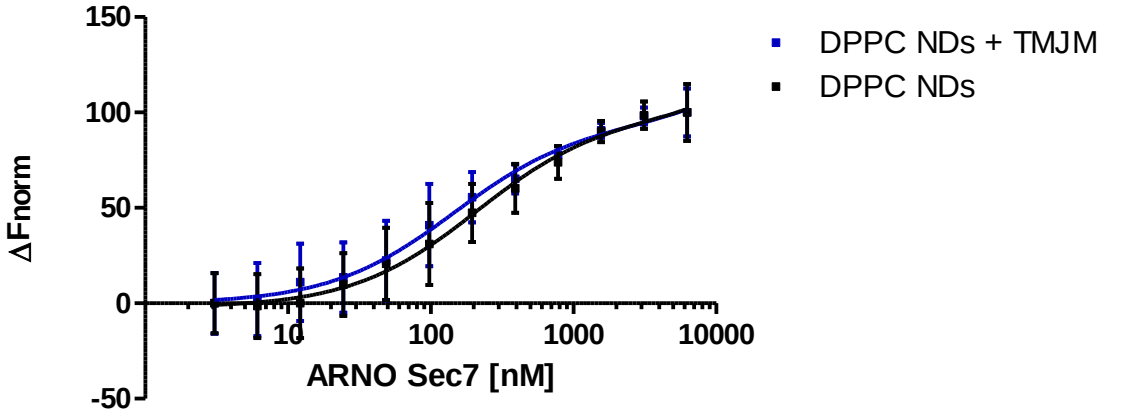

Figure 57: MST analysis of DPPC NDs containing EGFR TMJM and ARNO Sec7

MST analysis was performed in MSP standard buffer at 25 °C with 20 % LED power and 40 % MST power. Gel filtrated DPPC nanodiscs (NDs) labeled with GFP were used. Serial dilutions of nanodiscs after gel filtration were performed to establish the fluorescence moiety. NDs were diluted 1:20 after gel filtration. The thermophoresis with temperature-jump is shown as normalized fluorescence (ΔFnorm) and is plotted against the logarithmic ARNO Sec7 concentration. The data of two independent experiments are shown as mean±SEM. Almost the same behavior was observed for empty DPPC NDs (blue curve) and TMJM containing NDs (black curve), probably due to unspecific interactions.

Due to the difficulties in studying the interaction of JM domain with ARNO Sec7 in nanodiscs, other membrane model systems were used.

IV.2.4 Membrane Sheets

Membrane sheets are native plasma membranes adherent to a glass support. Cells which adhered to coverslips, are then subjected to a short ultrasound pulse and only the basal membrane remains attached to the support (Zilly et al. 2011). The following experiments were performed with the collaboration of Professor Thorsten Lang (Life and Medical Sciences Institute, University of Bonn).

Membrane sheets constitute the most complex *in vitro* membrane system to study protein clustering, protein-protein, and protein-lipid interactions. Membrane sheets were used to test the activity of EGFR upon the addition of ARNO and the interaction between the two proteins. For all the following experiments 20-35 membrane sheets for each coverslips were analyzed.

IV.2.4.1 EGFR activity on membrane sheets incubated with ARNO

EGFR activity was assayed using membrane sheets. HeLa membrane sheets were prepared as reported in Paragraph VII.2.6. Different experimental approaches were tested for assay optimization. Initially, the membrane sheets were pre-incubated for 5 minutes with buffer containing 1 mM Na-orthovanadate, a phosphatase inhibitor. The reaction was started by adding 1 mM ATP in the presence of 12.5 ng/ml, 25 ng/ml or 50 ng/ml EGF and stopped after 1 minute (Figure 58). Phosphorylated EGFR was measured with anti-pTyr1086 antibody. Samples were imaged by fluorescence microscopy.

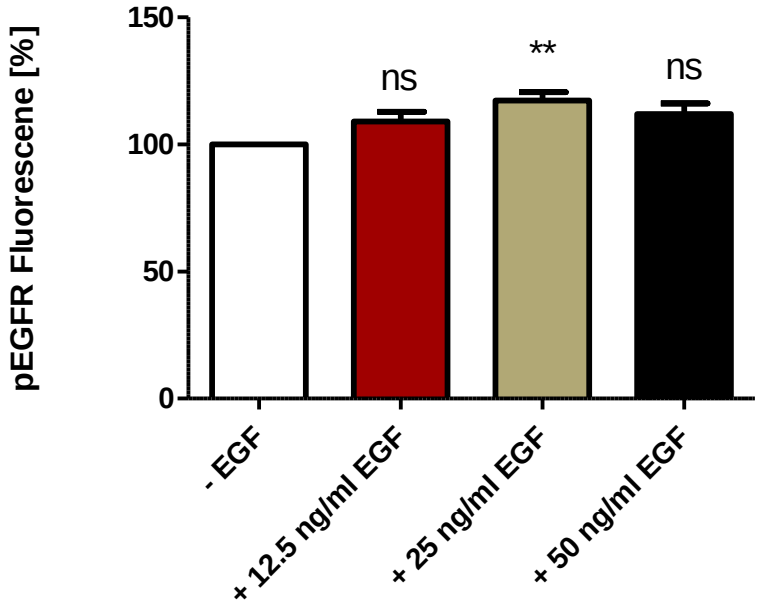

Figure 58: EGFR phosphorylation on HeLa membrane sheets with pre-incubation and stimulation with different EGF concentrations for 1 minute (n=3)

HeLa membrane sheets were pre-incubated for 5 minutes in buffer in presence of 1 mM of phosphatase inhibitor (Na-othovanadate). Then, the membrane sheets were stimulated for 1 minute with 1 mM ATP and three different EGF concentrations: 12.5 ng/ml, 25 ng/ml and 50 ng/ml, respectively. The phosphorylation of EGFR was measured with anti-pTyr1086 antibody. The bar chart shows the mean±SEM. Significance is calculated with one way ANOVA on Rank analysis. There is a statistically significant difference (p=0.006). The columns were compared with Dunn's Method. The comparison between the column 1 and column 2, column 1 and 3, and column 1 and 4 are reported (ns: not significant; **:$p<0.01$). No relevant increase of EGFR phosphorylation was observed.

The receptor was already in a highly active state prior to stimulation. For this reason no EGF-dependent EGFR stimulation was observable. EGFR activity was completely maximized during the pre-incubation time.

The experiment was repeated stimulating the receptor in the presence of 50 ng/ml EGF and 1 mM ATP for 1 minute, without pre-incubation (Figure 59). Furthermore, the influence of ARNO on the phosphorylation level of the EGFR was observed. HeLa membrane sheets were incubated with 100 nM ARNO full-length and stimulated with 50 ng/ml EGF and 1 mM ATP for 1 minute.

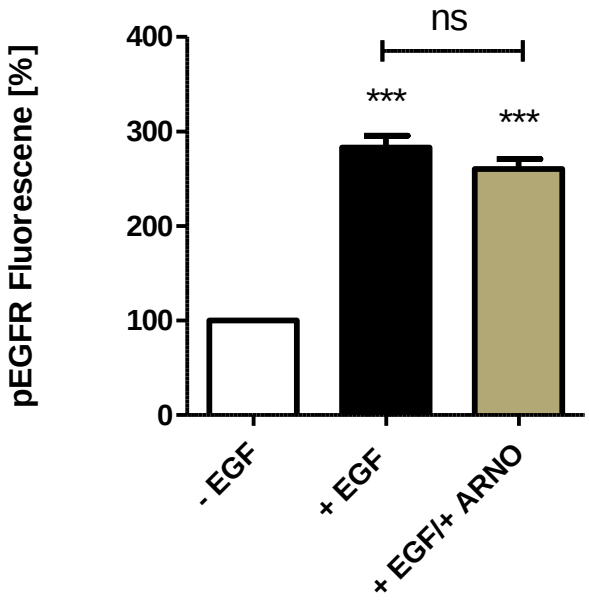

Figure 59: EGFR phosphorylation on HeLa membrane sheets without pre-incubation, in presence of 100 nM of ARNO (n=3)

HeLa membrane sheets were stimulated for 1 minute with 1 mM ATP and 50 ng/ml EGF with or without 100 nM ARNO. The phosphorylation of EGFR was measured with anti-pTyr1086 antibody. The bar chart shows the mean±SEM. Upon EGF addition, there was a three times increase of the phosphorylation level of the EGFR. No ARNO-dependent EGFR phosphorylation was observed. Significance is calculated with one way ANOVA on Rank analysis. There is a statistically significant difference ($p<0.001$). The columns were compared with Dunn's Method. The comparison between the column 1 and column 2, column 1 and 3, column 2 and 3, are reported (***: $p<0.001$; ns: not significant).

The receptor on membrane sheets was active, and upon EGF addition, gave a twofold increase in phosphorylation. The results showed that ARNO has no influence on EGFR phosphorylation on HeLa membrane sheets.

To exclude the cell-type influence, the same experiment with H460 cells was repeated (Figure 60).

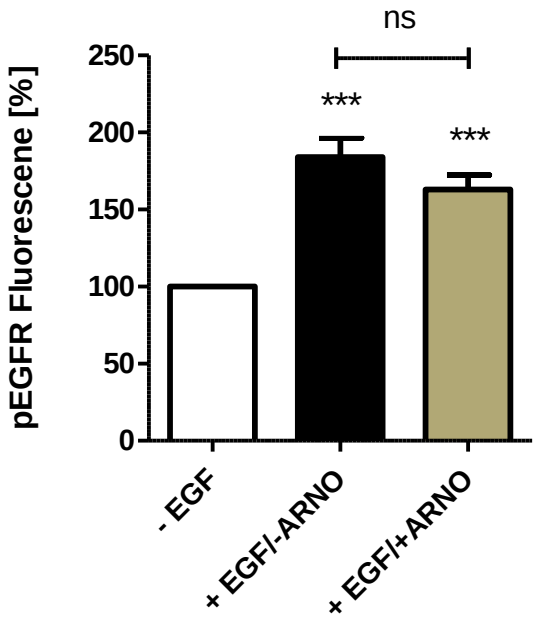

Figure 60: EGFR phosphorylation on H460 membrane sheets in presence of 100 nM of ARNO (n=2)

H460 membrane sheets were stimulated for 1 minute with 1 mM ATP and 50 ng/ml EGF with or without 100 nM ARNO. The phosphorylation of EGFR was measured with anti-pTyr1086 antibody. The bar chart shows the mean±SEM. No ARNO-dependent EGFR phosphorylation was observed. Significance is calculated with one way ANOVA on Rank analysis. There is a statistically significant difference ($p<0.001$). The columns were compared with Dunn's Method. The comparison between the column 1 and column 2, column 1 and 3, column 2 and 3, are reported (***: $p<0.001$; ns: not significant).

In H460, a similar increase in phosphorylation (nearly 100 %) was observed upon EGF addition. Nevertheless, ARNO has no effect on EGFR phosphorylation on membrane sheets.

IV.2.4.2 EGFR-ARNO co-localization on membrane sheet

Since ARNO had no effect on EGFR activation on membrane sheets, it was analyzed if ARNO co-localized at the plasma membrane with EGFR. HeLa cell line prepared membrane sheets were used for this purpose. Flag-ARNO at the concentration of 1 µM was incubated on membrane sheets for 5 minutes. Membrane sheets were stained with anti-EGFR antibody and anti-Flag antibody for ARNO detection. The Figure 61 shows representative images for membrane sheets incubated with buffer as a negative control or with Flag-ARNO. EGFR was stained in green, while ARNO in red and imaged with fluorescence microscopy. When membrane sheets were incubated with buffer, no co-localization between EGFR and ARNO channel was visible. When ARNO was added,

merging images, the overlapping spots in the red (ARNO) and green (EGFR) channel appear yellow. The co-localization results are represented graphically with a scatterplot (Figure 62). In the diagram, the pixel intensity of the red channel (x-axis) is plotted against the green pixel intensity (y-axis) of the background corrected membrane mean intensities. In a scatterplot, if co-localization between two proteins is present, the points cluster around a straight line, as is seen with ARNO and EGFR. In the buffer control, the points were localized in a small group, with no influence from the red channel (ARNO) on distribution.

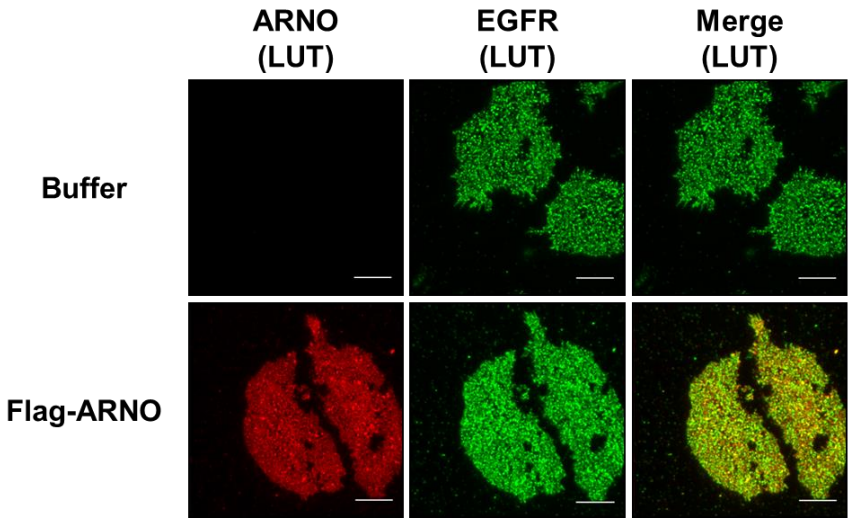

Figure 61: Representative images for Flag-ARNO co-localization with EGFR on HeLa membrane sheets

HeLa membrane sheets were incubated with 1 µM Flag-ARNO. ARNO was stained in red (using anti- Flag antibody to detect the N-terminal tag of ARNO), while EGFR was stained in green (using anti-EGFR sc03 antibody). The overlap between the two channels is indicated as "merge". In yellow is indicated the co-localization between ARNO and EGFR. No co-localization was visible when the membrane sheets were incubated with buffer. All the pictures are shown with the same lookup tables (LUT). The scale bar indicates 7.5 µm.

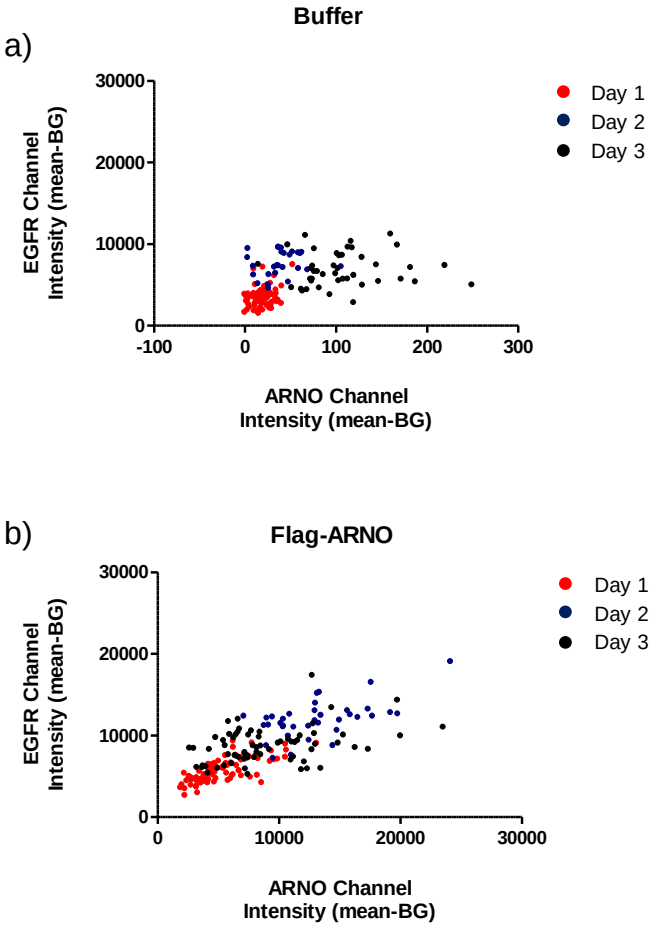

Figure 62: Scatterplot of the EGFR mean pixel intensity (y-axis) and ARNO pixel intensity (x-axis) of Flag-ARNO of background subtracted mean membrane sheet (mean-BG) intensity (n=3)

Scatterplot of three different experiments: day 1 in red, day 2 in blue and day 3 in black.
a) When membrane sheets were incubated only with buffer, no influence of the ARNO channel is visible on the scatterplot. **b)** The scatterplot of the membrane sheets incubated with ARNO shows points clustering around a straight line, indicating an equal contribution from the two channels for the total intensity.

To quantify the correlation between ARNO and EGFR, the Pearson's correlation coefficient (PCC) was used. The PCC was calculated with the following formula:

$$PCC = \frac{\sum_i (R_i - \bar{R}) \times (G_i - \bar{G})}{\sqrt{\sum_i (R_i - \bar{R})^2 \times \sum_i (G_i - \bar{G})^2}}$$

R refers to the intensity of the pixel, i, of the red channel and G to the pixel intensities of the green channel. $\bar{R}$ and $\bar{G}$ are the mean intensities of the red and green channel, respectively. PCC has values ranging from 1, for a perfect co-localization, to -1 for intensity inversely related. PCC values around 0 indicate no correlation between the two

intensities (Dunn et al. 2011). In Figure 63, the PCC for the co-localization of ARNO and EGFR in region of intersest (ROIs, 50x50 pixel) on the membrane, is reported.

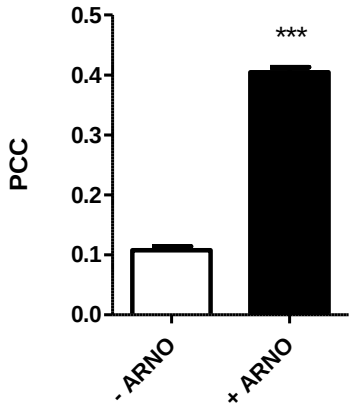

Figure 63: Pearson's correlation coefficient for ARNO and EGFR on HeLa membrane sheets within ROIs (n=3)

The PCC is calculated with the formula reported above within defined region of interest, termed ROI (50x50 pixels). When ARNO was not incubated with the membrane sheets, the PCC had a value around 0, indicating no correlation between the two proteins. Upon ARNO incubation, the PCC reached a value of 0.42, indicating a moderate degree of correlation between ARNO and EGFR. Significance calculated with Mann-Whitney test. (***: $p<0.001$ with $p<0.0001$).

The PCC calculated for ARNO-EGFR was 0.42, indicating a moderate degree of correlation between the two proteins.

IV.2.4.3 The effect of ARNO on EGFR clustering

Many membrane proteins organize themselves at the plasma membrane in microdomains or clusters. Cluster formation is controlled by lipid-lipid, protein-lipid, and protein-protein interactions (Zilly et al. 2011). The mechanism of cluster formation currently is not entirely understood. A recent study shows that EGFR can cluster at the plasma membrane due to the interaction between the JM region and anionic phospholipids, such as PIP_2 (Wang et al. 2014).

During the co-localization analysis of ARNO with EGFR on membrane sheets, another phenomenon was observed. A preliminary way to analyze membrane clustering on membrane sheets, using fluorescence microscopy, is to calculate the relative standard deviation (RSD) of EGFR channel intensity. The RSD is calculated within 50x50 pixel ROIs with the following formula:

$$RSD = \frac{SD_i}{(M_i - B_i)}$$

Where SD is the membrane standard deviation of the pixel intensity, i, of the channel. M is the intensity of the membrane ROI and B the intensity of the background ROI. The RSD gives information about the degree of clustering. Low RSD values indicate a homogenous pixel intensity distribution within a ROI, while high RSD values indicate that the pixel intensity is concentrated in spots, representing the protein cluster areas.

During the co-localization experiments, it was observed that the RSD of EGFR upon the addition of ARNO significantly decrease, while EGFR intensity increases. In Figure 64 the RSD and EGFR intensity on membrane sheets incubated with buffer as a negative control or with Flag-ARNO is reported.

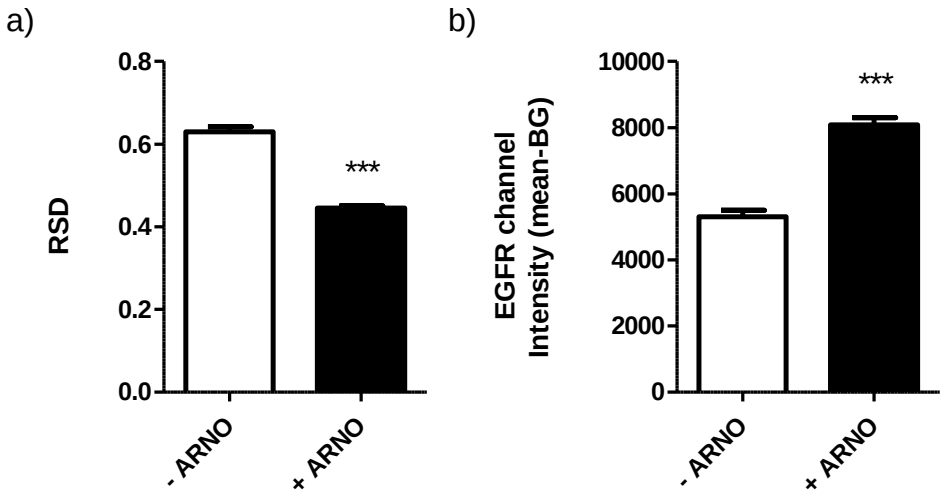

Figure 64: ARNO effect on the EGFR relative standard deviation on HeLa membrane sheets and on EGFR channel intensity (n=3)

a) The RSD gives information about the clustering degree of EGFR on HeLa membrane sheets. The RSD was measured on membrane sheets incubated with buffer or with 1 µM Flag-ARNO. The RSD goes from 0.63 to 0.45 upon ARNO addition. The RSD decreased and therefore, the degree of clustering of EGFR decreased too. **b)** Total EGFR channel intensity increased upon ARNO addition.
Significance was calculated with Mann-Whitney test. (***: $p<0.001$ with $p<0.0001$).

ARNO seemed to have an effect on the degree of clustering of EGFR. Upon ARNO addition, the degree of cluster decreased (since the RSD value decreased), going from 0.6 when the membrane sheets were incubated only with buffer, to 0.4.

Different explanations for ARNO's effect on the RSD are possible: ARNO decreases EGFR clustering at the plasma membrane. The binding of ARNO to EGFR makes EGFR more accessible to antibody staining by decreasing packing density in

clusters or by inducing conformation changes. In the latter case, the clusters may also become larger, which could be investigated in further studies employing super resolution microscopy.

IV.2.4.4 A mutation on ARNO PH domain affects EGFR co-localization and clustering

To understand whether the PH domain contributed to ARNO/EGFR co-localization and clustering, a Flag-tagged ARNO mutated construct, containing a single point mutation (R280C; R: Arginine; C: Cysteine) at the PH domain was developed. The PH domain, as described in Section II.4.1.1 is important for recruitment of proteins to the plasma membrane and interaction with PIP_ns. A single point mutation in the PH domain of ARNO was made to block the interaction with PIP_ns at the cell membrane.

Firstly, the co-localization of the mutated construct versus the wild-type construct was measured. In Figure 65 representative HeLa membrane sheets are shown. The binding of ARNO to the membrane sheets was drastically reduced in the ARNO construct containing the point mutation. The co-localization results were represented graphically in a scatterplot (Figure 66). As expected, for the mutated ARNO, the points were randomly distributed showing no correlation between EGFR channel (green) and ARNO channel (red).

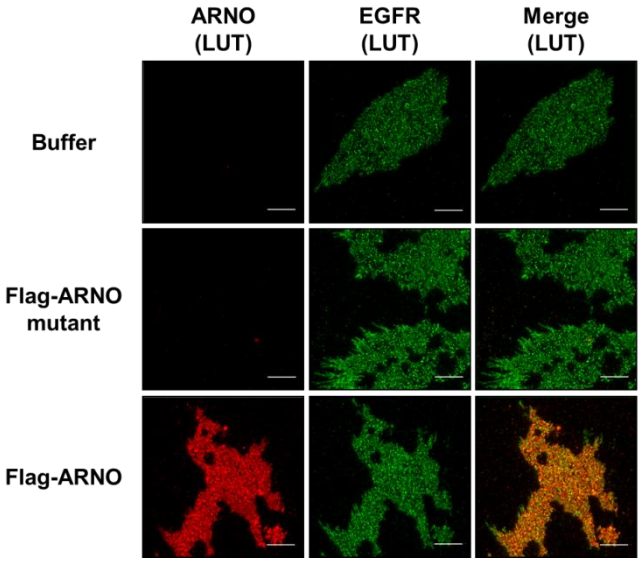

Figure 65: Representative images for mutant Flag-ARNO and wild-type Flag-ARNO co-localization with EGFR on HeLa membrane sheets

HeLa membrane sheets were incubated with 1 µM mutant Flag-ARNO or 1 µM wild-type Flag-ARNO. ARNO was stained in red, while EGFR was stained in green. The overlap between the two channels is indicated as "merge". In yellow, is indicated the co-localization between wild-type Flag-ARNO and EGFR. No co-localization was visible when the membrane sheets were incubated with buffer, as well as for point mutant Flag-ARNO. All the pictures are shown with the same lookup tables (LUT). The scale bar indicates 7.5 µm.

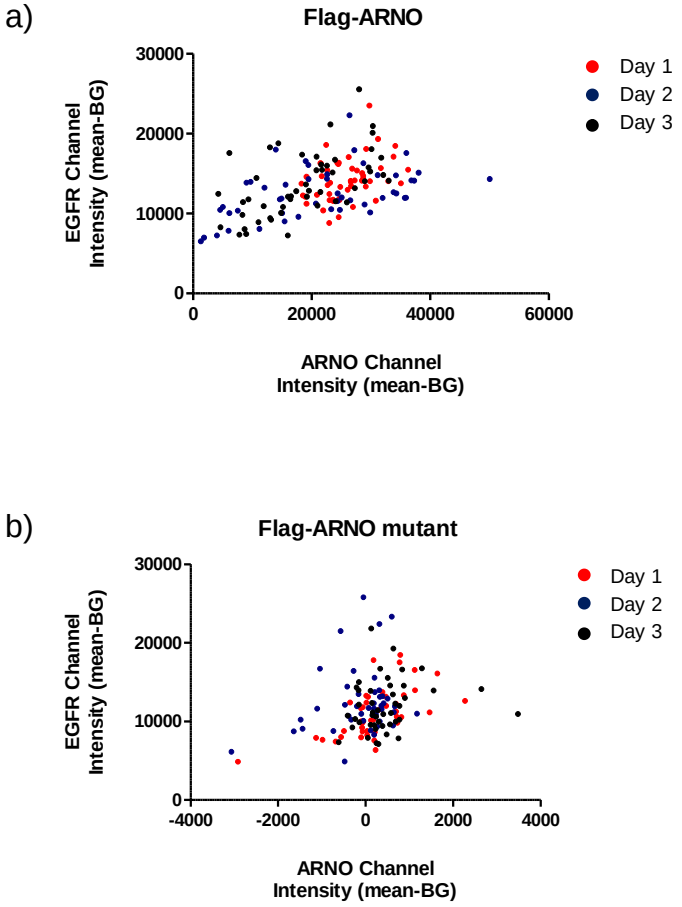

Figure 66: Scatterplot of EGFR mean pixel intensity (y-axis) and ARNO mean pixel intensity (x-axis) of wild-type Flag-ARNO vs. mutant Flag-ARNO of background subtracted mean membrane sheet (mean-BG) intensity (n=3)

Scatterplot of three different experiments: day 1 in red, day 2 in blue and day 3 in black.
a) When membrane sheets were incubated with wild-type Flag-ARNO, the points are clustering around a straight line. **b)** The scatterplot of the membrane sheets incubated with mutant Flag-ARNO shows a disordered distribution. Not an equal contribution from the two channels was visible.

The degree of co-localization was then calculated as the Pearson's correlation coefficient (Figure 67).

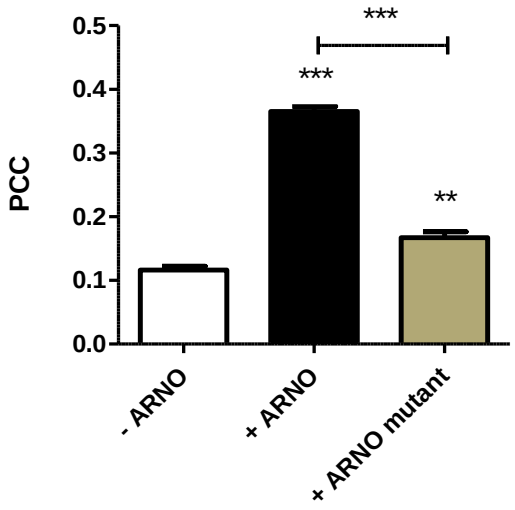

Figure 67: Pearson's correlation coefficient for wild-type ARNO or mutated ARNO and EGFR on HeLa membrane sheets (n=3)

The PCC was calculated within defined ROI (50x50 pixel). Wild-type ARNO showed, as previously seen, a middle co-localization value of 0.4. ARNO containing a PH mutation is unable to bind the PIP_2 and the co-localization drastically drops to 0.17, comparable to the buffer control with a PCC value of 0.12. Significance was calculated with one way ANOVA on Rank analysis. There is a statistically significant difference ($p<0.001$). The columns were compared with Dunn's Method. The comparison between the column 1 and column 2, column 1 and 3, column 2 and 3, are reported (***: $p<0.001$; **: $p<0.01$).

To understand if the effect observed for the wild-type ARNO on EGFR clustering was due only to the membrane interaction, the RSD for mutated ARNO was calculated. Also EGFR intensity was measured (Figure 68).

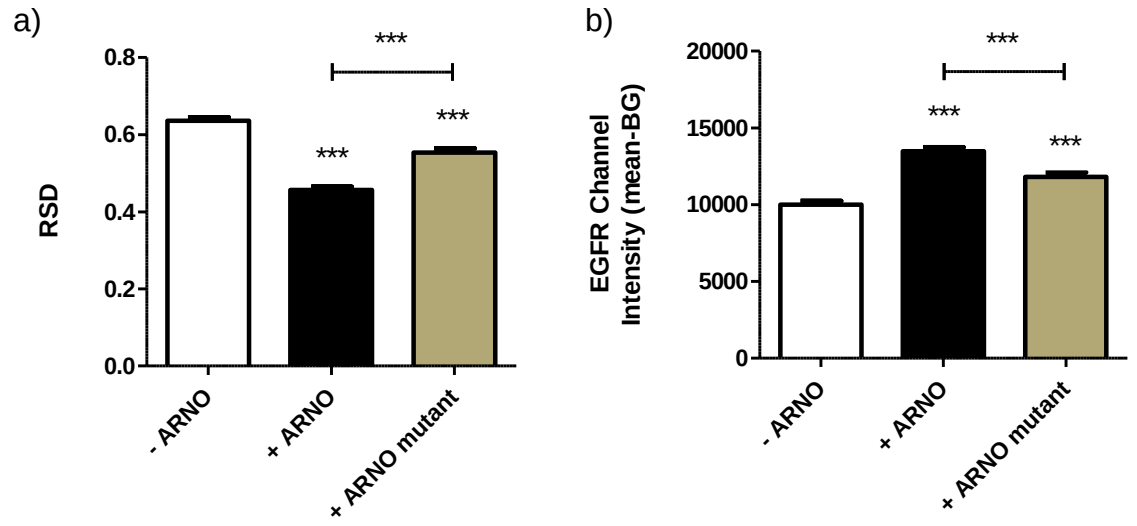

Figure 68: Different effect of ARNO constructs on EGFR relative standard deviation (RSD) and on EGFR intensity (n=3)

a) The RSD gives information about the clustering degree of EGFR on HeLa membrane sheets. The RSD was measured on membrane sheets incubated with buffer or 1 µM wild-type Flag-ARNO or 1 µM Flag-mutated ARNO. The RSD slightly decreased for the mutated ARNO (0.55) compared to the buffer RSD (0.64). For wild-type ARNO, the RSD had again a value around 0.4, meaning a decrease of EGFR clustering. **b)** Total EGFR channel intensity increased upon wild-type ARNO addition, and it was slight higher than the buffer control when the mutated ARNO was present.
Significance was calculated with one way ANOVA on Rank analysis. There is a statistically significant difference ($p<0.001$). The columns were compared with Dunn's Method. The comparison between the column 1 and column 2, column 1 and 3, column 2 and 3, are reported (***: $p<0.001$).

Only a slight effect on the clustering degree of the EGFR was visible for ARNO with a mutant PH domain.

In the light of these results, the PH domain is important to transport ARNO to the plasma membrane to increase its local concentration. ARNO could directly hinder tight EGFR clustering by binding or inducing conformational changes. Conformational changes alone may already be sufficient for increased accessibility. Alternatively, the PIP_2 microenvironment may be altered via PH domain binding PIP_2 at the plasma membrane. A point mutation of the PH domain of ARNO strongly reduces the membrane recruitment of ARNO. A small effect on the receptor clustering was still observed for this mutant, potentially due to the fact that the Sec7 domain still interacts with the JM region. Interaction of ARNO with the JM domain, which interacts with PIP_2, may also alter EGFR clustering by altering EGFR-PIP_2 interactions. Nevertheless, the effect is

drastically reduced if compared with wild-type ARNO, indicating a role of the PH domain in the receptor activation. Moreover, other cytosolic co-factors could also assist in the interaction between ARNO and EGFR in the living cell.

Fluorescence microscopy is a useful tool to study the co-localization between proteins, but due to the resolution limits, it is not possible to assay if a direct interaction between ARNO and EGFR takes place or if additional factors are required. Furthermore, to understand which domains of ARNO are involved in the interaction, deletion studies are necessary.

V. Discussion

V.1 Nanodiscs as a model system to study membrane-ARNO interactions

The comprehension of protein-membrane interactions and the influence of phospholipid composition on protein recruitment and activation is a major goal of biochemical and biophysical research (Contreras et al. 2011). Nanodiscs are an useful tool to study membrane-protein interactions and protein-protein interactions (Schuler et al. 2013). Cytohesins act as GEFs for Arf, in particular Arf1 and Arf6 (Cohen et al. 2007). Cytohesins are involved in membrane trafficking, vesicle formation and signal pathways important for cell growth and development (Casanova 2007). In Famulok's research group, the role of cytohesin-2 (ARNO) PH domain has been investigated. The PH domain recruits cytohesins to the plasma membrane, due to the interaction with PIP_ns (Kolanus 2007). In order to use an *in vitro* system to observe the interaction between ARNO PH domain and anionic lipids, nanodiscs containing PIP_2 have been produced.

V.1.1 Protein Expression and Purification

The first steps for this part of the project were the expression and purification of the PH domain of ARNO and the membrane scaffold protein, necessary for nanodisc assembly.

The PH domain was expressed in *E. coli* as an N-terminal SBP-tagged construct (Figure 13). The SBP-tag was used for the purification. The purification was performed as described by Keefe et al. (2001). The SBP-tag contains 38 amino acids residues and it was selected to bind selectively to streptavidin with a Kd of 2.5 nM (Keefe et al. 2001). The SBP-tag binds to an improved version of streptavidin, termed strep-tactin.

One liter of bacterial culture was cultivated overnight at 20 °C to increase protein yield and avoid protein aggregates formation. Cell lysate was applied to strep-tactin immobilized beads to allow the binding between the protein of interest and the conjugated matrix. After a wash step, performed to remove unspecific binding to the beads, ARNO PH was eluted using 2.5 mM desthiobiotin. Desthiobiotin is a modified form of biotin and binds with lower affinity to the strep-tactin matrix, allowing mild elution conditions and

bead recycling (Hirsch et al. 2002). After elution, a buffer exchange was performed in order to remove desthiobiotin for further experiments. The final protein yield for 1 liter culture was 2.8 mg.

Nanodiscs are surrounded by two membrane scaffold proteins that keep the hydrophobic tails of the phospholipids protected from the aqueous environment. Membrane scaffold protein 1 deleted 1 (MSP1D1) is a modified form of the human Apolipoprotein A-1 (Apo A-1) (Bayburt et al. 2002). MSP1D1 was expressed as a His-tagged construct followed by a TEV cleavage site in *E. coli* using the protocol reported by Sligar and co-workers available online (Sligar's Laboratory Website) (Figure 14). Two liters of bacterial culture were cultivated at 37 °C until the logarithmic phase of bacterial growth was reached (corresponding to an OD_{600} between 0.6 and 0.8). The protein was expressed for a maximum of 3 hours at 37 °C. Upon that time, proteolytic processes are started. Cell lysate was incubated with Ni-NTA agarose beads, which bind to the His-tag on the protein. In order to remove unspecific binding, several washing steps with different detergents were performed. MSP1D1 was eluted with buffer containing imidazole, and the protein was dialyzed overnight against MSP standard buffer for further nanodiscs assembly. Some precipitate was also present after dialysis. The final protein yield for 2 liters of culture was 15 mg.

V.1.2 Nanodiscs production with natural phospholipids

PIP_2 and PIP_3 are anionic phospholipids constituting less than 1% of the cellular membrane lipids (Czech 2000). In order to visualize PIP_ns at the plasma membrane, PH domains are used (Kavran et al. 1998). Grp-1 (cytohesin-3) PH domain, was the first member of the cytohesins family identified to interact with PIP_3 with high efficiency (Klarlund 1997). Subsequently, ARNO PH was identified to be recruited at the membrane, due to the interaction with PIP_ns (Venkateswarlu et al. 1998).

In order to validate nanodiscs as a suitable model to study membrane-protein interaction, PIP_2 was inserted into the phospholipid bilayer. Nanodiscs were assembled using natural phospholipids. Nanodiscs not containing PIP_2 were used as a negative control. The assembly procedure was adapted from Bayburt et al. (2002).

First, phospholipids and membrane scaffold protein were mixed in the appropriate amount, in order to achieve almost 100 % nanodisc formation, avoiding the presence of

free MSP1D1 or free lipids in the mixtures. For this reason, several different MSP to phospholipids ratios have been tested.

Second, to assess the formation of nanodiscs, HPLC (high pressure liquid chromatography) analytical gel filtration was performed. Sligar and co-workers reported that formed nanodiscs have the same elution time of the reference protein catalase (Sligar's Laboratory Website). Catalase is a globular protein with a Stokes diameter of 10.2 nm and it eluted at 13.3 minutes (Figure 15). PCPE-nanodiscs and PIP_2-nanodiscs were loaded on a Superdex 200 10/300 column and the elution time of the main peak was compared with the catalase peak. For PCPE-nanodiscs, three MSP to phospholipids ratio were analyzed with gel filtration: 1:60, 1:40 and 1:20 (Figure 16). In the 1:60 ratio, the nanodisc peak was visible at 12.8 minutes but an aggregate peak was eluting at the column void volume, at 9.4 minutes, due to the presence of a too high lipid amount. In the 1:40 ratio, the nanodisc main peak eluted at 13.3 minutes, and was corresponding to the same elution time of catalase. Nevertheless, aggregate traces were visible at around 10 minutes, indicating the presence of an excess of lipids. On the other side, when a 1:20 MSP to phospholipid ratio was used, free MSP1D1 as a shoulder of the main nanodisc peak (13.7 minutes) was visible at around 16 minutes. For this reason, an intermediate ratio between 1:40 and 1:20 was chosen, to avoid aggregate formation and the presence of free-MSP in the mixtures. PCPE-nanodiscs were produced with a 1:30 MSP to phospholipids ratio.

Also for PIP_2-nanodiscs, three different MSP:phopsholipids were tested: 1:60, 1:40 and 1:20 (Figure 17). After careful evaluation for PIP_2-nanodiscs a 1:30 ratio was also chosen, because aggregates caused by lipid excess in the 1:60 and 1:40 ratios were visible. Furthermore, for the 1:20 ratio, after the nanodisc peak at 13.8 minutes, free MSP was eluting at 16 minutes.

To evaluate nanodiscs formation, dynamic light scattering (DLS) was performed in the group of Professor Gerd Bendas (University of Bonn). DLS gives information about the size of the molecules in solution, according to their Brownian motion. The sample was irradiated with a monochromatic laser beam and the light was scattered in a time dependent manner according to the molecules movements. The intensity of the scattered light was then analyzed with an autocorrelation function, which gives information about the motion of the particle in solution, their diffusivity and the dimensions (Lorber et al. 2012). DLS was used to evaluate the polydispersity of nanodiscs and their dimensions in solution. DLS analysis of PCPE-nanodiscs (Figure 18a)

measured particles with a diameter of 16.18 nm and 94 % volume distribution, while the measured diameter for PIP_2-nanodiscs (Figure 18b) was 15.34 nm with a 98 % volume distribution. These results indicated an almost 100 % monodispersed samples and complete nanodiscs formation. The DLS measurement revealed nanodisc dimensions circa 5 nm bigger than the dimensions reported by Bayburt et al. (2002; 2003). This can be due to the fact that natural phospholipids were used. Natural phospholipids are heterogeneous preparations, with different fatty acid chains distribution, if compared with synthetic phospholipids. The predominant fatty acid species for egg PC have a chain length of 16:0 (32.7 %) and 18:1 (32.0 %). PE contains 19.5 % of fatty acids with a chain length of 20:4. Brain PIP_2, the chain length distribution is for 37 % 18:0, 36.8 % 20:4 and 7.7 % is unknown. Therefore the final dimension of the nanodisc bilayer can be influenced by the presence of unsaturated fatty acids. Furthermore, the DLS measurement was performed at room temperature and not at 4 °C, as for gel filtration experiment. Unsaturated fatty acids and higher temperature could increase the membrane fluidity (Hagve 1988; Nicolson 2014).

V.1.3 ARNO PH domain interacts with PIP_2-nanodiscs

To prove that nanodiscs are a suitable system to study membrane-ARNO interaction, a pull-down assay with PIP_2-nanodiscs and PCPE-nanodiscs was performed. ARNO PH fused at the N-terminal part with a SBP-tag was mixed with PCPE-nanodiscs or PIP_2-nanodiscs and then incubated with strep-tactin magnetic beads (Figure 19). Magnetic beads presented several advantages, they are usually smaller than non-magnetic beads and therefore the binding surface increase and fewer beads are required. Furthermore, magnetic beads can be easily removed from the suspension, without time consuming processes (Sepmag 2010). The pull-down assay was performed on ice, to avoid protein denaturation. In order to remove unspecific binding, several washing steps were performed. To displace ARNO PH from its interaction site on the beads, desthiobiotin at the appropriate concentration was used. The pull-down assay (Figure 20) shows no co-elution between PCPE-nanodiscs and the PH domain, as expected. ARNO PH domain interacts selectively with nanodiscs containing PIP_2. Two bands were visible in the pulled-down fraction: MSP1D1, indicating the presence of nanodiscs and ARNO PH domain.

V.1.4 Cyplecksins inhibit the binding of ARNO PH domain

Cyplecksins covalently target the cytohesins-PH domains. Cyplecksins are 5-bromo-pyrimidine-2,4,6-triones identified and synthetized by Doctor Mohammed Hussein, from Famulok's group. Inactive analogues were also produced (Figure 21). To understand if cyplecksins inhibits the membrane recruitment of ARNO PH domain in membrane surrogate systems, PIP_2-nanodiscs were used. A similar pull-down assay to the one previously described, with strep-tactin magnetic beads was performed. The compounds were pre-incubated with ARNO PH domains and subsequently nanodiscs were added to the mixtures. Also in this experiment, several washing steps were performed in order to remove unspecific binding. Cyplecksins inhibit the membrane recruitment of ARNO PH domain to the membrane but the inactive analogues have no effect (Figure 22).

From these results, nanodiscs demonstrate the ability to be a reliable system to detect the PIP_2 interaction and to test small-molecules inhibitors.

V.2 Different membrane-like environments to study EGFR-ARNO interaction and EGFR activation

Cytohesins were identified as cytoplasmic activators for EGFR in Famulok's research group. In particular, cytohesins work as enhancer for EGFR phosphorylation in living cells (Bill 2011). H460 cells treated with SecinH3, an inhibitor for cytohesins, showed a reduction of EGFR phosphorylation. On the other hand, the overexpression of cytohesin-2 in H460 cells led to an increase of EGFR activation level. From cell-free reconstitution experiments it was concluded that ARNO enhances EGFR phosphorylation by direct interaction, probably by enhancing the formation of the active asymmetric dimer.

Starting from this point, the aim of this work was to gather further characterization on the activation mechanism of EGFR driven by cytohesins, in native-like membrane systems using phosphorylation as readout. During this work, the findings that cytohesins are directly involved in the activation of the EGFR were challenged (Anastasi et al. 2016). Therefore, the key experiments of the earlier publication by Bill et al. (2010) involving EGFR activation by cytohesin-2 were repeated in our group. Whereas all the cellular data could be reproduced and the cytohesin-dependent stimulation of EGFR phosphorylation also be observed in HeLa cells, the cell-free reconstitution of the EGFR activation could not be reproduced. As a consequence, the publication was retracted by the authors (Bill et al. 2016). The discrepancy between the cellular and the cell-free data emphasizes further that deeper insight into the cytohesin-dependent activation of EGFR is needed.

EGFR is not a prototypical RTK, because its activation is regulated not only from the binding of a ligand to the extracellular domain, but more complex mechanisms are involved. Peculiar to EGFR is the regulating function of the juxtamembrane (JM) domain (Lemmon et al. 2014). The JM domain is a short intracellular region sited directly after the transmembrane (TM) domain. The JM domain contributes to the stabilization of the kinase domain in the active conformation. Moreover, the JM domain seems to also contribute to the inactive state of the receptor, via a direct interaction between the positively charge residues of the receptor and the anionic lipids of the plasma membrane (Arkhipov et al. 2013; Endres et al. 2013). The TM domain consists of a single α-helix

spanning through the membrane bilayer, comprised between the amino acid residues 621 to 644 (Jura et al. 2009a). Endres et al. (2013) recently identified the TM domain as another regulation motif for EGFR activation, underling the importance of a conformational change in the transmembrane segment to remove the JM domain from its inactive conformation at the plasma membrane and to keep the kinase domain in an active state. Moreover, recent studies in Famulok's research group (personal communication from Benjamin Weiche, Anton Schmitz and Michael Famulok) suggested that the interaction site for ARNO on EGFR is located on the JM domain.

To further investigate the regulation mechanism involved in EGFR-ARNO interaction, truncated EGFR constructs containing only the TM and the JM regions were embedded in membrane surrogates. Starting from simplified systems, like micelles and bicelles, and ending with more complex membrane-like environments, such as nanodiscs and membrane sheets, the interaction between cytohesin-2 and EGFR was studied.

V.2.1 Micelles

Detergent and phospholipids are amphiphilic molecules consisting of a hydrophilic head group and a lipophilic tail. In aqueous environments, they form micelles, spherical structures, to minimize the interaction of the hydrophobic tails with the solvent. Due to their nature, micelles constitute the most simplified membrane-like system and are a useful tool to solubilize membrane proteins.

V.2.1.1 EGFR phosphorylation in micelles

In order to study the activation of EGFR in micelles, a constitutively dimerized form of the receptor, namely lz-EGFR-TS, was used (Figure 23). In the lz-EGFR-TS construct, the extracellular domain was replaced by a leucine-zipper dimerization module. Since the construct is purified as already dimerized form, to evaluate receptor phosphorylation, no stimulation with an extracellular ligand was required. A Flag-tag was present at the N-terminal part, while the C-terminal part of the receptor had a SBP-tag used for purification. Lz-EGFR-TS was expressed in Sf9 insect cells by Yvonne Aschenbach, from Famulok's group. For the purification, strep-tactin beads were used. Protein expression was not high and the final product contained a variety of contaminants (Figure 24). For this reason, only an approximate determination of the protein

concentration was possible. Since lz-EGFR-TS eluted as a double band, a Western Blot with an anti-Flag antibody, for the N-terminal part, and a streptavidin-conjugated dye, for the C-terminal part, was performed to understand if during the purification the receptor was subjected to protease cleavage. Both antibodies recognized the upper band at 76 kDa, indicated in Figure 24.

Preliminary experiments were performed to understand if the receptor embedded in micelles was active and able to undergo phosphorylation. Since the receptor presented a basal phosphorylation level upon purification, the tyrosine-protein phosphatase YopH was used to dephosphorylate the protein. The addition of ATP led to an increase of the receptor phosphorylation level within 20 seconds (Figure 25). Interestingly, it was possible to observe that an upper band appeared after stimulation, due to the phosphorylation of several tyrosine residues on the C-terminal tail of the receptor. From these results, it is possible to assert that lz-EGFR-TS activity was conserved upon purification and micelles offer an easy solution to study EGFR activity in a native-like environment.

As a second step, the influence of ARNO on lz-EGFR-TS phosphorylation in micelles was observed. Bill (2011) reported that the Sec7 domain is sufficient to enhance EGFR phosphorylation. For this reason, the micelles containing the receptor were incubated with ARNO Sec7 or GST as a negative control protein (Figure 26). GST was used as a control, since GST monomers have almost the same molecular weight of Sec7. No influence of ARNO Sec7 on *in vitro* activation of EGFR was observed. These results are in contrast to the study of Bill (2011). It has to be considered, however, that Bill (2011) examined the phosphorylation of lz-EGFR in intact cells.

V.2.1.2 EGFR-ARNO interaction in micelles

After determining that it was not possible to observe an influence of ARNO on EGFR activation in micelles, it was investigated whether the absence of the effect was due to micelles not being suitable for the interaction. Famulok's research group has evidence that ARNO interacts with EGFR, directly binding to the JM domain (personal communication from Benjamin Weiche, Anton Schmitz and Michael Famulok). Furthermore, two recent studies highlighted the role of the JM domain on the regulation of EGFR activity (Arkhipov et al. 2013; Endres et al. 2013).

Discussion

First, to verify if micelles were a suitable environment for the interaction, a truncated form of the receptor, i.e. HST-EGFR-TMJM, containing the TM domain and the JM domain of EGFR was expressed and purified in bacteria. Initially the construct was expressed with a His-tag and a SBP-tag at the N-terminal part (Figure 27). In bacteria, the construct was accumulated in inclusion bodies during the protein expression. The formation of inclusion bodies in bacteria remains not completely understood (Ramón et al. 2014). Protein purification from inclusion bodies requires harsh denaturing conditions. Urea at high concentration was used to extract the protein from the inclusion bodies. Since the HST-EGFR-TMJM is a short peptide containing only 120 amino acids residues, no complex renaturation processes were required. Urea was simply removed by dialysis overnight against the desired buffer containing detergents for micelle formation. The final purity of the protein was around 70 % due to its low expression (Figure 28).

Second, a GST-tagged ARNO Sec7 construct was purified from *E. coli*. Protein expression was very high and the final protein yield was 50 mg starting from 2 liters of bacterial culture (Figure 29). To test if the Sec7 construct was correctly folded after purification, its catalytic activity was tested. For this purpose, a fluorescence-based nucleotide exchange assay was performed (Figure 30). An increase of tryptophan fluorescence was observed within 10 minutes, and the slope was calculated with a linear regression model. ARNO Sec7 was active at nanomolar concentration. The protein conserved its structure and activity upon purification.

In order to analyze and characterize ARNO-EGFR interaction, a GST pull-down assay was performed (Figure 31). From the bead fraction, it was possible to observe an unspecific interaction of the peptide with the glutathione beads, in presence or absence of ARNO Sec7. For this reason, it was not possible to draw a clear conclusion about ARNO Sec7 and EGFR TMJM interaction with GST pull-down. To avoid unspecific binding of TMJM peptide to GST beads, a pull-down assay with strep-tactin beads, interacting with the N-terminal SBP-tag of HST-EGFR-TMJM, was performed. Nevertheless, no elution of the peptide was visible in the pulled down fraction, meaning that in this case unspecific interaction with the beads was also observed. Because of the infeasibility of performing a reliable pull-down assay, other biochemical assays to investigate the interaction were used.

Crosslinking is used to “freeze” molecular interactions at a given point in time, and it is a useful tool to detect weak and transient binding events between proteins. To perform crosslinking, other constructs for EGFR and ARNO were expressed and purified.

A new EGFR-TMJM peptide was used, i.e. His-EGFR-TMJM-SBP. The construct contained a His-tag at the N-terminal part and a SBP-tag at the C-terminal (Figure 32). The presence of the SBP-tag at the C-terminal increased the yield (circa 13 mg from 2 liters of bacterial culture) and the purity of the final product (Figure 33). This was probably due to the increased binding capacity of the His-tag to the beads, since no steric hindrance of the SBP-tag was present anymore.

In addition to the Sec7 domain, an almost full-length form of the cytohesin-2 was used to increase the efficiency of crosslinking. The polybasic region (PBR) of ARNO is responsible for the interaction with acidic phospholipids at the plasma membrane (Nagel et al. 1998a). The construct, termed ARNOΔPBR, contained a 14 amino acids C-terminal deletion of the polybasic region. During the purification, degradation processes were occurring and degradation products were visible in the eluted fractions (Figure 34). Gel-filtration was performed to remove contaminants and the final protein yield was 10 mg starting from 2 liters of bacterial culture.

For the crosslinking assay, the crosslinker BS3 was used. Since BS3 interacts only with primary amine, and the polybasic region (PBR) of ARNO contains five lysine residues almost in succession, the ARNO domain was removed, to prevent the possibility that during the crosslinking only ARNO:ARNO complexes were formed.

Previous crosslinking experiments performed in Famulok's research group by Doctor Benjamin Weiche showed that the JM domain of EGFR is sufficient for ARNO binding. As a proof of principle, the experiment with JM domain and ARNOΔPBR was repeated (Figure 35). The JM domain does not required the presence of detergents to be soluble, and for this reason no micelles were formed. Two different concentrations of BS3 were used: 1.5 mM and 0.5 mM. The crosslinking experiment showed that the JM domain binds to ARNOΔPBR. Interestingly, the crosslinked band intensity between ARNO and the JM peptide became stronger when the lower BS3 concentration (0.5 mM) was used. Probably, high BS3 concentration (1.5 mM) shifts the reaction equilibrium to the formation of higher order ARNO and ARNO/JM complexes, which are not resolved in the gel.

The crosslinking experiment was repeated with micelles containing His-EGFR-TMJM-SBP and using as a negative control the TM and JM regions of the insulin receptor (IR). Insulin-receptor is a RTK, which regulates the glucose homeostasis, tissue growth and cellular metabolism (Kitamura et al. 2003). Cytohesins have an effect on insulin signaling. Hafner et al. (2006) have shown that the Sec7 antagonist, SecinH3,

blocked the insulin-dependent repression of the insulin-regulated gene for insulin-like growth factor binding protein (IGFBP1) in HepG2 cells. Furthermore, SecinH3 diminished GTP-bound Arf6 membrane recruitment upon insulin stimulation. Similar results were obtained with the knock-down of cytohesins-2 and 3. Nevertheless, the IR density at the cell membrane and the receptor phosphorylation were not affected by SecinH3 treatment, indicating that cytohesins play a role in the downstream signaling of IR, probably facilitating the formation of the IR-IRS1 complex (Hafner et al. 2006). Lim et al. (2010) recently identified a scaffold protein termed connector enhancer of KSR1 (CNK1) as a binding partner for cytohesins. The CNK1/cytohesin complex is necessary for the activation of the IR downstream signaling (Lim et al. 2010). Taking that into account, no direct binding between the IR-JM domain and ARNO seems to be involved in the receptor activation mechanism.

The crosslinking experiments between EGFR-TMJM and ARNOΔPBR revealed no interaction between the two proteins (Figure 36). No crosslinking between ARNO and IR was observed, as expected.

Since the crosslinking assay detected the interaction between the peptide JM and ARNO, but no interaction was observed between ARNO and EGFR-TMJM in micelles, two explanations are possible. First, micelles are not a suitable model to study the interaction. The detergent concentration required to maintain the protein in solution can be high enough to disrupt the protein-protein interaction. Second, the JM domain may interact with the detergent, and the interaction with ARNO is not strong enough to displace the detergent molecules.

Taking that into account, other membrane model systems were evaluated.

V.2.2 Bicelles

Bicelles are phospholipids bilayer formed by long-chain and short-chain lipids. Bicelles were used to study EGFR-ARNO interactions. For bicelle formation, phospholipid powders were mixed together in phosphate buffer at pH 7.2, to increase long-term bicelle stability (Ottiger, Bax 1998). Bicelles formation was assayed by DLS (Figure 37) and the resulting diameter was around 6 nm, with almost 100 % sample homogeneity. During DLS analysis, the sample was diluted and DHPC was supplemented into the dilution buffer to keep the q ratio stable and avoid the disassembly of bicelles (Beaugrand et al. 2014).

For the reconstitution of membrane proteins into bicelles, the lyophilization of the protein is often necessary (Dürr et al. 2012). The insertion of transmembrane proteins into bicelles requires a high amount of protein, generally above 10 mg/ml (Ujwal, Bowie 2011). Since the amount of lz-EGFR-TS purified was not enough to allow the insertion into bicelles, and lyophilization of the protein was not possible, only bicelles containing the TMJM peptide were produced. For this reason, the interaction between ARNO and EGFR, but not the phosphorylation in bicelles was studied.

DLS was used to analyze bicelles containing His-EGFR-TMJM-SBP (Figure 38) but no variation in the diameters was observed. In order to analyze if the peptide was assembled into bicelles, an indirect control experiment was performed (Figure 39). From the SDS-PAGE gel, it was possible to observe that the TMJM was present only in the soluble fraction when the bicelles were formed. Protein precipitate was also visible, due to an incomplete protein solubilization during sample preparation. The bicelles containing His-EGFR-TMJM-SBP were used within a week, to avoid the degradation of the sample.

V.2.2.1 EGFR-ARNO interaction in bicelles

To analyze the interaction between ARNOΔPBR and His-EGFR-TMJM-SBP, BS3 crosslinking was performed (Figure 40). Two different ARNO concentrations were used for this experiment and upon BS3 addition a crosslinked band with the peptide was visible at ~60 kDa. This result indicated a weak but reliable interaction of the EGFR-TMJM peptide with ARNO.

In order to understand if the Sec7 domain alone was sufficient for the interaction, the crosslinking experiment was repeated with two different Sec7 concentrations (Figure 41). ARNO Sec7 interacted with EGFR-TMJM in a concentration-dependent manner in bicelles. As mentioned before, studies in Famulok's research group and in the group of Doctor Manuel Etzkorn, suggested that the interaction site with ARNO is located on the JM-A segment of EGFR. To provide evidence towards that, two different constructs of the His-EGFR-TMJM-SBP peptide were produced, in which the JM segment was scrambled (Table 1). The JM-A segment is important for protein dimerization, probably due to the tendency to form a coiled-coil structure. Generally, a coiled-coil motif can contain from two to five α-helices and it is a common domain in proteins, which act as transcription factors and are involved in cell growth and proliferation (Mason, Arndt 2004). According to the program "prediction of coiled-coil regions in proteins" (COILs)

the motif is partially conserved in JM sc1, while no coiled-coil tendency was found for JM sc2. In the crosslinking experiments performed with wild-type EGFR-TMJM or the two scrambled versions (Figure 42), the interaction between wild-type EGFR-TMJM was observed. A weaker crosslinked band for the EGFR-TMJM sc1 and no interaction with the sc2 were detected. These data support the theory that for the interaction with ARNO is necessary an intact JM segment, in which a coiled-coil domain is formed.

In addition to the above experiment, a control experiment with the PH domain was performed (Figure 43). No interaction with EGFR-TMJM was detected for the PH domain, providing further evidence that Sec7 is the binding site for the EGFR.

Bicelles provide a reliable system to study protein-protein interactions. A recent publication of Mineev et al. (2015) reveals two different conformations of the EGFR-TMJM peptide in micelles and bicelles. In micelles, the JM domain is embedded or attached to the surface of the micelles. For this reason, the JM domain could not be free to interact with proteins present in the surrounding environment. Furthermore, Mineev et al. (2015) reported that the JM domain in bicelles does not interact with the phospholipid bilayer. For this reasons, interactions with other proteins could easily take place.

These findings could explain why no interaction between ARNO and EGFR-TMJM was detected in micelles, but weak interactions were observed when bicelles were used. Moreover, it was observed that the JM domain in bicelles is more flexible than in micelles, in which it forms a compact α-helix structure. The flexibility of the JM domain in bicelles may also explain the weak nature of the interaction observed with ARNO (Mineev et al. 2015).

V.2.3 Nanodiscs

Going through the different membrane systems, nanodiscs were the next choice to study EGFR-ARNO interactions. Since there were difficulties with natural phospholipids for nanodiscs production and storage, synthetic phospholipids were used to reduce the variability of the fatty acid chain (Amin, Hazelbauer 2012).

Nanodisc assembly was assayed with FPLC (fast protein liquid chromatography) analytical gel filtration and DLS. A Superdex 200 10/300 GL column was calibrated with gel filtration standard protein mixtures (Table 2). The protein γ-globulin, used for the calibration, has almost the same Stokes diameter of catalase, the reference protein used by Sligar and co-workers to assay the assembly of nanodiscs (Sligar's Laboratory Website).

Nanodiscs, formed with synthetic phospholipids, eluted at almost the same volume as γ-globulin, indicating a proper disc formation (Figures 44 and 45). The DLS analysis (Figure 46) confirmed that the nanodiscs were correctly assembled, with a diameter approximately of 10 nm. Further evidences on nanodisc shape and integrity were gathered with negative staining electron microscopy (Figure 47). Negative staining images of nanodiscs showed discoidal particles as single molecules or as chain aggregates. Since the nanodisc samples were gel filtered before electron microscopy analysis, the formation of nanodisc piles was probably caused by the under-vacuum drying phase necessary for the sample preparation. A 10 nm diameter was measured for the single nanodisc particles, although bigger particles with an 18 nm diameter were also found. Also in this case, the presence of bigger particles can be explained with sample degradation or with contaminants still present after purification of the nanodiscs.

V.2.3.1 EGFR phosphorylation in nanodiscs

In order to study EGFR activation in nanodiscs, the lz-EGFR-TS construct was reconstituted into nanodiscs membranes. The assembly protocol was adapted from Mi et al. (2008). To analyze if the receptor was properly inserted into the discs bilayer, an indirect control experiment was performed (Figure 48). The assembly process of nanodiscs starts when the detergent used to solubilize the lipids is removed with hydrophobic beads. Lz-EGFR-TS cannot stay in solution without detergent in the absence of nanodiscs. No traces of free lz-EGFR-TS were present in the supernatant upon detergent removal in the absence of nanodiscs. Only if nanodiscs were formed, lz-EGFR-TS was observed in the supernatant fraction after bead incubation.

Lz-EGFR-TS was then tested for phosphorylation into nanodiscs (Figure 49). Compared to the previously used micelles system, the kinetics of the receptor in nanodiscs were very slow and even after 10 minutes of stimulation the complete receptor activation was not reached. Seeing that the receptor already expressed a basal phosphorylation level after purification, the protein phosphatase YopH was then used. In presence of YopH, the receptor could reach a higher phosphorylation level, within 3 minutes (Figure 50). Moreover, Flag-ARNO Sec7 or ARNO Sec7 without tag, in order to exclude the possibility that the presence of a tag may influence the protein activity, were added to the reaction mixture. No changes of EGFR phosphorylation was detected in presence of ARNO Sec7 constructs.

Discussion

Nanodiscs showed a slower kinetic activation of EGFR compared to the micellar system. This is presumably due to membrane constriction and lipid-protein interactions, whereby the receptor cannot be easily phosphorylated, as compared with the detergent-solubilized receptor. These data are in agreement with previous studied published by Mi et al. (2008) and He et al. (2015), in which EGFR activation in nanodiscs or nanolipoprotein particles was studied between 2 to 18 hours. As the focus of this thesis was about the early activation stages of EGFR, the activation kinetics were only evaluated for a short incubation. Bill (2011) reported that in living cells ARNO enhances EGFR phosphorylation in the early stimulation stages (5 minutes stimulation). Taking that into account, a difference on the phosphorylation level within the first stimulation minutes was expected.

Nanodiscs and micelles provide only an artificial system in which transmembrane proteins can maintain their conformation but other regulatory factors are missing. For this reason, more complex membrane-like systems were used to evaluating ARNO effect on EGFR activity.

V.2.3.2 EGFR-ARNO interaction in nanodiscs

A series of different studies reported the use of nanodiscs to reconstitute transmembrane protein to study their structure, the conformation and the interaction with other associated factors (Alvarez et al. 2010; Bayburt, Sligar 2010; Denisov, Sligar 2011; Näsvik Öjemyr et al. 2012).

The previously used His-EGFR-TMJM-SBP construct was inserted into nanodiscs to study the interaction with ARNO. The assembly of the peptide in the discs bilayer was assayed with an indirect control. The peptide was purified in micelles and subsequently incubated with lipids and the membrane scaffold protein for the nanodisc assembly. At the same time, another mixture containing only the peptide and lipids was prepared. Both mixtures were incubated with hydrophobic beads, and only if the peptide was correctly integrated into the nanodiscs, could it remain soluble (Figure 51).

To test the interaction between His-EGFR-TMJM-SBP and ARNO, a GST pull-down with DMPC-nanodiscs and DPPC-nanodiscs was performed. DMPC and DPPC differ in the length of the fatty acid chain, 14:0 and 16:0 respectively. Longer side chains increase the transient temperature of the lipids and therefore the membrane fluidity can be modulated, changing the experiment parameters. GST pull-down with DMPC-nanodiscs

containing His-EGFR-TMJM-SBP was performed at 25 °C, close at the transition temperature of DMPC phospholipids (Figure 52). At the transition temperature, the membrane motility increases and becomes more fluid. Protein-protein interaction can be favored in these conditions. From the pulled down fraction, it was possible to observe a co-elution between GST-Sec7 and EGFR-TMJM, but no MSP1D1 was eluted. It is possible that during the interaction, the TMJM peptide was pulled out from the nanodiscs bilayer.

To verify this hypothesis, another pull-down experiment was performed at 37 °C with DPPC-nanodiscs (Figure 53). Two parameters were changed: lipid, and temperature. First, DPPC was used because the fatty acid chain is longer than DMPC chain. This may allow a better insertion of the peptide into the membrane. Additionally, DPPC has a transition temperature at 41 °C. The pull-down was performed at 37 °C to test the binding at a physiological temperature and to be close, but not above, the transition temperature of DPPC. In this way the membrane fluidity may be sufficient to facilitate the interaction, but since the bilayer is still in the gel phase, the peptide should not be removed from the nanodiscs. From the pulled down fraction it is possible to observe a co-elution between ARNO and nanodiscs containing His-EGFR-TMJM-SBP (Figure 53a). From the streptavidin Western Blot, the TMJM peptide was detected in the pulled down fraction only where Sec7, and not the control protein GST, was added (Figure 53b). Nevertheless, no MSP1D1 was detected in the pulled down fraction. For this reason, other approaches were used.

Another pull-down experiment was performed with Ni-NTA Agarose beads. This was to anchor the His-tagged TMJM to the beads. In this way, during the interaction, the peptide cannot be easily removed from the discs bilayer. In the Ni-NTA pull-down assay (Figure 54), it was possible to observe the co-elution of GST-ARNO Sec7, the scaffold protein of the nanodiscs, and EGFR-TMJM. The peptide is interacting with Sec7, and it is not removed from the discs bilayer. The same experiment was repeated at 25 °C (data not shown), but no interaction between ARNO Sec7 and EGFR-TMJM was visible, suggesting a primary role of the membrane motility for the interaction. Clarifications of these data are necessary. Other pull-down experiments were performed to gather evidence for the interaction. Nevertheless, no further reliable results were obtained from the pull-down experiments, underling the weak and transient nature of the interaction between ARNO and Sec7.

For this reason, crosslinking in nanodiscs was also performed. As was done for the bicelles experiments, BS3 was used to crosslink ARNOΔPBR with His-EGFR-TMJM-SBP for nanodiscs. As a negative control, nanodiscs containing the IR-TMJM were used. No crosslinking was observed between EGFR-TMJM and ARNO (Figure 55).

Endres et al. (2013) proposed that the JM domain, in its inactive state, is interacting with the plasma membrane, preventing the formation of the asymmetric dimer. To understand if the absence of protein interaction was due to the fact that BS3 crosslinker is not able to enter the membrane, the DSS crosslinker was used, which is a membrane permeable analogue of BS3. Even using DSS, no crosslinking between ARNO and EGFR-TMJM was visible (Figure 56).

It is interesting to observe that, the EGFR-TMJM construct embedded in nanodiscs, as well as the IR-TMJM construct, before crosslinker incubation, were almost only present in monomeric form. The proteins were visible at ~13 kDa, and almost no dimer was visible at ~25 kDa. After crosslinker addition, the dimer band became stronger for both constructs. For bicelles, the dimer was present before BS3 addition (see Figure 40) and when incubated with ARNO, a crosslinking between the two proteins was visible. In micelles, no interaction between EGFR-TMJM and ARNO was detected and almost no dimeric form of the receptor was observed (see Figure 36). These observations suggest that the receptor presents as a pre-formed dimer in membrane surrogate systems, may easily interact with ARNO. These results highlight an important regulatory role of the TM region of EGFR. Further analysis and experiments to clarify this theory are necessary.

As only weak interactions were detected with pull-down experiments, and no crosslinking was observed between ARNOΔPBR and EGFR-TMJM, another technique was used to investigate the interaction. Microscale thermophoresis (MST) is a useful technique to detect protein-protein interactions in a nanomolar range and without high protein consumption (Jerabek-Willemsen et al. 2011). DPPC-nanodiscs were directly produced with a MSP1D1-GFP labeled construct. Empty nanodiscs and nanodiscs containing TMJM presented the same thermophoretic pattern (Figure 57). The sigmoidal binding curves probably result from an unspecific interaction between the nanodiscs and Sec7. Since no reliable interactions between EGFR and ARNO were detected by using nanodiscs, other *in vivo* like membrane system were evaluated.

V.2.4 Membrane Sheets

Membrane sheets were prepared starting from cells adhered to a glass support, termed a cover slip. Cells were subjected to an ultrasound pulse and the plasma membrane remained immobilized on the glass support. These membrane sheets allow the access to the intracellular leaflet, to study other membrane-associated proteins. Furthermore, since the cytosolic component is removed, membrane sheets are a useful tool to study membrane proteins via fluorescence imaging studies, without the problem of cell autofluorescence (Perez et al. 2006). Membrane sheets constitute a more complex surrogate system, as the composition of the plasma membrane is completely native.

V.2.4.1 EGFR activity on membrane sheets stimulated with ARNO

To analyze the activation of EGFR on membrane sheets, different concentrations of EGF were tested. After membrane sheet preparation, the cover slips were pre-incubated with buffer and phosphatase inhibitor. The receptor phosphorylation was analyzed with pTyrosine antibody specific for a tyrosine residue on the C-terminal tail of the receptor (Tyr1086). Fluorescence microscopy was used to quantify the phosphorylation level on membrane sheets. No increase in phosphorylation level was observed upon EGF addition (Figure 58). This phenomenon was due to the fact that the receptor presented a high phosphorylation level, previous to EGF addition. During the pre-incubation time, the receptor almost completely recovered its activation level.

The experiment was repeated without pre-incubating the membrane sheets and adding ARNO in the stimulation mixtures, to observe if the protein had an effect on receptor activation (Figure 59). The addition of EGF allowed a two-time increase of the phosphorylation level of EGFR. Nevertheless, EGFR stimulation in membrane sheets is lower than the one measured in cellular systems (Bill 2011). Moreover, no enhancement of EGFR activation was observed upon ARNO addition.

Another cell line was used for membrane sheet preparation and evaluation of the effect of ARNO. H460 membrane sheets were treated as in the previous experiment (Figure 60). The phosphorylation of EGFR doubled upon EGF stimulation, but no effect was observed on membrane sheets incubated with ARNO.

Discussion

In all membrane systems no ARNO-dependent EGFR phosphorylation was observed. These results are contradictory with the data reported by Bill (2011), although it has to be considered that in Bill (2011) the cell-free experiments were performed with a soluble form of EGFR lacking any membrane-like environment. There is evidence that ARNO has an effect on EGFR phosphorylation in cell systems, but cell-free results were not able to be reproduced. In the cell-free systems only a low level of EGFR phosphorylation and no effect of ARNO on EGFR activation were detected. This can be explained by different factors: First, EGFR necessitates a co-factor that helps the activation and the interaction with ARNO, resembling the role of CNK1/cytohesin interaction for the IR pathway (Lim et al. 2010). Second, in cell-free models important regulatory systems of EGFR activity are missing. Protein phosphatases and endocytosis processes can also down-regulate EGFR activity. The equilibrium between inhibitory mechanisms and kinase activity regulates receptor phosphorylation (Segatto et al. 2011). In the latter case, the receptor in cell-free systems could already be in the proper conformation for activation and no enhancers are required to reach the fully activated state.

V.2.4.2 EGFR clustering and co-localization with ARNO on membrane sheets

Since an interaction between ARNO and EGFR was observed, albeit weak and transient in the previously illustrated experiment, the question was asked if ARNO was co-localizing at the plasma membrane with EGFR. Bill (2011) observed 60 % co-localization between the two endogenous proteins on H460 membrane sheets. HeLa membrane sheets were incubated with Flag-ARNO or with buffer as control. The plasma membrane sheets were immunostained for endogenous EGFR (green) and for the added ARNO (red) (Figure 61). The overlay between EGFR and ARNO spots, indicated as “merge”, appeared yellow. The results were also interpreted using a scatterplot (Figure 62) of the each sheets mean EGFR and mean ARNO intensities. Only when ARNO was incubated with the plasma membrane sheets, was a distribution along a straight line observed, indicating that increased EGFR levels correlated with an increased amount of bound ARNO. A random distribution (at ARNO background levels) was present when the membrane sheets were incubated buffer only. This correlation was quantified using the

Pearson's correlation coefficient (PCC) of ARNO and EGFR mean intensities, showing a medium-high correlation (Figure 63).

Independent from co-localization, another interesting phenomenon was observed. ARNO has an effect on EGFR clustering degree (Figure 64a). The relative standard deviation (RSD) is an indicator for the degree of clustering of EGFR molecules. The RSD for EGFR fluorescence was calculated in dependency on Flag-ARNO. The RSD decreased from 0.63 before ARNO addition, to 0.45 upon ARNO addition, indicating a reduction in the degree of clustering for EGFR. Since the RSD is also inversely proportional to the fluorescence intensity, the decrease of the RSD value may simply be caused by an increased EGFR intensity. Indeed, upon ARNO addition, EGFR intensity was increased by two times (Figure 64b). Therefore, ARNO may or may not decrease EGFR clustering, but it appears to make EGFR more accessible thereby giving a brighter EGFR fluorescence signal. In turn, this may indicate a less dense packing within clusters or a conformational rearrangement. The formation of EGFR agglomerates at the plasma membrane influences receptor activation (Ichinose et al. 2004). It is reported that pre-formed EGFR dimers are present at the plasma membrane, without EGF stimulation (Moriki et al. 2001). A recent study described that EGFR clusters at the plasma membrane, due to the interaction between the JM domain and negatively charged phospholipids, like PIP_2 (Wang et al. 2014). Taking that into account, it was evaluated if a PH mutated form of ARNO was still able to co-localize with EGFR at the plasma membrane (Figure 65). In the PH mutated ARNO construct the arginine residue in position 280 is substituted with a cysteine residue to impair the binding to PIP_ns on the cell membrane (Nagel et al. 1998b). The PH domain point mutation ARNO construct cannot interact with PIP_2 on the membrane, and the scatterplot revealed a random distribution between the ARNO and EGFR staining intensities, compared to the wild-type ARNO construct (Figure 66). Quantification with PCC confirmed a drastic decrease in the co-localization value with EGFR for the PH mutant compared to wild-type ARNO. Interestingly, the PCC value for the PH mutant ARNO is still slightly higher than for the buffer control (Figure 67). Then, EGFR clustering upon addition of the two constructs was assessed (Figure 68a). Furthermore, since the RSD can be influenced by the overall fluorescence intensity (see above), the mean EGFR channel intensities were also recorded (Figure 68b). In Figure 68a, EGFR staining shows a high RSD value (0.64) in the absence of added ARNO, a slightly lower value for the PH mutant ARNO (0.55) and the lowest value for wild-type ARNO (0.4). This indicates that wild-type ARNO decreases EGFR

clustering (as measured by RSD) strongly, while PH mutant ARNO has a less pronounced effect. However, as described above, these results may also be interpreted as an increased accessibility of EGFR receptor upon ARNO addition, with a weaker effect for the PH-domain point mutation.

If compared with the buffer control, the PH mutant ARNO exhibited a low co-localization with EGFR at the plasma membrane. This can be due to the fact that a weak interaction between the Sec7 domain of ARNO and EGFR was still taking place. As this interaction is probably happening with a very high Kd, the accumulation at the plasma membrane via the PH domain could be indispensable for the interaction with the Sec7 domain. Another hypothesis is that ARNO requires a co-factor for the interaction with the receptor. Summarizing, ARNO PH domain is required for the membrane recruitment and also for strong co-localization with EGFR at the plasma membrane. The PH domain mutation, which disrupts the interaction with PIP_2, significantly decreases the co-localization degree between the two proteins.

Since fluorescence microscopy presents resolution limits, other high-resolution microscopy techniques are necessary to further investigate this problem. In particular, using STED (stimulated emission depletion) microscopy it would be possible to measure co-localization at smaller scales. In addition, STED microscopy would allow to measure EGFR cluster dimensions directly before and after ARNO addition, shining light on the issue of decreased EGFR clustering. Using different ARNO truncated constructs, the role of different ARNO domains for co-localization, interaction and clustering can also be investigated. Another way around, in order to understand which domain(s) of EGFR is/are responsible for the interaction with ARNO, competition experiments with soluble EGFR functional regions could be performed.

Intriguingly, this implies a potentially new function of ARNO. In particular, the degree of EGFR clustering decreases in the presence of ARNO, and this effect depends on the ARNO PH domain. Wang et al. (2014) published that EGFR clustering is due to the interaction with anionic lipids. Furthermore they reported the presence of larger EGFR clusters in lung cancer cells compared to normal lung cells. EGFR clusters can be disrupted by PIP_2 depletion. ARNO might have an indirect effect on receptor clustering, binding to PIP_2 in EGFR proximity. This theory is supported by the fact that EGFR, in presence of the PH mutant, had a RSD value comparable to base level. The remaining small differences can be due to the fact that the Sec7 domain is still able to interact with EGFR and slightly influence clustering. Wang et al. (2014) proposed that a direct

interaction between the EGFR JM domain and PIP_2 at the plasma membrane leads to an increase of receptor cluster dimensions, while Endres et al. (2013) and the related paper of Arkhipov et al. (2013), highlighted a strong interaction between anionic lipids and positive residues on the JM domain in the receptor inhibited conformation. A hypothesis is that a mutually supportive interaction between PIP_2-JM, JM-ARNO Sec7 and PIP_2-ARNO PH can regulate EGFR activation, initially creating a PIP_2 microenvironment, then allowing the interaction between Sec7 and the JM domain to occur and helping the displacement of the JM from the plasma membrane for the formation of the active asymmetric dimer.

VI. Conclusion

VI.1 Which is the right membrane system?

Plasma membranes are extremely heterogenic systems and *in vitro* models, and while accurate, they can never reach the native complexity. On the other hand, having simplified systems in which transmembrane proteins can be studied, represent one of the major goals of biochemical research in the past twenty years. Micelles are usually the first choice to solubilize membrane proteins. The type of detergent is often crucial and particular attention should be paid to the CMC to ensure proper micelle formation. However, since detergents may disrupt weak hydrophobic and, for ionic detergents, ionic interactions, micelles are not suited to study transient protein-protein interactions (Catoire et al. 2014).

As plasma membranes are constituted of two phospholipids layers, bicelles represent a more native-like system in which transmembrane proteins can be studied. Bicelles can be easily prepared and they can self-assemble. Transmembrane proteins can be inserted into the bilayer and used for structural studies and they are accessible from both sides of the membrane. A disadvantage of bicelles is that the protein amount required is very high and often the desired protein yield is not reached. Moreover, to reconstitute a transmembrane protein into bicelles, lyophilization processes can be necessary. For complex globular proteins, enzymes or proteins with kinase activity, reconstitution from a lyophilized powder is especially challenging.

Further, nanodiscs were used to study protein-lipid and protein-protein interactions. Nanodiscs possess several advantages: modulation of the phospholipid composition, size control depending on the MSP type, and reconstitution of protein in oligomeric state (Borch, Hamann 2009). Nevertheless, finding the optimal ratio between phospholipids and membrane scaffold proteins for the proper nanodiscs assembly and for the membrane protein insertion can be very challenging. Also, the purification processes to obtain the desired nanodisc products can be tedious and time-consuming.

The last membrane system analyzed was plasma membrane sheets. Membrane sheets are the most *in vivo* like systems, suitable for protein interaction studies and fluorescence imaging. Starting from whole cells, the endogenous transmembrane proteins are still present. Membrane sheets can be incubated with exogenous proteins, or co-

transfection of two different proteins of interest can also be performed. As membrane sheets are adhered with their basal membrane to the glass support, the study of proteins from the extracellular side can be difficult.

Taking all of these considerations together, it is possible to deduce that the choice of the membrane system depends on the biochemical and biophysical assays that are required to investigate one particular membrane protein. Multiple assays may be used to fully evaluate a particular interaction. Different parameters have to be considered: the capacity of the transmembrane protein to resist to harsh conditions, such as detergents. Second, bilayer model systems can be preferable since they resemble the structure of the native membranes. Third, phospholipid bilayers allow the study of transmembrane proteins from both sides of the membrane. Furthermore, the expression, purification and reconstitution of desired transmembrane proteins into surrogate membranes can be difficult and time consuming. In this latter case, membrane sheets can be the appropriate system. For this reason, careful considerations of protein characteristics and of the design of experiments are always necessary.

VI.2 A new function for ARNO?

As part of a large research project into the role of ARNO in EGFR activation, this PhD project aimed to develop and implement *in vitro* systems to investigate the effects of ARNO on a molecular basis. Bill (2011) showed that ARNO increases the phosphorylation level of EGFR in living cells and for the soluble intracellular domain of EGFR. They propose that ARNO helps the formation of the asymmetric dimer. In all the experiments with *in vitro* systems reported here, the enhancement of EGFR activation upon ARNO addition was not observed.

Nevertheless, albeit weak and difficult to detect, observations were made regarding the interaction between the two proteins, with different limitations arising on the type of membrane system used. The current explanation for this interaction is based on Sec7 domain binding to the JM domain of EGFR, based on work in Famulok's research group showing that the JM region plays a relevant role in ARNO-EGFR interaction (personal communication from Benjamin Weiche, Anton Schmitz and Michael Famulok).

Furthermore, a new possible effect of ARNO on EGFR in membrane sheets was observed. ARNO either decreases EGFR clustering, or, more likely, increases EGFR

accessibility. A point mutation in the ARNO PH domain reduces membrane recruitment of ARNO, and the effect of ARNO on EGFR clustering. However, the remaining effects indicate interactions involving the Sec7 domain of ARNO and the JM domain of EGFR that may be significant. Nevertheless, the effect is drastically reduced if compared with wild-type ARNO, stressing the importance of the PH domain in the modulation of EGFR clustering. Moreover, the ARNO-EGFR interaction may be needed to induce conformational changes helping receptor activation, to alter the PIP_2 microenvironment, or to recruit other cytosolic co-factors.

These findings open the way to understanding the mechanism by which ARNO functions as activator for EGFR. As previously described, EGFR receptor is highly involved in different cancer types. Identifying the mechanism of activation of EGFR is crucial for developing new possible anti-EGFR treatments. Further experiments to elucidate the molecular details for the interaction are now even more necessary.

VII. Material and Methods

VII.1 Material

VII.1.1 Equipment

Equipment, type	Manufacturer
Analytical Balance	Sartorius, BP 211D
Autoclave	Systec
Blotting Chamber, semi-dry	BioRad
Centrifuges	Beckmann; Eppendorf
Christ Alpha 2-4 LD Freeze Dryers	SciQuip
Electrophoresis apparatus	BioRad
FPLC, ÄKTA	GE Healthcare Life Science
French Press	Thermo Scientific
Gel dryer	BioRad, Model 583
Heating blocks	Bachofer
HPLC, Agilent 1100	Agilent Technologies
Incubator (bacteria) Innova4430	Eppendorf
Incubator (mammalian cells)	Binder
Infinite M1000 Pro	Tecan
Microscope Nikon Eclipse TS100	Nikon
Microscope Olympus IX81-ZDC (AG Lang)	Olympus
Microwave	Bosch
MST-Monolith NT.115	Nano Temper
Nanoqant Infinite M200	Tecan
Odyssey Imager	Licorn
Over-head-tumbler	Heidolph
Peristaltic Pump	Mettler Toledo
pH-Meter	Mettler Toledo
Pipette-boy	Brand GmbH + Co.
Pipettes	Eppendorf
Plate reader, Enspire	PerkinElmer
Protino Ni-NTA Columns 5 ml	Macherey Nagel
Q1R column 1 ml (IEX)	Amersham Biosciences
SDS-PAGE equipment and chambers	BioRad
Sonifier	Bandelin Sonoplus
Sterile hood (bacteria)	Infors HT
Sterlie hood (mammalian cells)	Heraeus

Superdex 200 HR 10/30 column	GE Healthcare Life Science
UV/Vis Spectrophotometer	Thermo Spectronic
Vacuum-Pump AC500	HLC
Vortex Zx3	Velp Scientifica
Water bath	GFL
Water purification system	TKA-Lab

VII.1.2 Chemicals and Reagents

Reagent	Manufacturer
Acetic acid	Roth
Acetone	Roth
Acrylamide-Bisacrylamide solution (37.5:1)	Roth
Agarose	Bio-Budget Technologies
Alexa647-NHS	Invitrogen
Ammoniumperoxidisulfat (APS)	Roth
Biotin	Sigma-Aldrich
Bis(sulfosuccinimidyl)suberate (BS3)	Thermo Scientific
β-mercaptoethanol	Roth
Bradford Assay reagent	BioRad
Bromophenol blue	Merck
BSA	Sigma-Aldrich
Chloroform	VWR Chemical
Coomassie Brilliant Blue R250	Biorad
Desthiobiotin	Sigma-Aldrich
Dimethylsulphoxide (DMSO)	Fluka
Disuccinimidyl suberate (DSS)	Thermo Scientific
Dithiothreitol (DTT)	Roth
Ethylendiaminetetraacetic acid (EDTA)	AppliChem
Ethanol	Roth
Gel filtration standard mix	BioRad
Glycerol	Roth
Glycine	Roth
HEPES	Roth
Hydrochloric acid	VWR Chemical
Imidazole	Roth
Isopropanol	Roth
Magnesium chloride	Acros organics
Methanol	Roth
N,N,N’,N’-Tetramethylendiamine (TEMED)	Merck

PAGE Ruler Prestained Plus	Thermo Scientific
Protease Inhibitor Cocktail	Roche
Sodium bicarbonate	Merck
Sodium chloride	Roth
Sodium cholate	Sigma-Aldrich
Sodium dodecyl sulphate (SDS)	Roth
Sodium orthovanadate	AppliChem
TEMED	Roth
TetraSpeck beads 100 nm	Thermo Scientific
Thimerosal	AppliChem
TMA-DPH	Thermo Scientific
Trifluoroacetic acid	Roth
Tris	Roth
Triton X-100	AppliChem
Tween20	AppliChem
Uranylformate	SPI-Chem
Urea	Roth

VII.1.3 Consumables

Reagent	Manufacturer
Amberlite XAD-2	Supleco Analytical
Amicon Ultra Centrifugal Filters	Millipore
Blotting papers	Macherey-Nagel
Capillaries for MST	NanoTemper
Cell culture dishes	TPP
Cell culture flasks	TPP
Cell culture plates	TPP
Centrifugation tubes (15 ml and 50 ml)	Falcons or TPP
Dialysis membrane	Spectra/Por
Disposable columns	BioRad
Disposable cuvettes	Roth
Glutathione agarose beads	Protino
Glutathione magnetic beads	Pierce
Hamilton Syringes	Sigma-Aldrich
Membrane filters	Sigma-Aldich
NAP-5 and NAP- 10 columns	GE healthcare
Ni-NTA beads	Qiagen
Nitrocellulose papers	Wathman
Parafilm	Roth

Petri dishes	Faust
Pipette tips	Eppendorf and Peske
Reaction tubes (1.5 ml and 2 ml)	Eppendorf or Sarstedt
Serological pipettes (2 ml, 5 ml, 10 ml, 25 ml, 50 ml)	Sarstedt
Strep-tactin magnetic beads (MagStrep "type 2HC")	Iba
Strep-tactin superflow high capacity	Iba
Syringes	Braun

VII.1.4 Cell culture

VII.1.4.1 Cell culture reagents

Reagents	Manufacturer
Agar	Roth
Ampicillin	Sigma-Aldrich
Chloramphenicol	Sigma-Aldrich
DMEM	PAN
EGF	Peprotech
Fetal Calf Serum (FCS)	Biochrom
Glutamine	PAN
Isopropyl β-1-thiogalactopyranoside (IPTG)	Carbolution Chemicals
Kanamycin	Sigma-Aldrich
LB Medium	Roth
MEM	PAN
Metafecten	Biontex
NEAA (100x)	PAN
PBS Dulbecco's (1x) pH 7.4	PAN
Penicillin/Streptomycin	PAN
RPMI	PAN
Trypsin/EDTA (10x)	PAN

VII.1.4.2 Bacterial strains

Bacterial strains	Supplier
E. coli BL21DE3	Famulok's group (V. Fieberg)
E. coli BL21DE3 (RIL)	Agilent technologies
XL10-Gold	Agilent technologies

VII.1.4.3 Mammalian cell lines

Mammalian cell lines	Supplier
H460 (human lung cancer cell) - adherent	ATCC
HeLa (human cervix cancer cell) - adherent	ATCC

VII.1.5 Phospholipids

Phospholipid	Manufacturer
1,2-diheptanoyl-*sn*-glycero-3-phosphocholine 07:0 (DHPC)	Avanti Polar Lipids
1,2-dihexanoyl-*sn*-glycero-3-phosphocholine 06:0 (DHPC)	Avanti Polar Lipids
1,2-dimyristoyl-*sn*-glycero-3-phosphocholine 14:0 (DMPC)	Avanti Polar Lipids
1,2-dimyristoyl-*sn*-glycero-3-phospho-L-serine 14:0 (DMPS)	Avanti Polar Lipids
1,2-dipalmitoyl-*sn*-glycero-3-phosphocholine 16:0 (DPPC)	Avanti Polar Lipids
L-α-phosphatidylcholine (PC, Egg, Chicken)	Avanti Polar Lipids
L-α-phosphatidylethanolamine (PE, Liver, Bovine)	Avanti Polar Lipids
L-α-phosphatidylinositol-4,5-bisphosphate (PIP_2, Brain, Porcine)	Avanti Polar Lipids

VII.1.6 Antibodies

VII.1.6.1 Primary antibodies

Antibody target	Dilution v/v	Manufacturer
Apo-A1 sc-13549 (mouse)	1:1,000	Santa Cruz
Cytohesin 1/ARNO sc-9727 (goat)	1:1,000	Santa Cruz
EGFR sc-03 (rabbit)	1:1,000 (1:100 for microscopy)	Santa Cruz
FLAG M2 (mouse)	1:500	Sigma-Aldrich
GST sc-138 (mouse)	1:1,000	Santa Cruz
Penta-His (mouse)	1:500	Thermo Fisher
Phospho-Tyrosine sc-7020 (rabbit)	1:1,000	Santa Cruz
Phospho-Tyrosine 1086 EGFR (rabbit)	1:100	Cell Signaling

VII.1.6.2 Secondary antibodies

Antibody target	Dilution v/v	Manufacturer
Anti-goat (594 nm)	1:200	Life Technologies
Anti-mouse (594 nm)	1:200	Life Technologies
Anti-mouse (800 nm)	1:20,000	Licor
Anti-rabbit (488 nm)	1:200	Life Technologies
Anti-rabbit (594 nm)	1:200	Life Technologies
Anti-rabbit (800 nm)	1:20,000	Licor
Streptavidin-cojugated dye (800 nm)	1:20,000	Santa Cruz

VII.2 Methods

VII.2.1 Protein Expression and Purification

VII.2.1.1 Transformation of *E. coli* competent cells

The desired plasmids were introduced into BL21DE3 or BL21DE3 (RIL) *E. coli* strains. The RIL *E. coli* strain has the advantage of expressing extra tRNA genes for a few rare codons (R: arginine, I: isoleucine and L: leucine), increasing the expression efficiencies of heterologous proteins.

100 µl of chemically competent *E. coli* were thawed on ice for 10 minutes. 10 ng of DNA plasmid were added directly with the cells. The cells were incubated for 20 minutes on ice. Then, the cells were heat shocked for 1 minute at 42 °C and subsequently flash cooled on ice for 2 minutes. 500 µl of LB medium was added to the cells and the culture was grown for 1 hour at 37 °C, 1,000 rpm (rounds per minute).

Then the cells were centrifuged for 2 minutes at 3,500 rpm, and almost all the supernatant was discarded, the cell pellet was resuspended in the remaining 100 µl of LB (Luria Bertani) medium. The culture was plated on an Agar plate containing the appropriate antibiotic. The plate was incubated overnight at 37 °C in the incubator. The day after, the plate was removed from the incubator and stored for a maximum of 1 month at 4 °C.

Table 3: Bacterial media

Medium	Components
LB medium	20 g LB broth/1 L water
LB-Agar medium	LB medium supplemented with 15 g/L Agar

VII.2.1.2 Large-scale culture and preparation of glycerol stock

E. coli cells containing the plasmid of interest were growth overnight at 37 °C in 100 mL of LB medium, supplemented with the corresponding antibiotic. The small-volume culture was transferred into 1 L LB medium and grown at 37 °C until an OD (opticl density) at 600 nm between 0.6 and 0.8 was reached. A small aliquot of cell culture was removed and mixed with an equal volume of glycerol medium for the long-term storage at -80 °C.

Table 4: Storage Buffer for bacteria

Medium	Components
Glycerol medium	50 mM Tris-HCl pH 7.8 300 mM NaCl 40 % Glycerol

VII.2.1.3 Induction of protein expression and cell harvest

Protein expression was induced by the addition of 1 mM IPTG (isopropyl β-D-1-thiogalactopyranoside) to the culture medium. IPTG is a non-hydrolysable molecular mimic of allolactose. IPTG releases the Lac-Repressor from the Lac-Operon located in the *E. coli* genome and the T7 RNA polymerase is expressed. IPTG also releases the Lac-Repressor from the T7 promoter on the expression plasmid. Thus, the T7 RNA polymerase can bind to the T7 promoter and protein expression is induced.

All the construct reported in Table 5 were cloned by Doctor Anton Schmitz from Famulok's group. pMSP1D1 was a gift from Stephen Sligar (Addgene plasmid # 20061). Expression conditions were set up for each construct, as reported in Table 5. After expression, the cell culture was harvested at 5,000 rpm for 20 minutes at RT (Beckman Centrifuge, JLA 8.100 rotor). Cell pellets were stored at -80 °C until further processing.

Table 5: Plasmids list for expression in *E. coli*. (o/n: overnight)

Constructs	Temperature	Induction Time	Antibiotic µg/ml	*E. coli* Strain
pET28-HT-ARNO-Sec7	37 °C	5 h	Kanamycin 50	DE3
pET28-HTF-ARNO	20 °C	o/n	Kanamycin 50	DE3
pET28-HTF-ARNO-R280C (PH mutant)	20 °C	o/n	Kanamycin 50	DE3
pET28-ST-ARNO-PH	20 °C	o/n	Kanamycin 50	DE3-RIL
pGEX6P-ARNO-Sec7	37 °C	5 h	Ampicillin 100	DE3
pIBA101-HT-ARNO	20 °C	o/n	Ampicillin 100	DE3-RIL
pIBA101-HT-ARNO-ΔPBR	20 °C	o/n	Ampicillin 100	DE3-RIL
pMSP1D1	37 °C	3 h	Kanamycin 50	DE3-RIL
pMSP1D1-mEGFP	37 °C	3 h	Kanamycin 50	DE3-RIL

VII.2.1.4 Cell lysis

E. coli cell pellets were thawed and resuspended in the appropriated lysis buffer supplemented with 1x Protease Inhibitor Cocktail.

The resuspended cells were disrupted using the French press for two cycles with a maximum pressure of 1,200 PSI (pound-force per square inch, 82 bar) for *E. coli* cells.

Lysate was clarified via centrifugation at 2,0000 rpm for 20 minutes at 4 °C (Beckman Centrifuge, JA 25.50 rotor). The supernatant, containing the soluble protein, was used for further purification steps.

Table 6: Lysis buffers

Buffer	Components
ARNO constructs - Lysis buffer	50 mM Tris-HCl pH 7.8 at 4 °C 300 mM NaCl 5 % v/v Glycerol
MSP constructs - Lysis buffer	40 mM Tris-HCl pH 8.0 at 4 °C 300 mM NaCl 1% v/v Triton X-100 20 mM Imidazole

VII.2.1.5 Affinity Chromatography

Affinity chromatography is a technique to purify proteins through the reversible interaction between an affinity tag and a coupled matrix. A variety of different coupled matrix and affinity tags are commercially available.

VII.2.1.5.1 Nickel-NTA Affinity Chromatography

For the purification of the constructs reported in Table 5, containing a His-tag, a Ni-NTA Agarose matrix was used. His-tag interacts with Ni-NTA Agarose beads. Nitrilotriacetic acid (NTA) is a chelating agent and forms four coordination sites with Nickel molecules. Nickel molecules can form two reversible coordination sites with histidine residues of tagged proteins. Protein elution is achieved by adding a competitor, such as imidazole.

The supernatant after cell lysis was incubated for 1 hour at 4 °C and overhead tumbled with the appropriate amount of Ni-NTA Agarose beads. The amount of beads used were set on a case to case basis (generally 1 mL beads was used).

After incubation, the beads coupled with the protein of interest were separated from the supernatant by centrifugation at 1,500 rpm for 10 min at 4 °C. The beads were washed with washing buffer, and transferred to a disposable column. Three washing steps were performed. The protein was eluted by adding one beads-volume of elution buffer to the beads. The elution buffer was incubated with the beads for 10 minutes. The flow-through was then collected from the disposable column using a peristaltic pump. Three elution steps were generally performed. Samples from each purification steps were collected for SDS-PAGE analysis.

Table 7: Purification buffers for His-tagged constructs

Buffer	Components
ARNO constructs - Washing buffer	50 mM Tris-HCl pH 7.8 300 mM NaCl 20 mM Imidazole 5 % v/v Glycerol
ARNO constructs - Elution buffer	50 mM Tris-HCl pH 7.8 300 mM NaCl 350 mM Imidazole 5 % v/v Glycerol
MSP constructs - Washing buffer I	40 mM Tris-HCl pH 8.0 at 4 °C 300 mM NaCl 1% v/v Triton X-100 20 mM Imidazole
MSP constructs - Washing buffer II	40 mM Tris-HCl pH 8.0 at 4 °C 300 mM NaCl 50 mM cholate 20 mM Imidazole
MSP constructs - Washing buffer III	40 mM Tris-HCl pH 8.0 at 4 °C 300 mM NaCl 50 mM Imidazole
MSP constructs - Elution buffer	40 mM Tris-HCl pH 8.0 at 4 °C 300 mM NaCl 500 mM Imidazole

VII.2.1.5.2 Strep-tactin Affinity Chromatography

Strep-tactin is a derivate of streptavidin and binds to the streptavidin binding peptide (SBP)-tag. 600 µL strep-tactin beads were equilibrated with 25 mL lysis buffer. The supernatant containing the protein was then incubated with the beads for 1 hour at 4 °C. After incubation, the beads were sedimented at 1,500 rpm for 10 minutes at 4 °C.

Supernatant was discarded and the beads were transferred into a disposable column. The beads were washed with the wash buffer. One beads-volume of elution buffer was used. Elution buffer was incubated with the beads for 10 minutes on ice. The eluate was collected with the help of a peristaltic pump. Three elution steps were performed. Purification fractions were analyzed by SDS-PAGE and Western Blot.

Table 8: Purification buffers for SBP-tagged constructs

Buffer	Components
Wash buffer	50 mM Tris-HCl pH 7.8 at 4 °C 300 mM NaCl 5 % v/v Glycerol
Elution buffer	50 mM Tris-HCl pH 7.8 at 4 °C 300 mM NaCl 5 % v/v Glycerol 2.5 mM desthiobiotin

VII.2.1.5.3 Glutathione Affinity Chromatography

Glutathione agarose beads were used for the purification of GST-ARNO Sec7 construct. Glutathione beads bind to the GST-tag present at the N-terminal part of the construct. Glutathione-S-transferase Glutathione S-transferase (GST) is a dimeric protein. The GST-tag is composed of 220 amino acid residues, and it is often used to increase protein solubility. 2 mL of glutathione beads were incubated with the cell lysate for 1 hour at 4 °C. The same steps reported in Section VII.2.1.5.1 were performed to purify the protein.

Table 9: Purification buffers for GST-tagged construct

Buffer	Components
Wash buffer	50 mM Tris-HCl pH 7.8 at 4 °C 300 mM NaCl 5 % v/v Glycerol
Elution buffer	50 mM Tris-HCl pH 7.8 at 4 °C 300 mM NaCl 5 % v/v Glycerol 10 mM glutathione

VII.2.1.6 TEV digestion

For certain experimental applications, the affinity tag of the purified proteins was removed. The constructs reported in Table 5 contain a tobacco etch virus (TEV) cleavage site between the affinity tag and the protein of interest. A molar ratio of TEV to protein of 1 to 50 was used. The TEV digestion was performed overnight in the dialysis buffer.

After overnight dialysis, the protein was centrifuged at 5,000 rpm, for 10 minutes at 4 °C to remove the precipitate. The supernatant was applied onto a Ni-NTA matrix to remove the uncleaved protein and the His-tagged TEV protease.

Fractions of the flow-through containing the cleaved protein, the wash and elution fractions were collected and analyzed by SDS-PAGE. The fractions containing the cleaved protein were pooled together, divided into aliquots and stored at -80 °C.

Table 10: Dialysis buffers

Buffer	Components
ARNO constructs - Dialysis buffer	20 mM Tris-HCl pH 7.8 at 4 °C 150 mM NaCl 5 % Glycerol
MSP constructs - Dialysis buffer	20 mM Tris-HCl pH 7.4 at 4°C 100 mM NaCl 0.5 mM EDTA

VII.2.1.7 FPLC-gel filtration chromatography

A final purification step via FPLC-gel filtration is often necessary to remove impurities from the final protein product. Gel filtration is a technique that allows the separation of molecules according to their hydrodynamic volume. Generally Superdex or Sepharose matrix are used. These matrixes contain pores of different size. Small molecules can pass through the pores, while bigger molecules are excluded. In this way, it is possible to separate high molecular weight molecules, that are eluted earlier, from small size molecules. HiLoad™ 16/600 Superdex™ 200 (GE Healtcare) column or HiLoad™ 16/600 Superdex™ 75 (GE Healtcare) were used. Gel filtration columns were equilibrated with 3 column volumes of gel filtration buffer. 1 mL protein sample was applied onto the column. Elution fractions were collected and analyzed by SDS-PAGE and protein concentration was measured with UV-Absorption at 280 nm. Only the most pure fractions and with the highest protein concentrations were pooled together, further

concentrated with Vivaspin concentrators (Sartorius) or Amicon concentrators (Millipore), aliquoted and stored at -80 °C.

Table 11: Gel filtration buffers

Buffer	Components
ARNO constructs - gel filtration buffer	20 mM Tris-HCl pH 7.8 at 4 °C 150 mM NaCl 5 % Glycerol
MSP constructs - gel filtration buffer	20 mM Tris-HCl pH 7.4 at 4°C 100 mM NaCl 0.5 mM EDTA

VII.2.1.8 Expression and Purification of protein from inclusion bodies

Inclusion bodies are insoluble protein aggregates that accumulate in the cytoplasm of the host cell. The expression of hydrophobic heterologous protein in *E. coli* often leads to the formation of inclusion bodies, especially if the amount of expressed protein is high. For the purification of the proteins from inclusion bodies, the use of high concentration of denaturants, such as urea, is necessary (Singh et al. 2015).

VII.2.1.8.1 Purification of EGFR-TMJM constructs

The constructs reported in Table 12 were cloned by Doctor Anton Schmitz from Famulok's group.

Table 12: Plasmids list for expression in *E. coli* as unsoluble proteins. (o/n: overnight)

Constructs	Temperature	Induction Time	Antibiotic µg/ml	*E. coli* Strain
pET28-6H2W-EGFR-TMJM-SBP	37 °C	o/n	Kanamycin 50	DE3
pET28-6H2W-EGFR-TMJM-sc1-SBP	37 °C	o/n	Kanamycin 50	DE3
pET28-6H2W-EGFR-TMJM-sc2-SBP	37 °C	o/n	Kanamycin 50	DE3
pET28-HT-IR-TMJM-SBP	37 °C	o/n	Kanamycin 50	DE3
pET28-HST-EGFR-TMJM	37 °C	o/n	Kanamycin 50	DE3
pET28-HST-IR-TMJM	37 °C	o/n	Kanamycin 50	DE3

2 L of culture which was made into a cell pellet was resuspended in 20 mL lysis buffer on ice. Cells were made into a lysate form with French Press for three times at maximum 1,200 psi. Cell lysate was clarified with centrifugation for 20 minutes, 20,000 rpm at 4 °C (Beckman Centrifuge, JA 25.50 rotor). The supernatant was discarded and the cell pellet was washed three times with 20 mL washing buffer. Between each washing step, the cell pellet was resuspended and centrifuged again.

Cell pellet was then stirred for 1 hour at room temperature (RT) with the extraction buffer. The cell suspension was centrifuged for 20 minutes, 20,000 rpm at RT (Beckman Centrifuge, JA 25.50 rotor). The supernatant was incubated for 1 hour with Ni-NTA beads at RT. The protein was eluted three times in the elution buffer. Urea was removed overnight via dialysis against water. Protein precipitate was collected and lyophilized (Christ Alpha 2-4 LD Freeze Dryers). Lyophilized protein was stored at -20 °C.

Table 13: Buffers for protein purification form inclusion bodies

Buffer	Components
Lysis buffer	50 mM Tris-HCl pH 8.0 at 4 °C 100 mM NaCl
Wash buffer	50 mM Tris-HCl pH 8.0 at 4 °C 100 mM NaCl 1 M Urea 0.5 % Triton X-100
Extraction buffer	50 mM Tris-HCl pH 8.0 at RT 300 mM NaCl 8 M Urea 0.2 % SDS
Purification buffer	50 mM Tris-HCl pH 8.0 at RT 300 mM NaCl 8 M Urea 0.2 % Sodium Cholate 20 mM Imidazole
Elution buffer	50 mM Tris-HCl pH 8.0 at RT 300 mM NaCl 8 M Urea 0.2 % Sodium Cholate 350 mM Imidazole
Dialysis buffer	20 mM HEPES pH 8.0 at 4 °C 100 mM NaCl 0.5 mM EDTA 0.2 % Sodium Cholate

VII.2.1.9 Protein purification from Sf9 insect cells

VII.2.1.9.1 Expression of lz-EGFR-TS and cell harvest

pFB-lzEGFR-TS was expressed in baculovirus-infected Sf9 (*Spodoptera frugiperda*) insect cells from Yvonne Aschenbach (Famulok's group). The construct was designed by Dr. Anton Schmitz. Infection was performed for three days at 21 °C. Insect cells were harvested at 2,000 rpm for 15 minutes at 4 °C (Beckman Centrifuge, JLA 8.100 rotor).

VII.2.1.9.2 Purification of lz-EGFR-TS

1.5 L cell pellet was resuspended in 25 mL lysis buffer supplemented with 1x Protease Inhibitor Cocktail. Cell lysate was incubated for 30 minutes on ice. Cells were passed through the French Press for two cycle at maximum 1,000 PSI (69 bar). Cell lysate

was centrifuged at 14,000 rpm for 20 minutes at 4 °C (Beckman Centrifuge, JA 25.50 rotor). Supernatant was incubated with 2 mL Strep-tactin beads. The purification was performed as reported in Section VII.2.1.5.2.

The construct has a C-terminal SBP-tag that was used for the purification. 2 mL Strep-tactin beads were equilibrated with 25 mL lysis buffer. The supernatant containing lz-EGFR-TS protein was then incubated with the beads for 1 hour at 4 °C. After incubation, the beads were sedimented at 1,500 rpm for 10 minutes at 4 °C. Supernatant was discarded and the beads were transferred into a disposable column. The beads were washed three times with the wash buffer. 2 mL elution buffer was incubated with the beads for 10 minutes on ice. The eluate was collected with the help of a peristaltic pump. Three elution steps were performed. Purification fractions were analyzed by SDS-PAGE and Western Blot.

Table 14: Purification buffers for protein expressed in Sf9 cells

Buffer	Components
Lysis buffer	20 mM Tris-HCl pH 8.0 at 4 °C 400 mM NaCl 10% v/v Glycerol 0.1 % v/v Triton X-100 1 mM EDTA
Wash buffer	20 mM Tris-HCl pH 8.0 at 4 °C 400 mM NaCl 10% v/v Glycerol 0.1 % v/v Triton X-100 1 mM EDTA
Elution buffer	20 mM Tris-HCl pH 8.0 at 4 °C 400 mM NaCl 10% v/v Glycerol 0.1 % v/v Triton X-100 1 mM EDTA 2.5 mM desthiobiotin

VII.2.2 Determination of protein concentration

VII.2.2.1 Absorption

Protein concentration can be calculated using the absorption at 280 nm of amino acids containing an aromatic ring. The concentration was calculated using the Lambert-Beer Law:

$$A_{280} = \varepsilon \times c \times l$$

ε = extinction coefficient ($mol^{-1} * cm^{-1}$)

c = protein concentration (mol/L)

l = path length (cm)

VII.2.2.2 Bradford Assay

The Bradford assay was performed using the BioRad Bradford reagent. The assay is based on the color shift of the Coomassie Brilliant Blue G-250 dye from 465 nm to 595 nm upon protein binding.
BioRad Bradford reagent was diluted 1:5 in water. Different BSA concentrations were used as standards. 2 µl of protein were mixed with 150 µl of diluted Breadford reagent. Absoption at 595 nm was measured using Varioskan plate reader.

VII.2.3 Analysis of purified proteins

VII.2.3.1 SDS-PAGE

SDS-polyacrylamide gel electrophoresis (PAGE) was performed according the protocol of Laemmli (Laemmli 1970). SDS (sodium dodecyl sulphate) is an anionic detergent used to confer a negative net charge to the proteins. Proteins can be separate according to their size, moving from the negative to the positive pole, when an appropriate voltage is applied. Biphasic gels with a thickness of 1 mm were used. A 4 % stacking gel was casted on the upper part of the gel and a separating gel on the lower part. Different percentage of bis-acrylamide were used to cast the separating gel, depending on the molecular weight of the analyzed proteins. The gel mixture was prepared according to

Table 16. Polymerization was started upon addition of APS (ammonium persulfate) and TEMED (tetramethylethylenediamine).

Protein samples were mixed with 1x sample buffer and boiled at 95 °C for 5 minutes. 5 µl samples and a molecular weight pre-stained protein standard were loaded onto the gel. Gels were run in BioRad gel chambers at 200 Volt in 1x running buffer. Gels were run until the bromophenol blue contained in the sample buffer had reached the lower part of the gel. Gels were further analyze by Coomassie staining or used for Western Blot.

Table 15: Buffers for gel and sample preparation for SDS-PAGE

Buffer	Components
4x Stacking Gel buffer	60.6 g/L Tris-HCl pH 6.8 4 g/L SDS
4x Separating Gel buffer	181.7 g/L Tris-HCl pH 8.8 4 g/l SDS
6x Sample buffer	50 mM Tris pH 6.8 30 % Glycerol 15 % w/v SDS 600 mM DTT Bromophenol blue

Table 16: Recipe for SDS-PAGE preparation

1 gel	Separating Gel						Stacking Gel
	6 %	7.5 %	8 %	10 %	12.5 %	15 %	4 %
acrylamide	1000 µL	1250 µL	1333 µL	1667 µL	2083 µL	2500 µL	213 µL
water	2712 µL	2462 µL	2379 µL	2045 µL	1629 µL	1212 µL	975 µL
4x separating gel buffer	1250 µL						-
4x stacking gel buffer	-						400 µL
TEMED	8 µL						2 µL
APS	30 µL						10.4 µL

VII.2.3.2 Coomassie Staining

SDS-PAGE gels were covered with Coomassie staining solution and incubated at room temperature for at least 30 minutes. Coomassie staining solution was then removed,

and the gel was destained overnight in the destaining solution. Gels were scanned using Odyssey Image Scanner (Licor).

Table 17: Buffers for protein gel staining

Buffer	Components
Coomassie staining	30 % v/v methanol 10 % v/v acetic acid 700 mg/L Coomassie Brilliant Blue G-250
Coomassie destaining	30 % v/v methanol 10 % v/v acetic acid

VII.2.3.3 Western Blot

After SDS-PAGE, proteins were transferred onto a nitrocellulose membrane according to the Kyhse-Andersen protocol (Kyhse-Andersen 1984). A semi-dried blot was performed. The nitrocellulose membrane was equilibrated in anode II buffer, while the gel was equilibrated in cathode buffer. The gel and the nitrocellulose membrane were then piled with filter papers (Machery-Nagel) as reported in Figure 69. The transfer was performed applying 2 mA/cm^2 of gel for 45 minutes.

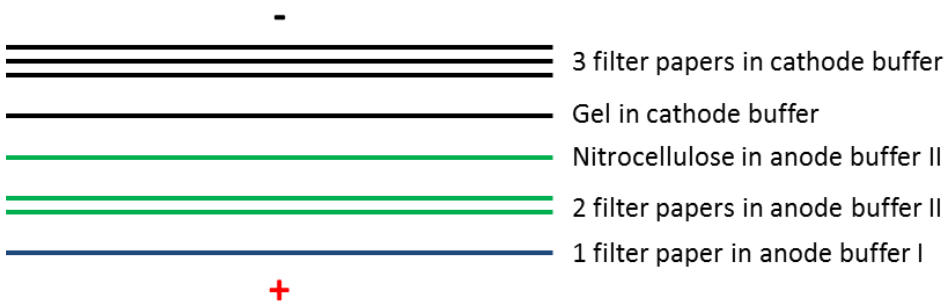

Figure 69: Western Blot transfer schema

Then, the nitrocellulose paper was incubated for 1 hour at room temperature with the blocking solution. The primary antibody was then applied onto the membrane for 1 hour at room temperature. The membrane was washed 3 times for 5 minutes with TBS-T and incubated overnight with the secondary antibody at 4 °C. Primary antibodies were diluted in 5 % BSA/TBS-T with 1:500 Thimerosal. Antibody dilutions are reported in Section VII.1.6. The secondary antibodies anti-mouse (800 nm) and anti-rabbit (800 nm) were diluted 1:20,000 in in 5 % BSA/TBS-T with 1:500 Thimerosal.

Table 18: Western Blot buffers

Buffer	Components
Anode buffer I	300 mM Tris-HCl pH 10.4
Anode buffer II	25 mM Tris-HCl pH 10.4
Cathode buffer	25 mM Tris-HCl pH 9.4 40 mM glycine
TBS-T	20 mM Tris-HCl pH 7.6 136 mM NaCl Tween20 0.1 % v/v
Blocking buffer	5 % w/v BSA in TBS-T

VII.2.4 Bicelles

Bicelles are mixtures of short-chain and long-chain phospholipids. Bicelles arrange in solution to form phospholipids bilayers and are suitable for the insertion of membrane proteins.

VII.2.4.1 Bicelles assembly

DMPC (1,2-dimyristoyl-sn-glycero-3-phosphocholine) or DPPC (1,2-dipalmitoyl-sn-glycero-3-phosphocholine) were mixed with DHPC (1,2-dihexanoyl-sn-glycero-3-phosphocholine). One of the most important parameters for bicelles assembly is the q factor. The q factor is the molar ratio between DMPC or DPPC and DHPC.

DMPC/DHPC or DPPC/DHPC were mixed together as a powder in a round-shaped glass vial. The q factor was set at 0.25. A pH around 7 is recommended to reduce oxidation processes. The final concentration of phospholipids was 46 mM in 10 mM phosphate buffer pH 7.2. The phospholipids were vortexed for 1 minute at room temperature and then incubated at 4 °C for 15 minutes. The mixture was warmed up in a water bath at 38 °C for 20 minutes and vortexed again for 5 minutes. This cool-warm process was repeated for three cycles, until the mixture appeared clear. Bicelles formation was controlled with DLS.

VII.2.4.2 Dynamic Light Scattering (DLS)

DLS was performed in the group of Professor Gerd Bendas, University of Bonn. A Nanotrac Ultra (Microtrac) dynamic light scattering system was used. Prior to DLS

analysis, samples were centrifuged at 14,000 rpm for 10 minutes at 4 °C in a table top centrifuge, to remove aggregates. For the sample preparation for DLS measurement, the final concentration of DHPC has to be above 7 mM, otherwise bicelles are not stable and disassemble. DHPC was supplemented into the dilution buffer. Diameters and the percent of monodisperse populations in solution were calculated using FLEX Software.

VII.2.4.3 Incorporation of EGFR-TMJM constructs in bicelles

His-EGFR-TMJM-SBP and the scrambled version 1 and 2 were added as lyophilized powder (3 mg) to the already formed bicelles. Upon protein addition, the mixture was incubated for 15 min at 4 °C. Subsequently, the mixture was incubated in water bath at 38 °C for 20 minutes, vortexed and centrifuged in a table-top centrifuge for 10 minutes at 14,000 rpm at room temperature. The supernatant with the protein incorporated in bicelles was stored at 4 °C and used within a week. To calculate the amount of protein incorporated in bicelles, absorption at 280 nm was measured. Empty bicelles were used as blank. Bicelles formation was controlled with DLS. Incorporation of His-EGFR-TMJM-SBP into bicelles was controlled by SDS-PAGE.

VII.2.5 Nanodiscs

Nanodiscs are phospholipids bilayers surrounded by two amphiphilic helical molecules, termed membrane scaffold proteins (Bayburt et al. 2002; Bayburt, Sligar 2003). Different phospholipids were used for the assembly of nanodiscs, as reported in Section VII.1.5. Membrane scaffold protein was purified as described in Paragraph VII.2.1.

VII.2.5.1 Preparation of nanodiscs reconstitution mixture

VII.2.5.1.1 PCPE- and PIP_2-nanodiscs preparation

For the preparation of nanodiscs L-α-phosphatidylcholine (PC, egg, chicken), L-α-phosphatidylethanolamine (PE, liver, bovine), and L-α-phosphatidylinositol-4,5-bisphosphate (PIP_2, brain, porcine) were used. Two different nanodisc compositions were prepared, as reported in Table 19.

Table 19: PCPE- and PIP_2-nanodiscs composition

Nanodisc	Phospholipid	MSP1D1:phospholipids molar ratio
PCPE-nanodiscs	80 mol % L-α-phosphatidylcholine 20 mol% L-α-phosphatidylethanolamine	1:30
PIP_2-nanodiscs	75 mol % L-α-phosphatidylcholine 20 mol % L-α-phosphatidylethanolamine 5 mol % L-α-phosphatidylinositol-4,5-bisphosphate	1:30

Nanodiscs were prepared following the Sligar's protocol (Bayburt, Sligar 2010). Phospholipids were dissolved in chloroform: PC at 20 mM and PE at 10 mM respectively. PIP_2 was dissolved in chloroform/methanol/water (20:9:1, 1 mM). Hamilton syringes were used to take the desired volume of phospholipids. Phospholipids were transferred in round-bottom vials and chloroform was dried under-vacuum overnight. A lipid thin layer was formed by rotating the vial during the drying process. For PIP_2-containing mixture, during the evaporation process the vial was immersed in a water bath at 34 °C for 5 minutes to increase PIP_2 homogenization. Phospholipid film was solubilized at the final concentration of 50 mM in 100 mM sodium cholate buffer.

Table 20: Buffers for the preparation of nanodiscs containing natural phosholipids

Buffer	Components
MSP standard buffer	20 mM Tris-HCl pH 7.4 at 4°C 100 mM NaCl 0.5 mM EDTA
Sodium cholate buffer	100 mM Sodium cholate in MSP standard buffer

The sodium cholate concentration was twice the concentration of lipid. The phospholipid thin layer was vortexed, warmed up and sonicated until the mixture appeared clear.

The appropriate amount of cholate-solubilized phospholipids and membrane scaffold protein were mixed. Typically a 1:30 MSP1D1:phospholipids molar ratio for PCPE-nanodiscs and PIP_2-nanodiscs was used. The sodium cholate in the final mixture had to be above the critical micellar concentration (CMC), between 12 mM and 40 mM. The MSP:phospholipids ratio is critical for the properly nanodiscs formation.

The nanodisc reaction mixtures were incubated for at least 15 minutes at 4 °C. The assembly process took place upon detergent removal. Amberlite XAD-2 beads (Sigma)

were used. Typically 0.5-0.8 g damp beads per ml mixture were used. Beads were washed twice with 1 ml methanol, water and MSP standard buffer. Phospholipids-cholate-MSP1D1 mixture was incubated overnight with the Amberlite beads at 4 °C and overhead tumbled.

Beads were then removed with two centrifugation steps in a table-top centrifuge at maximum speed at 4 °C. Nanodiscs formation was confirmed by gel filtration analysis on a Superdex 200 10/300 GL column (GE Healthcare) and with dynamic light scattering (DLS, Nanotrac, Microtrac). Nanodiscs were stored at 4 °C and used within a week.

VII.2.5.1.2 DMPC- and DPPC-nanodiscs preparation

For the preparation of nanodiscs with synthetic lipids 1,2-dimyristoyl-sn-glycero-3-phosphocholine (DMPC) or 1,2-dipalmitoyl-sn-glycero-3-phosphocholine (DPPC) were used. DMPC and DPPC were dissolved in chloroform at 50-100 mM for storage. Two different nanodiscs compositions were prepared, as reported in Table 21.

Table 21: DMPC- and DPPC-nanodiscs composition

Nanodisc	Phospholipid	MSP1D1:phospholipids molar ratio
DMPC-nanodiscs	1,2-dimyristoyl-*sn*-glycero-3-phosphocholine	1:60
DPPC-nanodiscs	1,2-dipalmitoyl-*sn*-glycero-3-phosphocholine	1:70

For the preparation of DMPC- and DPPC-nanodiscs the same steps as reported in Section VII.2.5.1.1 were performed. Briefly, the desired amount of phospholipids was dried for 3 hours under vacuum. The phospholipid film was rehydrated in phospholipid rehydration buffer at the final concentration of 10 mM. The MSP1D1:phospholipids molar ratio was set to 1:60 for DMPC and 1:70 for DPPC. In 200 µL assembly reaction, 10 µM MSP1D1 was incubated with 600 µM DMPC or 700 µM DPPC in the assembly buffer.

Table 22: Buffers for the preparation of nanodiscs containing synthetic phosholipids

Buffer	Components
Phospholipid rehydration buffer	10 mM Tris-HCl pH 7.4 at RT 100 mM NaCl 20 mM Triton X-100
Assembly buffer	10 mM Tris-HCl pH 7.4 at RT 100 mM NaCl 1 mM Triton X-100

The phospholipids-detergent-MSP1D1 mixtures were incubated for 1 hour at 25 °C for DMPC and 37 °C for DPPC, respectively. The mixtures were incubated overnight with Amberlite beads at 4 °C and overhead tumbled. Beads were removed and nanodiscs assembly was checked with gel filtration and DLS. Nanodiscs were stored at 4 °C and used within a week.

VII.2.5.2 Incorporation of membrane proteins into nanodiscs

For the incorporation of membrane proteins into nanodiscs the MSP to target protein ratio, the detergent and the assembly temperature are important parameters. It is suggested to establish the conditions to assembly "empty" discs and then to proceed with the insertion of membrane proteins.

VII.2.5.2.1 Insertion of lz-EGFR-TS in nanodiscs

Lz-EGFR-TS (for purification see Section VII.2.1.9.2) was incorporated into DPPC-nanodiscs. The MSP1D1 to phospholipids ratio was set to 1:70. The protocol was adapted from Mi et al. (2008). In 200 µL assembly reactions, 10 µM MSP1D1, 700 µM DPPC and 1 µM lz-EGFR-TS were mixed together at 45 °C for 1 hour. The final Triton X-100 concentration was kept between 2.0 mM and 2.5 mM. The final assembly steps were performed as reported in Section VII.2.5.1.2. To verify the insertion of the transmembrane protein, a negative control preparation was mixed. 200 µL mixtures containing 700 µM DPPC and 1 µM lz-EGFR-TS or 10 µM MSP1D1 and 1 µM lz-EGFR-TS were prepared. The same steps as for the nanodiscs assembly were repeated. Proper nanodiscs formation was checked by analytical SDS-PAGE.

VII.2.5.2.2 Insertion of His-EGFR-TMJM-SBP in nanodiscs

For the incorporation of His-EGFR-TMJM-SBP into nanodiscs, DMPC or DPPC were used. The phospholipid films were rehydrated in sodium cholate buffer at the final concentration of 50 mM. The volumes of solubilized phospholipids, MSP1D1, transemembrane protein and buffer for the reconstitution mixtures were calculated. The MSP:phopholipids ratios reported in Table 21 were used. The molecular ratio of MSP1D1 to His-EGFR-TMJM-SBP was set to 3:1. The same assembly protocol reported in Section VII.2.5.2.1 was used.

VII.2.5.3 Analysis of nanodiscs assembly

VII.2.5.3.1 Dynamic Light Scattering (DLS)

DLS was performed in the group of Professor Gerd Bendas, University of Bonn. A Nanotrac Ultra (Microtrac) dynamic light scattering system was used. DLS was performed as reported in Section VII.2.4.2. Samples were diluted 1:10 in MSP standard buffer and applied into the sample cell.

VII.2.5.3.2 Analytical FPLC-gel filtration chromatography

Analytical gel filtration was performed on a Superdex 200 10/300 GL column (GE Healthcare) in MSP standard buffer with a flow rate of 0.4 mL/min. 100 µL nanodisc sample was injected. BioRad protein standard was used as a molecular weight reference. Nanodisc fractions of 0.2 mL were collected and analyzed by 12.5 % SDS-PAGE.

VII.2.5.3.3 Analytical SDS-PAGE

SDS-PAGE was performed as reported in Section VII.2.3.1. To evaluate the incorporation of lz-EGFR-TS into nanodiscs an analytical 12.5% SDS-PAGE was performed. To calculate the amount of transmembrane protein embedded into nanodiscs, a titration gel was performed. 10 µL of purified lz-EGFR-TS protein was loaded onto the gel. The following protein concentrations were used: 1 µM, 750 nM, 500 nM, 200 nM and 100 nM.

VII.2.5.3.4 Negative Staining Electron Microscopy (EM)

For the preparation of the samples for negative staining, a modified protocol from Ohi et al. (2004) was used. Briefly, a 0.75% uranylformate staining solution was prepared dissolving 0.0375 g uranylformate in 5 ml boiling ddH_2O by stirring for 5 minutes in the

dark. Subsequently, 6 µl of 5 M NaOH solution were added to the mixture and it was stirred again for 5 minutes in the dark. The prepared solution was then filtered through a 0.22 µm filter to remove insoluble particles. A glow-discharged carbon-coated electron microscopy (EM) grid was prepared using a plasma cleaner (Diener, Femto). Then, the sample was adsorbed on the grid and washed with two drops of double deionized H_2O and two drops of the heavy metal solution. The excess of fluid was removed with filter paper. The sample was completely dried using a suction pump. Samples can be stored dry for at least one year.

Nanodiscs after gel filtration in EM Buffer were let adhere on the EM grid. Nanodiscs were imaged with a JEM-2200 FS (JEOL) Microscope. Images were taken with a TemCam-F416 (TVIPS) camera.

Table 23: Electron Microscopy buffer

Buffer	Components
EM buffer	10 mM Tris-HCl pH 7.4 at 4 °C 25 mM KCl 0.5 mM EDTA

VII.2.6 Membrane Sheets

VII.2.6.1 Cell culture

Cells were grown at 37 °C with 5 % CO_2 in 75 cm^2 flasks. Cells were split every 3 days or when a confluence of 70-90 % was reached. HeLa cells were cultivated in MEM medium supplemented with 10 % FCS and 4 mM glutamine. H460 cells were cultivated in RPMI medium supplemented with 10 % FCS and 4 mM glutamine. Penicillin/Streptomycin was added to the medium at a final concentration of 60 U/ml each.

Cell medium was removed and the cells were rinsed once with Dulbecco´s PBS (calcium- and magnesium-free). Cells were deatached from the flask by incubation with Trypsin-EDTA for 3 minutes at 37 °C followed by addition of MEM medium. Cells were pelleted for 3 minutes at 1,000 rpm. The supernatant was removed and the cell pellet was resuspended in the desired volume of complete medium. The appropriate cell amount was further cultivated.

VII.2.6.2 Coverslip cleaning and coating

Round glass coverslips (Ø 25 mm, thickness 1.0) were rinsed with water, ethanol, and water. Directly afterwards, coverslips were washed with 1 M HCl for ~2 hours and subsequently washed with water. Another 2 hours incubation step was performed in 1 M NaOH. Coverslips were then washed with water and rinsed in ethanol overnight. The day after, ethanol was removed and coverslips were sterilized at 150 °C.

For the coating, coverslips were transferred into six-well plates. Poly-L-lysine at the concentration of 0.1 mg/mL was added to the coverslips (500 µL for each coverslip) and incubated for 30-45 minutes at room temperature. Then, the liquid was removed and the coverslips were dried for 1 hour and directly sterilized for 20 minutes using UV lamp. Coverslips were stored at 4 °C and used within a month.

VII.2.6.3 Preparation of membrane sheets

$1.5x10^5$ HeLa cells or H460 cells were plated onto poly-L-lysine coated coverslips. Cells were cultivated as reported in Section VII.2.6.1. Cells were left to adhere for 5 hours and then starved overnight. For the preparation of membrane sheets, the procedure was adapted from previously described protocols (Avery 2000; Lang 2001). Coverslips were immersed in ice-cold sonication buffer (composition depending on the experimental requirements, see Table 24) and treated with ultrasound for 100 ms. Membrane sheets were used to investigate the effect of ARNO on EGFR phosphorylation and the EGFR-ARNO co-localization at the plasma membrane.

Table 24: Sonication buffers

Buffer	Components
Sonication buffer (phosphorylation assay)	20 mM HEPES pH 7.2 150 mM NaCl
Sonication buffer (co-localization)	20 mM HEPES pH 7.2 120 mM potassium glutamate 20 mM potassium acetate 10 mM EGTA

VII.2.7 Phosphorylation Assay

To evaluate the activity of EGFR reconstituted in artificial membrane systems, *in vitro* phosphorylation assays were performed.

VII.2.7.1 Phosphorylation Assay in micelles

Triton X-100 micelles containing 100 nM lz-EGFR-TS were incubated in presence of 200 nM YopH (Tyrosine-protein phosphatase from *Yersinia pseudotuberculosis*), and 10 µM BSA in 1x Phosphorylation Buffer. The mixture was incubated for 5 minutes at room temperature. Subsequently, 600 nM ARNO Sec7, 600 nM GST or reaction buffer were added. Samples before stimulation were taken. The reaction was started by the addition of 1 mM ATP. The receptor was stimulated for 10 and 20 seconds and then stopped by ETDA addition at the concentration of 20 mM. Samples were analyzed by SDS-PAGE and anti-pTyr Western Blot. The antibody was diluted 1:10,000 in 5 % BSA/TBS-T with 1:500 Thimerosal.

Table 25: Buffers for EGFR-phosphorylation assay

Buffer	Components
Phosphorylation Buffer	10 mM Tris-HCl pH 7.4 100 mM NaCl 5 mM $MgCl_2$ 0.1 % Triton X-100
10x Phosphatase Inhibitor	25 mM NaO_7P_2 10 mM β-Glycerophosphate 10 mM Na_3VO_4
Reaction Buffer	10 mM Tris-HCl pH 7.4 100 mM NaCl

VII.2.7.2 Phosphorylation Assay in nanodiscs

Briefly, in 100 µL reaction mixtures 100 nM lz-EGFR-TS-containing nanodiscs, 1x Phosphatase Inhibitors, and Phosphorylation Buffer were mixed together. Eventually, different ARNO constructs at the concentration of 600 nM were added: ARNO Sec7, Flag-ARNO Sec7, Flag-ARNO PH or reaction buffer. The mixtures were incubated for 10 minutes at room temperature. Samples before stimulation were taken. The reaction was started by the addition of 1 mM ATP. The receptor was stimulated for 1 and 3

minutes and then stopped by addition of 20 mM ETDA. Samples were analyzed by SDS-PAGE and anti-pTyr or anti-EGFR sc03 Western Blot. Both antibodies were diluted 1:10,000 in 5 % BSA/TBS-T with 1:500 Thimerosal.

VII.2.7.3 Phosphorylation Assay in membrane sheets

Coverslips were removed from sonication buffer and were incubated upside-down on different reaction mixture drops on parafilm. Sonication buffer was supplemented with 5 mM $MgCl_2$ and 1 mM Na-orthovanadate. The coverslips were pre-incubated for 5 minutes at room temperature. Coverslips were stimulated in presence of 1 mM ATP and three different EGF concentrations, 50 ng/mL, 25 ng/mL and 12.5 ng/mL respectively, for 1 minute.

In another experiment, 50 ng/ml EGF or 50 ng/ml EGF and 100 nM ARNO without His-tag were incubated for 5 minutes in presence of 1 mM ATP. No pre-incubation was performed. Samples were directly fixed after stimulation and further analyzed as reported in Section VII.2.13.1.

VII.2.8 Nucleotide Exchange Assay

To measure the catalytic activity of GST-ARNO Sec7 a tryptophan fluorescence assay on NΔ17Arf1 was performed. A 500 µM GTP mixture in PBS pH 7.4 and 3 mM $MgCl_2$ was prepared. NΔ17Arf1 at the concentration of 2.8 µM was then pre-incubated for 15 minutes at 37 °C with 80 µM GDP in PBS pH 7.4 and 2 mM EDTA. The GDP-bound Arf1 was stabilized by adding 3 mM $MgCl_2$ to the mixture and it was incubated for 5 minutes at 37 °C. Different ARNO Sec7 concentrations (0 nM, 10 nM, 15 nM) were incubated with 700 nM GDP-Arf1 in PBS pH 7.4 and 3 mM $MgCl_2$ (total volume 80 µL). The reaction was started by adding 10 µl GTP (50 nM). The tryptophan fluorescence was measured a 280 nm excitation and 340 nm emission for 600 seconds in a black 96-well plate. The fluorescence signal was detected every 5 seconds. The measurement was performed on an Infinite 200 Pro Tecan Reader (Tecan). The GraphPadPrism Software was used for the line fitting by linear regression.

VII.2.9 Pull-down Assay

Pull-down is a technique to measure biochemical interactions between two or more proteins. Similarly to affinity chromatography, pull-down used tag-conjugated beads. The affinity tag binds to the "bait" protein contained in the solution. Washing steps are performed to remove the unbound proteins. Then, the "pray" protein is added to the mixture and binds to the "bait" protein. After a washing step, the protein-protein complex is eluted. Analysis was performed by SDS-PAGE.

VII.2.9.1 Pull-down Assay of nanodiscs and ARNO PH domain

20 µL Strep-tactin magnetic beads were equilibrated in 200 µL wash buffer for two times. 8 µM PCPE-nanodiscs or PIP_2-nanodiscs were mixed with 16 µM ST-ARNO-PH in wash buffer in the presence of 2 % v/v DMSO. The reaction mixture was incubated with the beads for 30 minutes on ice and vortexed every 5 minutes. The mixtures and the beads were put on a magnetic rack. The supernatant was removed and the beads were washed 3 times with 100 µL of wash buffer. 25 µL elution buffer was incubated for 10 minutes with the beads. Loaded samples and eluted samples were analyzed by 12.5 % SDS-PAGE.

Table 26: Buffers for nanodiscs-ARNO PH pull-down

Buffer	Components
Wash buffer	50 mM Tris-HCl pH 7.8 at 4°C 150 mM NaCl 5 % Glycerol
Elution buffer	50 mM Tris-HCl pH 7.8 at 4°C 150 mM NaCl 5 % Glycerol 10 mM biotin

VII.2.9.2 Pull-down Assay of nanodiscs and ARNO PH domain in presence of Cyplecksins

Cyplecksins are barbiturate derivatives that inhibit the membrane recruitment of the PH domain of ARNO. Cyplecksins were synthetized and kindly provided by Doctor Mohammed Hussein, from Famulok's group. ST-ARNO-PH was incubated for 15 minutes on ice in the presence of 100 µM cyplecksins 1-3 or 100 µM of cyplecksins

inactive analogues (MH 40 A and MH 40 B). The final concentration of DMSO was 2 % v/v. Subsequently, 8 µM PIP_2-nanodiscs were added and further incubated for 15 minutes on ice. Pull-down assay was performed as reported in Section VII.2.9.1.

VII.2.9.3 GST Pull-down Assay of micelles and GST-ARNO Sec7

HST-EGFR-TMJM in 0.2 % sodium cholate micelles at the concentration of 10 µM was pre-incubated with 30 µM GST-ARNO Sec7 in wash buffer for 30 minutes at 4 °C. 20 µL GST magnetic beads were pre-equilibrated in 200 µL wash buffer for two times. The mixtures and the beads were incubated for 1 hour at 4 °C. The supernatant after beads incubation was removed and the beads were washed for 3 times with 100 µL wash buffer. 20 µL elution buffer was incubated for 10 minutes with the beads at 4 °C. Total fraction, the supernatant and the pull down fraction were analyzed by 15 % SDS-PAGE.

Table 27: GST pull-down with micelles

Buffer	Components
Wash buffer	50 mM Tris-HCl pH 7.8 at 4°C 100 mM NaCl 5 % Glycerol 0.2 % sodium cholate
Elution buffer	50 mM Tris-HCl pH 7.8 at 4°C 100 mM NaCl 5 % Glycerol 10 mM glutathione

VII.2.9.4 GST Pull-down Assay of nanodiscs and GST-ARNO Sec7

15 µM empty DPPC-nanodiscs or 15 µM DPPC-nanodiscs containing 10 µM EGFR-TMJM peptide were preincubated with 30 µM GST-ARNO Sec7 (or 30 µM GST protein as a negative contriol) in wash buffer for 30 minutes at 25 °C or 37 °C. 20 µL GST magnetic beads were pre-equilibrated in 200 µL wash buffer for two times. The mixtures and the beads were incubated for 1 hour at 25 °C or 37 °C. The supernatant after beads incubation was removed and the beads were washed for 3 times with 100 µL of wash buffer. 20 µL elution buffer were incubated for 10 minutes with the beads at the

respective temperatures. Total fraction, the supernatant and the pull down fraction were analyzed by 15 % SDS-PAGE and streptavidin or anti-His Western Blot. Strevtavidin conjugated-dye was diluted 1:10,000 in 5 % BSA/TBS-T with 1:500 Thimerosal. Anti-His antibody was diluted 1:500 in 5 % BSA/TBS-T with 1:500 Thimerosal.

Table 28: GST pull-down in nanodiscs

Buffer	Components
Wash buffer	50 mM Tris-HCl pH 7.8 at 4°C 100 mM NaCl 5 % Glycerol
Elution buffer	50 mM Tris-HCl pH 7.8 at 4°C 100 mM NaCl 5 % Glycerol

VII.2.9.5 Ni-NTA Pull-down Assay of nanodiscs and GST-ARNO Sec7

40 µL Ni-NTA Agarose beads were pre-equilibrated in 400 µL wash buffer for three times. 20 µM empty DPPC-nanodiscs or 20 µM DPPC-nanodiscs containing 13 µM EGFR-TMJM peptide were pre-incubated with the beads in wash buffer for 30 minutes at 37 °C. Then, 30 µM GST-ARNO Sec7 was incubated with nanodiscs and beas for 30 minutes at 37 °C. The supernatant after beads incubation was removed and the beads were washed three-time with 400 µL wash buffer. 25 µL elution buffer was incubated for 10 minutes with the beads at 37 °C. Total fraction, the supernatant and the pulled down fraction were analyzed by 15 % SDS-PAGE and GST Western Blot. Anti-GST antibody was diluted 1:1,000 in in 5 % BSA/TBS-T with 1:500 Thimerosal.

Table 29: Ni-NTA pull-down in nanodiscs

Buffer	Components
Wash buffer	20 mM Tris-HCl pH 7.4 at RT 100 mM NaCl 0.5 mM EDTA 20 mM Imidazole
Elution buffer	20 mM Tris-HCl pH 7.4 at RT 100 mM NaCl 0.5 Mm EDTA 300 mM Imidazole

VII.2.10 Crosslinking

Chemical crosslinking was performed with bis(sulfosuccinimidyl)suberate (BS3) or with the water insoluble analogue disuccinimidyl suberate (DSS). BS3 in an homobifunctional, water-soluble noncleavable crosslinker, with a spacer arm of 11.4 Å. BS3 contains an *N*-hydroxysulfosuccinimide (NHS) ester that reacts with primary amines at pH 7-9, contained in the side chain of lysine residues or at the N-terminal part of polypeptides (Thermo Scientific Pierce 2010). The chemical structure of BS3 is reported in Figure 70.

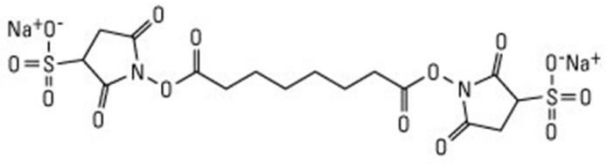

Figure 70: BS3 crosslinker structure (from Thermo Fisher Website)

DSS is a lipophilic noncleavable crosslinker. DSS is the membrane permeable analogue of BS3. The crosslinker structure is reported in Figure 71.

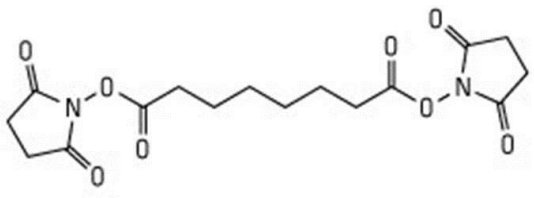

Figure 71: DSS crosslinker structure (from Thermo Fisher Website)

VII.2.10.1 Crosslinking in micelles

A 50 µL reaction mixture containing 10 µM JM peptide or 10 µM His-EGFR-TMJM-SBP or 10 µM HT-IR-TMJM-SBP was incubated in presence or absence of 30 µM ARNOΔPBR for 30 minutes at 20 °C. Samples before crosslinker addition were taken. BS3 crosslinker at the concentration of 1.5 mM or 0.5 mM was added and incubated for 10 minutes at room temperature. Reaction was stopped by the addition of 50 mM Tris-HCl at pH 7.5. Samples were analyzed by SDS-PAGE.

Table 30: Crosslinking buffers for micelles

Buffer	Components
Crosslinking buffer for JM peptide	20 mM HEPES pH 8.0 at RT 150 mM NaCl
Crosslinking buffer for TMJM constructs	20 mM HEPES pH 8.0 at RT 150 mM NaCl 0.4 % sodium cholate

VII.2.10.2 Crosslinking in bicelles

Different ARNO constructs at the concentrations of 10 µM and 50 µM respectively, were pre-incubated with 46 mM bicelles containing His-EGFR-TMJM-SBP for 30 minutes at 38 °C. Samples before crosslinker addition were taken. BS3 at the concentration of 2.0 mM was added to the mixtures and incubated for 10 minutes at room temperature. The reaction was stopped by the addition of 6x sample buffer (see Table 15). Samples were analyzed by SDS-PAGE and streptavidin, anti-ARNO and anti-Flag Western Blot. See Section VII.1.6.1 and VII.1.6.2 for primary and secondary antibody dilutions, respectivly.

Table 31: Crosslinking buffer for bicelles

Buffer	Components
Crosslinking buffer	7 mM DHPC 10 µM BSA in 10 mM Phosphate Buffer pH 7.2 at RT

VII.2.10.3 Crosslinking in nanodiscs

Nanodiscs containing His-EGFR-TMJM-SBP or HT-IR-TMJM-SBP at the concentration of 20 µM were pre-incubated with 30 µM ARNOΔPBR for 30 minutes at 20 °C. BS3 or DSS crosslinker at the concentration of 0.5 mM was added to the mixture and incubated for 5 minutes. The reaction was stopped by the addition of 6x sample buffer (see Table 15). Samples were analyzed by SDS-PAGE and streptavidin Western Blot.

Table 32: Crosslinking buffer for nanodiscs

Buffer	Components
Crosslinking buffer	20 mM HEPES pH 8.0 at RT 150 mM NaCl

VII.2.11 MembraneScale Thermophoresis (MST)

To perform the MST analysis the Monolith NT.115 instrument (NanoTemper) was used. DPPC-nanodiscs with or without His-EGFR-TMJM-SBP were assembled with a MSP1D1-mEGFP fusion construct. Nanodiscs after gel filtration were diluted 20 times and incubated with a serial dilution of ARNO Sec7 (from 50 µM to 1.5 nM) in MSP standard buffer. Standard capillaries were used. The MST measurement was performed with 20 % LED power and 40 % MST power. The same experiment was repeated also in presence of 1.5 mg/mL BSA to reduce unspecific interactions. The thermophoresis with the temperature jump is calculated as a change in the normalized fluorescence (ΔFnorm), which is defined as the ratio between the hot and cold fluorescence in a defined area (Figure 72) (Jerabek-Willemsen et al. 2014).

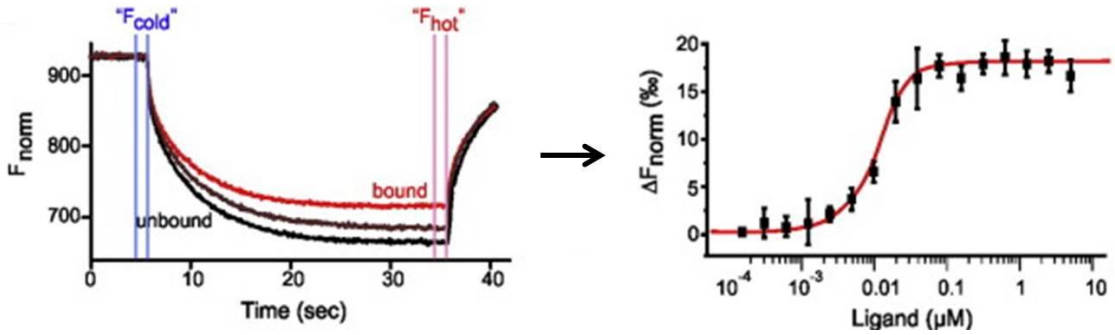

Figure 72: Typical MST binding experiment

The fluorescent molecule trace (in black) changes upon ligand binding (in red). The analysis is performed calculating the normalized fluorescence difference (ΔFnorm). The fluorescence is defined as the Fhot/Fcold ratio. Different ligand concentrations are used to obtain a binding curve (Jerabek-Willemsen et al. 2014).

VII.2.12 Co-localization in membrane sheets

Coverslips were removed from sonication buffer and were incubated upside-down on different reaction mixture drops on parafilm. Wild-type Flag-ARNO or PH mutant (R280C; R: arginine, C: cysteine) Flag-ARNO at the concentration of 1 µM were

incubated on the membrane sheets for 5 minutes at room temperature. Samples were directly fixed after incubation and further analyzed as reported in Section VII.2.13.

VII.2.13 Microscopy

VII.2.13.1 Immunofluorescence on membrane sheets

After incubation with the different reaction mixtures, membrane sheets were fixed for 30 minutes at room temperature with 4 % PFA (paraformaldehyde) in PBS. Eventually 20 mM EDTA were added to stop the reaction after the phosphorylation assay. Coverslips were quenched with 50 mM NH_4Cl in PBS for 20 minutes. Membrane sheets were rinsed with PBS three times for 5 minutes each. Coverslips were then incubated for 1 hour at room temperature with 3 % BSA in PBS.

For the phosphorylation assay analysis, phospho-tyrosine 1086 EGFR (rabbit) antibody was diluted 1:100 in PBS containing 3 % of BSA. Coverslips were incubated for 1 hour at room temperature with the primary antibody. Membrane sheets were washed three times for 10 minutes each in PBS. The secondary antibody anti-rabbit Alexa 594 was diluted 1:200 in PBS containing 1 % BSA in PBS and centrifuged for 2 minutes at 14,000 rpm at room temperature. Coverslips were incubated with the secondary antibody for 1 hour at room temperature in the dark. After incubation, coverslips were washed again for three times for 10 minutes each in PBS. Samples were then prepared for imaging.

For the co-localization analysis, FLAG M2 (mouse) antibody for Flag-ARNO constructs detection was diluted 1:500 in PBS containing 3 % of BSA. Coverslips were washed three times in PBS for 5 minutes each. Subsequently, the secondary antibody donkey anti-mouse Alexa 594 was incubated for 1 hour at room temperature in the dark. The same coverslips were subsequently incubated with an anti-EGFR sc-03 (rabbit) antibody 1:100 diluted in PBS containing 3 % of BSA for EGFR detection. The coverslips were incubated for 1 hour at room temperature with the primary antibody. Membrane sheets were washed three times for 5 minutes each in PBS. The secondary antibody donkey anti-rabbit Alexa 488 was diluted 1:200 in PBS containing 3 % BSA. The antibody was incubated for 1 hour at room temperature in the dark. After incubation, coverslips were washed again for three times for 5 minutes each in PBS. Samples were then prepared for imaging.

VII.2.13.2 Fluorescence Microscopy

Membrane sheets were imaged in 500 µL of a 10 % saturated TMA-DPH (trimethylammonium diphenylhexatriene) solution in PBS. For colocalization experiments, 80 µl of a 1:1,000 dilution of fluorescent beads (TetraSpeck beads, 100 nm size) were added for image alignment purposes (see below). Membrane sheets were imaged with an Olympus IX81-ZDC Microscope, with a 60x 1.49 NA Apochromat objective applying 1.6x and a 2x magnifying lenses (Olympus). Images were taken with a digital 16bit EM-CCD camera (ImagEM Enhanced C9100-13, 16 µm pixel size, Hamamatsu Photonics, Hamamatsu) at 100 % EM gain. An MT20E illumination system (Olympus) equipped with a 150 W Xenon lamp was used for illumination. Alexa 488 was imaged with the filter set F36-525 EGFP. Alexa 594 was imaged with the filter set F36-503 TRITC HC. TMA-DPH fluorescence was imaged using filter set F36-500 DAPI HC. Fluorescent microspheres were imaged using the filter set F46-009 Cy5 ET narrow bandpass (AHF Analysentechnik). Images were analyzed with ImageJ Software (version 1.48 or higher).

For unbiased quantification of the fluorescence intensity, regions of interest (ROIs) were selected in TMA-DPH channel. The ROIs dimension was set to 50x50 pixels. The ROI was transferred to the Alexa 594 channel image to measure the mean pixel intensity within the ROI. Similarly, the mean background intensity in the Alexa 594 channel was determined using a ROI placed outside the membrane sheet area and subtracted from the mean sheet intensity. This procedure was repeated for all quantified image channels. For each coverslips 20-35 membrane sheets were analyzed and the background-corrected intensities were averaged. Values are given as mean ± SEM.

For co-localization experiments, different image channels were aligned by shifting images laterally using the ImageJ plugin AlignSlice. Correct alignment was verified using the positions of added fluorescent beads (see above) as a reference.

VIII. Appendix

VIII.1 Original gel figures

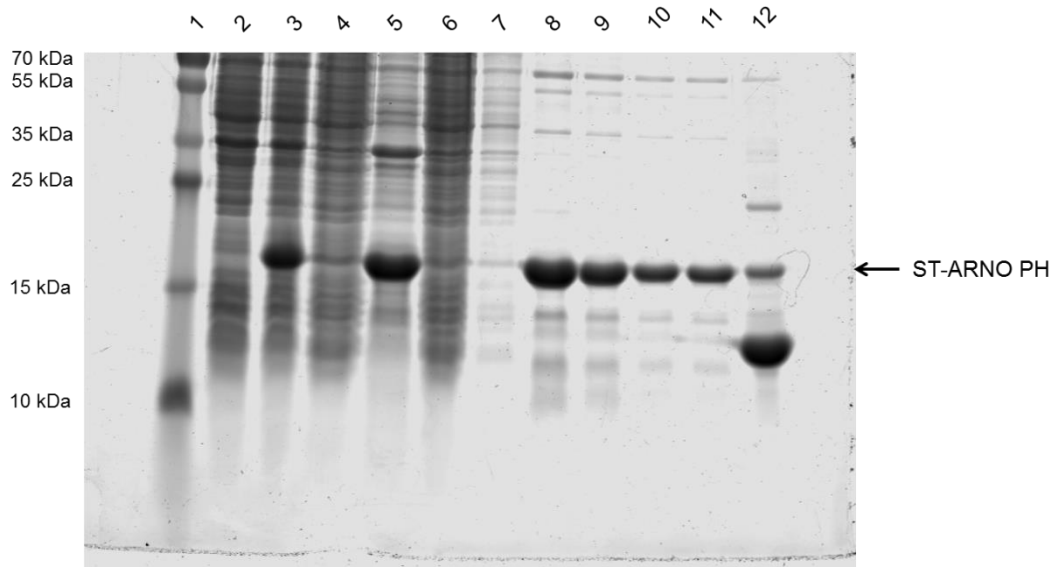

Supporting Figure 1: Original SDS-PAGE of ST-ARNO PH expression and purification (see Figure 13)

15 % SDS-PAGE stained with Coomassie Brilliant Blue. Lane 11 shows the elution 4 and the lane 12 shows the beads fraction. ST-ARNO PH is indicated with an arrow.

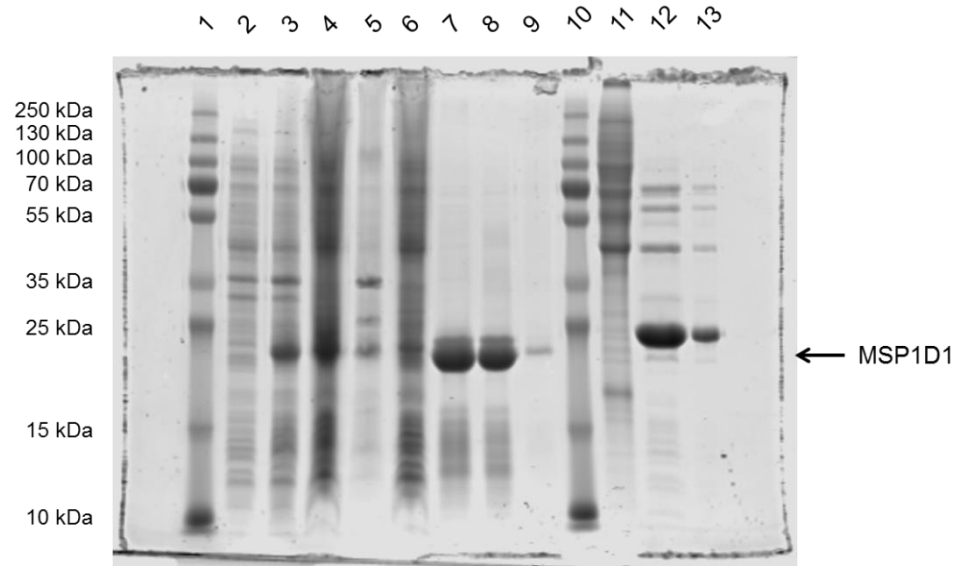

Supporting Figure 2: Original SDS-PAGE of MSP1D1 expression and purification (see Figure 14)

12.5 % SDS-PAGE stained with Coomassie Brilliant Blue. In lanes 10, 11, 12 and 13 there are protein samples evaluated for Volkmar Fieberg from Famulok's group and they were not used in this PhD Thesis.

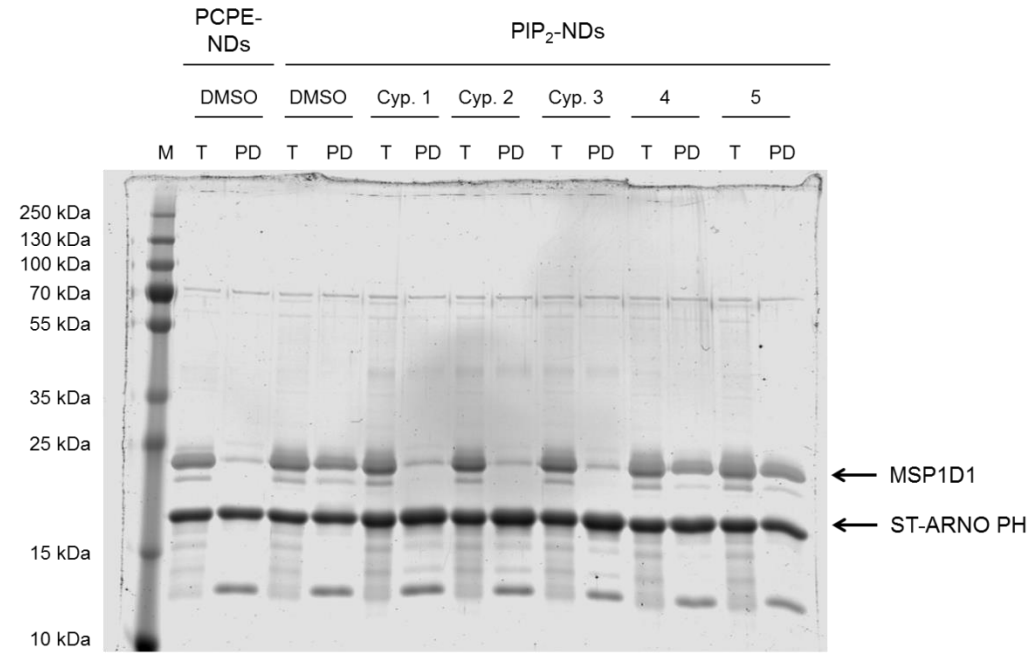

Supporting Figure 3: Original SDS-PAGE of Figures 20 and 22

Pull-down assay of ARNO PH incubated with PCPE-NDs (nanodiscs) or PIP_2-NDs in presence of 2 % DMSO. PIP_2-NDs and ARNO PH were incubated with 100 µM Cyplecksins (Cyp.) 1, 2 or 3 or the inactive analogues MH 40 A (4) or MH 40 B (5). The input or total (**T**) fractions and the pull-down (**PD**) fractions were analyzed by SDS-PAGE and visualized by Coomassie staining. The prestained molecular weight marker (**M**) was loaded in the first lane.

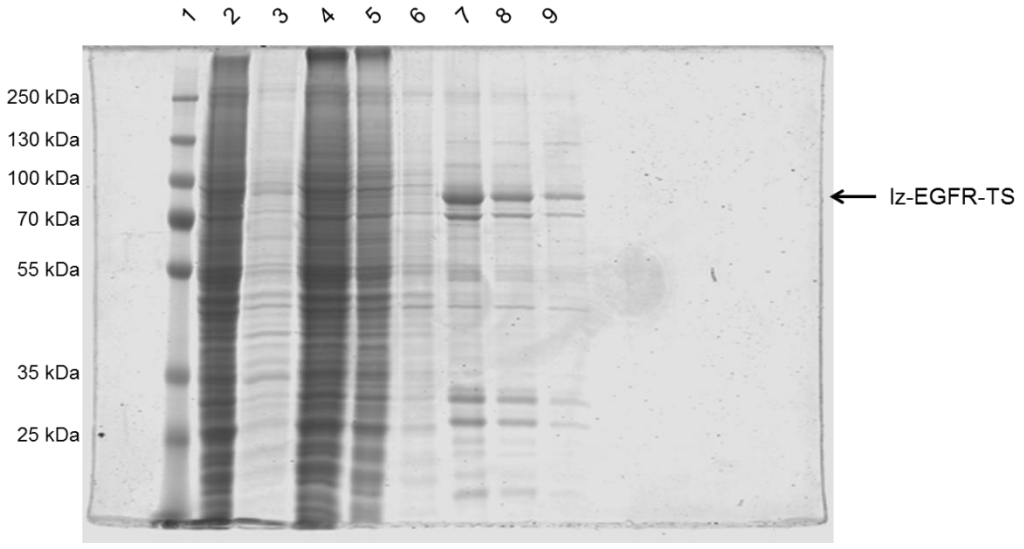

Supporting Figure 4: Original SDS-PAGE of the purification of lz-EGFR-TS from Sf9 cells (see Figure 24)

10 % SDS-PAGE stained with Coomassie Brilliant Blue.

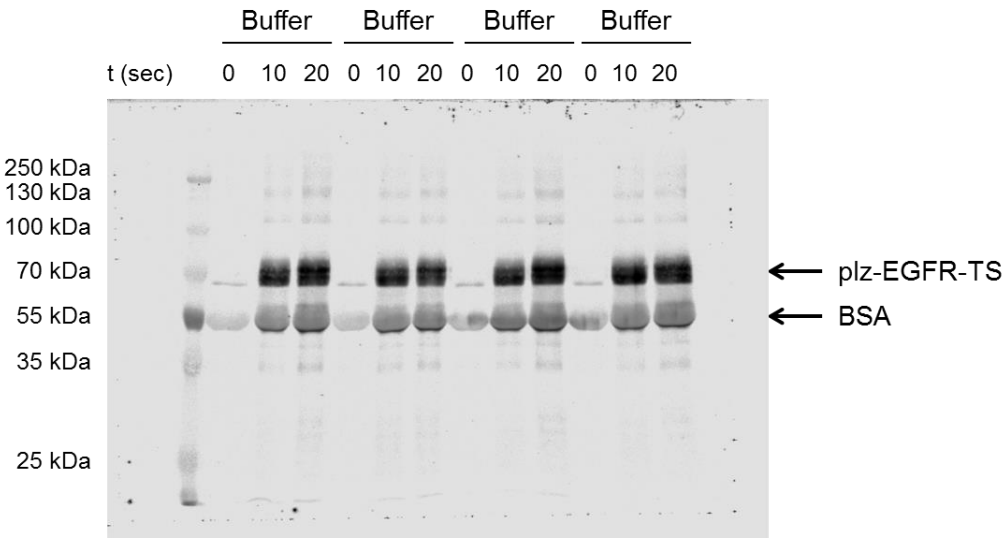

Supporting Figure 5: Original Western Blot of lz-EGFR-TS phosphorylation in micelles (see Figure 25)

Western Blot analysis is performed with anti-pTyr antibody. The receptor was incubated only with Buffer.

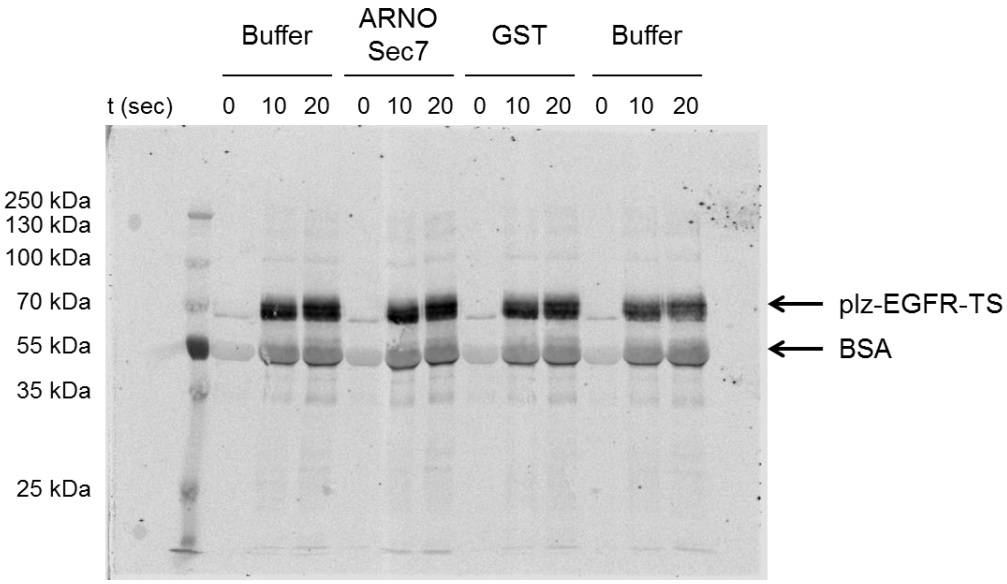

Supporting Figure 6: Original Western Blot of the Influence of ARNO Sec7 on lz-EGFR-TS phosphorylation in micelles (see Figure 26)

Western Blot analysis is performed with anti-pTyr antibody. Influence of ARNO Sec7 on lz-EGFR-TS phosphorylation in micelles.

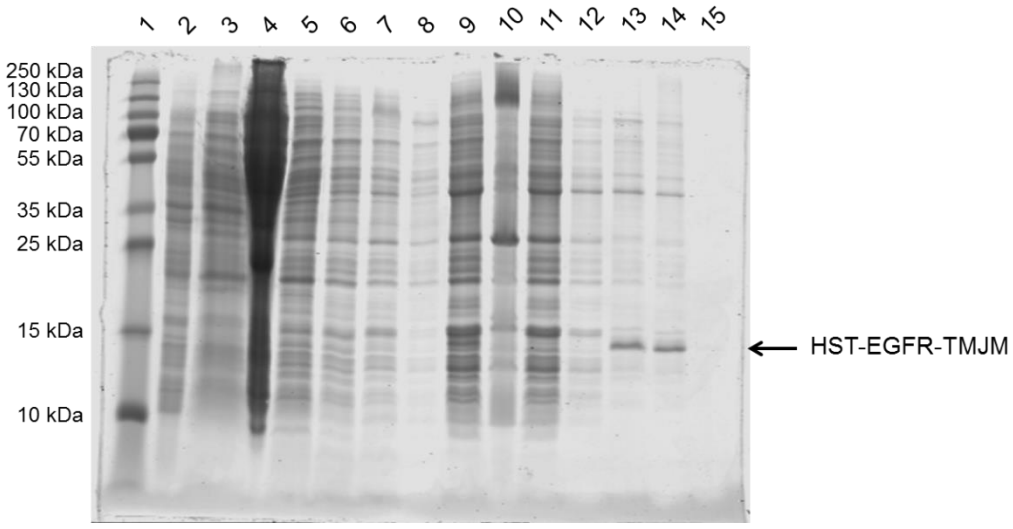

Supporting Figure 7: Original SDS-PAGE of HST-EGFR-TMJM expression and purification from inclusion bodies (see Figure 28)

15 % SDS-PAGE stained with Coomassie Brilliant Blue.

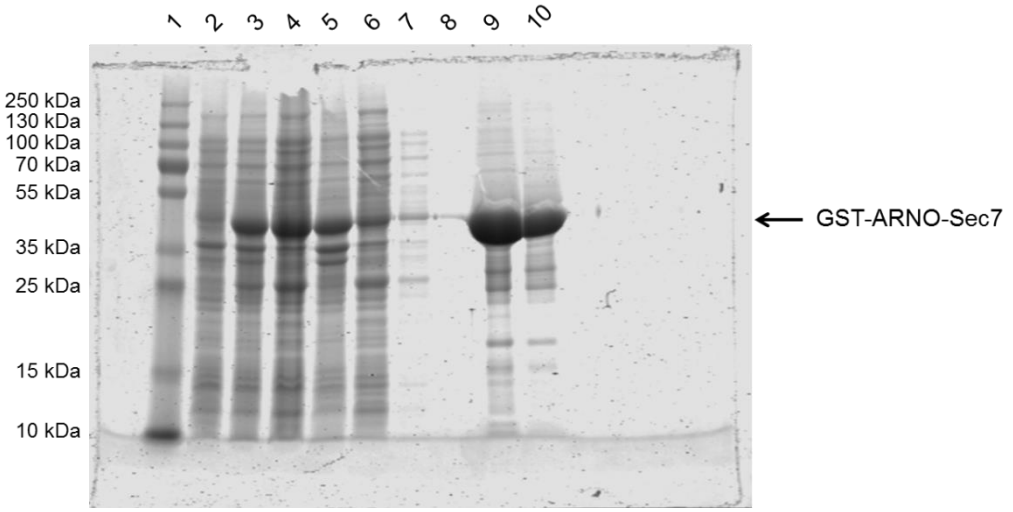

Supporting Figure 8: Original SDS-PAGE of GST-ARNO Sec7 expression and purification (see Figure 29)

12.5 % SDS-PAGE stained with Coomassie Brilliant Blue.

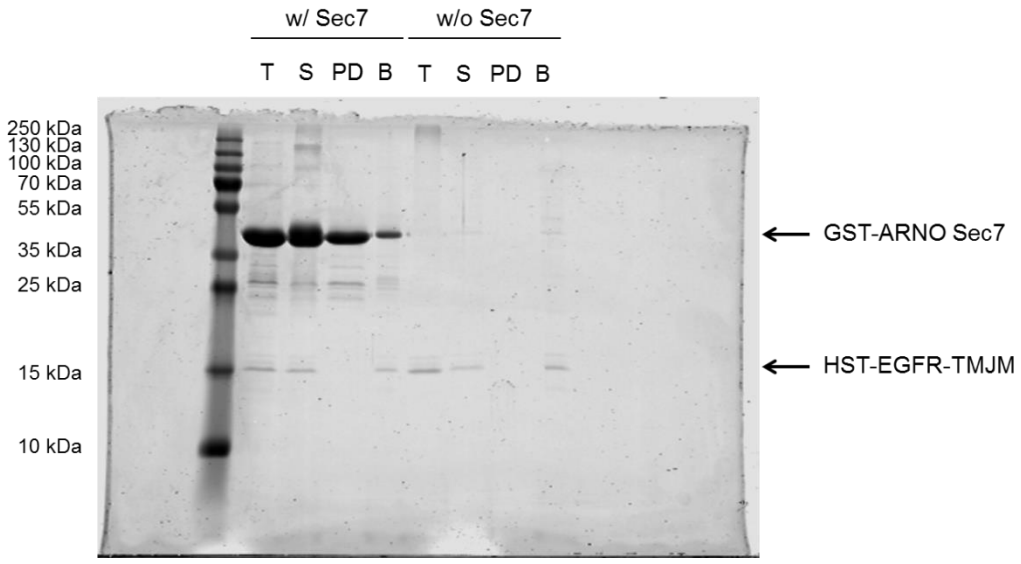

Supporting Figure 9: Original SDS-PAGE of GST-pull-down of HST-EGFR-TMJM in micelles in presence of GST-ARNO Sec7 (see Figure 31)

15 % SDS-PAGE stained with Coomassie Brilliant Blue. The protein pull-down was performed with glutathione beads in the presence (with: w/) or absence (without: w/o) of GST-ARNO Sec7. **T**: Total protein; **S**: Supernatant after bead incubation; **P**: Pulled-down fraction; **B**: Bead fraction.

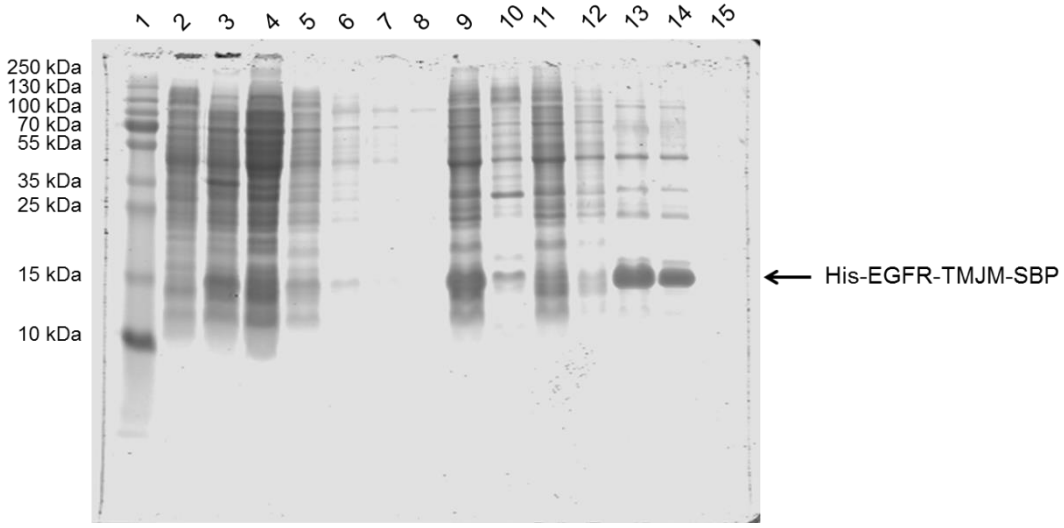

Supporting Figure 10: Original SDS-PAGE of His-EGFR-TMJM-SBP expression and purification from inclusion bodies (see Figure 33)

15 % SDS-PAGE stained with Coomassie Brilliant Blue.

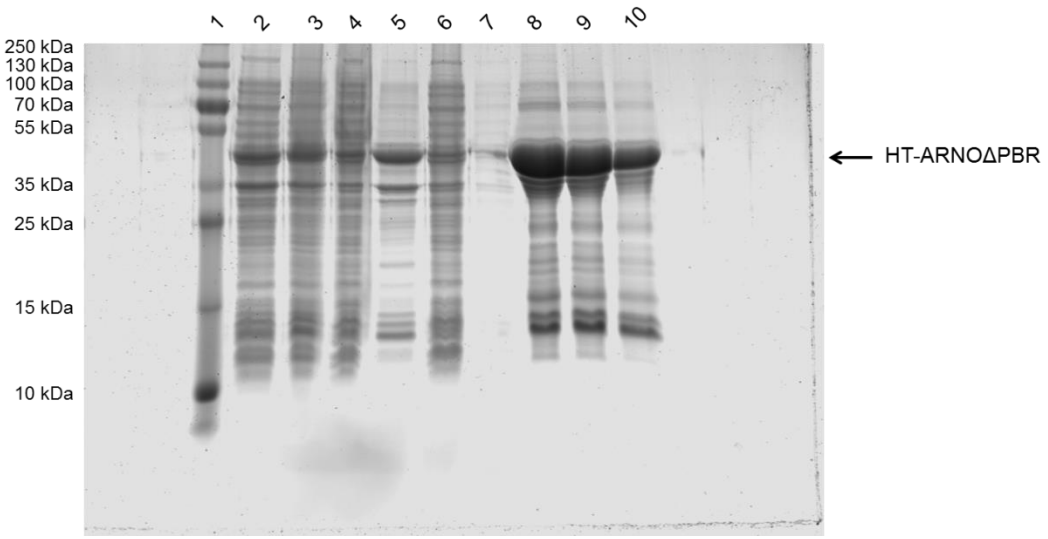

Supporting Figure 11: Original SDS-PAGE of HT-ARNOΔPBR expression and purification (see Figure 34)

12.5 % SDS-PAGE stained with Coomassie Brilliant Blue.

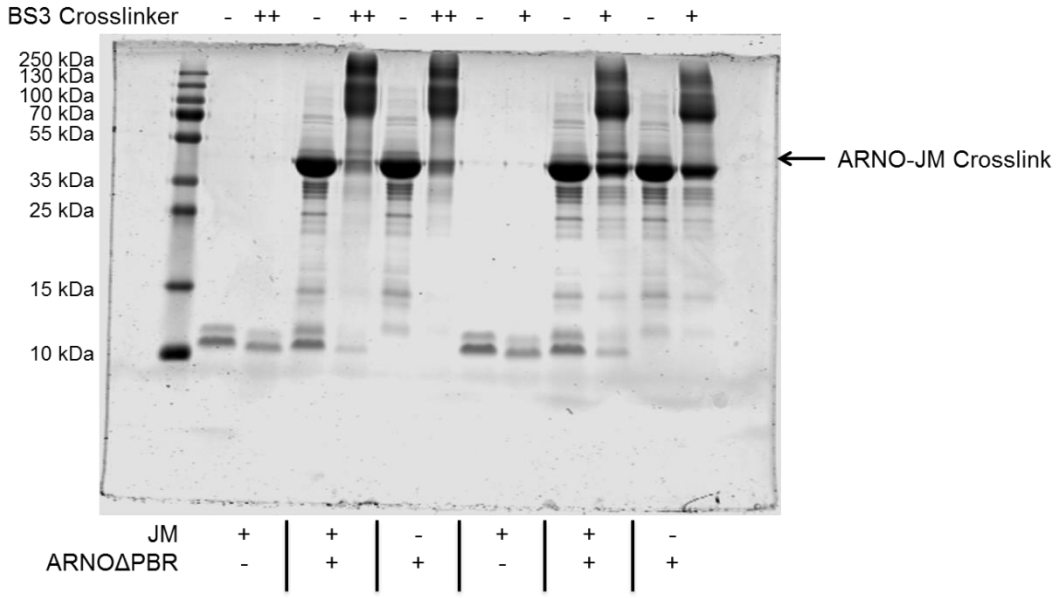

Supporting Figure 12: Original SDS-PAGE of the crosslinking between ARNOΔPBR and JM peptide with different BS3 concentrations (see Figure 35)

15 % SDS-PAGE stained with Coomassie Brilliant Blue.

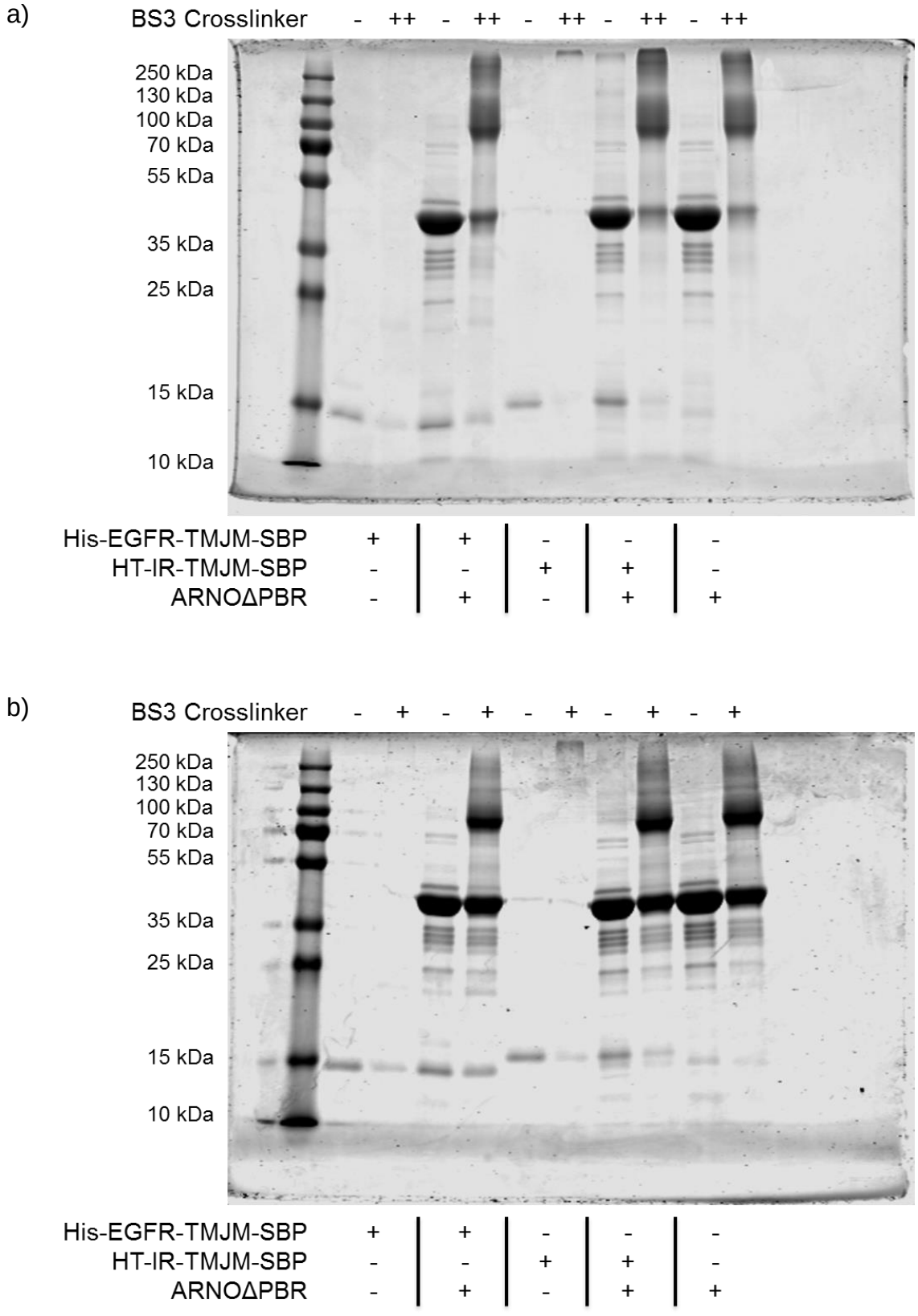

Supporting Figure 13: Original SDS-PAGE of the crosslinking between ARNOΔPBR and TMJM constructs in micelles (see Figure 36 a and b)

12.5 % SDS-PAGE stained with Coomassie Brilliant Blue. The BS3 was used at two different concentrations: **a)** 1.5 mM (++) and **b)** 0.5 mM (+).

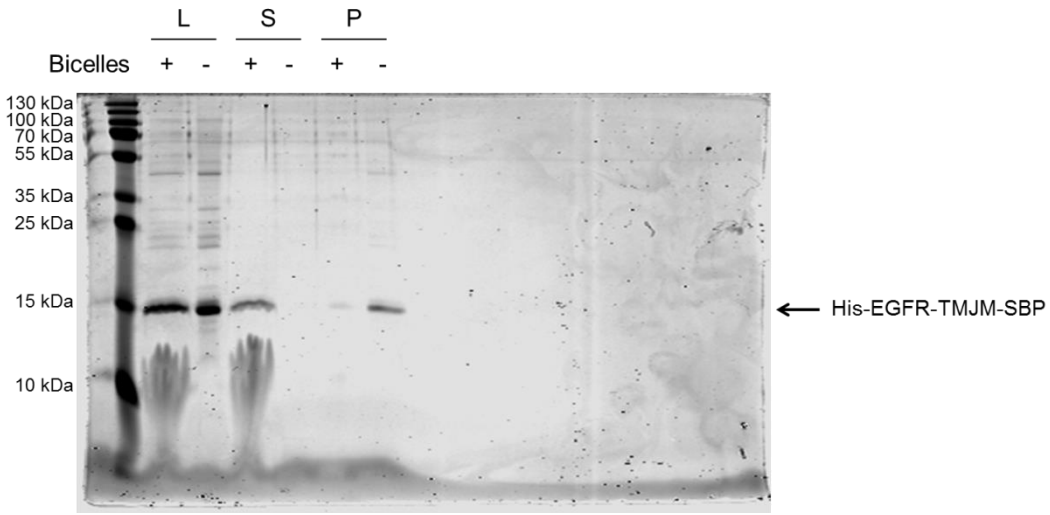

Supporting Figure 14: Original SDS-PAGE of the control of His-EGFR-TMJM-SBP assembly into bicelles (see Figure 39)

15 % SDS-PAGE stained with Coomassie Brilliant Blue. **L**: Load; **S**: Supernatant; **P**: Precipitate.

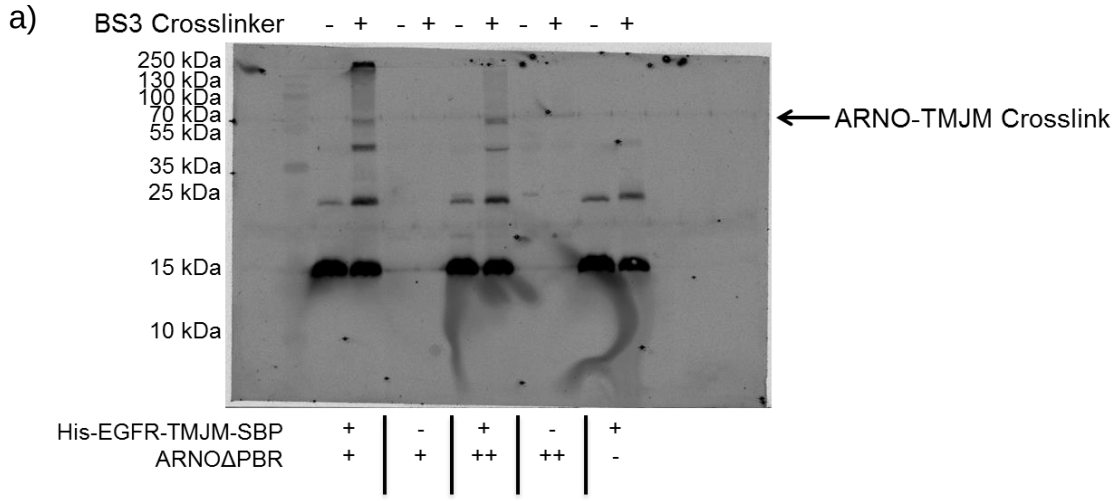

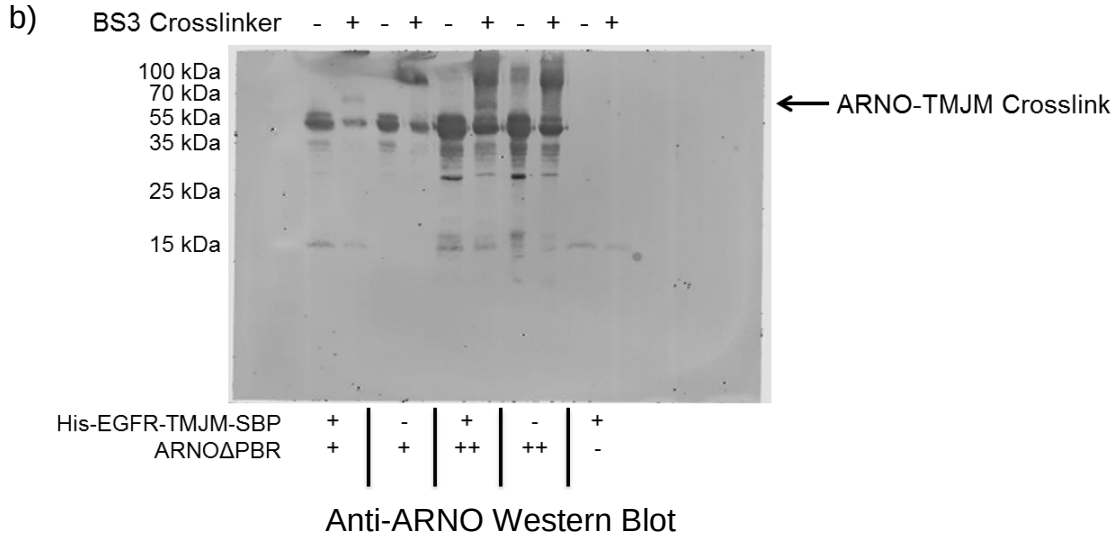

Supporting Figure 15: Original Western Blots of the crosslinking between ARNOΔPBR and EGFR-TMJM embedded into bicelles (see Figure 40 a and b)

BS3 crosslinking agent was incubated with two different HT-ARNOΔPBR concentrations, 10 µM (+) and 50 µM (++) respectively, and bicelles containing His-EGFR-TMJM-SBP. Analysis was performed by SDS-PAGE and **a)** Streptavidin Western Blot detecting the SBP-labeled EGFR-TMJM or **b)** anti-ARNO Western Blot.

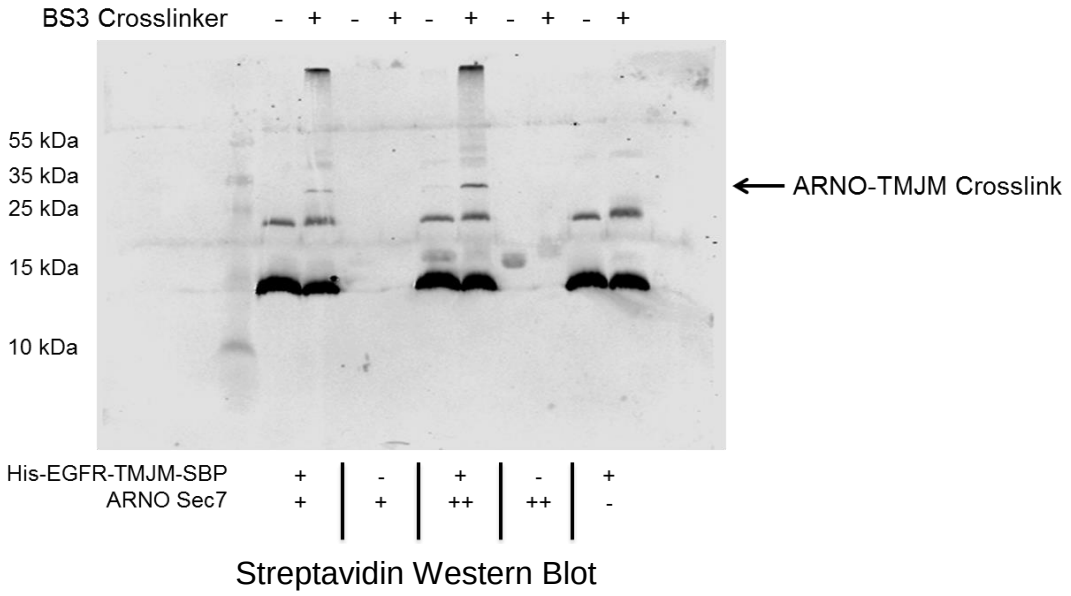

Supporting Figure 16: Original Western Blot of the crosslinking between ARNO Sec7 and EGFR-TMJM embedded into bicelles (see Figure 41)

BS3 was incubated with two different ARNO Sec7 concentrations, 10 µM (+) and 50 µM (++) respectively, and bicelles containing HT-EGFR-TMJM-SBP. Analysis was performed with SDS-PAGE and streptavidin Western Blot detecting the SBP-tagged EGFR-TMJM.

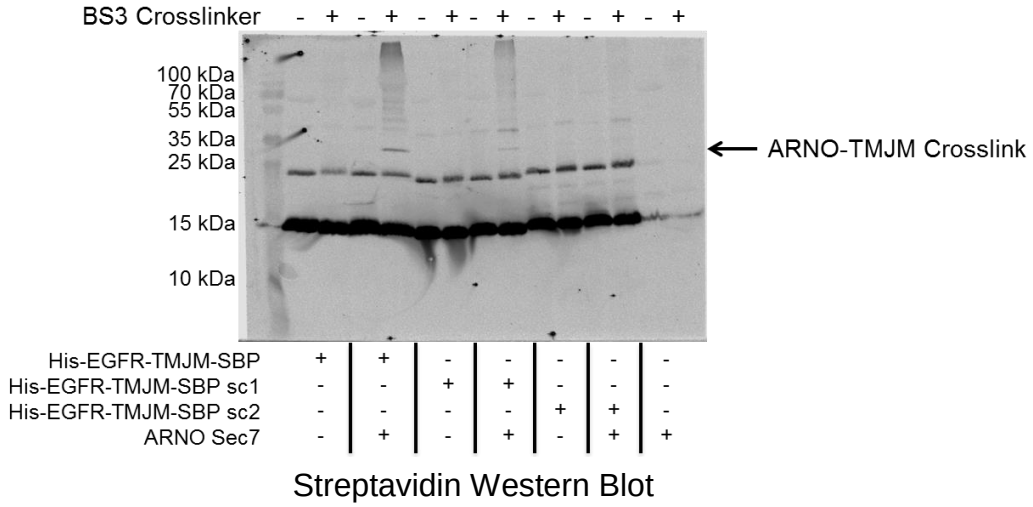

Supporting Figure 17: Original Western Blot of the Crosslinking between ARNO Sec7 and EGFR-TMJM wild-type, sc1 and sc2 embedded into bicelles (see Figure 42)

Crosslinking agent BS3 was incubated with 10 µM ARNO Sec7 and bicelles containing His-EGFR-TMJM-SBP wild-type, scrambled version 1 (sc1), or 2 (sc2). Analysis was performed with SDS-PAGE and streptavidin Western Blot detecting the SBP-tagged EGFR-TMJM.

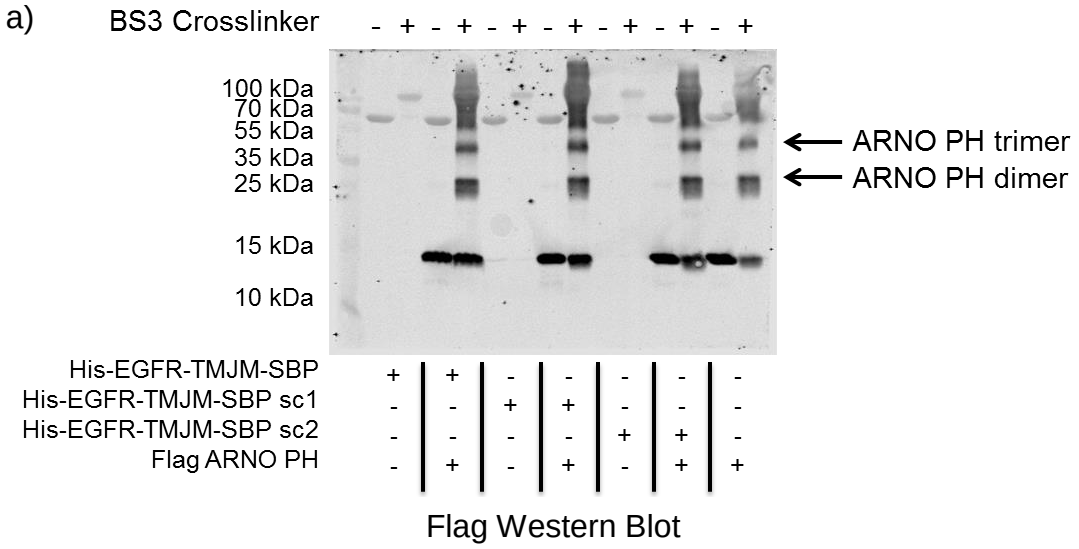

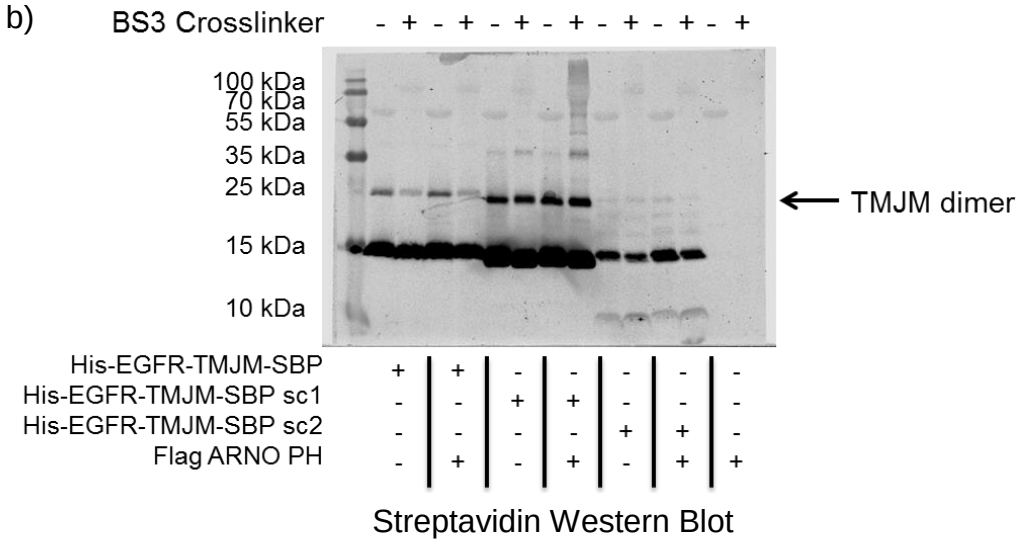

Supporting Figure 18: Original Western Blots of the crosslinking between ARNO PH and EGFR-TMJM wild-type, sc1 and sc2 embedded into bicelles (see Figure 43 a and b)

BS3 was incubated with 10 µM Flag ARNO PH and bicelles containing His-EGFR-TMJM-SBP wild-type and scrambled version 1 (sc1) and 2 (sc2). The TMJM domains contained within bicelles had a concentration of 5 µM. Analysis was performed by SDS-PAGE and **a)** anti-Flag Western Blot detecting the N-terminal part of ARNO PH domain and **b)** streptavidin Western Blot detecting the SBP-labeled EGFR-TMJMs.

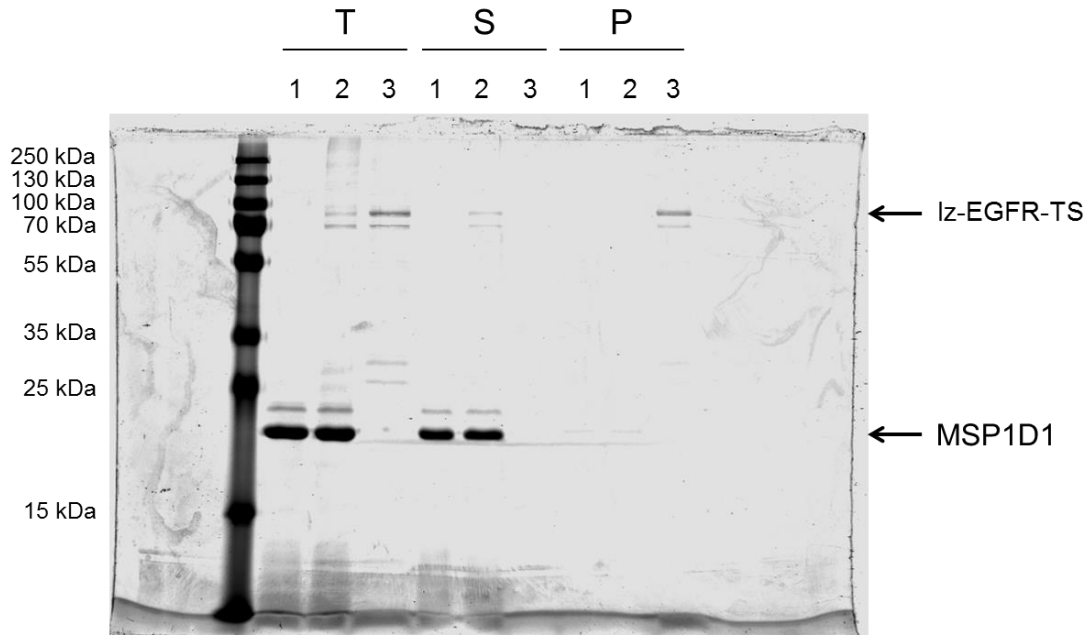

Supporting Figure 19: Original SDS-PAGE of the control of lz-EGFR-TS assembly into nanodiscs (see Figure 48)

12.5 % SDS-PAGE stained with Coomassie Brilliant Blue. Empty nanodiscs (1), nanodiscs containing lz-EGFR-TS (2) or lz-EGFR-TS alone (3). **T**: Total mixtures before incubation; **S**: Supernatant; **P**: Precipitate.

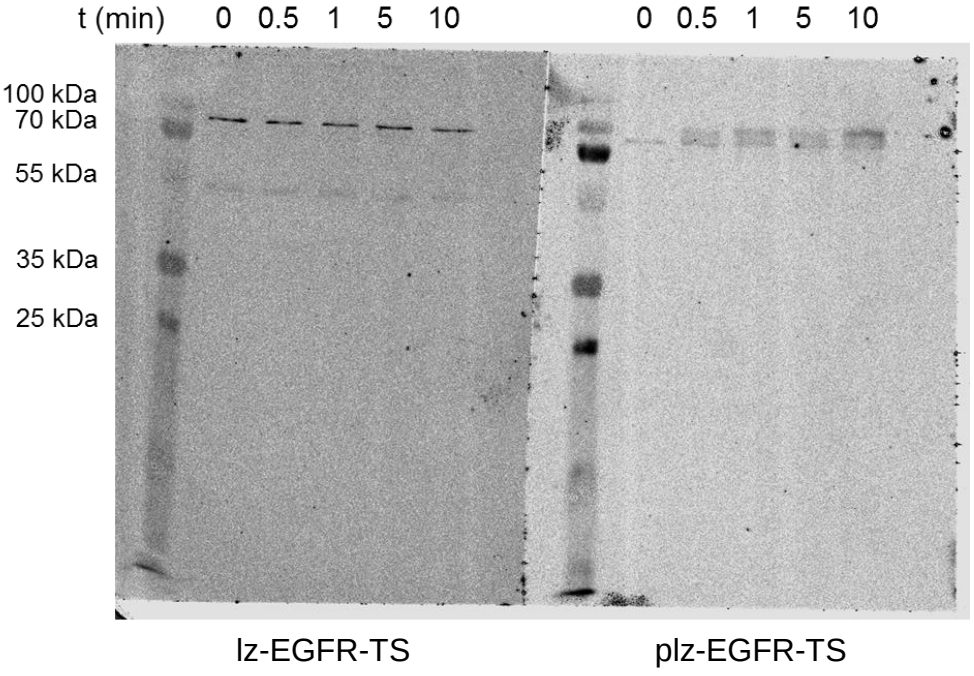

Supporting Figure 20: Original Western Blots of the phosphorylation of lz-EGFR-TS into nanodiscs (see Figure 49)

Western Blot analysis with anti-EGFR sc03 antibody (left panel) and pTyr antibody (right panel).

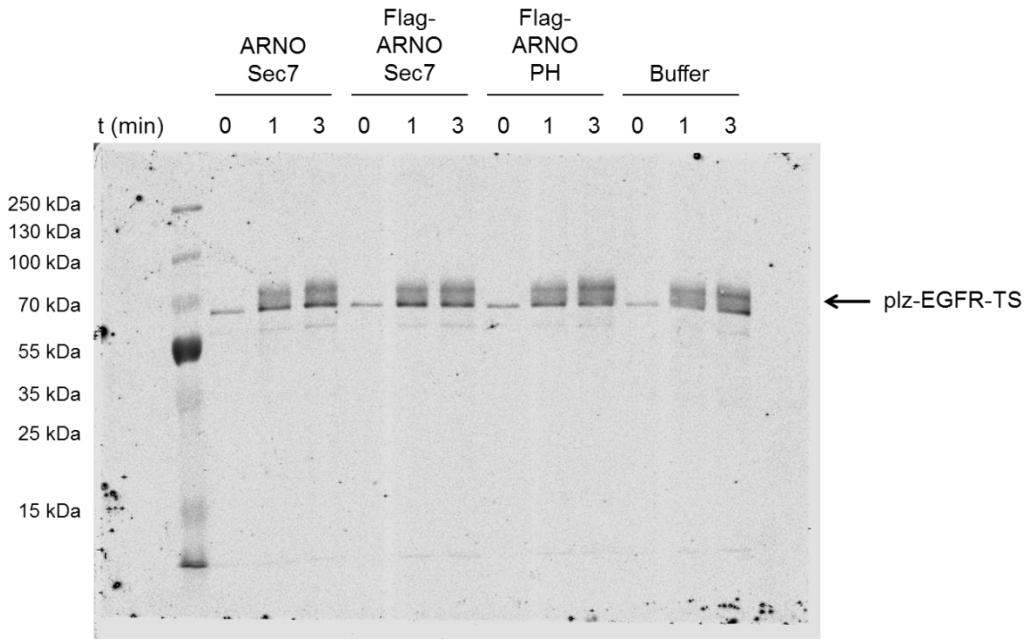

Supporting Figure 21: Original Western Blot of the phosphorylation of lz-EGFR-TS in nanodiscs in presence of ARNO Sec7, or Flag-ARNO Sec7, or Flag-ARNO PH (see Figure 50, upper panel)

Western Blot with anti-pTyr antibody.

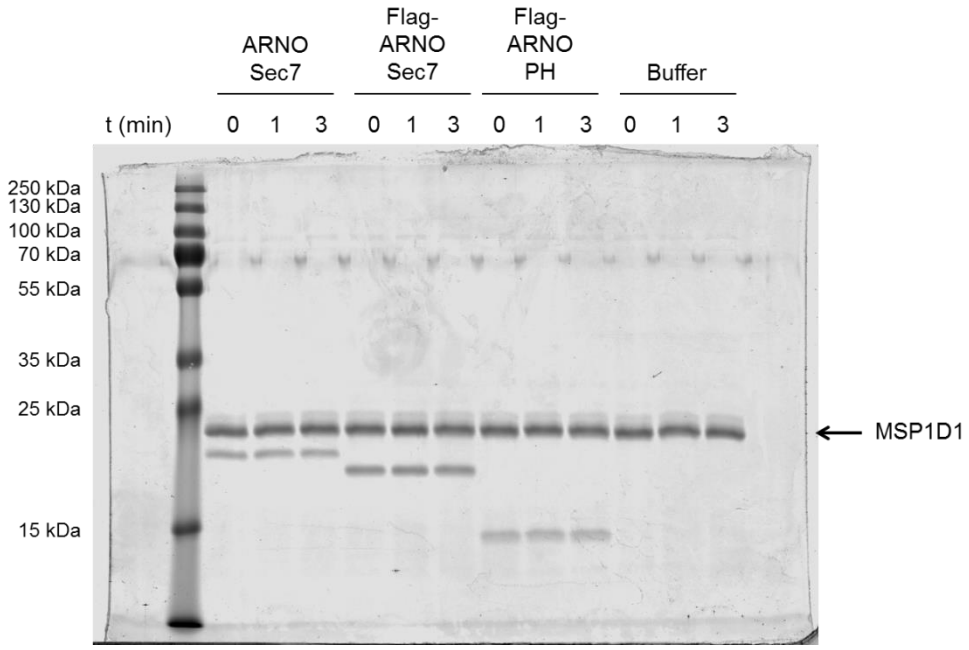

Supporting Figure 22: Original SDS-PAGE of the phosphorylation of lz-EGFR-TS in nanodiscs in presence of ARNO Sec7, or Flag-ARNO Sec7, or Flag-ARNO PH (see Figure 50, lower panel)

12.5 % SDS-PAGE stained with Coomassie Brilliant Blue.

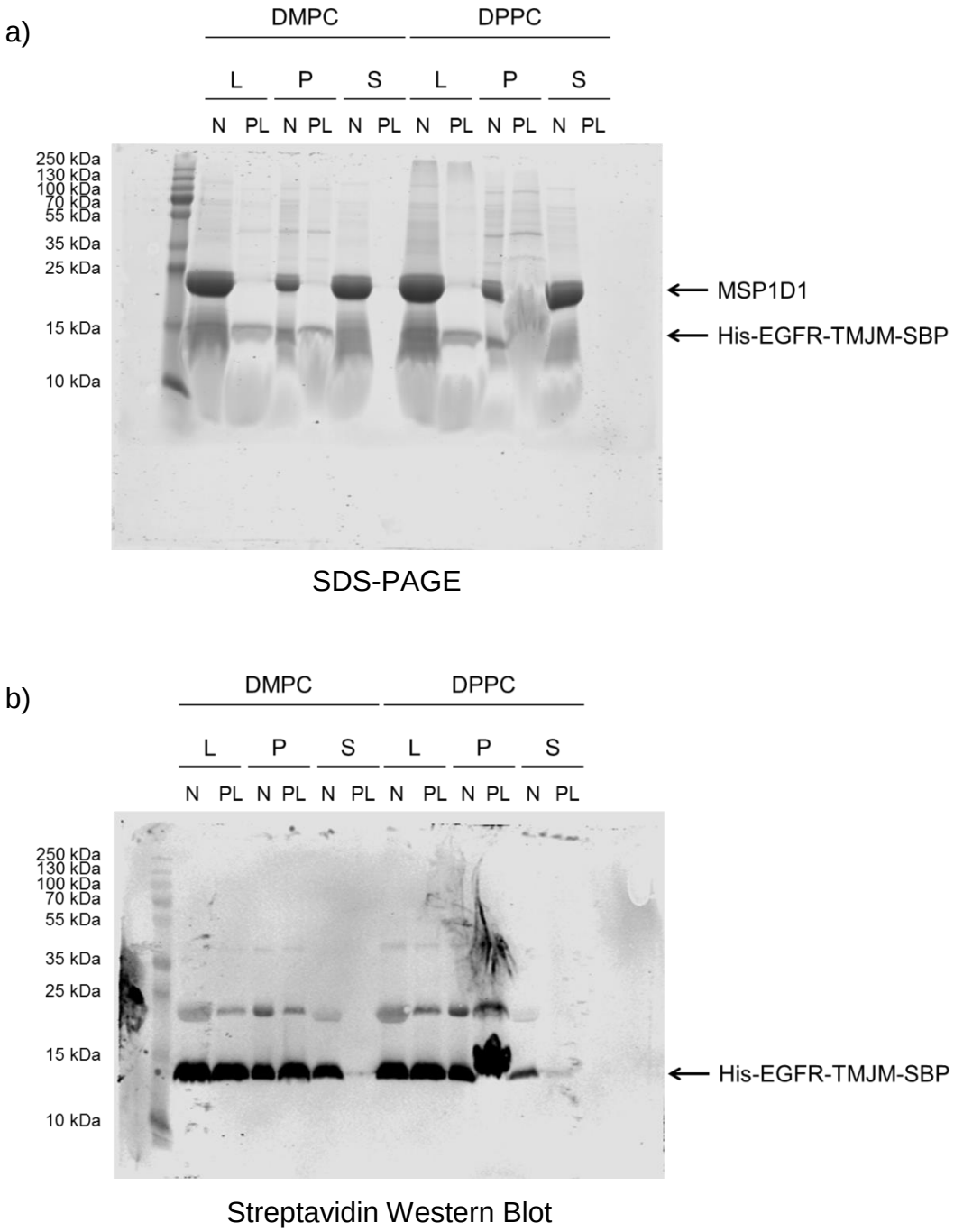

Supporting Figure 23: Original SDS-PAGE and Western Blot of the control of EGFR-TMJM assembly into nanodiscs (see Figure 51 a and b)

A phospholipids-MSP1D1 mixture or phospholipids only were mixed with His-EGFR-TMJM-SBP. DMPC- and DPPC-phospholipids were used. In Figure 51 is reported only the left part of the gel with DMPC-phospholipids. **L**: Load; **P**: Precipitate; **S**: Supernatant; **N**: Nanodiscs; **PL**: Phospholipids. **a)** 15 % SDS-PAGE stained with Coomassie Brilliant Blue. **b)** Western Blot performed using streptavidin-800 conjugated dye, recognizing the SBP-tag at the C-terminus of the TMJM peptide.

a)

Legend:
1 - NDs/Sec7
2 - NDs + TMJM/Sec7

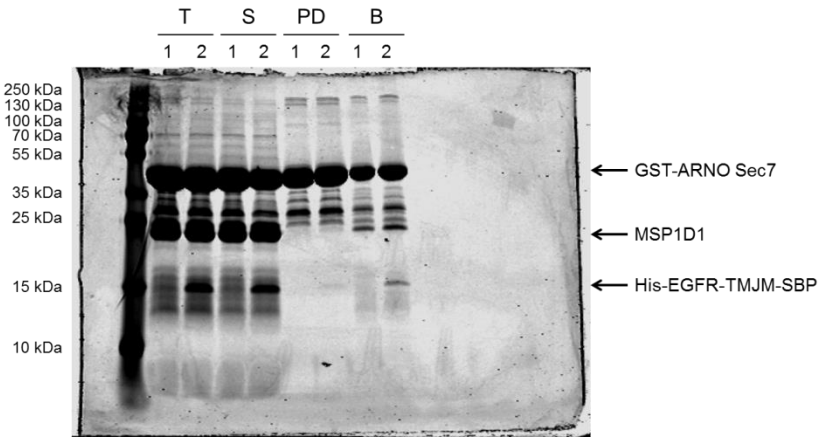

SDS-PAGE

b)

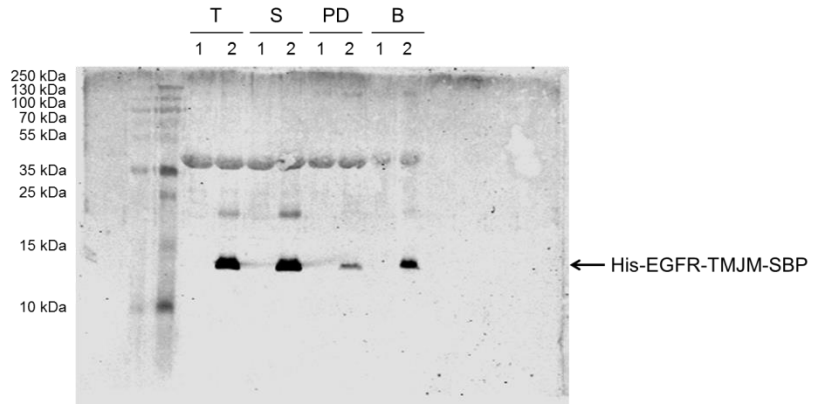

Streptavidin Western Blot

c)

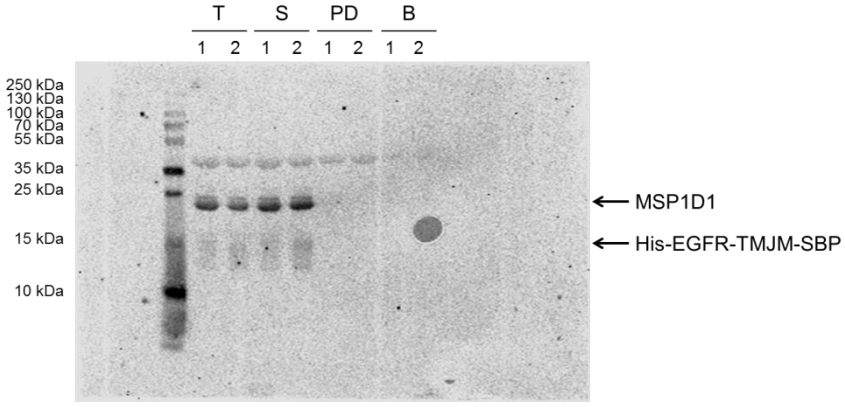

His Western Blot

Supporting Figure 24: Original SDS-PAGE and Western Blots of the GST pull-down at 25 °C with DMPC-nanodiscs to analyze TMJM-Sec7 interaction (see Figure 52 a, b and c)

T: Total protein; **S**: Supernatant after beads incubation; **PD**: Pulled-down fraction; **B**: Bead fractions were collected and analyzed. **a)** 15 % SDS-PAGE stained with Coomassie Brilliant Blue. **b)** Western Blot performed with streptavidin-800 conjugated dye, recognizing the SBP-tag at the C-terminus of TMJM peptide. **c)** Western Blot performed with anti-His antibody detecting the N-terminal part of MSP1D1 protein and the N-terminal part of His-EGFR-TMJM-SBP construct.

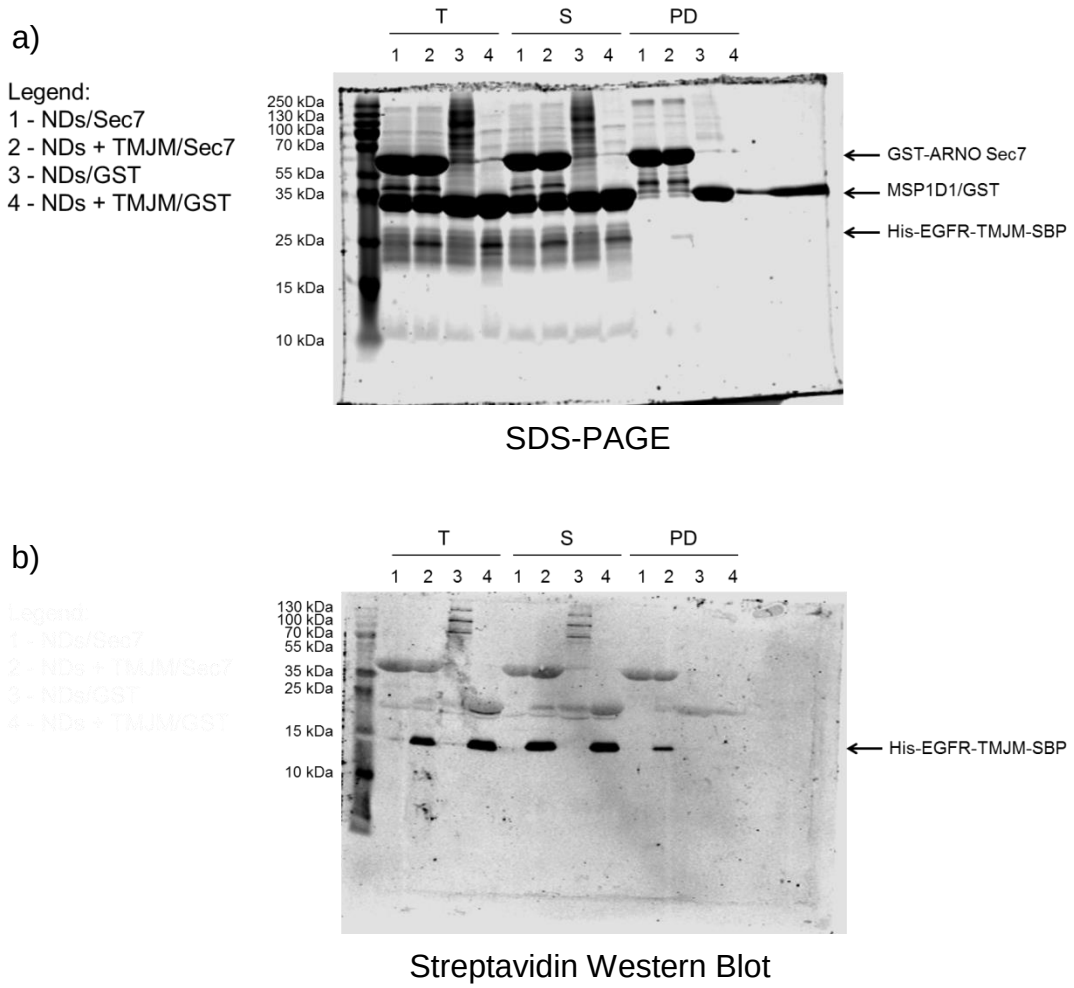

Supporting Figure 25: Original SDS-PAGE and Western Blot of the GST pull-down at 37 °C with DPPC-nanodiscs to analyze TMJM-Sec7 interaction (see Figure 53 a and b)

T: Total protein; **S**: Supernatant after beads incubation; **PD**: Pulled-down fractions were collected and analyzed. **a**) 15 % SDS-PAGE stained with Coomassie Brilliant Blue. **b**) Streptavidin Western Blot was performed with streptavidin-800 conjugated dye, recognizing the SBP-tag at the C-terminus of TMJM peptide.

a)

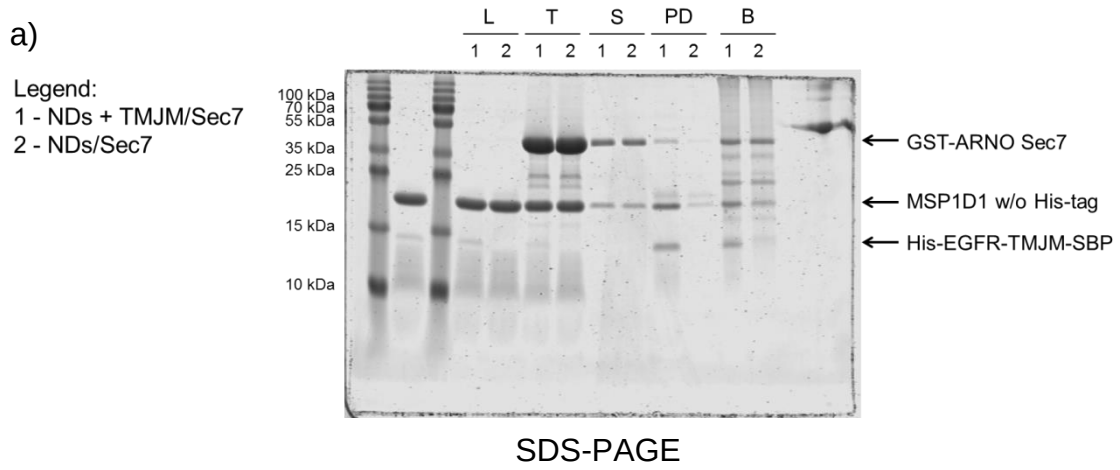

SDS-PAGE

b)

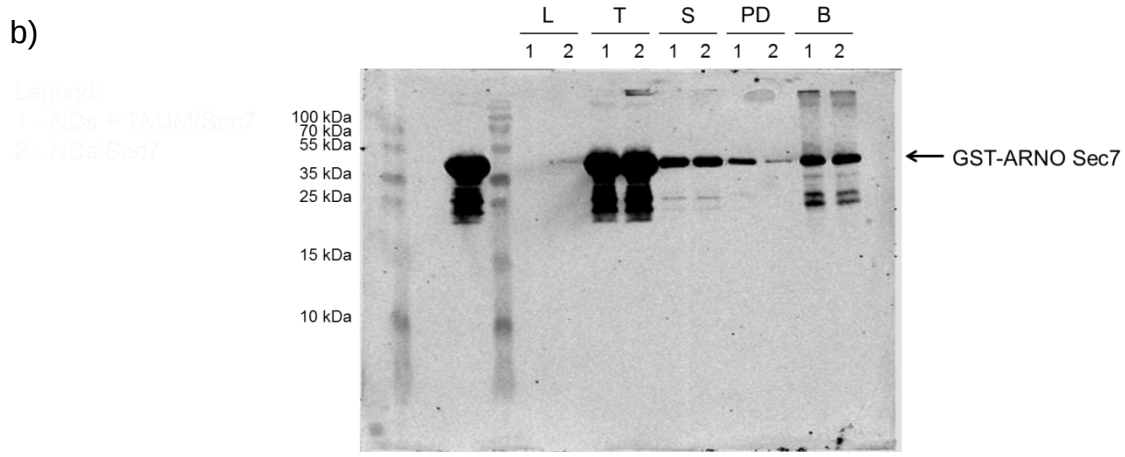

GST Western Blot

Supporting Figure 26: Original SDS-PAGE and Western Blot of the Ni-NTA Agarose beads pull-down at 37 °C to analyze TMJM-Sec7 interaction (see Figure 54 a and b)

L: Loaded fractions before ARNO addition **T**: Total protein; **S**: Supernatant after beads incubation; **PD**: Pulled-down fractions were collected and analyzed. The left part of the gels was wrongly loaded. **a**) 15 % SDS-PAGE stained with Coomassie Brilliant Blue. **b**) GST Western Blot was performed with anti-GST antibody, recognizing ARNO.

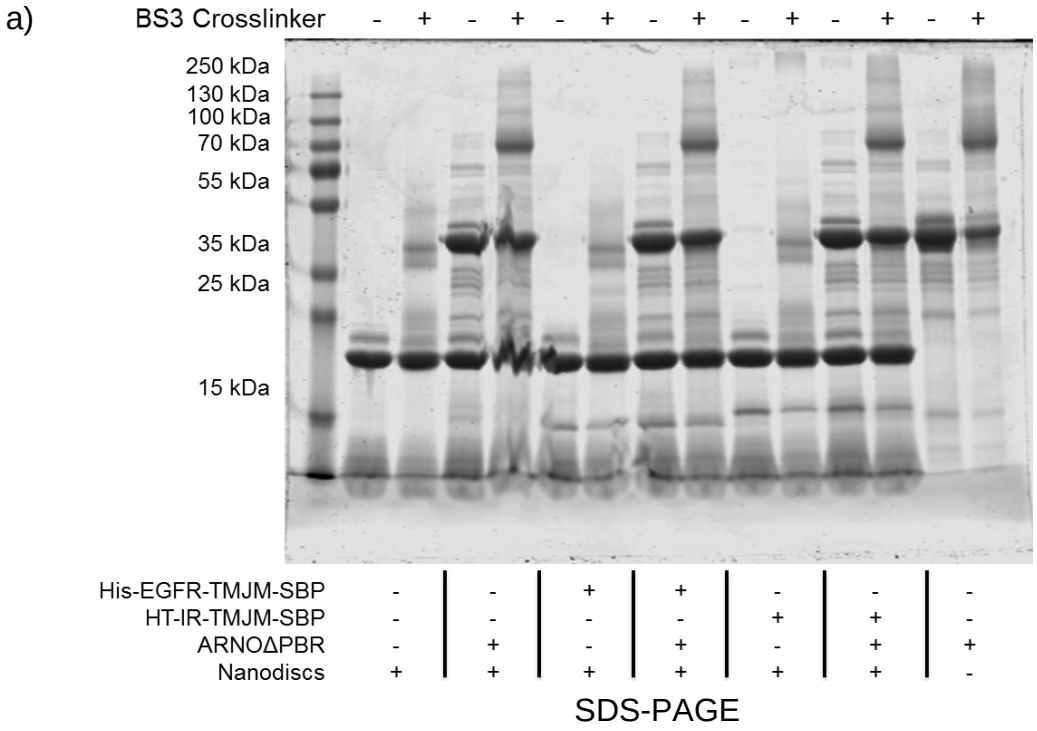

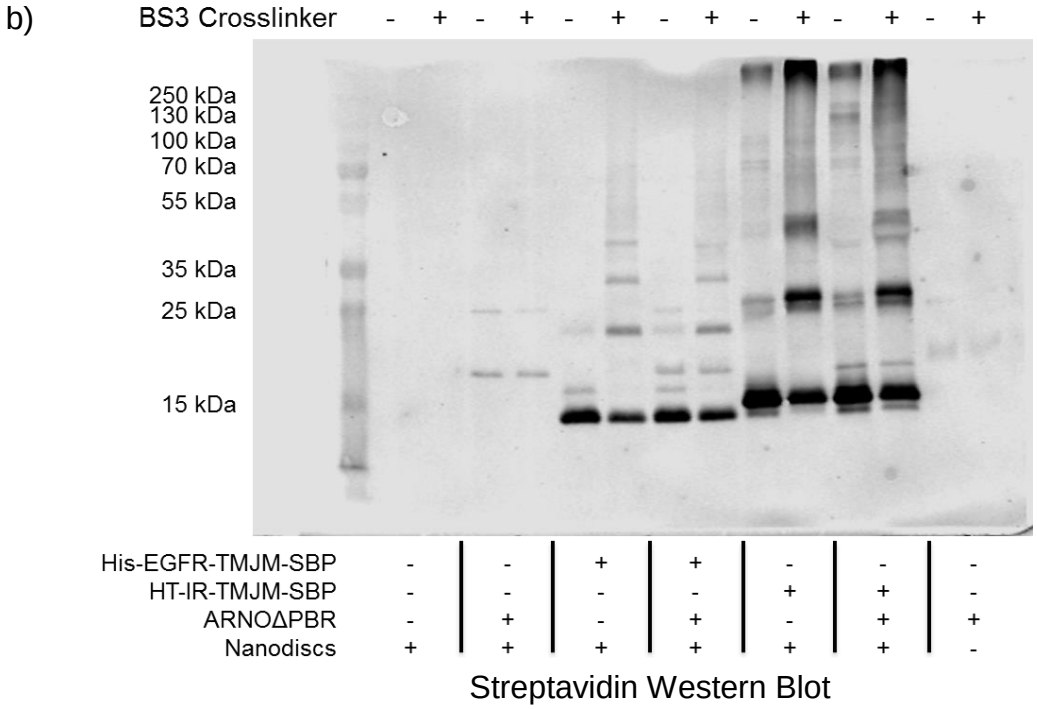

Supporting Figure 27: Original SDS-PAGE and Western Blot of BS3 crosslinking with nanodiscs containing EGFR-TMJM and ARNOΔPBR (see Figure 55 a and b)

a) 15 % SDS-PAGE stained with Coomassie Brilliant Blue and **b**) Western blot using a streptavidin-800 conjugated dye. No crosslinking between ARNO and EGFR-TMJM was visible using BS3 crosslinker.

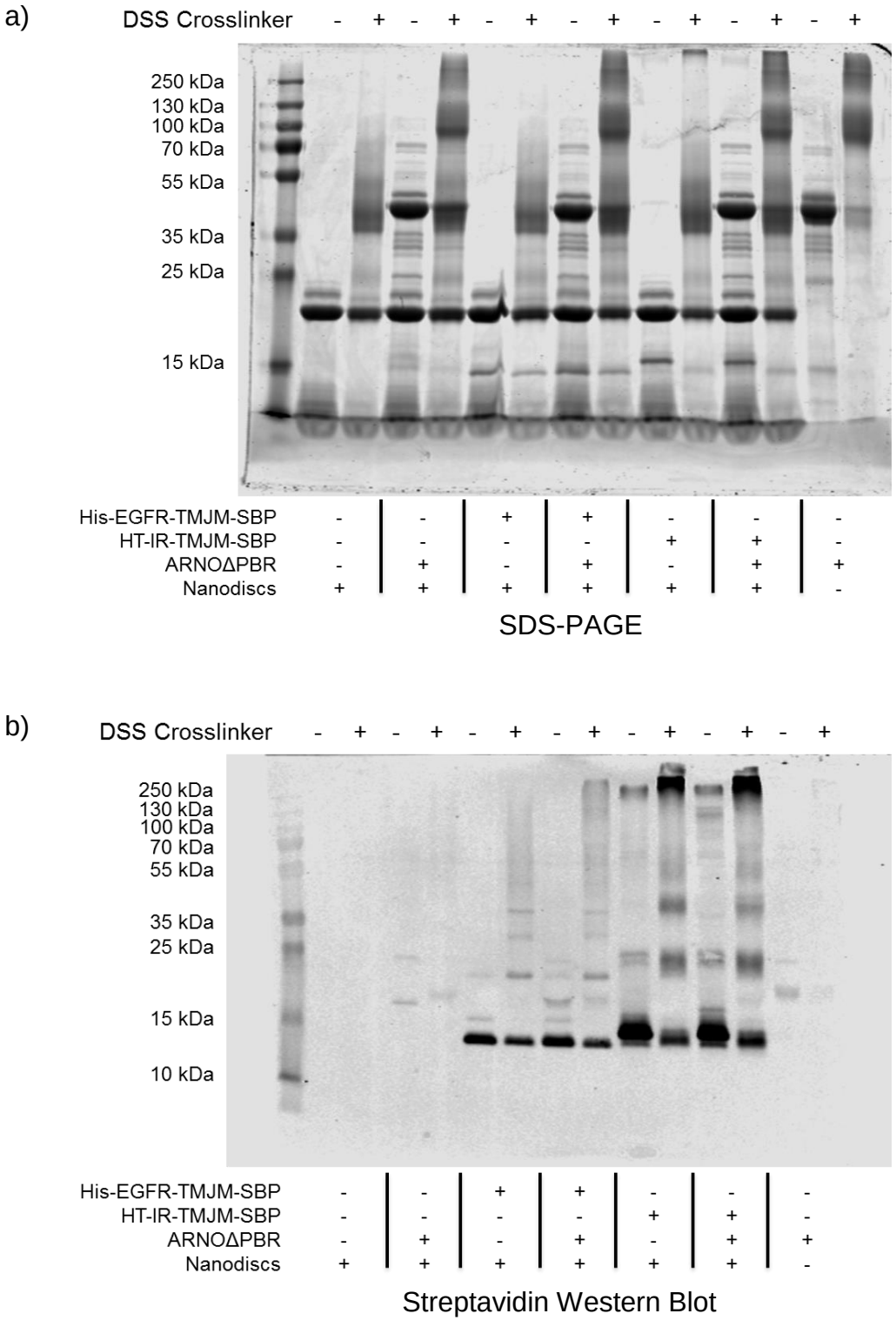

Supporting Figure 28: Original SDS-PAGE and Western Blot of DSS crosslinking of nanodiscs containing EGFR-TMJM and ARNOΔPBR (see Figure 56 a and b)

a) 15 % SDS-PAGE stained with Coomassie Brilliant Blue and **b)** Western blot using a Streptavidin-800 conjugated dye.

Acknowledgments

I would like to thank all the people that advised and helped me along these years.

First of all I express my gratitude to Professor Michael Famulok to give me the opportunity to work on a really interesting project, to encourage me and to welcome me in his group. I will always be grateful for this opportunity.

I am thankful to my supervisor Doctor Anton Schmitz for his helpful advices and support, to teach me how research can be challenging and to help me through difficult times. Furthermore, I am now completely confused about which article has the word “mango” in German.

I express my gratitude to Professor Thorsten Lang to encourage me and to motivate me at the end of my PhD project. I had a great time in his group and I would like to thank Gero for introducing me to the secrets of microscopy and the patience showed in teaching it. I sincerely thank Dennis, Elisa, Helena, Yahya, Pascal, Rebecca and Thomas for welcoming me and to feed me every week with a lot of cakes and candies.

I am very grateful to Professor Günter Mayer and Doctor Stefan Goertz for accepting to be the referees of this thesis.

My gratitude goes to all the members of the Famulok’s and Mayer’s group for the great time we spent together. I express my sincere thanks to Ben, Christine and Mo, for guiding me during the beginning of my PhD. I say a huge thank to all the people that help me to correct this PhD Thesis. In particular I would like to thank the small Caesar’s group: Christian, Maren, Max, Nora, Yvonne and Volkmar, best known as Volky. You always helped me to see the light at the end of the tunnel and I am extremely grateful for all the advice in the everyday lab-life. And after two years spent in the Caesar’s basement to improve my Kicker’s performance, I gained the title of “the wall”.

I would like to thank my German/Italian/Canadian/Spanish friends to make this experience one of the best of my life. And special thanks go to: Elisabetta, my fabulous flat mate, to make me feel like home and to prepare “pasta al pesto” as first aid; Christian or Mr. Nuss to be a fantastic friend and to be always here for me; Anna, who makes me lose weight walking at the speed of light; Alice to be the best long-distance friend ever.

Acknowledgments

I say thank to one of the most important people in my life, Falk, to be always by my side, to encourage me and to accept me as I am. Without you all this would not be possible at all. And the best part still has to come!

And last but not least to my big, huge, fat Italian family. I am extremely grateful for the deep love and support you always give me also from another country. Big thanks go to a small dog Priscilla, to always welcome me when I come back home. I would like to dedicate this work to my parents, Emanuela and Umberto, for their love and comprehension. I will always be grateful for all the sacrifices you made for me. To you goes my deepest love.

References

Alberts et al. (2002): The Lipid Bilayer. 4th edition: New York: Garland Science (Molecular Biology of the Cell).
Available online at http://www.ncbi.nlm.nih.gov/books/NBK26871/.

Alvarez, F. J. D.; Orelle, C.; Davidson, A. L. (2010): Functional Reconstitution of an ABC Transporter in Nanodiscs for Use in Electron Paramagnetic Resonance Spectroscopy. In *J. Am. Chem. Soc.* 132 (28), pp. 9513–9515. DOI: 10.1021/ja104047c.

Amin, D. N.; Hazelbauer, G. L. (2012): Influence of Membrane Lipid Composition on a Transmembrane Bacterial Chemoreceptor. In *Journal of Biological Chemistry* 287 (50), pp. 41697–41705. DOI: 10.1074/jbc.M112.415588.

Anastasi, S.; Zhu, S.-J.; Ballarò, C.; Manca, S.; Lamberti, D.; Wang, L.-J. et al. (2016): Lack of Evidence that CYTH2/ARNO Functions as a Direct Intracellular EGFR Activator. In *Cell* 165 (5), pp. 1031–1034. DOI: 10.1016/j.cell.2016.05.009.

Arkhipov, A.; Shan, Y.; Das, R.; Endres, N. F.; Eastwood, M. P.; Wemmer, D. E. et al. (2013): Architecture and membrane interactions of the EGF receptor. In *Cell* 152 (3), pp. 557–569. DOI: 10.1016/j.cell.2012.12.030.

Arnold, T.; Linke, D. (2008): The Use of Detergents to Purify Membrane Proteins. In *Current Protocols in Protein Science*, p. 4.8.1. DOI: 10.1002/0471140864.ps0408s53.

Avanti Polar Lipids Website (a). Available online at http://avantilipids.com/tech-support/liposome-preparation/bicelle-preparation/.

Avanti Polar Lipids Website (b). Available online at https://avantilipids.com/tech-support/faqs/transition-temperature/.

Avery, J. (2000): A Cell-free System for Regulated Exocytosis in PC12 Cells. In *The Journal of Cell Biology* 148 (2), pp. 317–324. DOI: 10.1083/jcb.148.2.317.

Bayburt, T. H.; Grinkova, Y. V.; Sligar, S. G. (2002): Self-Assembly of Discoidal Phospholipid Bilayer Nanoparticles with Membrane Scaffold Proteins. In *Nano Lett.* 2 (8), pp. 853–856. DOI: 10.1021/nl025623k.

Bayburt, T. H.; Sligar, S. G. (2003): Self-assembly of single integral membrane proteins into soluble nanoscale phospholipid bilayers. In *Protein Science* 12 (11), pp. 2476–2481. DOI: 10.1110/ps.03267503.

Bayburt, T. H.; Sligar, S. G. (2010): Membrane protein assembly into Nanodiscs. In *FEBS letters* 584 (9), pp. 1721–1727. DOI: 10.1016/j.febslet.2009.10.024.

Beaugrand, M.; Arnold, A. A.; Hénin, J.; Warschawski, D. E.; Williamson, P. T. F.; Marcotte, I. (2014): Lipid Concentration and Molar Ratio Boundaries for the Use of Isotropic Bicelles. In *Langmuir* 30 (21), pp. 6162–6170. DOI: 10.1021/la5004353.

Berger, M. B.; Mendrola, J. M.; Lemmon, M. A. (2004): ErbB3/HER3 does not homodimerize upon neuregulin binding at the cell surface. In *FEBS letters* 569 (1-3), pp. 332–336. DOI: 10.1016/j.febslet.2004.06.014.

References

Bessman, N. J.; Bagchi, A.; Ferguson, K. M.; Lemmon, M. A. (2014): Complex Relationship between Ligand Binding and Dimerization in the Epidermal Growth Factor Receptor. In *Cell Reports* 9 (4), pp. 1306–1317. DOI: 10.1016/j.celrep.2014.10.010.

Bill, A. (2011): Cytohesins are cytoplasmic ErbB receptor activators. Dissertation. Rheinischen Friedrich-Wilhelms-Universität Bonn. Available online at http://hss.ulb.uni-bonn.de/2011/2583/2583.htm.

Bill, A.; Schmitz, A.; Albertoni, B.; Song, J.-N.; Heukamp, L. C.; Walrafen, D. et al. (2010): Cytohesins are cytoplasmic ErbB receptor activators. In *Cell* 143 (2), pp. 201–211. DOI: 10.1016/j.cell.2010.09.011.

Bill, A.; Schmitz, A.; Albertoni, B.; Song, J.-N.; Heukamp, L. C.; Walrafen, D. et al. (2016): Retraction Notice to: Cytohesins Are Cytoplasmic ErbB Receptor Activators. In *Cell* 165 (5), p. 1293. DOI: 10.1016/j.cell.2016.05.013.

Bishayee, A.; Beguinot, L.; Bishayee, S. (1999): Phosphorylation of Tyrosine 992, 1068, and 1086 Is Required for Conformational Change of the Human Epidermal Growth Factor Receptor C-Terminal Tail. In *Molecular Biology of the Cell* 10 (3), pp. 525–536. DOI: 10.1091/mbc.10.3.525.

Blume-Jensen P.; Hunter, T. (2001): Oncogenic kinase signalling. In *Nature* (411), pp. 355–365. DOI: 10.1038/35077225.

Borch, J.; Hamann, T. (2009): The nanodisc. A novel tool for membrane protein studies. In *Biological Chemistry* 390 (8). DOI: 10.1515/BC.2009.091.

Bose, R.; Zhang, X. (2009): The ErbB kinase domain: structural perspectives into kinase activation and inhibition. In *Experimental cell research* 315 (4), pp. 649–658. DOI: 10.1016/j.yexcr.2008.07.031.

Brouillette, C. G.; Anantharamaiah, G. M.; Engler, J. A.; Borhani, D. W. (2001): Structural models of human apolipoprotein A-I. A critical analysis and review. In *Biochimica et Biophysica Acta (BBA) - Molecular and Cell Biology of Lipids* 1531 (1-2), pp. 4–46. DOI: 10.1016/S1388-1981(01)00081-6.

Burgess, A. W.; Cho, H.-S.; Eigenbrot, C.; Ferguson, K. M.; Garrett, T. P. J.; Leahy, D. J. et al. (2003): An Open-and-Shut Case? Recent Insights into the Activation of EGF/ErbB Receptors. In *Molecular cell* 12 (3), pp. 541–552. DOI: 10.1016/S1097-2765(03)00350-2.

Cantley, L. C. (2002): The Phosphoinositide 3-Kinase Pathway. In *Science* 296 (5573), pp. 1655–1657. DOI: 10.1126/science.296.5573.1655.

Casanova, J. E. (2007): Regulation of Arf activation: the Sec7 family of guanine nucleotide exchange factors. In *Traffic (Copenhagen, Denmark)* 8 (11), pp. 1476–1485. DOI: 10.1111/j.1600-0854.2007.00634.x.

Catoire, L. J.; Warnet, X. L.; Warschawski, D. E. (Eds.) (2014): Micelles, Bicelles, Amphipols, Nanodiscs, Liposomes, or Intact Cells: The Hitchhiker's Guide to the Study of Membrane Proteins by NMR.

Cherfils, J.; Ménétrey, J.; Mathieu, M.; Le Bras, G.; Robineau, S.; Béraud-Dufour, S. et al. (1998): Structure of the Sec7 domain of the Arf exchange factor ARNO. In *Nature* 392 (6671), pp. 101–105. DOI: 10.1038/32210.

Ciardiello, F.; Tortora, G. (2008): EGFR Antagonists in Cancer Treatment. In *N Engl J Med* 358 (11), pp. 1160–1174. DOI: 10.1056/NEJMra0707704.

Clayton, A. H. A. (2005): Ligand-induced Dimer-Tetramer Transition during the Activation of the Cell Surface Epidermal Growth Factor Receptor-A Multidimensional Microscopy Analysis. In *Journal of Biological Chemistry* 280 (34), pp. 30392–30399. DOI: 10.1074/jbc.M504770200.

Cohen, L. A.; Honda, A.; Varnai, P.; Brown, F. D.; Balla, T.; Donaldson, J. G. (2007): Active Arf6 Recruits ARNO/Cytohesin GEFs to the PM by Binding Their PH Domains. In *Molecular Biology of the Cell* 18 (6), pp. 2244–2253. DOI: 10.1091/mbc.E06-11-0998.

Contreras, F.-X.; Ernst, A. M.; Wieland, F.; Brügger, B. (2011): Specificity of intramembrane protein-lipid interactions. In *Cold Spring Harbor perspectives in biology* 3 (6). DOI: 10.1101/cshperspect.a004705.

Cronin, T. C.; DiNitto, J. P.; Czech, M. P.; Lambright, D. G. (2004): Structural determinants of phosphoinositide selectivity in splice variants of Grp1 family PH domains. In *The EMBO journal* (19), pp. 3711–3720. DOI: 10.1038/sj.emboj.7600388.

Czech, M. P. (2000): PIP2 and PIP3. In *Cell* 100 (6), pp. 603–606. DOI: 10.1016/S0092-8674(00)80696-0.

Dawson, J. P.; Berger, M. B.; Lin, C. C.; Schlessinger, J.; Lemmon, M. A.; Ferguson, K. M. (2005): Epidermal Growth Factor Receptor Dimerization and Activation Require Ligand-Induced Conformational Changes in the Dimer Interface. In *Molecular and Cellular Biology* 25 (17), pp. 7734–7742. DOI: 10.1128/MCB.25.17.7734-7742.2005.

Denisov, I. G.; Grinkova, Y. V.; Lazarides, A. A.; Sligar, S. G. (2004): Directed Self-Assembly of Monodisperse Phospholipid Bilayer Nanodiscs with Controlled Size. In *J. Am. Chem. Soc.* 126 (11), pp. 3477–3487. DOI: 10.1021/ja0393574.

Denisov, I. G.; Sligar, S. G. (2011): Cytochromes P450 in nanodiscs. In *Biochimica et biophysica acta* 1814 (1), pp. 223–229. DOI: 10.1016/j.bbapap.2010.05.017.

Di Paolo, G.; Camilli, P. de (2006): Phosphoinositides in cell regulation and membrane dynamics. In *Nature* 443 (7112), pp. 651–657. DOI: 10.1038/nature05185.

Domingues, A.; Fernandez, A.; Gonzalez, N.; Iglesias, E.; Montenegro, L. (1997): Determination of Critical Micelle Concentration of SomeSurfactants by Three Techniques. In *Journal of Chemical Education* (74), pp. 1227–1231. DOI: 10.1021/ed074p1227.

Donaldson, J. G.; Jackson, C. L. (2011): ARF family G proteins and their regulators: roles in membrane transport, development and disease. In *Nature reviews. Molecular cell biology* 12 (6), pp. 362–375. DOI: 10.1038/nrm3117.

Downward, J.; Parker, P.; Waterfield, M. D. (1984): Autophosphorylation sites on the epidermal growth factor receptor. In *Nature* (311), pp. 483–485. DOI: 10.1038/311483a0.

References

D'Souza-Schorey, C.; Chavrier, P. (2006): ARF proteins: roles in membrane traffic and beyond. In *Nature Reviews Molecular Cell Biology* 7 (5), pp. 347–358. DOI: 10.1038/nrm1910.

Duhr, S.; Braun, D. (2006): Why molecules move along a temperature gradient. In *Proceedings of the National Academy of Sciences of the United States of America* 103 (52), pp. 19678–19682. DOI: 10.1073/pnas.0603873103.

Dunn, K. W.; Kamocka, M. M.; McDonald, J. H. (2011): A practical guide to evaluating colocalization in biological microscopy. In *American journal of physiology. Cell physiology* 300 (4), p. C723-42. DOI: 10.1152/ajpcell.00462.2010.

Dürr, U. H. N.; Gildenberg, M.; Ramamoorthy, A. (2012): The magic of bicelles lights up membrane protein structure. In *Chemical reviews* 112 (11), pp. 6054–6074. DOI: 10.1021/cr300061w.

Endres, N. F.; Das, R.; Smith, A. W.; Arkhipov, A.; Kovacs, E.; Huang, Y. et al. (2013): Conformational coupling across the plasma membrane in activation of the EGF receptor. In *Cell* 152 (3), pp. 543–556. DOI: 10.1016/j.cell.2012.12.032.

Engelman, D. M. (2005): Membranes are more mosaic than fluid. In *Nature* 438 (7068), pp. 578–580. DOI: 10.1038/nature04394.

Ferguson, K. M. (2008): Structure-based view of epidermal growth factor receptor regulation. In *Annual review of biophysics* 37, pp. 353–373. DOI: 10.1146/annurev.biophys.37.032807.125829.

Ferguson, K. M.; Berger, M. B.; Mendrola, J. M.; Cho, H.-S.; Leahy, D. J.; Lemmon, M. A. (2003): EGF Activates Its Receptor by Removing Interactions that Autoinhibit Ectodomain Dimerization. In *Molecular cell* 11 (2), pp. 507–517. DOI: 10.1016/S1097-2765(03)00047-9.

Fuller, S. J.; Sivarajah, K.; Sugden, P. H. (2008): ErbB receptors, their ligands, and the consequences of their activation and inhibition in the myocardium. In *Journal of Molecular and Cellular Cardiology* 44 (5), pp. 831–854. DOI: 10.1016/j.yjmcc.2008.02.278.

Garavito, R. M.; Ferguson-Miller, S. (2001): Detergents as tools in membrane biochemistry. In *The Journal of biological chemistry* 276 (35), pp. 32403–32406. DOI: 10.1074/jbc.R100031200.

Garrett, T. P. J.; McKern, N. M.; Lou, M.; Elleman, T. C.; Adams, T. E.; Lovrecz, G. O. et al. (2002): Crystal Structure of a Truncated Epidermal Growth Factor Receptor Extracellular Domain Bound to Transforming Growth Factor α. In *Cell* 110 (6), pp. 763–773. DOI: 10.1016/S0092-8674(02)00940-6.

Glover, K. J.; Whiles, J. A.; Wu, G.; Yu, N.-j.; Deems, R.; Struppe, J. O. et al. (2001): Structural Evaluation of Phospholipid Bicelles for Solution-State Studies of Membrane-Associated Biomolecules. In *Biophysical journal* 81 (4), pp. 2163–2171. DOI: 10.1016/S0006-3495(01)75864-X.

Glück, J. M.; Koenig, B. W.; Willbold, D. (2011): Nanodiscs allow the use of integral membrane proteins as analytes in surface plasmon resonance studies. In *Analytical Biochemistry* 408 (1), pp. 46–52. DOI: 10.1016/j.ab.2010.08.028.

Glück, J. M.; Wittlich, M.; Feuerstein, S.; Hoffmann, S.; Willbold, D.; Koenig, B. W. (2009): Integral Membrane Proteins in Nanodiscs Can Be Studied by Solution NMR Spectroscopy. In *J. Am. Chem. Soc.* 131 (34), pp. 12060–12061. DOI: 10.1021/ja904897p.

Goñi, F. M. (2014): The basic structure and dynamics of cell membranes. An update of the Singer–Nicolson model. In *Biochimica et Biophysica Acta (BBA) - Biomembranes* 1838 (6), pp. 1467–1476. DOI: 10.1016/j.bbamem.2014.01.006.

Gotoh, N.; Tojo, A.; Hino, M.; Yazaki, Y.; Shibuya, M. (1992): A highly conserved tyrosine residue at codon 845 within the kinase domain is not required for the transforming activity of human epidermal growth factor receptor. In *Biochemical and biophysical research communications* 186 (2), pp. 768–774. DOI: 10.1016/0006-291X(92)90812-Y.

Hafner, M.; Schmitz, A.; Grüne, I.; Srivatsan, S. G.; Paul, B.; Kolanus, W. et al. (2006): Inhibition of cytohesins by SecinH3 leads to hepatic insulin resistance. In *Nature* 444 (7121), pp. 941–944. DOI: 10.1038/nature05415.

Hagn, F.; Etzkorn, M.; Raschle, T.; Wagner, G. (2013): Optimized Phospholipid Bilayer Nanodiscs Facilitate High-Resolution Structure Determination of Membrane Proteins. In *J. Am. Chem. Soc.* 135 (5), pp. 1919–1925. DOI: 10.1021/ja310901f.

Hagve, T.-A. (1988): Effects of unsaturated fatty acids on cell membrane functions. In *Scandinavian Journal of Clinical and Laboratory Investigation* 48 (5), pp. 381–388. DOI: 10.1080/00365518809085746.

Haley, J. D.; Gullick, W. J. (2009): EGFR Signaling Networks in Cancer Therapy: Humana Press. Available online at https://books.google.de/books?id=lUPbzFYc-TsC.

He, W.; Scharadin, T. M.; Saldana, M.; Gellner, C.; Hoang-Phou, S.; Takanishi, C. et al. (2015): Cell-free expression of functional receptor tyrosine kinases. In *Sci. Rep.* 5, p. 12896. DOI: 10.1038/srep12896.

Hirsch, J. D.; Eslamizar, L.; Filanoski, B. J.; Malekzadeh, N.; Haugland, Rosaria P.; Beechem, J. M.; Haugland, Richard P. (2002): Easily reversible desthiobiotin binding to streptavidin, avidin, and other biotin-binding proteins. Uses for protein labeling, detection, and isolation. In *Analytical Biochemistry* 308 (2), pp. 343–357. DOI: 10.1016/S0003-2697(02)00201-4.

Hubbard, S. R. (2004): Juxtamembrane autoinhibition in receptor tyrosine kinases. In *Nature reviews. Molecular cell biology* 5 (6), pp. 464–471. DOI: 10.1038/nrm1399.

Hubbard, S. R. (2013): The insulin receptor: both a prototypical and atypical receptor tyrosine kinase. In *Cold Spring Harbor perspectives in biology* 5 (3), pp. a008946. DOI: 10.1101/cshperspect.a008946.

References

Hunter, T. (1998): The role of tyrosine phosphorylation in cell growth and disease. In *Harvey lectures* 94, pp. 81–119. DOI: 10.1098/rstb.1998.0228.

Hussein, M.; Bettio, M.; Schmitz, A.; Hannam, J. S.; Theis, J.; Mayer, G. et al. (2013): Cyplecksins are covalent inhibitors of the pleckstrin homology domain of cytohesin. In *Angewandte Chemie (International ed. in English)* 52 (36), pp. 9529–9533. DOI: 10.1002/anie.201302207.

Ichinose, J.; Murata, M.; Yanagida, T.; Sako, Y. (2004): EGF signalling amplification induced by dynamic clustering of EGFR. In *Biochemical and biophysical research communications* 324 (3), pp. 1143–1149. DOI: 10.1016/j.bbrc.2004.09.173.

Imaoka T. S., Lynham J. A., Haslam R. J. (1983): Purification and Characterization of the 47,000-dalton ProteinPhosphorylated during Degranulation of Human Platelets. In *The Journal of biological chemistry* (258).

Inoue, A.; Setoguchi, K.; Matsubara, Y.; Okada, K.; Sato, N.; Iwakura, Y. et al. (2009): Dok-7 Activates the Muscle Receptor Kinase MuSK and Shapes Synapse Formation. In *Sci. Signal.* 2 (59), pp. ra7-ra7. DOI: 10.1126/scisignal.2000113.

Jerabek-Willemsen, M.; André, T.; Wanner, R.; Roth, H. M.; Duhr, S.; Baaske, P.; Breitsprecher, D. (2014): MicroScale Thermophoresis: Interaction analysis and beyond. In *Fluorescence studies of biomolecular association processes.Towards a detailed understanding of spectroscopic, thermodynamic and structural aspects* 1077, pp. 101–113. DOI: 10.1016/j.molstruc.2014.03.009.

Jerabek-Willemsen, M.; Wienken, C. J.; Braun, D.; Baaske, P.; Duhr, S. (2011): Molecular interaction studies using microscale thermophoresis. In *Assay and drug development technologies* 9 (4), pp. 342–353. DOI: 10.1089/adt.2011.0380.

Johnston, J.; Navaratnam, S.; Pitz, M.; Maniate, J.; Wiechec, E.; Baust, H. et al. (2006): Targeting the EGFR Pathway for Cancer Therapy. In *CMC* 13 (29), pp. 3483–3492. DOI: 10.2174/092986706779026174.

Jura, N.; Endres, N. F.; Engel, K.; Deindl, S.; Das, R.; Lamers, M. H. et al. (2009a): Mechanism for activation of the EGF receptor catalytic domain by the juxtamembrane segment. In *Cell* 137 (7), pp. 1293–1307. DOI: 10.1016/j.cell.2009.04.025.

Jura, N.; Shan, Y.; Cao, X.; Shaw, D. E.; Kuriyan, J. (2009b): Structural analysis of the catalytically inactive kinase domain of the human EGF receptor 3. In *Proceedings of the National Academy of Sciences of the United States of America* 106 (51), pp. 21608–21613. DOI: 10.1073/pnas.0912101106.

Jura, N.; Zhang, X.; Endres, N. F.; Seeliger, M. A.; Schindler, T.; Kuriyan, J. (2011): Catalytic control in the EGF Receptor and its connection to general kinase regulatory mechanisms. In *Molecular cell* 42 (1), pp. 9–22. DOI: 10.1016/j.molcel.2011.03.004.

Kahn, R. A.; Randazzo, P.; Serafini, T.; Weiss, O.; Rulka, C.; Clark, J. et al. (1992): The amino terminus of ADP-ribosylation factor (ARF) is a critical determinant of ARF activities and is a potent and specific inhibitor of protein transport. In *J. Biol. Chem.* 267 (18), pp. 13039–13046.

Available online at http://www.jbc.org/content/267/18/13039.full.pdf.

Kavran, J. M.; Klein, D. E.; Lee, A.; Falasca, M.; Isakoff, S. J.; Skolnik, E. Y.; Lemmon, M. A. (1998): Specificity and Promiscuity in Phosphoinositide Binding by Pleckstrin Homology Domains. In *Journal of Biological Chemistry* 273 (46), pp. 30497–30508. DOI: 10.1074/jbc.273.46.30497.

Keefe, A. D.; Wilson, D. S.; Seelig, B.; Szostak, J. W. (2001): One-Step Purification of Recombinant Proteins Using a Nanomolar-Affinity Streptavidin-Binding Peptide, the SBP-Tag. In *Protein Expression and Purification* 23 (3), pp. 440–446. DOI: 10.1006/prep.2001.1515.

Kholodenko, B. N.; Demin, O. V.; Moehren, G.; Hoek, J. B. (1999): Quantification of Short Term Signaling by the Epidermal Growth Factor Receptor. In *Journal of Biological Chemistry* 274 (42), pp. 30169–30181. DOI: 10.1074/jbc.274.42.30169.

Kitamura, T.; Kahn, C. R.; Accili, D. (2003): Insulin receptor knockout mice. In *Annual review of physiology* 65, pp. 313–332. DOI: 10.1146/annurev.physiol.65.092101.142540.

Klarlund, J. K. (1997): Signaling by Phosphoinositide-3,4,5-Trisphosphate Through Proteins Containing Pleckstrin and Sec7 Homology Domains. In *Science* 275 (5308), pp. 1927–1930. DOI: 10.1126/science.275.5308.1927.

Klarlund, J. K.; Tsiaras, W.; Holik, J. J.; Chawla, A.; Czech, M. P. (2000): Distinct polyphosphoinositide binding selectivities for pleckstrin homology domains of GRP1-like proteins based on diglycine versus triglycine motifs. In *The Journal of biological chemistry* 275 (42), pp. 32816–32821. DOI: 10.1074/jbc.M002435200.

Kolanus, W. (2007): Guanine nucleotide exchange factors of the cytohesin family and their roles in signal transduction. In *Immunological reviews* 218, pp. 102–113. DOI: 10.1111/j.1600-065X.2007.00542.x.

Kolanus, W.; Nagel, W.; Schiller, B.; Zeitlmann, L.; Godar, S.; Stockinger, H.; Seed, B. (1996): αLβ2 Integrin/LFA-1 Binding to ICAM-1 Induced by Cytohesin-1, a Cytoplasmic Regulatory Molecule. In *Cell* 86 (2), pp. 233–242. DOI: 10.1016/S0092-8674(00)80095-1.

Krause, M. R.; Regen, S. L. (2014): The Structural Role of Cholesterol in Cell Membranes. From Condensed Bilayers to Lipid Rafts. In *Acc. Chem. Res.* 47 (12), pp. 3512–3521. DOI: 10.1021/ar500260t.

Kyhse-Andersen, J. (1984): Electroblotting of multiple gels: a simple apparatus without buffer tank for rapid transfer of proteins from polyacrylamide to nitrocellulose. In *Journal of biochemical and biophysical methods* 10 (3-4), pp. 203–209.

Laemmli, U. K. (1970): Cleavage of Structural Proteins during the Assembly of the Head of Bacteriophage T4 227 (5259), pp. 680–685. DOI: 10.1038/227680a0.

Lang, T. (2001): SNAREs are concentrated in cholesterol-dependent clusters that define docking and fusion sites for exocytosis. In *The EMBO journal* 20 (9), pp. 2202–2213. DOI: 10.1093/emboj/20.9.2202.

References

Lang, T. (2003): Imaging SNAREs at work in ‘unroofed’ cells – approaches that may be of general interest for functional studies on membrane proteins. In *Biochm. Soc. Trans.* 31 (4), pp. 861–864. DOI: 10.1042/bst0310861.

Le Maire, M.; Arnou, B.; Olesen, C.; Georgin, D.; Ebel, C.; Møller, J. V. (2008): Gel chromatography and analytical ultracentrifugation to determine the extent of detergent binding and aggregation, and Stokes radius of membrane proteins using sarcoplasmic reticulum Ca2+-ATPase as an example. In *Nature protocols* 3 (11), pp. 1782–1795. DOI: 10.1038/nprot.2008.177.

Lemmon, M. A. (2008): Membrane recognition by phospholipid-binding domains. In *Nat Rev Mol Cell Biol* 9 (2), pp. 99–111. DOI: 10.1038/nrm2328.

Lemmon, M. A.; Ferguson, K. M. (2000): Signal-dependent membrane targeting by pleckstrin homology (PH) domains. In *Biochem. J.* 350 (1), pp. 1–18. DOI: 10.1042/bj3500001.

Lemmon, M. A.; Ferguson, K. M.; Abrams, C. S. (2002): Pleckstrin homology domains and the cytoskeleton. In *Protein Domains* 513 (1), pp. 71–76. DOI: 10.1016/S0014-5793(01)03243-4.

Lemmon, M. A.; Schlessinger, J. (2010): Cell signaling by receptor tyrosine kinases. In *Cell* 141 (7), pp. 1117–1134. DOI: 10.1016/j.cell.2010.06.011.

Lemmon, M. A.; Schlessinger, J.; Ferguson, K. M. (2014): The EGFR Family. Not So Prototypical Receptor Tyrosine Kinases. In *Cold Spring Harbor perspectives in biology* 6 (4), pp. a020768-a020768. DOI: 10.1101/cshperspect.a020768.

Leventis, P. A.; Grinstein, S. (2010): The Distribution and Function of Phosphatidylserine in Cellular Membranes. In *Annu. Rev. Biophys.* 39 (1), pp. 407–427. DOI: 10.1146/annurev.biophys.093008.131234.

Li, Lunyi; Shi, Xiaoshan; Guo, Xingdong; Li, Hua; Xu, Chenqi (2014): Ionic protein–lipid interaction at the plasma membrane. What can the charge do? In *Trends in biochemical sciences* 39 (3), pp. 130–140. DOI: 10.1016/j.tibs.2014.01.002.

Lim, J.; Zhou, M.; Veenstra, T. D.; Morrison, D. K. (2010): The CNK1 scaffold binds cytohesins and promotes insulin pathway signaling. In *Genes & Development* 24 (14), pp. 1496–1506. DOI: 10.1101/gad.1904610.

Liu, Y.; Kahn, R. A.; Prestegard, J. H. (2010): Dynamic structure of membrane-anchored Arf•GTP. In *Nat Struct Mol Biol* 17 (7), pp. 876–881. DOI: 10.1038/nsmb.1853.

Lorber, B.; Fischer, F.; Bailly, M.; Roy, H.; Kern, D. (2012): Protein analysis by dynamic light scattering: Methods and techniques for students. In *Biochemistry and Molecular Biology Education* 40. DOI: 10.1002/bmb.20644.

Lu, Z.; van Horn, W. D.; Chen, J.; Mathew, S.; Zent, R.; Sanders, C. R. (2012): Bicelles at low concentrations. In *Molecular pharmaceutics* 9 (4), pp. 752–761. DOI: 10.1021/mp2004687.

Mason, J. M.; Arndt, K. M. (2004): Coiled coil domains: stability, specificity, and biological implications. In *Chembiochem : a European journal of chemical biology* 5 (2), pp. 170–176. DOI: 10.1002/cbic.200300781.

Mendelsohn, J.; Baselga, J. (2000): The EGF receptor family as targets for cancer therapy. In *Oncogene* 19 (56), pp. 6550–6565. DOI: 10.1038/sj.onc.1204082.

Mendrola, J. M.; Berger, M. B.; King, M. C.; Lemmon, M. A. (2002): The Single Transmembrane Domains of ErbB Receptors Self-associate in Cell Membranes. In *J. Biol. Chem.* 277 (7), pp. 4704–4712. DOI: 10.1074/jbc.M108681200.

Mi, L.-Z.; Grey, M. J.; Nishida, N.; Walz, T.; Lu, C.; Springer, T. A. (2008): Functional and structural stability of the epidermal growth factor receptor in detergent micelles and phospholipid nanodiscs. In *Biochemistry* 47 (39), pp. 10314–10323. DOI: 10.1021/bi801006s.

Mineev, K. S.; Panova, S. V.; Bocharova, O. V.; Bocharov, E. V.; Arseniev, A. S. (2015): The Membrane Mimetic Affects the Spatial Structure and Mobility of EGFR Transmembrane and Juxtamembrane Domains. In *Biochemistry* 54 (41), pp. 6295–6298. DOI: 10.1021/acs.biochem.5b00851.

Moriki, T.; Maruyama, H.; Maruyama, I. N. (2001): Activation of preformed EGF receptor dimers by ligand-induced rotation of the transmembrane domain11Edited by B. Holland. In *Journal of Molecular Biology* 311 (5), pp. 1011–1026. DOI: 10.1006/jmbi.2001.4923.

Nagel, W.; Schilcher, P.; Zeitlmann, L.; Kolanus, W. (1998a): The PH Domain and the Polybasic c Domain of Cytohesin-1 Cooperate specifically in Plasma Membrane Association and Cellular Function. In *Molecular Biology of the Cell* 9 (8), pp. 1981–1994. DOI: 10.1091/mbc.9.8.1981.

Nagel, Wolfgang; Zeitlmann, Lutz; Schilcher, Pierre; Geiger, Christiane; Kolanus, Johanna; Kolanus, Waldemar (1998b): Phosphoinositide 3-OH Kinase Activates the β2Integrin Adhesion Pathway and Induces Membrane Recruitment of Cytohesin-1. In *J. Biol. Chem.* 273 (24), pp. 14853–14861. DOI: 10.1074/jbc.273.24.14853.

Näsvik Öjemyr, L.; Ballmoos, C. von; Gennis, R. B.; Sligar, S. G.; Brzezinski, P. (2012): Reconstitution of respiratory oxidases in membrane nanodiscs for investigation of proton-coupled electron transfer. In *FEBS letters* 586 (5), pp. 640–645. DOI: 10.1016/j.febslet.2011.12.023.

Nath, A.; Atkins, W. M.; Sligar, S. G. (2007): Applications of Phospholipid Bilayer Nanodiscs in the Study of Membranes and Membrane Proteins †. In *Biochemistry* 46 (8), pp. 2059–2069. DOI: 10.1021/bi602371n.

Nic, M.; Jirat, J.; Kosata, B. (Eds.) (2009): IUPAC Compendium of Chemical Terminology. Research Triagle Park, NC: IUPAC.

Nicolson, G. L. (2014): The Fluid—Mosaic Model of Membrane Structure. Still relevant to understanding the structure, function and dynamics of biological membranes after more

than 40years. In *Biochimica et Biophysica Acta (BBA) - Biomembranes* 1838 (6), pp. 1451–1466. DOI: 10.1016/j.bbamem.2013.10.019.

O'Connor, C. M.; Adams, M. (Eds.) (2010): Essentials of Cell Biology: Cambridge, MA: NPG Education. Available online at http://www.nature.com/scitable/ebooks/cell-biology-for-seminars-14760004/118244378.

Ogiso, H.; Ishitani, R.; Nureki, O.; Fukai, S.; Yamanaka, M.; Kim, J.-H. et al. (2002): Crystal Structure of the Complex of Human Epidermal Growth Factor and Receptor Extracellular Domains. In *Cell* 110 (6), pp. 775–787. DOI: 10.1016/S0092-8674(02)00963-7.

Ohi, M.; Li, Y.; Cheng, Y.; Walz, T. (2004): Negative Staining and Image Classification – Powerful Tools in Modern Electron Microscopy. In *Biological procedures online* 6, pp. 23–34. DOI: 10.1251/bpo70.

Olayioye, M. A. (2000): The ErbB signaling network: receptor heterodimerization in development and cancer. In *The EMBO journal* 19 (13), pp. 3159–3167. DOI: 10.1093/emboj/19.13.3159.

Ottiger, M.; Bax, A. (1998): Characterization of magnetically oriented phospholipid micelles for measurement of dipolar couplings in macromolecules. In *Journal of Biomolecular NMR* 12 (3), pp. 361–372. DOI: 10.1023/A:1008366116644.

Palmer, I.; Wingfield, P. T. (2012): Preparation and extraction of insoluble (inclusion-body) proteins from Escherichia coli. In *Current protocols in protein science / editorial board, John E. Coligan ... [et al.]* Chapter 6, p. Unit6.3. DOI: 10.1002/0471140864.ps0603s70.

Pandit, A.; Shirzad-Wasei, N.; Wlodarczyk, L. M.; van Roon, H.; Boekema, E. J.; Dekker, J. P.; Grip, W. J. de (2011): Assembly of the Major Light-Harvesting Complex II in Lipid Nanodiscs. In *Biophysical journal* 101 (10), pp. 2507–2515. DOI: 10.1016/j.bpj.2011.09.055.

Perez, J.-B.; Martinez, K. L.; Segura, J.-M.; Vogel, H. (2006): Supported Cell-Membrane Sheets for Functional Fluorescence Imaging of Membrane Proteins. In *Adv. Funct. Mater.* 16 (2), pp. 306–312. DOI: 10.1002/adfm.200500236.

Peters, K.; Richards, F. M. (1977): Chemical cross-linking: reagents and problems in studies of membrane structure. In *Annual review of biochemistry* 46, pp. 523–551. DOI: 10.1146/annurev.bi.46.070177.002515.

Prosser, R. S.; Evanics, F.; Kitevski, J. L.; Al-Abdul-Wahid, M. S. (2006): Current applications of bicelles in NMR studies of membrane-associated amphiphiles and proteins. In *Biochemistry* 45 (28), pp. 8453–8465. DOI: 10.1021/bi060615u.

Ram, P.; Prestegard, J. H. (1988): Magnetic field induced ordering of bile salt/phospholipid micelles. New media for NMR structural investigations. In *Biochimica et Biophysica Acta (BBA) - Biomembranes* 940 (2), pp. 289–294. DOI: 10.1016/0005-2736(88)90203-9.

Ramón, A.; Señorale-Pose, M.; Marín, M. (2014): Inclusion bodies. Not that bad… In *Front. Microbiol.* 5. DOI: 10.3389/fmicb.2014.00056.

Recenttec Website.
Available online at http://www.recenttec.com/product/?product_id=228.

Red Brewer, M.; Choi, S. H.; Alvarado, D.; Moravcevic, K.; Pozzi, A.; Lemmon, M. A.; Carpenter, G. (2009): The juxtamembrane region of the EGF receptor functions as an activation domain. In *Molecular cell* 34 (6), pp. 641–651. DOI: 10.1016/j.molcel.2009.04.034.

Rey L., May J. C. (Ed.) (2010): Freeze-Drying/Lyophilization Of Pharmaceutical & Biological Products, Third Edition (Drugs and the Pharmaceutical Sciences). Chapter 7: Freezing- and Drying-Induced Perturbationsof Protein Structure and Mechanisms ofProtein Protection by Stabilizing Additives: Informa Healthcare (206).

Rigaud J.-L. (2002): Membrane proteins: functional and structural studies using reconstituted proteoliposomes and 2-D crystals. In *Reconstitutionofmembraneproteins Brazilian Journal of Medical and Biological Research*, pp. 753–766.

Roskoski, R. (2014): The ErbB/HER family of protein-tyrosine kinases and cancer. In *Pharmacological research* 79, pp. 34–74. DOI: 10.1016/j.phrs.2013.11.002.

Russ, W. P.; Engelman, D. M. (2000): The GxxxG motif. A framework for transmembrane helix-helix association. In *Journal of Molecular Biology* 296 (3), pp. 911–919. DOI: 10.1006/jmbi.1999.3489.

Sanders, C. R.; Landis, G. C. (1995): Reconstitution of Membrane Proteins into Lipid-Rich Bilayered Mixed Micelles for NMR Studies. In *Biochemistry* 34 (12), pp. 4030–4040. DOI: 10.1021/bi00012a022.

Sanders, C. R.; Prestegard, J. H. (1990): Magnetically orientable phospholipid bilayers containing small amounts of a bile salt analogue, CHAPSO. In *Biophysical journal* 58 (2), pp. 447–460. DOI: 10.1016/S0006-3495(90)82390-0.

Schlessinger, J.; Lemmon, M. A. (2003): SH2 and PTB Domains in Tyrosine Kinase Signaling. In *Science Signaling* 2003 (191), pp. re12-re12. DOI: 10.1126/stke.2003.191.re12.

Schuler, M. A.; Denisov, I. G.; Sligar, S. G. (2013): Nanodiscs as a new tool to examine lipid-protein interactions. In *Methods in molecular biology (Clifton, N.J.)* 974, pp. 415–433. DOI: 10.1007/978-1-62703-275-9_18.

Segatto, O.; Anastasi, S.; Alemà, S. (2011): Regulation of epidermal growth factor receptor signalling by inducible feedback inhibitors. In *Journal of cell science* 124 (Pt 11), pp. 1785–1793. DOI: 10.1242/jcs.083303.

Sepmag (Ed.) (2010): The Advanced Guide to Biomagnetic Protein Purification.

Serebryany, E.; Zhu, G. A.; Yan, E. C. Y. (2012): Artificial membrane-like environments for in vitro studies of purified G-protein coupled receptors. In *Biochimica et Biophysica Acta (BBA) - Biomembranes* 1818 (2), pp. 225–233. DOI: 10.1016/j.bbamem.2011.07.047.

References

Sharpe, S.; Barber, K. R.; Grant, C. W. M. (2000): Val 659 →Glu Mutation within the Transmembrane Domain of ErbB-2. Effects Measured by 2 H NMR in Fluid Phospholipid Bilayers †. In *Biochemistry* 39 (21), pp. 6572–6580. DOI: 10.1021/bi000038o.

Shih, Amy Y.; Arkhipov, Anton; Freddolino, Peter L.; Sligar, Stephen G.; Schulten, Klaus (2007): Assembly of lipids and proteins into lipoprotein particles. In *The journal of physical chemistry. B* 111 (38), pp. 11095–11104. DOI: 10.1021/jp072320b.

Simons, K.; Ikonen, E. (1997): Functional rafts in cell membranes. In *Nature* 387 (6633), pp. 569–572. DOI: 10.1038/42408.

Simons, K.; Sampaio, J. L. (2011): Membrane Organization and Lipid Rafts. In *Cold Spring Harbor perspectives in biology* 3 (10), pp. a004697-a004697. DOI: 10.1101/cshperspect.a004697.

Simons, K.; Vaz, W. L. C. (2004): Model systems, lipid rafts, and cell membranes. In *Annual review of biophysics and biomolecular structure* 33, pp. 269–295. DOI: 10.1146/annurev.biophys.32.110601.141803.

Singer, S. J.; Nicolson, G. L. (1972): The Fluid Mosaic Model of the Structure of Cell Membranes. In *Science* 175 (4023), pp. 720–731. DOI: 10.1126/science.175.4023.720.

Singh, A.; Upadhyay, V.; Upadhyay, A. K.; Singh, S. M.; Panda, A. K. (2015): Protein recovery from inclusion bodies of Escherichia coli using mild solubilization process. In *Microb Cell Fact* 14 (1), p. 687. DOI: 10.1186/s12934-015-0222-8.

Sligar's Laboratory Website.
Available online at http://sligarlab.life.uiuc.edu/nanodisc/protocols.html.

Stamos, J.; Sliwkowski, M. X.; Eigenbrot, C. (2002): Structure of the Epidermal Growth Factor Receptor Kinase Domain Alone and in Complex with a 4-Anilinoquinazoline Inhibitor. In *J. Biol. Chem.* 277 (48), pp. 46265–46272. DOI: 10.1074/jbc.M207135200.

Struppe, J.; Whiles, J. A.; Vold, R. R. (2000): Acidic Phospholipid Bicelles. A Versatile Model Membrane System. In *Biophysical journal* 78 (1), pp. 281–289. DOI: 10.1016/S0006-3495(00)76591-X.

Tanford, C. (1974): Theory of micelle formation in aqueous solutions. In *J. Phys. Chem.* 78 (24), pp. 2469–2479. DOI: 10.1021/j100617a012.

Taniguchi, C. M.; Emanuelli, B.; Kahn, C. R. (2006): Critical nodes in signalling pathways: insights into insulin action. In *Nature reviews. Molecular cell biology* 7 (2), pp. 85–96. DOI: 10.1038/nrm1837.

Tanner, K. G.; Kyte, J. (1999): Dimerization of the Extracellular Domain of the Receptor for Epidermal Growth Factor Containing the Membrane-spanning Segment in Response to Treatment with Epidermal Growth Factor. In *Journal of Biological Chemistry* 274 (50), pp. 35985–35990. DOI: 10.1074/jbc.274.50.35985.

Thermo Scientific Pierce (Ed.) (2010): Protein Interaction Technica Handbook.

Thiel, K. W.; Carpenter, G. (2007): Epidermal growth factor receptor juxtamembrane region regulates allosteric tyrosine kinase activation. In *Proceedings of the National Academy of Sciences of the United States of America* 104 (49), pp. 19238–19243. DOI: 10.1073/pnas.0703854104.

Tsuboi, T.; Lippiat, J. D.; Ashcroft, F. M.; Rutter, G. A. (2004): ATP-dependent interaction of the cytosolic domains of the inwardly rectifying K+ channel Kir6.2 revealed by fluorescence resonance energy transfer. In *Proceedings of the National Academy of Sciences* 101 (1), pp. 76–81. DOI: 10.1073/pnas.0306347101.

Ujwal, R.; Bowie, J. U. (2011): Crystallizing membrane proteins using lipidic bicelles. In *Methods (San Diego, Calif.)* 55 (4), pp. 337–341. DOI: 10.1016/j.ymeth.2011.09.020.

Venkateswarlu, K.; Oatey, P. B.; Tavaré, J. M.; Cullen, P. J. (1998): Insulin-dependent translocation of ARNO to the plasma membrane of adipocytes requires phosphatidylinositol 3-kinase. In *Current Biology* 8 (8), pp. 463–466. DOI: 10.1016/S0960-9822(98)70181-2.

Versace, R. E.; Lazaridis, T. (2015): Modeling Protein–Micelle Systems in Implicit Water. In *J. Phys. Chem. B* 119 (25), pp. 8037–8047. DOI: 10.1021/acs.jpcb.5b00171.

Wang, Ye; Gao, J.; Guo, X.; Tong, T.; Shi, X.; Li, L. et al. (2014): Regulation of EGFR nanocluster formation by ionic protein-lipid interaction. In *Cell research* 24 (8), pp. 959–976. DOI: 10.1038/cr.2014.89.

Wennerberg, K.; Rossman, K. L.; Der, C. J. (2005): The Ras superfamily at a glance. In *Journal of cell science* 118 (Pt 5), pp. 843–846. DOI: 10.1242/jcs.01660.

Whiles, J. A.; Deems, R.; Vold, R. R.; Dennis, E. A. (2002): Bicelles in structure–function studies of membrane-associated proteins. In *Bioorganic Chemistry* 30 (6), pp. 431–442. DOI: 10.1016/S0045-2068(02)00527-8.

Whitson, K. B.; Beechem, J. M.; Beth, A. H.; Staros, J. V. (2004): Preparation and characterization of Alexa Fluor 594-labeled epidermal growth factor for fluorescence resonance energy transfer studies: application to the epidermal growth factor receptor. In *Analytical Biochemistry* 324 (2), pp. 227–236. DOI: 10.1016/j.ab.2003.09.023.

Wu, M.; Huang, B.; Graham, M.; Raimondi, A.; Heuser, J. E.; Zhuang, X.i; Camilli, P. de (2010): Coupling between clathrin-dependent endocytic budding and F-BAR-dependent tubulation in a cell-free system. In *Nat Cell Biol* 12 (9), pp. 902–908. DOI: 10.1038/ncb2094.

Wu, S.-L.; Kim, J.; Bandle, R. W.; Liotta, L.; Petricoin, E.; Karger, B. L. (2006): Dynamic profiling of the post-translational modifications and interaction partners of epidermal growth factor receptor signaling after stimulation by epidermal growth factor using Extended Range Proteomic Analysis (ERPA). In *Molecular & cellular proteomics : MCP* 5 (9), pp. 1610–1627. DOI: 10.1074/mcp.M600105-MCP200.

Yarden, Y. (2001): Biology of HER2 and Its Importance in Breast Cancer. In *Oncology* 61 (Suppl. 2), pp. 1–13. DOI: 10.1159/000055396.

References

Yarden, Y.; Sliwkowski, M. X. (2001): Untangling the ErbB signalling network. In *Nature Reviews* (2), pp. 127–137. DOI: 10.1038/35052073.

Zhang, X.; Gureasko, J.; Shen, K.; Cole, P. A.; Kuriyan, J. (2006): An Allosteric Mechanism for Activation of the Kinase Domain of Epidermal Growth Factor Receptor. In *Cell* 125 (6), pp. 1137–1149. DOI: 10.1016/j.cell.2006.05.013.

Zhang, X.; Pickin, K. A.; Bose, R.; Jura, N.; Cole, P. A.; Kuriyan, J. (2007): Inhibition of the EGF receptor by binding of MIG6 to an activating kinase domain interface. In *Nature* 450 (7170), pp. 741–744. DOI: 10.1038/nature05998.

Zilly, F. E.; Halemani, N. D.; Walrafen, D.; Spitta, L.; Schreiber, A.; Jahn, R.; Lang, T. (2011): Ca2+ induces clustering of membrane proteins in the plasma membrane via electrostatic interactions. In *The EMBO journal* 30 (7), pp. 1209–1220. DOI: 10.1038/emboj.2011.53.